Loughborough University

This item is held in Loughborough University's Institutional Repository (https://dspace.lboro.ac.uk/) and was harvested from the British Library's EThOS service (http://www.ethos.bl.uk/). It is made available under the following Creative Commons Licence conditions.

creative commons

COMMONS DEED

Attribution-NonCommercial-NoDerivs 2.5

You are free:

- to copy, distribute, display, and perform the work

Under the following conditions:

Attribution. You must attribute the work in the manner specified by the author or licensor.

Noncommercial. You may not use this work for commercial purposes.

No Derivative Works. You may not alter, transform, or build upon this work.

- For any reuse or distribution, you must make clear to others the license terms of this work.
- Any of these conditions can be waived if you get permission from the copyright holder.

Your fair use and other rights are in no way affected by the above.

This is a human-readable summary of the Legal Code (the full license).

Disclaimer

For the full text of this licence, please go to:
http://creativecommons.org/licenses/by-nc-nd/2.5/

MODELLING AND CONTROL OF VARIABILITY IN PCB COPPER ELECTROPLATING

by

Ka-Kwai POON, Msc(Warwick)

A Doctoral Thesis
submitted in partial fulfilment of the requirements
for the award of Doctor of Philosophy
of Loughborough University

March 1998

© by Ka-Kwai POON 1998

ACKNOWLEDGEMENTS

I wish to express my sincere appreciation to my research supervisor, Prof. David Williams for his intellectual stimulus, encouragement and invaluable advice throughout the project. My thanks also go to Ms. SC Lee, technician of the Electronics Product Manufacturing Laboratory of City University of Hong Kong, who provided technical support in the course of experimentation. Finally, my sincere appreciation go to my wife, Agnes, for her utmost support and unceasing patience throughout my study.

TABLE OF CONTENTS

DECLARATION i

ACKNOWLEDGMENTS ii

TABLE OF CONTENTS iii

LIST OF FIGURES AND TABLES ix

LIST OF ABBREVIATIONS xv

ABSTRACT xx

1. INTRODUCTION 1

1.1 Introduction 1

1.2 The Areas of Investigation 2

1.3 Research Approach 3

1.4 Structure of the Thesis 4

2. MODELLING OF ELECTROPLATING 6

2.1 Introduction 6

2.2 The Acid Copper Electroplating Process 6

2.3 Modelling of Current Distribution 9

2.3.1 The Primary Current Distribution 10

2.3.2 The Secondary Current Distribution 11

2.3.3 The Tertiary Current Distribution 12

2.4 A Review of Recent Modelling Work 13

2.4.1 Scaling of current distribution modelling 13

2.4.2 Workpiece level modelling 16

2.4.2.1 Parallel Planar Electrodes – Two-Dimensional Analysis 16

2.4.2.2 Parallel Planar Electrodes – Three-Dimensional Analysis 22

2.4.2.3 Hull Cell Modelling 25

2.4.3 Pattern level modelling 27
2.4.4 Feature level modelling 32
2.4.4.1 Through-Hole Modelling 32
2.4.4.2 Empirical Modelling of Through-Hole Plating 42
2.5 Statistical Modelling of Acid Copper Plating Process 43
2.6 Summary 45

3. EXPERIMENTAL SETUP AND PROCEDURES 46
3.1 Introduction 46
3.2 Equipment and Apparatus 46
3.3 Acid Copper Pattern Plating 49
3.3.1 Material and Solution 49
3.3.2 Pattern Plating Process 49
3.4 Plated-Through Hole and Blind Via Plating 52
3.4.1 Solution and Material 52
3.4.2 Electroless Copper Plating 53
3.4.3 Acid Copper Plating 54
3.5 Measurement of Plating Thickness with X-ray Thickness Gauge/Microscope 55
3.5.1 Materials 55
3.5.2 Microsectioning Procedure 55
3.6 Measurement of Plating Thickness with Talysurf Roughness Measuring Machine 56
3.7 Summary 56

4. EXPERIMENTAL DESIGN AND ANALYSIS : PATTERN PLATING 57
4.1 Introduction 57
4.2 Quality Characteristic 58
4.3 Process Parameters 59
4.4 The Matrix Experiments 60

4.5 Experimental Study of Copper Plating of Uniform Patterns 62
4.5.1 Hull Cell Experiments : Factor Screening 62
4.5.2 Plating Bath Experiment : Locating Neighborhood of Optimum Region 67
4.5.2.1 Analysis of the Mean Responses 73
4.5.2.2 Analysis of the SD Responses 74
4.5.3 Finding the approximation : location of Optimum Region and the First Order Model 75
4.5.4 Second Order Model and Building and Optimization 78
4.5.5 Model Verification 83
4.6 Experimental Study of Copper Plating of Non-Uniform Patterns 85
4.6.1 The First-Order Model 88
4.6.2 Model Verification Using the 'Zebra" Pattern 92
4.6.2.1 Analysis Using the Left, Right and Central Region of the Board 92
4.6.2.2 Analysis Using the Upper and Lower Region of the Board 99
4.6.3 Model Verification Using a Simple Circuit Pattern 102
4.7 Summary 109

5. EXPERIMENTAL DESIGN AND ANALYSIS : PLATED THROUGH HOLE AND BLIND VIA PLATING 110
5.1 Introduction 110
5.2 Plated-Through Hole(PTH) Plating Workpiece Level Modelling 110
5.2.1 Factors Screening and the First-Order Model 110
5.2.1.1 Analysis of the Mean Responses 112
5.2.1.2 Analysis of the SD Responses 116
5.2.1.3 Building the First-Order Model of the SD Responses 118
5.2.1.4 Residual Analysis 120

5.2.2 Second-Order Model Building and Optimization of workpiece level Variation 120
5.2.2.1 Response Surfaces and Optimization 122
5.2.2.2 Residual Analysis 127
5.2.3 Model Verification 127
5.3 Blind Via (BV) Plating Workpiece Level Modeling 128
5.3.1 Factors Screening and the First-Order Model 128
5.3.1.1 Analysis of the Mean Response 129
5.3.1.2 Analysis of the SD Responses 132
5.3.1.3 Building the First-Order Model of the SD Response 133
5.3.1.4 Residual Analysis 134
5.3.2 Second-Order Model Building and Optimization of Workpiece Level Variation 134
5.3.2.1 Response Surface and Optimization 137
5.3.2.2 Residual Analysis 138
5.3.3 Model Verification 138
5.4 Combined Models for PTH and BV 140
5.4.1 PTH Crossed with the BV Model at the BV CCD Space 140
5.4.2 BV Crossed with the PTH Model at the PTH CCD Space 147
5.5 Summary 148

6. DISCUSSION AND CONCLUSION 153
6.1 Introduction 153
6.2 Summary of the Models 153
6.3 Discussion on the Pattern Plating Experiments 155
6.4 Discussion on the PTH and BV Plating Experiments 159
6.5 Limitations of the Study 161
6.6 Contributions of the Study 162
6.7 Suggestions for Future Work 163
6.8 Conclusions 164

REFERENCES 165

Appendix 3.1 List of Apparatus and Equipment A-1

Appendix 4.1 Alias Structure of the 2_{IV}^{6-2} Fractional Factorial Design used in the Screening Experiments of Uniform Pattern Plating A-12

Appendix 4.2 Raw Data of the Screening Runs of the Hull Cell Experiment, Uniform Pattern Plating Experiment A-13

Appendix 4.3 Raw Data of the Screening Runs of the Plating Bath Experiment, Uniform Pattern Plating A-14

Appendix 4.4 Normal Probability Plot of the Residuals of the Plating Bath Experiment, Uniform Pattern Plating A-17

Appendix 4.5 Raw Data of the Verification Run, Second-Order Model, Uniform Pattern Plating Experiment A-18

Appendix 4.6 Measurement Scheme and Typical Thickness Profile of the Nonuniform Pattern Plating Experiment A-20

Appendix 4.7 Raw Data of the Nonuniform Pattern Plating Experiment, First-Order Model A-21

Appendix 4.8 Raw Data of the Verification Experiment Using the "Zebra" Pattern, Nonuniform Pattern Plating A-24

Appendix 4.9 Response Graphs of the Upper, Lower, Left-centre, Centre-right Regions of the Board, Nonuniform Pattern Verification Experiment Using the "Zebra" Pattern A-27

Appendix 4.10 Raw Data of the Nonuniform Pattern Verification Experiment Using a Simple Circuit Pattern A-31

Appendix 5.1 Alias Structure of the 2_{VI}^{6-1} Fractional Factorial Design used in the Screening Experiments of PTH Plating A-33

Appendix 5.2 Raw Data of the Screening Runs of the PTH Experiments A-34

Appendix 5.3	Normal Probability Plot of the Residuals of the PTH Plating Experiment, First-Order Model	A-38
Appendix 5.4	Raw Data of the PTH CCD Experiments for the Second-Order Model Building	A-39
Appendix 5.5	Normal Probability Plot of the Residuals of the PTH Plating Experiment, Second-Order Model	A-41
Appendix 5.6	Raw Data of the PTH Verification Experiments	A-42
Appendix 5.7	Alias Structure of the 2_{IV}^{7-2} Fractional Factorial Design used in the Screening Experiments of BV Plating	A-45
Appendix 5.8	Raw Data of the Screening Runs of the BV Experiments	A-46
Appendix 5.9	Normal Probability Plot of the Residuals of the BV Plating Experiment, First-Order Model	A-50
Appendix 5.10	Raw Data of the BV Experiments for Locating the Approximate Optimum Region	A-51
Appendix 5.11	Raw Data of the BV CCD Experiments for the Second-Order Model Building	A-52
Appendix 5.12	Normal Probability Plot of the Residuals of the BV Plating Experiment, Second-Order Model	A-53
Appendix 5.13	Raw Data of the BV Verification Experiments	A-54
Appendix 5.14	Raw Data of the PTH Experiments conducted in the BV CCD Space	A-56
Appendix 5.15	Raw Data of the BV Experiments conducted in the PTH CCD Space	A-58
Appendix 6.1	Approximation Solutions of Wa_T and Wa_L	A-60

LIST OF TABLES AND FIGURES

Fig. 2.1	Schematic of the Acid Copper Plating Process	7
Fig. 2.2	The concept of *Active-Area Density* Proposed by [Mehdizadeh *et al.*,1992]	29
Fig. 3.1	The 200 Litre Plating Bath	47
Fig. 3.2	The Purpose-built Rectangular Testing Cell	47
Fig. 3.3	Seiko SFT 7155 XRF X-ray Coating Thickness Gauge	48
Fig. 3.4	Measurement of Deposit Thickness with Talysurf Profilometer	48
Fig. 3.5	Flow Chart of the Acid Copper Pattern Plating Process	50
Fig. 4.1	Test Pattern of the Screening Experiment (Not to Scale)	63
Fig. 4.2	Normal Probability Plots of the Screening Experiment	65
Fig. 4.3	Normal Probability Plots of the Residuals of the Screening Experiment	66
Fig. 4.4	Lithographic Pattern of the Plating Bath Experiment and the Measuring Points for the Determination of Standard Deviation (Not to Scale)	70
Fig. 4.5	Normal Probability Plots of the Plating Bath Experiment	72
Fig. 4.6	Analysis of Mean Plot for the Plating Bath Experiment (Mean Responses)	73
Fig. 4.7	Interaction Plots for the Parameter B, C and D	74
Fig. 4.8	Analysis of Mean Plot for the Plating Bath Experiment (SD Responses)	75
Fig. 4.9(a)	Interaction Plot of CD for the SD Responses	76
Fig. 4.9(b)	Mean Deposit Thickness compared with Faraday's Prediction for the Combination of C(+), D(+)	76
Fig. 4.10	Responses graph of the Projected 2^2 design and the Direction for further Experiment	77
Fig. 4.11	The Rotatable Central Composite Design and Response Values	81

Fig. 4.12	Response Surface and Contour Plot of the Second Order Model for Uniform Pattern Plating	81
Fig. 4.13	Contour Plot of the Second-Order Model for Uniform Pattern Plating	82
Fig. 4.14	Verification of the Second-Order Model for Uniform Pattern Plating	82
Fig. 4.15	Actual Average Plating Thickness compared with Faraday's Prediction of the Verification Run	84
Fig. 4.16	Difference between Actual Average Plating Thickness and Faraday's Prediction as a function of Average Current Density	84
Fig. 4.17(a)	Empirical Relationship between the Normalized Difference and the Average Current Density	86
Fig. 4.17(b)	Empirical Relationship between the Ratio of Actual Thickness to Faraday's Prediction and the Average Current Density	86
Fig. 4.18	The "Zebra" Pattern used in the Non-uniform Pattern Plating Experiment (Not in Scale)	87
Fig. 4.19	Current Efficiency of the Non-uniform Pattern Plating Experiment	89
Fig. 4.20	AB Interaction for the Non-uniform Pattern Plating Experiment	90
Fig. 4.21	Response Surface of the First-Order Model for the Non-Uniform Pattern Plating	91
Fig. 4.22	"Zebra" Patterns Used in the Verification Run	93
Fig. 4.23	Comparison of the Actual and Predicted Standard Deviation of the First-Order Model	93
Fig. 4.24	Variation of the Mean and Standard Deviation of the Deposit Thickness with AADR in the Verification Runs	95
Fig. 4.25	Variation of the Four Components of s^2 with AADR in the Verification Runs	97
Fig. 4.26	Correlation of the Four Components of s^2 with AADR in the Verification Runs	97
Fig. 4.27	Comparison of s^2 (SDO) and σ^2 calculated by Eq. 4.11	99

Fig. 4.28	Variation of the Mean and Standard Deviation of the Deposit Thickness with AADR in the Verification Runs (Board Partitioned into Upper and Lower Region)	100
Fig. 4.29	The Different in Pattern Level Variation of the Upper and Lower Region	102
Fig. 4.30	The Simple Circuit Patterns used in the Second Verification Runs	103
Fig. 4.31	Mean and SD Responses Graphs of the Second Verification Runs	104
Fig. 4.32	Variation of the Variance and Mean Components of s^2 with AADR	105
Fig. 4.33	Comparison of the Actual and Predicted Standard Deviation of the Original and Modified First Order Model	106
Fig. 5.1	Test Boards of the PTH Screening Experiment (Not to Scale)	112
Fig. 5.2	Plating Efficiency of the PTH Screening Experiment	113
Fig. 5.3	Normal Plot of the PTH Screening Experiment (Mean Responses)	114
Fig. 5.4	Analysis of Mean Plot of the Significant Location Parameters	116
Fig. 5.5	Interaction Plot of AB for the Mean Responses	116
Fig. 5.6	Normal Plot of the PTH Screening Experiment (SD Responses)	117
Fig. 5.7	Analysis of the Means Plot for the SD Responses	117
Fig. 5.8	Interaction Plots for the Parameters C, D and F	118
Fig. 5.9	Cube-plot of the Projected 2^3 full factorial of the PTH Screening Experiment (SD Responses)	120
Fig. 5.10a	Response Surface and Contour Plot of the PTH 8-term Second-order Model for the case of F = -1	123
Fig. 5.10b	Response Surface and Contour Plot of the PTH 8-term Second Order Model for the case of F = 1	123
Fig. 5.11	The Locus of the Optimum Combinations of parameter C and D for the whole range of F	125
Fig. 5.12	Predicted Minimum Standard Deviation of Plating Thickness at different levels of Corrected Aspect Ratio (F)	125
Fig. 5.13	The Dependence of the Minimum Variability on the Corrected Aspect Ratio	126

Fig. 5.14	Verification Results of the PTH 8-term Second-Order Model	128
Fig. 5.15	Normal Plot of the BV Screening Experiment (Mean Responses)	130
Fig. 5.16	Analysis of Mean Plot of the Significant Location Parameters	131
Fig. 5.17	Interaction Plots for the Parameters A, B, C, and D for the Mean Responses	132
Fig. 5.18	Normal Probability Plot of the BV Screening Experiment (SD Responses)	132
Fig. 5.19	Analysis of Mean Plot for the SD Responses	133
Fig. 5.20	Response Surface and Contour Plot of the BV 3-term First-Order Model	134
Fig. 5.21	Response Surface and Contour Plot of the BV Full Second-Order Model (SD Responses)	137
Fig. 5.22	Locus of the SD_{min} within the optimum Region	138
Fig. 5.23(a)	Relationship between SD_{min} and the Average Current Density	139
Fig. 5.23(b)	Locus of the Optimum Combination of parameter C and D	139
Fig. 5.24	Verification Results of the BV Full Second-Order Model	141
Fig. 5.25(a)	Intersection of the PTH and BV Response Surfaces in the BV CCD Space for F = -1	144
Fig. 5.25(b)	Intersection of the PTH and BV Response Surfaces in the BV CCD Space for F = 0	145
Fig. 5.25(c)	Intersection of the PTH and BV Response Surfaces in the BV CCD Space for F = +1	146
Fig. 5.26(a)	Intersection of the PTH and BV Response Surfaces in the PTH CCD Space for F = -1	150
Fig. 5.26(b)	Intersection of the PTH and BV Response Surfaces in the PTH CCD Space for F = 0	151
Fig. 5.26(c)	Intersection of the PTH and BV Response Surfaces in the PTH CCD Space for F = +1	152

Table 4.1	Factor Levels of the Screening Experiment	63
Table 4.2	Design Matrix and Responses of the Screening Experiment	64
Table 4.3(a)	ANOVA Table of the Screening Experiment (Mean Responses)	67
Table 4.3(b)	ANOVA Table of the Screening Experiment (SD Responses)	67
Table 4.4	Factors Levels of the Second Experiment	68
Table 4.5	Design Matrix and responses of the Plating Bath Experiment	69
Table 4.6(a)	ANOVA Table of the Plating Bath Experiment (Mean Responses)	71
Table 4.6(b)	ANOVA Table of the Plating Bath Experiment (SD Responses)	71
Table 4.7	Projected 2^2 Design with 8 replicates and the Responses	75
Table 4.8	The Central Composite Design and Responses	78
Table 4.9	Four extra axial points of the CCD and the Responses	79
Table 4.10	ANOVA Table of the 2nd Degree Model	80
Table 4.11	Actual and Predicted Responses of the Verification Run	82
Table 4.12	The Replicated 2^3 Design and the SD Responses	88
Table 4.13	ANOVA of the First Order Model for the Non-Uniform Pattern Plating Experiment	89
Table 4.14	Explanation of the Legends used in Fig. 4.23	94
Table 4.15	Explanation of the Legends used in Fig. 4.28	101
Table 4.16	Active Area Densities of the Circuit Patterns	103
Table 4.17	The Differences in A_c and n_c of the Two Verification Runs	107
Table 4.18	Recalculated Parameter Levels of AADR and AADP for the Two Verification Runs	109
Table 5.1	Factors Settings of the 2_{VI}^{6-1} PTH Screening Experiment	111
Table 5.2	Parameter Settings and the Responses of the PTH Screening Experiment	113
Table 5.3	ANOVA Table of the PTH Screening Experiment (Mean Responses)	114
Table 5.4	ANOVA Table of the PTH Screening Experiment (SD Responses)	119
Table 5.5	Factor levels and setting of the PTH CCD Experiment	121
Table 5.6	Factor levels and Responses of the PTH CCD Experiment	121

Table 5.7	ANOVA of the PTH 8-term Second Order Model (SD Responses)	122
Table 5.8	Factors Settings and Responses of the PTH Verification Experiment	127
Table 5.9	Parameter settings and the Responses of the BV Screening Experiment	129
Table 5.10	ANOVA Table of the BV Screening Experiment (Mean Responses)	130
Table 5.11	ANOVA Table of the BV Screening Experiment (SD Responses)	133
Table 5.12	Design Points and Responses in the Proximity of [C(-),D(-)]	135
Table 5.13	Factor levels and setting of the BV CCD Experiment	135
Table 5.14	Factor levels and Responses of the BV CCD Experiment	136
Table 5.15	ANOVA of the BV Second-Order Full Model (SD Responses)	136
Table 5.16	Factors Settings and Responses of the BV Verification Experiment	141
Table 5.17	Factor levels and setting of the Second PTH CCD Experiment in the BV CCD Space	142
Table 5.18	Responses of the Second PTH CCD Experiment in the BV CCD Space	142
Table 5.19	ANOVA of the PTH First-order Model in the BV CCD Experiment	143
Table 5.20	Factor levels and setting of the BV CCD Experiment	147
Table 5.21	Responses of the Second BV CCD Experiment in the PTH CCD Space	147
Table 5.22	ANOVA of the PTH First-Order Model in the BV CCD Space	148
Table 6.1	Summary of Coefficients of the Parameters in the Pattern, PTH and BV Models	154

LIST OF ABBREVIATIONS

a	area exposed to electrodeposition, cm^2
A	half-breadth of the cathode, cm
A	convection variable, dimensionless
A	atomic weight, g
A_c	area of the continuum with constant AAD, cm^2
A_{act}	active area of a region on an electrode surface, cm^2
A_{sup}	superficial area of a region on an electrode surface, cm^2
AAD	active area density, dimensionless
$\overline{AAD}$	average active area density over cathode surface, dimensionless
AADP	modified parameter catering for the combined effect of AADR, $\overline{AAD}$, and the scale effect, cm
AADR	ratio of the active area density of two neighbouring regions, dimensionless
BEM	boundary element method
BIEM	boundary integral equation method
c_0	surface concentration of the reacting ion, mol/cm^3
c_b	bulk concentration of the reacting ion, mol/cm^3
D	separation between the anode and cathode, cm
D_i	diffusion coefficient of the reacting cupric ion, cm^2/s
F	Faraday's constant, 96487 C/g-equivalent
FEM	finite element method
g	gap width between the cathode and auxiliary electrode, cm
i	current density of a point at a distance x from the edge of the electrode, mA/cm^2
I	total current passed (A)
I	ratio of the average current density of the auxiliary electrode and cathode
I_{opt}	optimum value of I giving minimum cathodic thickness variation
$\bar{i}$	average current density, A/cm^2

$i(z)$	current density of a point on the Hull cell panel, mA/cm^2
i_{ACT}	active current density, mA/cm^2
$i_{c,SUP}$	superficial current density at cathode, mA/cm^2
$i_{c,ACT}$	active current density at cathode, mA/cm^2
i_{avg}	average current density over the electrode, mA/cm^2
i_c	cathodic current density, mA/cm^2
$i_{c,\Omega}$	ohmic critical current density, mA/cm^2
i_e	current density at the entrance of a through-hole, mA/cm^2
i_{lim}	limiting current density, mA/cm^2
i_{max}	maximum current density along the cathode, mA/cm^2
i_{min}	minimum current density along the cathode, mA/cm^2
$\bar{i}$	average current density along a through-hole, mA/cm^2
$\bar{i}_{AUX}$	average current density on the auxiliary electrode, mA/cm^2
$\bar{i}_c$	average current density on the cathode, mA/cm^2
$\bar{i}_{c,SIUP}$	average superficial current density at cathode, mA/cm^2
$\bar{i}_{lim}$	average limiting current density, A/cm^2
$\bar{i}_{L,avg}$	average mass transfer limiting current density, mA/cm^2
i_0	exchange current density, mA/cm^2
j^*	dimensionless parameter for the gap cell
k_c	Wagner polarization parameter, dimensionless
$K(m)$	complete elliptic integral of the first kind
l	half length of the rectangular electrolytic cell, cm
L	characteristic length, cm
L	length of the electrode, cm
LAAD	the region with larger active area density in two neighbouring areas of different AAD
m	half length of the cathode, cm
n	half length of the anode, cm
n	number of electrons transferred

n_c	number of continuums over the substrate
N	average limiting current density for tubular electrode system, dimensionless
PCB	printed circuit board
r_{AUX}	radius of the cylindrical auxiliary electrode, cm
r_c	radius of the cylindrical cathode, cm
r_w	radius of the cylindrical cell, cm
R	universal gas constant, $J/mol^{-1}K^{-1}$
R_0	through-hole radius, cm
s	standard deviation of the deposit thickness over the whole board, μm
s_L	standard deviation of the deposit thickness of the pattern of the LAAD region, μm
s_N	standard deviation of the deposit thickness of the region with smaller line width, μm
s_S	standard deviation of the deposit thickness of the pattern of the SAAD region, μm
s_T	standard deviation of the deposit thickness of the pattern of the lower region, μm
SAAD	the region with smaller active area density in two neighbouring areas of different AAD
t	plating duration, second
T	temperature, Kelvin
Wa	Wagner number, dimensionless
Wa_L	Wagner number for linear kinetics, dimensionless
Wa_T	Wagner number for Tafel kinetics, dimensionless
x	distance measured from the center of the electrode, cm
$\bar{X}$	average deposit thickness over the whole board, μm
$\bar{X}_L$	average deposit thickness of the pattern of the LAAD region, μm

$\bar{X}_N$	average deposit thickness of the pattern of the region with smaller line width, μm
$\bar{X}_S$	average deposit thickness of the pattern of the SAAD region, μm
$\bar{X}_T$	average deposit thickness of the pattern of the region with thicker line width, μm
z	normalized distance measured from the low current density edge of a Hull cell panel, cm

Greek Symbols

α_a	anodic transfer coefficient, dimensionless
α_c	cathodic transfer coefficient, dimensionless
β_a	anodic Tafel slope, V
β_c	cathodic Tafel slope, V
ε	$\pi L / 2h$, dimensionless, in equation [2.15]
ε	mass transfer enhancement factor, dimensionless
ϕ	electrode potential, V
ϕ_E	equilibrium potential of an electrode, V
$(\gamma a)^2$	Thiele modulus parameter
η	total overpotential of an electrode, V
η_c	concentration overpotential of an electrode, V
η_s	surface overpotential of an electrode, V
κ	electrolyte conductivity, $\Omega^{-1}cm^{-1}$
ρ	density of copper g/cm^3
σ	normalized root-mean-square deviation of the cathodic current densities, cm
$\bar{\sigma}$	mean standard deviation of the deposit thickness from replicated experiments, μm
$\hat{\sigma}$	thickness standard deviation predicted by the statistical models, μm
σ_{opt}	minimum value of σ, cm

ξ	linear polarization parameter for tubular electrode system, dimensionless
$\xi_{T\kappa}$	linear polarization parameter for through-hole system, dimensionless

ABSTRACT

This thesis is concerned with the modelling and control of the acid copper electroplating process for the manufacturing of printed circuit boards (PCB). The objectives of this study were to investigate the effects of process and product parameters on the workpiece level uniformity during the acid copper plating of lithographic patterns, plated-through holes (PTH) and blind-via (BV), and to explore the minimization of the deposit thickness variation. The parameters studied were the average current density (ACD), plating duration, concentration of additive and sulphuric acid, electrode separation (ES), line width and active area density ratio (AADR) of the circuit pattern. The effects of the copper sulphate concentration, aspect ratio (CAR) and depth ratio were also studied for the PTH and BV plating. The results of the study enhance the understanding of the limitations of applying current distribution and statistical models to the copper electroplating of PCB at a workpiece level.

Multifactor two-level factorial and the central composite rotatable five-level experiments were designed, and a total of fourteen sets of experiment were conducted sequentially and used to generate statistical process models. For the plating of uniform patterns, ACD, ES and their quadratic effects were found to be significant and a 6-term second order model was built and verified to predict and minimize the workpiece level variability. The existence of a minimum plating variability was attributed to the minimum deviation from the Faraday's nominal thickness observed under a particular combination of ACD and ES. For non-uniform patterns, ACD, AADR and the ACD $\times$ ES interaction were found significant and an 8-term first-order prediction model was constructed. The minimum variability achievable was found to increase with the AADR, and was explained by the scattering effect of AADR on the average plating thickness. Verification of the model with patterns of same AADR but different line width revealed the limitation of the continuum concept, i.e. AADR alone is not sufficient to characterize a non-uniformly patterned substrate. Subsequent verification runs using a simple circuit pattern showed further that a composite parameter involving

the overall active area density, the continuum area and the number of AAD contrasts, was appropriate.

For the PTH plating, ACD, CAR, ACD^2 and the $ACD \times ES$, $ES \times CAR$ interactions were found significant but only ES, ES^2 and $ACD \times ES$ were active for BV plating. Second-order models were also developed for the two processes in their respective optimum regions and verified experimentally. The optimum values of ACD and ES, and the minimum variability achievable were found to increase with the corrected aspect ratio of the through-hole. Given the difference in the optimum regions of the PTH and BV plating, a new response surface of the PTH process was constructed at the optimum region of the BV process and vice versa. The process limiting the workpiece level uniformity under different combinations of ACD and ES was found by the intersections of these responses surfaces. Finally, process parameters limiting the simultaneous minimization of the plating variability of pattern, PTH and BV were discussed. It showed that under most situations, the workpiece level variability of BVs was higher than that of the PTHs.

CHAPTER 1
INTRODUCTION

1.1 Background

Most printed circuit boards (PCBs) nowadays are electroplated with copper because of its abundance and high electrical conductivity. With the current trends toward miniaturization, PCB manufacturers are continuously facing the challenge of producing quality boards with narrower conductors, smaller spaces, more layers per board and smaller diameter holes with larger hole length to diameter ratio*. The success of electroplating in PCB fabrication depends largely upon efforts to achieve uniform films of deposit in spite of difficulties presented by lithographic patterns, irregular surface topographies and high aspect ratio holes.

As electroplating is a Faradaic charge-transfer reaction, the rate of deposition depends on the current density (Faraday's law) and, in general, a uniform plating is achieved when the current density is evenly distributed over the electrode surface. Therefore, the challenge of deposit uniformity is usually posed as a problem of current density distribution by researchers in the field of electrodeposition. Although the mathematical expressions quantitatively describing the current distribution in electrochemical cells can be rigorously formulated, explicit solutions cannot be obtained, except for a few simple cases [Landau, 88], [Newman, 91b]. Simplifying assumptions are usually made by considering the extreme situations where the current distribution is dominated by a single mechanism. For example, a process controlled solely by electrolyte resistance yields the highly non-uniform *primary* distribution while at the other extreme is the mass transfer controlled *tertiary* distribution which is flow dependent. However, the prevailing current distribution in a practical cell is believed to assume some intermediate value bounded by those extremes [Landau, 88]. Moreover, when there is a competing reaction, such as hydrogen evolution, the current

* The ratio of the length to the radius of the through-hole and blind via is commonly known as the aspect ratio.

efficiency of plating, i.e. the fraction of the current density actually participating in the electrodeposition reaction, is no longer 100% but varies with current density [Dukovia, 90]. A discrepancy thus exists between the actual plating thickness distribution and the current density distribution under such circumstances, and its magnitude is hardly predictable.

In spite of the above limitations, mathematical treatments of the problem did show that the plating uniformity is jointly affected by a set of process and product parameters including the bath chemistry and geometry, electrolyte conductivity, electrode potential and current density, dimensions and densities of the features. For this type of multivariable process, statistical techniques can be used to advantage to study the effects of the various parameters on the actual plating thickness distribution and help the judicious manipulation of their levels to achieve desirable plating uniformity. Relatively little work in this area has been reported in the literature. These considerations therefore prompted the author to initiate the research reported in this thesis on the statistical modelling of the electroplating process for the control and minimization of plating thickness variations at a workpiece level.

1.2 The Areas of Investigation

This research was focused on the acid copper electroplating of PCB with lithographic patterns, plated-through holes (PTHs) and blind vias (BVs). These three features are commonly found in the PCB assemblies of most electronic products. The response variable of interest was the variation of the plating thickness of these features across the board surface. The process and product parameters studied included the average cathodic current density, plating duration, concentration of additive and sulphuric acid, electrode separation, line width, active area density ratio of the circuit pattern. The effects of the copper sulphate concentration, aspect ratio and depth ratio were also studied for the PTH and BV plating.

1.3 Research Approach

The above parameters were studied in fourteen sets of statistically designed experiments with the objectives of understanding how the workpiece level plating uniformity of the three features is affected by these parameters, and to investigate the possibility of minimizing the thickness variability using the statistical models developed.

For the study of multivariable processes, the traditional strategy of experimentation is to investigate the effects of several parameters one at a time. In this approach, the effect of a single parameter on the response is studied by varying the value (level) of this variable while holding the values of the other independent variables fixed [Box *et al.* 78]. This one-factor-at-a-time approach is shown to be inefficient and fails to consider any possible interaction between the parameters [Box *et al.* 78], [Dini 89], such interactions are not uncommon in chemical and electrochemical processes like electroplating. Moreover, this approach leads to erroneous conclusions regarding the stationary point (local maximum or minimum, if it exists) of the response in the presence of interactions because it assumes that the maximizing (or minimizing) value of one parameter is independent of the level of the others [Box *et al.*, 78], [Taylor, 89]. Statistically designed experiments, on the other hand, allow simultaneous studying of the effects of several parameters and their potential interactions in a reasonably small number of runs.

In the early eighties, Taguchi proposed his parameter-design approach of experimentation [Taguchi and Wu, 80], [Taguchi, 80, 86, 87], and was well received in the mid-eighties and early nineties with numerous successful implementations reported in the literature [Lin and Kackar, 85], [Pao *et al.*, 85], [Phadke, 86], [Goh and Roy, 89], [Haluzan and Reichenbach, 91], [Leisner *et al.*, 92].

However, such an approach was not adopted in this study mainly because of its controversial statistical analysis techniques [Hare, 90], [Nair, 92], [Myers and Montgomery, 95] and its lack of provision for adequately dealing with potential interactions between parameters [Ryan, 88], [Montgomery, 97]. In this research,

fractional factorial designs were used to screen out the significant parameters and obtain first-order models for the graphical analysis of their effects on the plating variability. These models indicate the influence of these parameters, and their interactions (if any), on the plating rate and variability within the process window, as well as the direction of optimizing these two performance measures. Response surface designs were then used to obtain second-order models and construct response surfaces for the optimization of the plating process to minimize the variability. One-factor and two-factor experiments were performed as complements to the factorial designs to verify the adequacy of the models built and help the interpretation of parameters' effects and the behaviour of the optimum solutions.

1.4 Structure of the Thesis

This introductory chapter is followed by five further chapters. Chapter two presents a review of the literature relevant to the thesis, which includes a brief description of the acid copper electroplating process; classification of the current distribution problem; previous modelling work performed at the workpiece, pattern and feature level; and the need for and appropriateness of statistical modelling of the electroplating process.

Chapter three shows the apparatus and materials used in the experiments and describes briefly the procedures of the acid copper plating, electroless copper plating, and methods of measuring the deposit thickness in this study.

Chapter four reports the design and analysis of statistical experiments performed on the acid copper plating of uniform and non-uniform patterns. It describes the factor screening and the building of the first and second order models for the workpiece level thickness variability of the process, followed by explanation and verification of these models. The verification runs confirmed the adequacy and predictive power of these models, and unveiled the effects of average current density, electrode separation and active area density contrast on the workpiece level plating uniformity. They also showed the limitation of the active area density contrast in characterizing a non-uniformly patterned substrate and a new composite parameter is suggested.

Chapter five gives an account of the experimental studies of the plating of through-holes and blind vias, which investigate, amongst others, the effects of the average current density and electrode separation on the workpiece level variability of the two features. The resulting models show that the optimum process conditions for the two features lie in different regions of the experimental space and therefore two separate response surfaces are developed. The chapter then explores the possibility of obtaining a compromise solution by intersecting the response surfaces of the two features when either one of them is optimized.

Finally, Chapter six contains an overall discussion summarizing all the significant parameters identified and their effects on the workpiece level plating uniformity of lithographic patterns, plated-through holes and blind vias. Experimental findings and the models developed are interpreted in the light of the results obtained in previous research work. The chapter ends with an assessment of the contributions and limitations of this study and some indications for future work.

CHAPTER 2

MODELLING OF ELECTROPLATING

2.1 Introduction

In this chapter, the research literature on the modelling of current-density distribution in the field of electrodeposition is reviewed. Research works are categorized according to their length scales and key contributions in each category are identified. Particular emphasis is placed on how the deposit uniformity is affected, and optimized, by the various process and product parameters of the system, rather than the electrochemistry and mathematics involved. A brief description of the process and related mathematical treatment of the problem, however, is given beforehand as a contextual preface to the subsequent review.

2.2 The Acid Copper Electroplating Process

Copper is perhaps the most commonly plated metal because of its low cost, abundant supply and, more importantly, its high electrical conductivity (highest other than silver). Plated copper is extensively used in circuitry on glass-epoxy for PCBs and the through-hole interlayer connections. Copper electroplating solutions containing nitrate, cyanide, chloride, acetate and fluorosilicate salts were used in the past, but the only solutions widely used today are alkaline copper pyrophosphate and acidic copper sulphate/sulphuric acid or copper fluoroborate/fluoroboric acid [Couch and Bikales, 61], [Dini, 64]. For the circuit processing industry, a relatively thick, ductile and rapidly formed deposit is preferable, and the trend towards the extensive use of acid copper sulphate bath is prominent in the last few decades. Fig. 1 shows a schematic diagram of the process. Typical bath compositions and process control techniques are well documented in the literature [Coombs, 88], [Parthasaradhy, 89].

The reactions taking place at the two electrodes are :

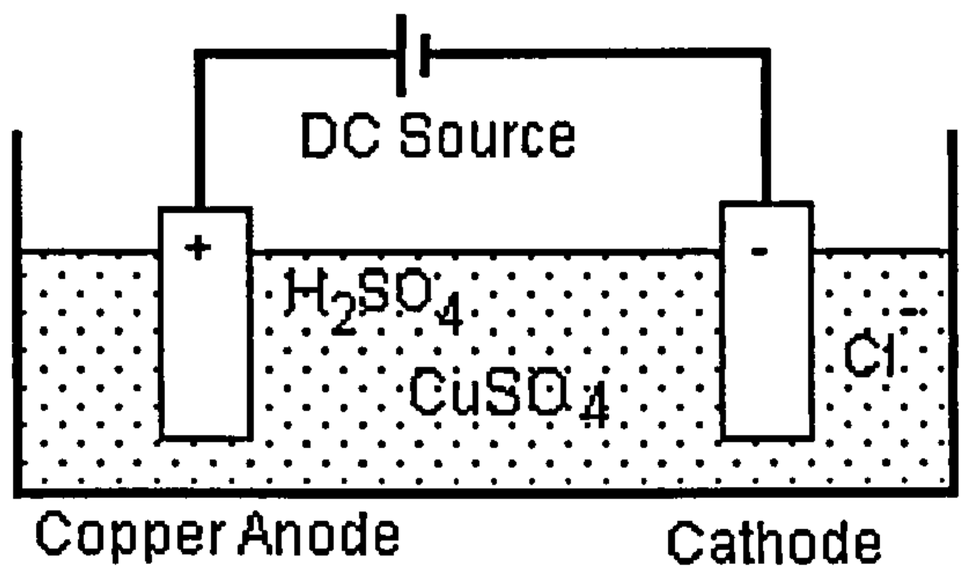

Figure 2.1 : Schematic of the Acid Copper Plating Process

$$Cu \rightarrow Cu^{2+} + 2e \qquad \text{(at the anode)}$$

$$Cu^{2+} + 2e \rightarrow Cu \qquad \text{(at the cathode)}$$

Strictly speaking, the reduction process taking place at the cathodic surface proceeds via two separate one electron transfer steps, i.e. the cupric ion (Cu^{2+}) is first reduced to the cuprous ion (Cu^{+}) before it is further reduced to its non-ionized state (Cu) [Mattson and Bockris, 59]. Typical components of an acid copper plating bath include copper sulphate ($CuSO_4$), sulphuric acid (H_2SO_4), chloride ion (Cl^-) and *brightener* (an organic additive).

Copper sulphate is the source of cupric ions. Too high a copper concentration leads to reduced cathodic polarization and may increase solution resistance if bisulphate species (HSO_4^-) are formed. On the contrary, hydrogen evolution and reduced cathodic current efficiency may result if the concentration is too low as the current density is increased. Anode passivation or excessive polarization at high current densities occurs at high total sulphate concentrations as a result of the formation of a precipitate film at the anodic surface when the solubility of copper sulphate is exceeded. Depletion of cupric ions may cause deposit "burning" at regions of high current density such as the edge of the PCB.

The primary function of sulphuric acid is to provide a high solution conductivity, typically about 0.5 ohm/cm. Specific conductivity increases almost linearly with acid

concentration from 25 to 150 g/litre [Skowronsk and Reinoso, 27], beyond which the changes become smaller due to bisulphate species formation. Increased acid concentrations generally reduce deposit grain size and promote plating uniformity, especially at a feature level [Lanzi and Landau, 88].

Acid copper baths usually contain chloride ions at 60 to 80 ppm. Chloride precipitates excessive heavy metal accumulations and influences deposition kinetics through adsorption at the adsorb surface [Gauvin and Winkler, 55]. Below 30 ppm, deposits will be coarse-grained and dull and the anodes will get polarized, causing plating to stop. The organic additives used in acid copper baths contain chemicals commonly known as brightener, levelers, and wetting agents or "carriers". The additives adsorb competitively at the cathodic surface and strongly influence deposit metallurgy and feature-level thickness distribution. The overall effect of additives on metallurgy is to disrupt the large columnar grain produced in the absence of additives and to form a fine equiaxial grain structure. Without additives, the deposition rates currently achieved in through-holes would be impossible [Yung and Romankiw, 89], and therefore they are the essential constituent in plating bath for high aspect ratio through-hole plating. The effective concentration range of these additives is often as large as a factor of ten [Pletcher, 82].

A wide variety of molecules are mentioned in patents and the literature as brightener [Sarma and Nageswar, 84], which usually contain pendant sulphur atoms (thiols, disulphides) and a functionality to increase water solubility. These molecules adsorb very strongly at the cathode owing to the pendant sulphur atom's high affinity for copper. Solution concentrations of only about 10 ppm are required to achieve the desired degree of surface coverage. Brighteners frequently participate directly in the copper redox and electro-crystallization processes and thus strongly influence deposit grain structure and metallurgy. Levelers are generally nitrogen-containing surfactant molecules including amines and amides which adsorb strongly at edges and surface irregularities and decrease the size of surface topography features that are present prior to plating [Mirkova *et al.*, 82]. Carriers are usually polyether glycol and polyoxyether molecules with molecular weights ranging from 2000 to 6000. They form an adsorbed

layer at the cathode which uniformly polarizes the interface and improves the throwing power of the solution [Mayer and Barbieri, 81].

2.3 Modelling of Current Distribution

In order to calculate the current-density distribution along a surface, the distribution of the electric potential has to be determined first. The *potential theory*, developed originally for solving thermodynamics and fluid flow problems, is found applicable and widely adopted in solving current and potential distribution problems, as reflected later in Sec. 2.4. While a comprehensive treatment of the potential-theory model is outside the scope of this thesis, a brief description of the model is advantageous before the recent literature is reviewed. Detailed explanation of the model can be found elsewhere, e.g. [Newman, 91a], [Deconinck, 92]. For the potential model to be applicable to an electrochemical system, the following assumptions have to be satisfied :

i/ uniform conductivity, κ, of electrolyte,

ii/ uniform temperature, T, of electrolyte,

iii/ negligible concentration gradient in the bulk electrolyte,

iv/ dilute electrolytic solution with small concentration of electroactive species.

The first three conditions are often satisfied when the electrolyte is well agitated, while the last one, which means also that the reacting ions represent only a small fraction of the ionic conductivity of the electrolyte, promotes uniform conductivity. Under such assumptions, the current distribution is determined by the ohmic potential drop in the electrolyte and by electrode overpotentials. The system of mass and charge transport equations can be simplified and solved to give an expression of the potential, ϕ, within the electrolyte :

$$\nabla^2 \phi = 0 \qquad [2.1]$$

which is also the well known Laplace's equation. The current density, i, is then given by the Ohm's law as the normal derivative of the potential, i.e.

$$i = -\kappa \frac{\partial \phi}{\partial n} \qquad [2.2]$$

where n is a unit vector normal to the surface. At all insulating boundaries where no current flows, Eq. [2.2] gives the boundary condition of

$$\frac{\partial \phi}{\partial n} = 0 \qquad [2.3]$$

The boundary conditions at the electrode surfaces contain expressions for electrode kinetics and concentration polarization and take the form

$$\phi = \phi_E - \eta \qquad [2.4]$$

where ϕ_E is the potential of the electrode itself and η is the total overpotential, which can be further decomposed into a kinetic or *surface overpotential*, η_s, and a *concentration overpotential* η_c, which arise, respectively, from the kinetic limitation of the electrode and the concentration gradient in the thin layer immediately adjacent to the electrode surface. The total overpotential is the driving force for the net current, i.e. electrodeposition, it takes positive value at the anode and negative value at the cathode. Current distribution is usually classified into three main groups according to the assumptions imposed on the total overpotential.

2.3.1 The Primary Current Distribution

When only the electric field effects are considered and the total overpotential is assumed to be zero, i.e. $\eta = 0$ in Eq. [2.4] above, the resulting distribution is called a *primary distribution.* The solution adjacent to the electrode is an equipotential surface and the boundary conditions are constant. However, the Laplace equation is not trivial to solve, even for relatively simple geometries [Newman, 91a]. The primary distribution is determined by geometric factors alone and, in particular, not affected by the conductivity and temperature of the electrolyte [Newman, 91a], [Deconinck, 92]. It is also the most non-uniform distribution among the three classes of distributions. Although the primary model is extremely restricted, the macroscopic current uniformity is largely determined by the primary distribution [Wagner, 51], [Kessler and Alkire, 76a, b], [Blue, 80]. Analytic solutions have been calculated by various authors for simple geometries and commonly used techniques include conformal mapping [Wagner, 51], [Hine *et al.*, 56], [Yoshida *et al.*, 67], [West *et al.*, 92], separation of variables [Newman, 66] and methods of images [Kasper, 40, 42]. Complex configurations can only be solved by numerical techniques such as the finite

element method (FEM) [Matlosz *et al.*, 87], [West and Newman, 91] or the boundary element method (BEM) [Bialecki *et al.*, 84], [Deconinck *et al.*, 85], [Blue 80].

2.3.2 The Secondary Current Distribution

When the electrode kinetics are considered in the absence of the concentration gradient, i.e $\eta = \eta_s$, the *secondary distribution* results. The potential along the electrode surfaces is no longer constant but depends on the local current density, i. The most commonly used expression of electrode kinetics is the *Butler-Volmer* equation,

$$i = i_0[e^{\alpha_a(F\eta_s/RT)} - e^{-\alpha_c(F\eta_s/RT)}] \qquad [2.5]$$

where i_0 is the exchange current density (mA/cm^2), α_a and α_c are the kinetic transfer coefficients of the anode and cathode, F is the Faraday's constant (C/g-equivalent), R is the universal gas constant (J/mol^{-1}K^{-1}), and T is the electrolyte temperature (Kelvin). The nonlinearity of the kinetics expression of Eq. [2.5] renders many current distribution problems intractable by analytical methods. To simplify the calculation, many analyses of secondary distribution have treated one of the two limiting cases of the Butler-Volmer kinetics. At high cathodic overpotential, (approximately, $\eta_s > 0.1$ V), the first exponential function can be neglected and the *Tafel* expression is obtained,

$$\eta_s = -\frac{RT}{\alpha_c F}\ln\frac{-i}{i_0} \qquad [2.6]$$

The term $RT/\alpha F$ is referred to as the *Tafel slope*. A similar Tafel expression could be obtained for the anode at high overpotential. At low overpotential, Eq. [2.5] can be linearized to give the *linear* approximation of the kinetic expression,

$$\eta_s = \frac{i}{i_0}\frac{(\alpha_a + \alpha_c)F}{RT} \qquad [2.7]$$

As a result of the additional resistance imposed by the electrode polarization at the electrode interface, the secondary distribution is always more uniform than the primary distribution. [Wagner, 51] defined a dimensionless group, which is now commonly known as the *Wagner number* [Ibl, 81], that characterizes the secondary distribution as

$$Wa = \frac{\kappa}{L}\frac{\partial \eta_s}{\partial i}\Big|_{i=\bar{i}} \qquad [2.8]$$

where $\bar{i}$ is the average current density (A/cm^2) and L is a characteristic length (cm) of the system. Wagner number is usually evaluated at either the Tafel limit, Wa_T, or the linear limit, Wa_L, which is given by

$$Wa_T = \frac{RT\kappa}{\alpha_c FL\bar{i}} \qquad [2.9]$$

$$Wa_L = \frac{RT\kappa}{(\alpha_a + \alpha_c)FLi_0} \qquad [2.10]$$

Semi-analytic solutions for the secondary distribution can be found for some configurations under the linear approximation [Wagner, 51], [Gnusin *et al.*, 65], [Shih and Pickering, 87], but normally numerical techniques are the only way to solve the problem because of the non-linear boundary conditions.

2.3.3 The Tertiary Current Distribution

When concentration gradient becomes significant, e.g. when the limiting current density is approached, the concentration overpotential is taken into account together with the surface overpotential, i.e. $\eta = \eta_s + \eta_c$, and the current distribution is said to be a tertiary distribution. If the electrolyte is well-agitated, the concentration variations are restricted to a thin and uniform layer adjacent to the electrode surface, known as the *diffusion layer* which is typically of the order of 0.01cm [Lyons, 74]. In the presence of an excess of supporting electrolyte, η_c can be approximated by

$$\eta_c = \frac{RT}{nF}\ln\frac{c_0}{c_b} \qquad [2.11]$$

where n is number of electrons transferred, c_0 and c_b are the surface and bulk concentration of the reacting ion. As the potential-theory model is no longer applicable in the diffusion layer, the problem has to be separated into two regions, a bulk region and a diffusion layer region. A solution for Laplace's equation in the bulk electrolyte where concentration variations can be ignored is first obtained while a separate solution to the convective diffusion equation is applied to the diffusion layer. The local current density profile computed from the potential gradient (bulk region) and the concentration gradient (diffusion layer) are then forced to be equal to each

other along the boundary of the two regions using iterative convergence methods. [Parrish and Newman, 69, 70], [Alkire and Mirarefi, 73], [Blue, 80], and [Dukovic, 93] illustrate the uses of different iterative schemes in solving the coupled Laplace's and convective diffusion equations.

Concentration overpotential counteracts equalization of current distribution over the peaks and troughs of the electrode surface on a microscale but promotes current uniformity on a macroscale. Generally, both effects exist at the same time and tend to cancel out each other. In spite of this, the tertiary distribution plays a significant role in the modelling of current distribution on a miniscale, which can be significantly affected by the mass transport and electrolyte hydrodynamics in the system. It has been solved by various authors to study the effect of electrolyte flow [Alkire and Mirarefi, 73], [Kessler and Alkire, 76a, b], [Hazlebeck and Talbot, 91b], [Chern and Cheh, 96a], and additives [Hazlebeck and Talbot, 91b], [Chern and Cheh, 96a] in a through-hole system, and the levelling effect of additives on a microscale [Dukovic, 90], [Madore *et al.*, 96].

On the other hand, the tertiary distribution is also used by some authors [Patel *et al.*, 75], [Middleman, 86], to specify the limiting case in which the electrodeposition is totally mass transfer controlled and ohmic and kinetics effects are neglected. Unlike potential theory problems, the treatment of transport limited systems is relatively straightforward, provided that the velocity distribution of the electrolyte required for solving the convective diffusion equation is obtainable.

2.4 A Review of Recent Modelling Work

2.4.1 Scaling of current distribution modelling

As mentioned earlier in Sec. 2.3, and pointed out by various authors [Deconinck, 92], [Geoffrey, 91], [Dukovic and Tobias, 90], analytical solutions of primary and secondary distributions are difficult to obtain for even the simplest geometries due to the non-linear electrode kinetics and mass transfer characteristics of the electrolyte.

There has been a trend to shift from an analytical to a computational and numerical treatment of the current distribution problem in the last two decades and, as commented upon by [Dukovic, 90], this is the driving force of the advancement of electroplating as a science. Approximate solutions obtained by numerical methods such as FEM or BEM, however, require the discretization of the boundaries into minute segments, usually in the order of microns. The number of nodal points required increases geometrically with the number of features on the workpiece and the complexity of the geometry [DeBecker and West, 96]. Taking the pattern plating of a PCB bare board as an example, if the board contains one hundred patterns and each pattern has fifty features, at least 100,000 nodes would be required for a boundary-element simulation if twenty node points per feature are needed for a reasonable approximation. Therefore, it is usually impractical to simulate numerically the current distribution over the entire workpiece, while accounting rigorously for all the geometric details of the features and patterns. It follows naturally that many researchers focus their modelling work on a particular length scale to simplify the task into a manageable one.

On the classification of length scales, [Kessler and Alkire, 76a] proposed three different length scales for the through-hole copper plating of multi-layer PCBs :

i/ macroscale - region of interest covers the entire board surface,
ii/ miniscale - region of interest being the individual through-holes,
iii/ microscale - surface roughness of the plated through-holes.

Such a classification was also adopted by [Yung *et al.*, 89] in their review paper on the copper plating of through and blind holes. [Dukovic, 90] suggested a similar but extended hierarchy of size scales which, in the view of this author, is particularly appropriate to the PCB electroplating. In his paper, current distribution studies are categorized into four levels :

i/ *workpiece scale* - distribution over the whole object undergoing electrodeposition, e.g. PCB panel, IC wafer,

ii/ *pattern scale* - distribution among the patterns on the surface of the workpiece with different density of features, e.g. lithographic patterns over an IC wafer or a PCB panel,

iii/ *feature scale* - distribution within an individual feature within a pattern, e.g. a through-hole, blind-via or conductor wire in a circuit pattern,

iv/ *roughness scale* - microscopic roughness or asperities of an individual feature.

[Mehdizadeh *et al.*, 92] adopted the same classification scheme and suggested characteristic lengths for the first three levels : 10 cm upward for the workpiece scale, in-between 10 μm and 10 cm for the pattern scale, 10 μm and below for the feature scale. However, a review of recent modelling work shows that classification based on absolute length is not appropriate. For example, the three-dimensional current distribution model developed by [Choi and Kang, 96] for a 5 cm x 5 cm cathode is best classified as a workpiece scale model while the modelling of through-hole plating [Yung and Romankiw, 89] is approached with at a feature scale, although its characteristic dimension seldom falls below 10μm. Moreover, as most of the current distribution problems are formulated and solved in dimensionless forms instead of absolute lengths, the characteristic dimensions suggested above can be considered as arbitrary only.

Another important reason for decomposing the problem into different length scales is that although the current distribution is governed by the same general phenomena, the dominating process parameters are different for each scale [Kessler and Alkire, 76a], [Pesco and Cheh, 89]. For example, ohmic resistance is considered dominating on a workpiece scale [Kessler and Alkire, 76a] while mass transfer resistance is significant within the concentration boundary layer over a particular feature [Kardos and Foulke, 62]. Scaling of the problem thus enables the researchers to simplify the calculation by making assumptions appropriate to the particular scale.

In the remaining sections of this chapter, recent research work on the computation of current distribution in electrodeposition is summarized at the workpiece, pattern and feature levels. Roughness scale studies are excluded as this thesis is concerned primarily with the fabrication of the PCB rather than electrocrystallization at the

microscopic scale. However, important work on the levelling effect of additives is discussed in the feature level modelling section. By the same token, only modelling work relating to the copper plating with applications in PCB fabrication is reviewed here. The modelling work is classified according to its principle objectives instead of following the arbitrary length scales as suggested by [Mehdizadeh *et al.*, 92].

2.4.2 Workpiece level modelling

The principle objective of workpiece scale modelling is to determine the distribution of current, and hence the deposition thickness, over the entire workpiece undergoing electrodeposition. Due to the limitations imposed by analytical methods, early investigations were confined to flat surface and simple geometries such as triangular [Wagner, 51] or sinusoidal profiles [Wagner, 54]. More complex configurations were attempted when numerical methods were later developed and applied to solve the problem. Except for the most recent work of [Choi and Kang, 96], the whole surface is electrochemically active in the workpiece level modelling problem.

2.4.2.1 Parallel Planar Electrodes - Two-Dimensional Analysis

The system of parallel planar electrodes embedded in insulating walls is of particular interest and relevance to the electronics industry due to its practical importance - most of the industrial electrolytic cells possess this geometrical characteristic. [Moulton, 05] presented a classical solution for the primary current distribution for two electrodes placed on the boundary of a rectangle, using the method of conformal mapping with the Schwarz-Christoffel transformation [Newman, 91a], [West *et al.*, 92]. [Wagner, 51] solved the primary current distribution for parallel electrodes using conformal mapping and obtained the expression below :

$$\frac{i}{i_{avg}} = \frac{2}{\pi\sqrt{1-(x/m)^2}} \qquad [2.12]$$

where i is the current density at a point of distance x from the center of the electrode (mA/cm^2), i_{avg} is the average current density over the electrode (mA/cm^2), $2m$ is the length of the cathode (cm), x is the distance measured from the center of the electrode (cm). Eq. [2.12] shows that primary current density is infinite at both ends of the

electrode and decreases exponentially and symmetrically until a minimum is reached at the centre. Secondary distribution under linear electrode polarization was also calculated by casting the solution in a Fredholm integral equation with the polarization parameter, k_c, as the constant term. The parameter k_c was defined as the product of the gradient of the cathodic polarization curve and the electrolyte conductivity. In his analysis, the lengths of both electrodes were equal and assumed to be small compared with the electrode separation, D, ($m << D$). The side walls, i.e. insulators perpendicular to the electrodes, were far removed ($l >> m$), where $2l$ represents the length of the cell. Using the same method due to [Moulton, 05], [Hine *et al.*, 56] later solved the primary current distribution on both sides of the electrodes for different ratios of electrode size, electrode separation and width of the gap between the electrode and the insulating side wall. They illustrated quantitatively, with a special case when the electrode separation equalled the cell width, that the larger the electrodes and the smaller the gap width, the more uniform the current distribution. In other words, when cells of the same size and form are considered, larger electrodes result in better uniformity in the current distribution. The effects of the back walls, assumed to be far removed, and electrode polarization were neglected in their model. As they were interested in the relative share of current at the two sides of the electrode under different cell geometries, the current distribution itself was not shown explicitly.

While the studies above were all concerned with working electrodes of equal lengths, [Yoshida *et al.*, 67a] and [Koseki *et al.*, 67b] considered the case of unequal electrode lengths. Similar to the work of [Hine *et al*, 56], they determined the primary current distribution for different values of electrode separation (D) and gap width using conformal mapping. The length of the anode ($2n$) was set to be smaller than that of the cathode ($2m$), and both of them were attached to the back wall but *not* touching the side wall ($m < l$). In their first paper, they developed a general equation for the primary distribution and showed that the result was in good agreement with [Wagner, 51] for the special case of equal electrode length, i.e. $n = m$. A modified equation was also developed specifically for the case when both edges of the cathode reached the side walls of the cell. Experimental data were then obtained from an acid copper plating process to validate the theoretical analysis and determine the effect of the electrode separation and gap width. Actual current distribution on the copper cathode was

obtained both by weighing of the electrodeposits, and from the equipotential lines constructed in the neighbourhood of the cathode [Evans, 60]. In summary, current uniformity was found to be enhanced when

i/ the anode was narrower than the cathode ($n < m$),
ii/ the electrode separation was smaller than the half length of the cathode ($D < m$),
iii/ the edges of the cathode were in contact with the side walls ($l = m$), although only a weak influence was observed.

Theoretical calculations were concluded to be in approximate agreement with the experimental results of the authors. However, the assumption of negligible polarization has restricted the current density used in their experiments to a very low value of 5 mA/cm^2, practical applicability of their model is therefore limited.

In a subsequent presentation, [Koseki, 68] incorporated the effect of electrolytic polarization into the model and solved the secondary distribution for linear polarization. A current density coefficient was added to the Fredholm integral equation derived by [Wagner, 51] to model the effects of the electrode lengths (m, n), separation (D) and cell length (l). According to his calculations, current distribution was more uniform when D was small, e.g. $D = m$, and the electrode length ratio, m/n was large, e.g. $m/n = 2$. The effect of polarization was that the optimal m/n ratio for uniform distribution could be reduced if the polarization parameter k_c was larger. Varying the geometrical factors in the cell such as D or m/n was found to be much more effective than modifying the gap width or the polarization characteristics in obtaining uniform current distribution.

In addition to [Wagner, 51] and [Koseki, 68], the secondary current distribution problem with linear polarization was also tackled by [Tobias and Wijsman, 53] in their study of electrode resistance effect in a rectangular cell. [Fomichev, 68] solved a similar problem for a platinum strip anode and compared his results with experimental studies. Secondary distribution under Tafel polarization was solved by [Gnusin *et al.*, 65] using the integral technique under the same assumptions of [Wagner, 51]. The distribution was obtained by rewriting the integral equation into a system of nonlinear

equations which was then solved numerically by the Newton method. [Parrish and Newman, 69, 70] considered the special case of two parallel planar electrodes embedded in the walls of a channel with fully developed laminar flow of electrolyte. Two dimensionless parameters were defined in their paper to characterize the current distribution :

- J - exchange current density, given by $ZFLi_0/RT\kappa$ [2.13]
- δ - average current density, given by $|\, i_{avg} \,|\, ZFL/RT\kappa$ [2.14]

where $Z = -n$ for systems with supporting electrolyte, and the characteristic length L is taken as the length of the electrode (cm). Current distributions were calculated as functions of different polarization parameters for the following four limiting cases.

i/ primary distribution ($J \rightarrow \infty$) : determined by the equation

$$\frac{i}{i_{avg}} = \frac{\varepsilon \cosh \varepsilon / K(\tanh^2 \varepsilon)}{\sqrt{\sinh^2 \varepsilon - \sinh^2 (2x\varepsilon / L)}} \qquad [2.15]$$

where ε is a dimensionless geometric factor given by $\pi L / 2D^*$, D is the height of the flow channel (cm) and $K(m)$ is the complete elliptic integral of the first kind. The above expression shows that the primary distribution depends *only* on geometric factors and it approaches infinity towards the ends of the electrode, i.e. $x \rightarrow L/2$. Asymptotic behaviour of the current distribution at electrode edges was studied in detail later by [Symrl and Newman, 89] and [West and Newman, 89] using singular perturbation analyses and the FDM.

ii/ secondary distribution under linear polarization (i.e. $i_{avg} << i_0$) : a doubly reiterative procedure involving Simpson's method and Gaussian quadrature integration was used to obtain the secondary distribution. The results agreed with [Wagner, 51], which considered only the extreme cases of $D / L \rightarrow \infty$ and $D / L << 1$. The current uniformity, defined as the ratio of the maximum to minimum current density, was plotted against the dimensionless parameter $(\alpha_a + \alpha_c)J^{\dagger}$ for different D/L ratios. It was found that the uniformity was higher when either of these were smaller, i.e.

---

* The symbol D is used here instead of h as used by Parrish to harmonize this presentation.

† This parameter, when divided by Z, gives the reciprocal of the Wagner number evaluated at the linear limit, i.e. Wa_L. Therefore, it can be regarded as the dimensionless group characterizing the secondary current distribution in the linear regime.

when bath conductivity (κ) was high or the electrode separation (D) was small. Similar conclusions were also reported by [Koseki, 68] for a rectangular cell.

iii/ secondary distribution under Tafel polarization (i.e. $i_{avg} >> i_0$) : results obtained were similar to ii/ above for both the current distribution and uniformity, except that δ ‡ was used as the dimensionless parameter in this case. Therefore, smaller average current density would enhance current uniformity in the high overpotential regime.

iv/ tertiary distribution : Tafel polarization was used in calculating the tertiary distribution at different fractions of the limiting current density, i_{lim}. At a small to medium fraction, i.e. $i_{avg} / i_{lim} < 0.75$, the cathodic current was highest at the edge where the electrolyte entered the channel. It dropped rapidly along the cathode before it rose up slightly again at the other end. This was explained as a compromise between the secondary and limiting distributions of current. At higher fraction of i_{avg} / i_{lim}, the primary distribution was approached.

For all the four cases discussed above, it was found also that the current distribution was insensitive to the D / L ratio when it was 10 or more.

[Blue, 80] developed a computer program to solve the tertiary distribution problem using the BIEM approach and used the copper plating of a multilayer board as an illustration. The plating tank under consideration had a depth of 84 cm, both the cathode and anode had a length of 46 cm and their separation was 16 cm. A concentration-dependent Butler-Volmer kinetics was used for the surface overpotential while two different expressions were developed for the concentration overpotential at the anode and cathode to cater for the vertical variations in the mass-transfer characteristic of the agitation by gas sparging. Interestingly, the resulting distribution was essentially the same as the primary distribution and therefore the author concluded that the primary distribution was quite adequate for predicting the plating thickness distribution when it was performed at a quarter of the limiting

‡ Similar to the case of J, δ divided by Z/α_c gives the reciprocal of the Wagner number evaluated at the Tafel limit, Wa_L. It can be regarded as the dimensionless group characterizing the secondary current distribution in the Tafel regime.

current density. However, no experimental verification of the calculated results was given in the paper.

Optimization of workpiece scale current uniformity using an auxiliary electrode was studied in detail by [Mehdizadeh *et al.*, 1990]. They developed a program to calculate the secondary current distribution under the Tafel kinetics using a BEM approach and determine the optimum current density of a ring auxiliary electrode to minimize the nonuniformity on a disk electrode. The current distribution was characterized by two dimensionless parameters :

- $Wa = RT\kappa \,/\, F\alpha_c \bar{i}_c r_c$ [2.16]
- $I = \bar{i}_{AUX} / \bar{i}_c$ [2.17]

where Wa is the Tafel form of the Wagner number, $\bar{i}_c$ is the average current density on the cathode (mA/cm^2), r_c is the radius of the cathode (cm) and $\bar{i}_{AUX}$ is the average current density on the auxiliary electrode (mA/cm^2). The nonuniformity of the current (thickness) distribution was quantified as the normalized root-mean-square deviation, σ, of the cathodic current density, i_c, from its average, $\bar{i}_c$, i.e.

$$\sigma^2 = \frac{1}{\pi r_c^{\,2}} \int_{r=0}^{r_c} \int_{\theta=0}^{2\pi} \left(\frac{i_c - \bar{i}_c}{\bar{i}_c} \right)^2 r \, d\theta \, dr \qquad [2.18]$$

A very strong influence of I on the secondary distribution was observed and the effect was found to be opposite on different regions of the electrode. As I was increased, the local current density on the edge was found to be decreased while that on the central part was increased, indicating that there should be some value of I that would minimize σ. An optimization algorithm was developed and incorporated into the BEM code to determine the optimum value I_{opt} that would give a minimum σ (σ_{opt}) for a particular value of $\bar{i}_c$. Effects of the following geometric factors on the optimal solution were modelled : the radius of the auxiliary electrode (r_{AUX}), the gap size between the cathode and auxiliary electrode (g), and the radius of the wall of the cell (r_w). A standard problem typical of acid copper plating was solved and parametric departures from this base case were examined in detail with several plottings.

i/ σ plotted against I for Wa values ranged from 0.01 to 10 : it was found that both σ_{opt}, I_{opt} and the sensitivity of σ toward I was lower at higher Wa numbers, i.e., better uniformity could be obtained at lower current density on the auxiliary electrode for a wider range of I when Wa is large.

ii/ σ plotted against I for r_{AUX} / r_c ratios ranged from 1.4 to 2.8 : both σ_{opt} and I_{opt} decreased with increasing r_{AUX} / r_c ratios but the sensitivity of σ toward I was higher at large r_{AUX} / r_c ratios. Therefore, a larger auxiliary electrode could enhance current uniformity but tighter control of $\bar{i}_{AUX}$ was required.

iii/ σ plotted against I for g / r_c ratios ranged from 0.01 to 0.1 : lower values of I_{opt} was obtained as g was decreased, but σ_{opt} varied curvilinearly, suggesting the existence of an optimum gap size. It was explained as a compromise between the undesirable edge effect and the current "thieving" action of the auxiliary electrode. As expected, this optimum gap size was found to be dependent on Wa and it was smaller for lower Wagner number.

iv/ σ plotted against I for r_w / r_c ratios ranged from 2 to 5 : similar to iii/ above, lower values of I_{opt} were obtained as r_w was decreased, i.e. when the wall was brought closer to the auxiliary electrode. However, σ_{opt} was found to be minimized when the cell was slightly bigger than the auxiliary electrode instead of touching it, although the latter case was expected based on the results of [Hine *et al*, 56] and [Koseki *et al.*, 67b]. It was suspected that when the wall was too close, the auxiliary electrode distribution was constrained in a disadvantageous way.

v/ σ_{opt} plotted against r_{AUX} / r_c for g / r_c ratios ranged from 0.006 to 0.13 (for fixed cell size of $r_w = 2r_c$) : a minimum was observed for each value of g considered and lower minima were obtained for smaller gaps and these occurred at higher values of r_{AUX}. Optimum combination of g and r_{AUX} for a given cell size could be obtained from the plot.

No experimental verification of the proposed model was given.

2.4.2.2 Parallel Planar Electrodes - Three-Dimensional Analysis

[Shih and Pickering, 87] presented the first three-dimensional modelling of the secondary current distribution under linear kinetics on a square planar electrode (2 cm

×2 cm) with the anode infinitely far away. The local current density function was expressed as a Fredholm integral equation of the second kind and solved numerically to give the secondary distribution over the whole cathodic surface. The same method had been employed by [Wagner, 51] and [Koseki, 68] in solving the two-dimensional secondary distribution problem. A three-dimensional plot of the current distribution showed that current density was highest at the four corners and lowest at the center of the board. The major difference between the three-dimensional and two-dimensional model, which predicted a maximum current density at the edges [Wagner, 51], [Parrish and Newman, 69, 70], was clearly presented. The ratios of the local current density to the average value from the center to the corner, center to the mid-edge, and midedge to corner was plotted for a wide range (0.006 - 10) of the Wagner polarization parameter k_c[1] / A, which was given by

$$k_c = \kappa(d\phi/di)_p \qquad [2.19]$$

where $(d\phi/di)_p$ is the slope of a point **p** on the linear portion of the cathodic polarization curve and A is the half-breadth of the electrode (cm). Current distribution was found to be more uniform when k_c/A was larger, a similar trend as observed in the two-dimensional case where a larger Wagner number implied a higher uniformity [Wagner, 51]. Higher current uniformity could be achieved by either increasing the bath conductivity (κ) or the $d\phi/di$ ratio. Rewriting the Wagner number in the form of k_c/A, the authors illustrated also the *scale effect* pointed out by [Agar and Hoar, 47] and [Hine *et al.*, 56], i.e. uniform distribution resulted when the electrode was small (k_c/A >> 1), whereas primary distribution was approached for the case of large electrode (k_c/A << 1). According to their calculations, k_c/A should be larger than 10 for the current distribution to be uniform within ±2.6% (center-to-corner), larger than 5 for a ±5.0% variation and larger than 2.5 for a ±8.5% variation. On the other hand, the largest cathodes for which a uniform distribution could be produced solely by controlling the bath composition to give a large k_c were found to be of the order of ≤ 1 cm only. This limit was calculated for a high-throwing bath with an equivalent Wagner number of 7.5. This is in agreement with the conclusion of [Koseki, 68] that controlling k_c alone is ineffective in obtaining

[1] The parameter k_c is actually the product of the Wagner number, *Wa*, and the characteristic length of the system, which is A is this case. k_c/A is therefore the Wagner number commonly used to characterize the current distributions in two-dimensional analysis, such a formulation facilitates the subsequent discussion of the scale effect in the three-dimensional case.

uniform distribution. Although experimental verification of the proposed model was not provided, they show that their semi-numerical solution method, when applied to a two-dimensional case, gave the same results as presented by [Wagner, 51]. [Dukovic, 90] and [Choi and Kang, 96] have also pointed out that the algorithm proposed was not readily extendable to more complicated systems.

A three-dimensional model was later developed by [Choi and Kang, 96] to predict the current distribution on a uniformly patterned cathode with an auxiliary electrode. Although the process under investigation was the electrodeposition of the permalloy (80% Ni-20% Fe) instead of copper, it is included here because i/ no similar modelling work is found in the literature for the copper plating process, and ii/ the electrodeposition of magnetic alloys has important applications in the computer industry [Shinoura, 96]. The cell used in their study consisted of two square electrodes (5 cm x 5 cm), separated by 4 cm and placed at the center of the bottom and ceiling of a rectangular cell (12 cm x 12 cm x 4 cm). In their calculation, the non-linear Butler-Volmer kinetics on the cathode was approximated by a simple log-type expression ($\eta = a + b \log i$) and the total overpotential (η) was not decomposed into a surface overpotential and a concentration overpotential. The relationship between the total overpotential (η) and the cathodic current density (i) was first determined experimentally in a *paddle cell* [Powers *et al.*, 72] at a fixed stirring speed, the logarithmic polarization curve was then obtained by least-squares fitting. The potential and current distribution problem was solved by the BEM with triangular type linear elements. Using the concept of *active-area-density* (AAD) (Sec. 2.4.3, Eq. [2.25]) developed by [Mehdizadeh *et al.*, 92, 93], they have modelled the effect of AAD on the three-dimensional current uniformity and determined the optimum size of auxiliary electrode as a function of the AAD. The corner and side effects found in [Shih and Pickering, 87] were also observable in the uniformly patterned cathode, and the effects were found to be more severe when the AAD was larger. This was explained by the fact that when the AAD increased, both the average superficial current density and the total current through the cell was increased [Mehdizadeh *et al.*, 93]. Their results show further that not only the AAD contrast among different regions of the cathodaic surface can promote thickness nonuniformity over the surface of the substrate (as

discussed in [Mehdizadeh *et al.*, 93] and Sec. 2.4.3 below), AAD itself has significant influence on the workpiece scale uniformity. Current distribution was more uniform for smaller AAD. On the other hand, it was found that the auxiliary electrode could reduce the workpiece scale nonuniformity, and uniform distribution could be obtained by proper combination of the auxiliary electrode and the AAD. It was explained by the contradicting effect of the size of the auxiliary electrode on the local current density over the corner/side parts and the central part of the cathode. A similar effect has also been reported by [Mehdizadeh *et al.*, 1990, see Sec. 2.4.2.1] for an unpatterned circular cathode with a ring auxiliary electrode. Optimum auxiliary electrode size was calculated for four different AAD values and they were found to increase with the AAD. However, it should be noted that the auxiliary electrode considered in their paper has the same potential as the cathode while it is generally understood that they need not be equal [Dalby *et al.*, 75], [Howe *et al.*, 79], and separate galvanostatic control of the two electrodes is more favorable in case of a large AAD. Finally, it is interesting to note that, although the cell configuration was clearly explained, no comparison with experimental data was given in their paper.

2.4.2.3 Hull Cell Modelling

Developed and described by [Hull, 39], the Hull cell is a versatile tool frequently used for maintenance and control of industrial plating baths, primarily because of its low cost, simplicity of operation, and its actual correlation with plating production [Duffek, 88]. Trial running of new process settings or bath ingredients can be conducted without interrupting normal production. It has a trapezoidal structure consisting of two nonparallel electrodes and two insulating walls. The cathode is tilted with respect to the anode so that a wide range of current densities can be obtained in a single experiment and the quality of deposits produced over a wide range of plating conditions can be studied. Technical aspects of Hull cell applications are discussed by [Duffek, 88] and [Sanicky, 85].

An empirical formula for the primary current distribution in a Hull cell panel (cathode) was given by [Norm, 83] as

$$\frac{i(z)}{i_{avg}} = 2.33\log\frac{1}{1-z} - 0.08 \qquad [2.20]$$

where $i(z)$ is the local current density of a point at a normalized distance z measured from the low current density edge and $0.186 < z < 0.941$. [West *et al*, 92] presented an analytical solution of the primary distribution using conformal mapping with two Schwartz-Christoffel transformations. Similar methods were also employed by [Moulton, 05], [Hine *et al.*, 56] and [Yoshida *et al.*, 67a] in solving primary distribution problems. The current distribution, estimated as

$$\frac{i(z)}{i_{avg}} = \frac{z^{1.273}}{(1-z)^{0.359}}(1.733 - 0.736z) \qquad [2.21]$$

was found to be in good agreement with the empirical solution of [Norm, 83]. Numerical calculations were performed by [Matlosz *et al.*, 87] with both the FEM and the BEM to determine the primary distribution. The numerical solutions obtained by both methods were in good agreement, and they matched well with the solution of [Norm, 83]. Using the two numerical techniques, they have also calculated the secondary current distribution with Butler-Volmer kinetics. Making use of the fact that there existed a one-to-one relationship between the applied potential and the average current density on the cathode, they performed a dimensional analysis and found that the dimensionless current density ($i(z)/i_{avg}$) was dependent on three dimensionless parameters only. For a fixed Hull geometry, the three parameters were

- $Wa_T = \dfrac{\beta_c \kappa}{i_{avg}\varepsilon}$ [2.22]
- $Wa_L = \dfrac{\kappa}{i_0\varepsilon(1/\beta_a + 1/\beta_c)}$ [2.23]
- β_a / β_c [2.24]

where β_c and β_a correspond to the cathodic and anodic Tafel slope, and the characteristic length ε was chosen as the difference in length of the two insulating side walls. Eq. [2.22] and [2.23] are indeed equivalent to the conventional definition of [Wagner, 51] (Eq. [2.9] & [2.10]) as the Tafel slope is given by $RT/\alpha F$ (Eq. [2.6]). The influences of the three parameters on the current nonuniformity, defined as the ratio of the maximum to minimum current density along the cathode, i_{max}/i_{min}, were determined. Two different iteration procedures were used in the finite element and

boundary element algorithm to cope with the nonlinear boundary conditions. Their calculations show that the current distribution ($i(z)/i_{avg}$) depended only on a single parameter for the limiting case of low and high cathodic overpotential, Wa_L and Wa_T, respectively. In either case the current uniformity increased with the dimensionless parameter. For the general case where the Butler-Volmer kinetics was applicable, the uniformity was influenced by all the three dimensionless parameters mentioned above. The general dependence of i_{max}/i_{min} on these parameters was reported as below :

- for small Wa_T, the Tafel approximation was applicable and the primary distribution was approached in the limit of very small Wa_T (e.g. < 0.5)
- for large Wa_T (e.g. > 100), the uniformity depended solely on Wa_L and uniform distribution was approached for high Wa_L values
- at intermediate values of Wa_T, the ratio β_a / β_c determined the optimal uniformity obtainable, minimum i_{max}/i_{min} ratio (even smaller than its final limiting value at high Wa_T) might exist within this range, e.g. when $Wa_T = 1$ and $\beta_a / \beta_c = 0.2$, the most uniform distribution was resulted when $Wa_T = 7$ instead of infinity.

They have also compared their numerical calculations with experimental results using a plating bath of copper sulphate ($CuSO_4$, 0.6*M*) and sulphuric acid (H_2SO_4, 1*M*) at 25 ^{0}C. Actual and predicted current distribution was compared for Wa_T values ranging from 0.063 to 1.60 using different average current densities, i_{avg}, of the cathode. Good agreement was reported except for large values of Wa_T (0.95 and 1.6) where the current efficiency was found to be low also.

2.4.3 Pattern level modelling

Pattern level modelling tackles the problem of current distribution over a plating surface with unevenly distributed electroactive areas. A typical example is through-mask plating, also known as pattern plating, of printed circuit boards with unevenly distributed lithographic patterns. Among the three levels of modelling, the pattern level problem has received little attention although the technology of through-mask plating has been reported in the literature [Romankiw *et al.*, 74] and widely used in PCB manufacturing for more than twenty years. This is evidenced by the fact that

literature containing a formal mathematical treatment of the problem is practically non-existent before 1988 [Dukovic, 90]. There are two possible reasons :

i/ the significant amount of work reported for workpiece and feature scale modelling, particularly through-hole plating, suggests that problems in these two domains are of sufficient complexity to demand the effort of most researchers in this area,

ii/ the numerical technique required to solve the pattern scale problem, notably the BEM, has evolved as a viable tool only after its successful application in solving problems at the other two scales.

During through-mask plating, it is observed that the distribution of the patterns has a very strong influence on the resulting current and thickness distribution over the substrate. Specifically, regions with sparsely populated patterns, e.g. isolated through-holes, tend to grow a thicker electrodeposit than those with higher pattern densities. This effect, which is well known by the industrial practitioners, was first described by [Romankiw *et al.*, 74] when they were fabricating a bubble domain memory chip with pattern plating and sputter etching. [Horkans and Romankiw, 77] later discussed such an effect in the pulse-plating of gold and explained it by the "crowding" of lines of current into these isolated patterns. [Yung *et al.*, 89] mentioned also the effect of circuit layout on the macroscale thickness uniformity. Methods suggested to mitigate this undesirable patterning effect include the use of on-board "current thieves", which utilizes dummy patterns on the board surface to even out the current distribution [Romankiw *et al.*, 74], an auxiliary cathode with separate galvanostatic control as off-board current thief [Dalby *et al.*, 75], [Berger *et al.*, 80] and non-conducting current shields positioned between the cathode and anode [Dalby *et al.*, 75], [Parthasaradhy, 89].

[Mehdizadeh *et al.*, 88] proposed the first, and so far the only, theoretical and mathematical model of current distribution over a patterned substrate using the potential-theory model for electrodeposition. In their 1992 paper [Mehdizadeh *et al.*, 92], they introduced their *active-area density* model and solved rigorously the secondary current distribution across two neighbouring regions with different active-area densities. The active-area density, AAD, is defined in their models as

$$AAD = \frac{A_{act}}{A_{sup}} \qquad [2.25]$$

where A_{act} is the active area exposed to electrodeposition over a particular region , e.g. the actual area of circuitry patterns over a PCB, and A_{sup} is the superficial area of that region, e.g. the geometric area of the PCB. As illustrated in Fig. 2.2, a large value of *AAD* represents a densely populated region and vice versa. It shows also that the *AAD* applies equally well to characterize the plating over topographic patterns such as the electrodeposition of copper bumps.

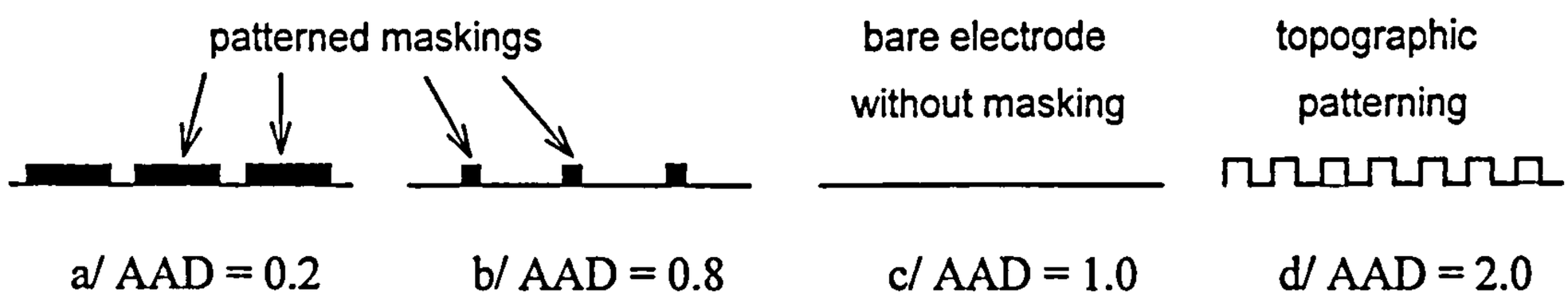

Fig. 2.2 : The Concept of *Active-Area Density* Proposed by [Mehdizadeh *et al.*, 1992]

To model the current crowding effect [Horkans and Romankiw, 77] of the surface pattern, Mehdizadeh *et al.* defined two different current densities, $i_{c,SUP}$ and $i_{c,ACT}$ at the cathode surface. The superficial current density, $i_{c,SUP}$, is the local average current per unit superficial area while the active current density, $i_{c,ACT}$, represents the current per unit active area that determines the local plating rate under Faraday's law. They are related by

$$i_{c,ACT} = \frac{i_{c,SUP}}{AAD} \qquad [2.26]$$

By using the $i_{c,ACT}$ as the current density in the Butler-Volmer equation of the cathodic kinetics, the patterning effect is successfully incorporated into the mathematical model. The potential problem is then solved numerically by the BEM using two nested levels of iteration to give the secondary current distribution across two adjacent zones with different AADs. The problem for a patterned cathode surrounded by a coplanar and concentric auxiliary electrode was also solved and the optimum current density at the auxiliary electrode was identified for a particular AAD. Two major assumptions were made in order to simplify the problem and achieve computational savings :

i/ mass transfer effect of the depositing metal and additives are neglected, i.e. the tertiary current distribution is not considered in the model,

ii/ a pattern over a particular region is approximated as a continuum and the patterned electrode is described entirely in terms of its AAD, i.e. individual features that constitute the pattern are disregarded.

Several important findings and practical implications derived from the model are summarized below.

- pattern scale nonconformity depends on different parameters for different Butler-Volmer kinetics :
  - at high overpotential, i.e. the Tafel regime, it depends on a single parameter, the Wagner number, Wa_T[†], only
  - in the intermediate regime, it depends on Wa_T , $Wa_L / \overline{AAD}$ and α_a / α_c, where $\overline{AAD}$ is the overall average active-area density of the whole substrate surface
  - at low overpotential, i.e. the linear regime, it depends again on a single parameter, $Wa_L / \overline{AAD}$

  similar parametric dependence was also observed in workpiece scale current distribution [Matlosz *et al.*, 1987], as mentioned earlier in section 2.4.2.3 above.
- AAD does have significant effect on the pattern scale current distribution, higher active current density, i_{ACT}, is found on the zone with lower AAD, i.e. sparely patterned area, and vice versa,
- the degree of non-uniformity, defined by the difference of the maximum and minimum of i_{ACT} within the region of interest, increases with the AAD ratio of the two neighbouring zones
- the AAD effects described above decrease with Wa_T, the Wagner number in Tafel form, therefore pattern-induced nonconformities can be reduced by
  - increasing the bath conductivity, κ

[†] in the AAD model, the modified Wagner number, Wa, evaluated at the Tafel ($_T$) and linear limits ($_L$) are given by

$$Wa_T = \frac{RT\kappa}{\alpha_c F L \bar{i}_{c,SUP}} \quad \text{and} \quad Wa_L = \frac{RT\kappa}{(\alpha_a + \alpha_c) F L i_0}$$

- using a smaller $\bar{i}_{c,SUP}$, the average superficial current density over the cathode, this, however, gives a reduced plating rate
- reducing the AAD contrast among different regions on the substrate
- reducing the size of the zone over which the AAD contrast occurs, i.e. reduced L
- reducing the average AAD over the entire substrate and hence the $\bar{i}_{c,SUP}$

- for a particular plating rate, a substrate with uniform patterns will have better thickness uniformity than an unmasked substrate as the $\bar{i}_{c,SUP}$ is smaller.

This comprehensive theoretical and mathematical treatment of the lithographic patterning effect was later verified experimentally and augmented by the same authors in [Mehdizadeh *et al.*, 93]. In their experiments, acid copper plating was performed on a patterned cathode (4.7 x 4.7 cm) under controlled agitation using a specially designed paddle cell [Powers *et al.*, 72]. Six different combinations of acid concentrations and $\bar{i}_{c,SUP}$ were used to simulate a wide range of Wa_T (0.4 to 7.6) values. The patterns consisted of alternate zones of parallel lines with 10% and 90% AAD and three different line widths were used. The deposit thickness over a line (0.7 cm) crossing two zones of different AAD (0.1 and 0.9) was measured with a profilometer and compared with theoretical predictions for all the three line widths.
For moderate and high values of Wa_T, good agreement was found between the measured and predicted values, showing that their AAD model using continuum approximation was accurate when mass transfer effects were negligible. However, in the region with high AAD, the model was found to under-predict the thickness in the case of low cathodic current density, and over-predict for a high current density. The deviation was found to be greater for baths with lower Wagner numbers. It was believed that non-negligible mass transfer effect was induced by the radial diffusion[1] over the lithographic pattern. The former model, which they named the *secondary model*, was further extended to include a simplified treatment of such an effect. In that *tertiary model*, the concentration overpotential, η_c, was included in the Butler-Volmer equation to obtain the tertiary current distribution for the mass transfer effect. An

[1] it refers to the radial enhancement of diffusion of the depositing reactant from the bulk of the electrolyte to the bottom of a trench, leading to the preferential growth of deposit at the two sides of the trench and thickness nonuniformity, [Romankiw, 79] and [Hume *et al.*, 84] discussed this effect in patterned electrodeposition.

enhancement factor ε was developed for a trench geometry (cross-section of a line) and used to construct a simplified expression for the concentration overpotential. The tertiary model was found to give better thickness prediction than the secondary model, especially in the case of high current density. The model shows that both active-area density effect and the pattern-driven mass transfer effects are contributing to the nonuniform current distribution over lithographic patterns.

2.4.4 Feature level modelling

In feature level modelling, the area of interest is limited to the small region of a single feature on the substrate being plated, e.g. a through-hole or a rectangular trench of a polymeric mask on a PCB. At this small scale, the influence of mass transfer and concentration overpotential, as well as the evolution of the electrode shape during the deposition process become highly important [Dukovic, 90]. All these add to the complexity and difficulty of the current distribution problem. A majority of the investigations undertaken at this level deals with the electroplating of through-holes, probably because of their extensive use in PCB fabrication and the importance of vias in circuit connectivity.

2.4.4.1 Through-Hole Modelling

[Alkire and Mirarefi, 73] calculated the current distribution within a tubular electrode under laminar flow and this is regarded as the first mathematical analysis of the through-hole problem [Yung *et al.*, 89], although the geometry and placement of the anode is different from a real through-hole situation. In their analysis, a tubular cathode was positioned between two long pipe sections of insulators while a single anode was placed either on the left (upstream) or right hand (downstream) side, with the electrolyte flowing from left to right. Two dimensionless groups that characterize the distribution were identified :

- linear polarization parameter, $\xi = \frac{2nF}{RT\kappa}\frac{L^2}{R_0}i_0$ [2.27]

- average limiting current density, $N = \frac{3nF}{RT\kappa}\frac{L^2}{R_0} i_{\lim}$ [2.28]

where L and R_0 are the length and radius of the tubular electrode (cm), and $i_{\lim}$ is the limiting current density determined from the convective diffusion equation within the diffusion layer region (A/cm^2), which is assumed to be thin with respect to R_0. The strongly coupled Laplace's equation and the convective diffusion equation were solved simultaneously through a complex iterative procedure. When the cathodic current was far below the limiting current ($< 0.25 i_{\lim}$) and secondary distribution was dominating, current distribution was found to depend only on ξ which denoted the ratio of potential loss in the electrolyte to surface overpotential. Uniform distribution was obtained for very small ξ ($<< 1$) when most of the cell potential was consumed by surface overpotential which was independent of the distance from the counterelectrode. In case of $\xi >> 1$, the nonuniform primary distribution is resulted. At the limiting current where the reaction was totally mass-transfer controlled, the current distribution was found to be independent of both N and ξ, and the position of the counterelectrode. It was given by $i_{\lim}(l/z)^{1/3}$ where z is the distance measured from the edge of the electrode where the electrolyte enters. A similar result was noticed by [Middleman, 86] for the through-hole system under the same assumption. At intermediate currents, the limiting distribution was encountered when N was small and the secondary distribution was approached when N is large. N reflects the relative ease of the mass transfer process and the passage of current through the electrolyte. These theoretical calculations were later verified experimentally in [Alkire and Mirarefi, 77a, 77b] with acid copper plating using a specially designed sectioned copper electrode. Good agreement was observed for a wide range of fractions of limiting current. The sufficiency of the above two dimensionless parameters in characterizing the current distribution has also unveiled the interesting fact that it is the ratio L^2/R_0 instead of the commonly used "aspect ratio" L/R_0 that determines the difficulty in achieving uniform plating of through-holes. Such a misconception was also pointed out by various subsequent authors [Kessler and Alkire, 76b], [Yung *et al.*, 89], [Hazlebeck and Talbot, 90]. Therefore, not all holes with the same aspect ratio are created equal for plating purposes. A thinner board with holes of smaller diameter will have more uniform deposition than a thicker one with holes of larger diameter because of the

smaller ξ value for the thinner board, even through they have the same aspect ratio and are plated at the same average current density.

Noting the difference between the tubular electrode and the actual through-hole, the model described above was used by [Kessler and Alkire, 76a, b] to develop an analytical model for predicting electroplated copper thickness distribution on multilayer PCBs. The original parameter N and a modified ξ, denoted $\xi_{T\kappa}$,were used as the dimensionless parameters, and

$$\xi_{T\kappa} = \frac{2\alpha_c F L^2}{RTR_0\kappa}\bar{i} \qquad [2.29]$$

where the length of the electrode, L, corresponds now to the thickness of the PCB. The substitution of i_0 by $\bar{i}$ in the above expression meant that the effect of plating additives was ignored in their model. Model predictions were compared with experimental data obtained from an acid copper plating process over a wide range of operating conditions including an actual multilayer board product. The model provided a conservative prediction for the PTH resistance, throwing power** as well as the actual plating thickness with acceptable over-all agreement. [Lanzi, 85] explained and rectified the error with a corrected Tafel slope reported by [Mattson and Bockris, 59]. Deposit uniformity was found to be highly correlated with $\xi_{T\kappa}$ in the absence of mass transfer limitation, i.e. high copper concentration and sufficient agitation. Moreover, criteria for uniform distribution were concluded from the comparison as follows :

i/ $\xi_{T\kappa} < 1$ or uniform $\xi_{T\kappa}$ throughout the whole panel : plating quality on the feature and workpiece level could be enhanced, respectively, by smaller average current density, $\bar{i}$, and an uniform primary current distribution, poor through-hole quality observed for $\xi_{T\kappa} > 1$ suggested that nonuniform distribution was mainly the result of large ohmic effects.

ii/ $\bar{i} < 0.25\bar{i}_{lim}$: where $\bar{i}_{lim}$ is the average limiting current density, this criterion was deduced from the observation that rough deposits occurred when $\bar{i} > 0.25\bar{i}_{lim}$ due to

** The throwing power is defined as the ratio of the plated copper thickness at the outer edge, t_S, of the hole to that in the center, t_H.

mass transfer limitations, which was also reported by [Gabe and Robinson, 71]. Such a criterion imposed a lower limit on the average electrolyte velocity within the hole for adequate electrolyte convection. For example, if a through-hole of R_0 = 0.023", L = 0.123" is to be plated in a 0.27M copper sulphate electrolyte with an average current density $\bar{i}$ = 40 mA/cm^2, a minimum average electrolyte convection of 4 cm/sec is required for a good deposit. As this limit was system dependent, a nomogram was provided in [Kessler and Alkire, 76a] to aid the determination of desirable values of $\xi_{T\kappa}$ and N from R_0, $\bar{i}$ and L, and hence the required electrolyte velocity for the plating system they have investigated.

The two criteria discussed above were also confirmed experimentally by [Engelmaier and Kessler, 78] for high conductivity acid-copper sulphate electrolyte in an 80 litre forced-flow plating system. The addition of brightener additive, which was not considered in Kessler and Alkire's model, was also experimented with. Plating quality was evaluated by the through-hole resistance, throwing power as well as metallographic examinations. Apart from the confirmation of the plating criteria, they found also that plating with the organic additive was considerably less sensitive to variations in the plating parameters which were likely to occur in the industrial production. The operating window could be widened to $\xi_{T\kappa} < 2$ and $\bar{i} < 0.25\bar{i}_{lim}$ to allow for more latitude for current density variations. Moreover, they have also estimated an equivalent electrolyte velocity of 0.25 cm/s and 1.7 cm/s for agitation with air sparging and natural convection, respectively. These values can serve as useful guidelines in determining whether additional means of agitation are required for a particular plating condition. In a recent study, [Chern and Cheh, 96a] simulated through-hole plating by a tubular electrode with an abrupt decrease in the radius in the middle section to form the through-hole. The tertiary current distribution inside the hole was solved with the methodology of [Parrish and Newman, 69, 70]. Theoretical predictions were compared with experimental results obtained from sectioned copper ring electrodes in a cylindrical channel. Satisfactory agreement was found at different current densities, aspect ratios and flow rates.

In all the models discussed above, the flow of the electrolyte was unidirectional only. [Patel *et al.*, 75] measured the wall mass transfer in fully developed pulsating laminar flow in a tube for different tube diameters, pulsating frequencies and amplitudes, and electrode lengths. The plating uniformity improvement due to flow reversal was not accommodated in their analysis. [Haak *et al.*, 81] investigated the relative importance of air sparging in comparison with mechanical board oscillation and their effects on the mass transport rate over the entire surface of the board as well as in the interior of the through-holes. However, no measurement of plating thickness uniformity along the hole axis was presented. [Middleman, 86] compared the effect of unidirectional and periodic alternating flow on the plating uniformity, assuming that the electrodeposition was entirely controlled by mass transfer. Although such an assumption was considered inappropriate for the through-hole plating problem [Dukovic, 90] and impractical [Hazlebeck and Talbot, 91a], his simplified analysis did show that periodic flow reversal was much more effective in promoting uniform reaction rate along the hole length than steady flow in one direction. The ratio of maximum to minimum plating rate in the region $0.1 \leq z / l \leq 0.9$ was reduced by 40% when flow reversal was introduced. [Hazlebeck and Talbot, 91b] found also that same deposit uniformity could be achieved at a much lower flow rate (one-tenth) by using a reversed flow process rather than unidirectional flow. However, [Pesco and Cheh, 89] showed that under normal operating conditions where through-holes were plated far below mass transfer limiting conditions, the effect of flow reversal on the current distribution was negligible. [Hazlebeck and Talbot, 91b] showed also that plating uniformity was virtually independent of the flow direction or periodic flow reversal when the plating was ohmic-limited. Finally, the fact that only mild convection was required to avoid mass transfer limitation, as pointed out by [Lanzi and Landau, 88] and [Yung *et al*, 89], was not recognized in Middleman's analysis.

Miniturization of modern electronic products requires the fabrication of thicker multi-layer boards (MLBs) with higher circuit density and longer, smaller through-holes in an industrial scale. These holes must be plated at sufficient rates with acceptable deposit thickness uniformity along the holes. Theoretical analysis of the plating of high aspect ratio (HAR) through-holes was carried out by [Lanzi and Landau, 88]. Limiting current density due to mass transfer and ohmic resistance effect was

calculated separately to examine which transport mechanism imposed the critical limit on the plating uniformity of HAR through-holes. Two expressions were developed :

- *mass transfer* : $\bar{i}_{L,avg} = \frac{FD_i c_b}{R_0}\left\{1.15A^{1/3} - 1.2 - 0.65A^{-1/3}\right\}$ [2.30]
- *ohmic resistance* : $i_{c,\Omega} = \pi^2 RTR_0\kappa / \alpha_c FL^2$ [2.31]

where $\bar{i}_{L,avg}$ is the average current density at the limiting mass transfer rate (mA/cm^2), D_i is the diffusion coefficient of the cupric ion (cm^2/s), A is a convection variable jointly determined by hole / bath geometry and electrolyte characteristic[††], $i_{c,\Omega}$ is the upper limit of the (secondary) current density at the centre of the hole imposed by the ohmic resistance (mA/cm^2). By comparing the functional dependence of $\bar{i}_{L,avg}$ and $i_{c,\Omega}$ on the parameter L^2/R_0, they found that the ohmic limit was much more sensitive to the through-hole dimensions : $i_{c,\Omega}$ decreased more rapidly than $\bar{i}_{L,avg}$ when L^2/R_0 became larger. Moreover, this limit was well below the mass transfer limit when L^2/R_0 was large, i.e., the ohmic limitation took effect at current densities well below those at which mass transfer became a significant limitation even for moderate amounts of agitation. It was therefore concluded that the ohmic rather than the mass transport resistance (as commonly perceived in the plating practice) imposed the critical limitation on the current density at which through-holes may be uniformly plated. [Yung *et al.*, 89] illustrated such dominating effect of the ohmic resistance with a numerical example and showed that only a small electrolyte velocity was needed to avoid mass transport limitations at a plating current density of 40 mA/cm^2, but uniform deposition was unattainable unless the current density was reduced to an extremely low level of 0.4 mA/cm^2. It follows that, unless the deposition process is totally mass-transfer controlled, increasing the level of $\bar{i}_{L,avg}$ by vigorous agitation or jet impingement [Alkire and Ju, 87] has limited enhancement effect when plating HAR holes with high current densities. On the contrary, the plating uniformity can be improved more effectively by reducing the effect of ohmic resistance, which can be achieved by

- increasing the electrolyte conductivity, κ,

[††] The full expression of A is $R_0^4 \rho V_0^2 / 2\mu D_i L^2 f_b^2$, where ρ is the electrolyte density, V_0 is the maximum MLB translation speed, μ is the electrolyte viscosity, f_b is the fraction of bath cross section not occupied by the MLB.

- reducing the hole length, L, and increasing the radius, R_0,
- miniaturing the hole for a given aspect ratio, thus reducing L^2/R_0,
- reducing α_c by altering the reaction kinetics with organic additives.

These recommendations were also ratified by the general model of [Hazlebeck and Talbot, 91a] for the case of ohmic-limited plating. Once again, their work demonstrates that it is the ratio L^2/R_0 rather than the commonly anticipated aspect ratio, L/R_0, that determines the difficulty of obtaining uniform plating within a hole geometry, as discussed earlier.

While all of the studies mentioned above were limited to the plating uniformity inside the hole, i.e. represented by the ratio of copper thickness at the entrance of the hole to the thickness at the centre of the hole, [Yung and Romankiw, 89] dealt with the additional problem of the ratio of the copper thickness on the surface of the board to that at the hole centre, commonly know as the surface-to-hole (S/H) ratio. In their model, both the two ratios were determined under the condition of unidirectional electrolyte flow and unlimited mass transfer. Through-hole plating was first simulated in a specially designed experimental gap cell, which allowed rapid and easy measurement of deposit thickness without tedious sectioning, to investigate the effect of gap aspect ratio, electrolyte velocity and current density on the thickness distribution. The experimental findings were verified with a mathematical model for the two-dimensional gap geometry, with good agreement found between actual and predicted entrance-to-centre thickness ratio over the range of aspect ratio (2.45 - 19.6) studied. Plating became more nonuniform as the current density was increased or the gap height was decreased as a result of the shifting from charge transfer control to ohmic resistance control of the plating behaviour in both situations. The shifting was reflected by the increase in magnitude of the dimensionless parameter j^*, adopted by these authors and originally proposed by [Alkire and Ju, 87] as

$$j^* = \frac{2nF\left(L/2\right)^2 \bar{i}}{RTR_0\kappa} \qquad [2.32]^{\ddagger\ddagger}$$

‡‡ It is noted that the local, instead of the average, current density is used in the original model of [Alkire and Ju, 87].

The influence of flow rate was not determinable because the electrolyte velocity in their experiments had exceeded the minimum convection requirement of [Kessler and Alkire, 76a] and mass transport limitation was not experienced. The applicability of the gap model to a hole geometry was then confirmed by a second set of experiments using Plexiglas boards with drilled holes. Model prediction of the S/H ratio was found to be accurate to within $\pm 20\%$, and was considered significant given the wide range of hole radius (0.01 - 0.125 cm), board thickness (0.25 - 0.80 cm) and current levels (100 - 800 mA) used in their experiments. They discussed also the effectiveness of additives in improving the feature-scale plating uniformity by examining the dominating mechanisms under different ranges of current densities.

i/ When the current density was extremely low ($j^* < 1$), the system behaviour was solely charge transfer controlled and the center-to-entrance thickness ratio depended on the dimensionless parameter ξ only, which was defined as

$$\xi = \frac{2nF\left(L/2\right)^2 i_0}{RTR_0\kappa} \qquad [2.33]$$

Under such condition, plating additives were, in theory, highly effective in promoting the plating uniformity by reducing the exchange current density, i_0, which yielded better centre-to-entrance thickness ratio according to their calculations. However, such conclusion became trivial if j^* was smaller than ξ, i.e. $\bar{i} < i_0$, where no electrodeposition took place.

ii/ In the region of medium current density ($1 < j^* < 15$), the electrodeposition was jointly controlled by charge transfer and ohmic resistance. An enhancement effect due to additives was still observable, although their effectiveness dropped rapidly with increasing plating current.

iii/ In the case of high current density ($j^* > 15$), as pointed out by [Lanzi and Landau, 88] and [Yung *et al.*, 89] above, the system was dominated by ohmic resistance. Plating additives were no longer effective in promoting thickness uniformity, which depended on the dimensionless parameter j^* and hence $\bar{i}$ alone.

With the better understanding of the fundamental mechanisms of the through-hole plating provided by the previous modelling work discussed above, particularly the

dominating effect of the ohmic resistance on the plating uniformity of HAR through-holes under practical operating conditions, the behaviour and intricate effect of additives in promoting feature-scale uniformity are being unveiled gradually by several recent studies. Although most of these studies are purely theoretical analyses without experimental verification, they do indicate the current trend of feature scale modelling work. Only modelling of additive effects on the acid copper plating of through-holes will be discussed below.

[Lanzi *et al.*, 89] calculated the secondary current distribution within a HAR through-hole when the local electrode kinetics was made variable along the hole length by the addition of organic additives. Mass transfer resistance was considered negligible as the ohmic limitation forced the process to be run well below the mass transfer limit, as pointed out by [Lanzi and Landau, 88]. It was found that current distribution inside the hole was independent of the exchange current density (i_0) once it was sufficiently small to bring about essentially irreversible kinetics. Therefore, the enhancement effect of additives by reducing the magnitude of i_0, as assumed by [Yung and Romankiw, 89], is significant only when i_0 is comparable to the operating current density range, which is unlikely under practical plating conditions. On the contrary, the cathodic transfer coefficient (α_c) was found to have a profound effect on the current distribution, and lower α_c gave more uniform deposit. This explains the validity of the various forms of the Wagner number, which is determined by the slope of the polarization curve and in turn by α_c[§§], as a dimensionless parameter characterizing the current and thickness uniformity in systems with and without additives. While it is known that certain organic additives, e.g. thiourea, can reduce the value of α_c and i_0 of a copper system [Turner and Johnson, 62], the calculations of [Lanzi *et al.*, 89] illustrated further that apparently minor electrode kinetic variations induced by additives could have a prominent effect on the through-hole secondary current distribution, even when the bath composition and the average current density were fixed. Such effects of additives on the kinetics explain partially the experimental error observed by [Kessler and Alkire, 76a, b], which neglected such effects and assumed a global Tafel kinetics (Eq. [2.29]) in their model. Improved plating

[§§] The slope of the polarization curve in the Tafel regime is given by the expression $RT / \alpha_c F$.

uniformity at smaller values of α_c and i_0 was also mentioned by [Chern and Cheh, 96b] in their tubular electrode through-hole model, although they assumed that α_c and i_0 were not affected by the presence of additives in their theoretical analysis.

[Hazlebeck and Talbot, 90] evaluated the additive effects when the electrolyte within the through-hole was stagnant. An empirical Butler-Volmer kinetic expression [Caban and Chapman, 77] was adopted for an additive-free bath while a special kinetic function for adsorption kinetics were developed for a bath containing additive based on a simple adsorption reaction mechanism. The effect of bulk cupric ion concentration, cupric ion diffusivity, through-hole dimensions, applied potential difference, and current density on deposition uniformity was correlated by the Thiele modulus parameter, $(\gamma a)^2$, defined as

$$(\gamma a)^2 = \frac{i_e}{D_t c_b} \frac{L^2}{R_0} \qquad [2.34]$$

where i_e is the current density at the entrance of the through-hole. The plating uniformity, defined as the ratio of the current density at the centre to that at the entrance of the hole, decreased with increasing Thiele modulus parameter for both additive-free and additive-containing bath. It follows that lower current density, higher cupric ion concentration and diffusivity, smaller diameter through-holes, and lower aspect ratio will all improve the plating uniformity. A bath with additives yielded more uniform deposit than a bath without additives as long as the value of $(\gamma a)^2$ was smaller than four. Interestingly, it was also found that a bath with lower sulphuric acid concentration, i.e., conductivity, provided higher uniformity for plating without convection, while the opposite was true for plating with convection. It is because in the former case the effect of ionic migration, which depends on the relative amount of acid and copper sulphate, becomes significant in addition to diffusion. [Newman, 91b] shows that the limiting current is increased when the relative amount of acid is lower in a stagnant diffusion cell. Although the assumption of stagnant electrolyte is not appropriate for industrial through-hole plating processes, their model is applicable to the plating of precision through-holes, such as magnetic recording heads and blind holes, where plating without convection becomes practical and inducing convection becomes difficult. In a later paper, [Hazlebeck and Talbot, 91a] developed a general

mathematical model which incorporated all the three transport mechanisms taking place in the through-hole, namely, electrical migration, diffusion and convection (unidirectional). The potential and concentration distribution inside the hole were solved by the method of orthogonal collocation. Uniformity of deposition was correlated with the plating variables in the general model and under the limiting cases of mass-transfer limited, ohmic-limited and mixed control, using a very different set of dimensionless groups. The enhancement effect of additives on the thickness uniformity through the reduction of the cathodic transfer coefficient (α_c) was confirmed again for ohmic-limited plating and the recommendations of [Lanzi and Landau, 88] was reiterated. According to their calculations, ohmic-limited plating resulted in highest uniformity at any plating rate when two counterelectrodes and unidirectional flow was employed. Minimum velocity and agitation required for ohmic-limited plating to prevail were determined for aspect-ratio up to 20.

2.4.4.2 Empirical Modelling of Through-Hole Plating

Although the multi-parameter nature of the electrodeposition process lends itself to modern methods of experimental design, little has been published in the literature on this approach to solving problems. Empirical modelling of the through-hole plating process with statistically designed experiments were attempted by a few authors. [Barringer and Carano, 86] used the 2^3 full factorial design to study the effects of bath temperature, levelling agent and the acid/copper ratio on the levelling power using visual and microsection rating as the responses. The full factorial, which was a cubic design, was wrongly recognized as the Box-Behnken spherical design [Box and Behnken, 60] by these authors and [Dini, 89], probably because of the inclusion of an additional centre point in their full factorial which did not enter into subsequent calculations. Levelling was found to be enhanced by lower bath temperature but not significantly affected by the acid/copper ratio and levelling agent. Their conclusions, which contradict previous theoretical predictions of temperature effect (Eqs. 2.27 - 2.33) and the findings of [Newman, 91b] discussed above, are doubtful in the light of the limited elaboration given in their paper. The effect of concentration of copper, formaldehyde, caustic soda, temperature and deposition time on the electroless deposition rate and coverage were studied by [Haluzan and Reichenbach, 91] with a

Taguchi L_{18} orthogonal array. [Forrest and Reed, 93] investigated the effects of the same set of parameters on the S/H ratio of electroplated copper in HAR through-holes using a replicated D-optimal design of 32 runs. They found that brightener concentration had the biggest impact on S/H ratio in comparison with the other two, and the best ratio was obtained when the brightener was at the middle of the experimental range. As their experiments were performed at low current densities, their results agreed with the analysis of [Yung and Romankiw, 89], which stated that additive effect was significant only in the low and medium current density regimes. However, the exact values of the current densities and the statistical analysis were not shown clearly. [Bokisa and McFarland, 93] employed a general factorial design to study the influence of aspect ratio, current density and copper sulphate concentration upon the S/H ratio of plated-through holes. Three levels of aspect ratio (3:1 to 10:1), six levels of sulphate concentration (15 - 90 g/L) and eight levels of current density (5 - 35 asf) were studied in 150*** runs of experiments. 22 main and interaction effects were identified as significant and a 23-term polynomial was obtained by multiple linear regression to predict the S/H ratio with a correlation coefficient greater than 0.99. Experimental verification of the prediction polynomial, however, was not done in their investigation.

Apart from the studies of levelling power and S/H ratio, statistically designed experiments were also used to establish coupon-to-board correlation [Harry, 89] and identify the primary failure mechanism of electrical opens during the tin plating of HAR through holes [Huffman and Witkowski, 1991].

2.5 Statistical Modelling of Acid Copper Plating Process

Acid copper plating is commonly employed in the manufacture of through hole printed circuit boards (PCB) during the pattern or panel plating process. A uniform plating thickness across the entire board is highly desirable as thin copper plating may result in over-etching or even open-trace problem during etching while over-plating

*** A few extra experiments were done at low current densities in smaller increments, adding up to a total of 50 runs for each aspect ratio.

may end up with under-sized or plugged holes, causing difficulties for subsequent components insertion or assembly. Inherent variation of plating thickness exists because of the non-uniform current distribution over the board surface.

Previous research based on fundamental electrochemical principals have successfully modelled the effect of the process parameters on the current distribution under well defined assumptions and polarization characteristic. However, the exact current-potential relationship, which is highly sensitive to the bath composition as well as the agitation mechanism, is not usually obtainable for a bath employing air and mechanical agitation simultaneously. More importantly, the actual deposit thickness follows the current distribution only when the current efficiency is 100% over the entire surface, which is difficult to achieve in an industrial environment where energy is lost in hydrogen and heat dissipation. However, this multivariable process is a good candidate to be investigated with statistical experimentation. Structured experimental investigation in the acid copper plating for PCB fabrication is as yet far from complete, especially in the pattern level variations. This is clearly reflected in the review of the current literature. Although some of the designs employed by previous researchers, especially those based on Taguchi method, are highly saturated designs with complex alias structures and low resolutions, their inefficiency being largely offset by the powerfulness of factorial designs. Generally, those works represent successful applications of simple designed experiments to obtain obvious directions of process improvement, usually in the form of a set of recommended factor settings. Empirical modelling and optimization of the process, however, can rarely be achieved and verified in a single set of experimental trials. Depending on the complexity of the process under investigation, different experimental techniques are needed to achieve specific purposes during the step-by-step modelling process. This thesis presents how planned matrix experiments, namely fractional factorials and central composite designs, are conducted sequentially to model empirically the main effects as well as possible interactions of major process parameters on the average plating thickness and its variations, and obtain the optimal combination of these factors to minimize the plating thickness variability within the allowable process windows.

2.6 Summary

The previous sections of this chapter present a review of the topics relevant to the work of this thesis. The review shows that previous researchers have been concentrating on the modelling of the deposite thickness itself and little work has been done in the modelling and control of the variability, particularly at the workpiece and pattern level. The rest of this thesis reports the experimental works and analysis performed in these areas.

CHAPTER 3

EXPERIMENTAL SETUP AND PROCEDURES

3.1 Introduction

This chapter describes the apparatus, equipment and materials used in the pattern, PTH and BV plating experiments. Detailed procedures of the electroless and acid copper plating, and the measurement of deposit thickness are also presented.

3.2 Equipment and Apparatus

Major equipment used in the experiments included the 200-litre plating bath for the acid copper plating of uniform pattern (Fig. 3.1), the purpose-built testing cell for the plating of non-uniform pattern, PTH and BV (Fig. 3.2), the Seiko SFT 7155 XRF X-ray coating thickness gauge (Fig. 3.3) and the Talysurf profilometer (Fig. 3.4) for the measurement of plating thickness. Two rectangular testing cells were assembled with PVC plates and have internal dimensions* of 35.6 $\times$ 6.4 $\times$ 15.2 cm and 55.9 $\times$ 6.4 $\times$ 15.2 cm, respectively. The second (longer) cell was needed as the electrode separations required in some of the experiments (Sec. 5.2.2, 5.4.2) were larger than the length of the first cell. Performing the experiments in the cells has the following advantages :

i/ the guide bar with equally spaced (1.3 cm) slots enabled easy and accurate positioning of the PCB for different values of electrode separation

ii/ it allowed a fresh set of plating solutions to be prepared for each set of experiments, and hence better control of bath composition, this is particularly important for electroless plating because of the instability of the plating solution

A detailed list of all the equipment and apparatus employed in this research is given in Appendix 3.1.

* The dimensions are given in the format of length $\times$ breadth $\times$ height.

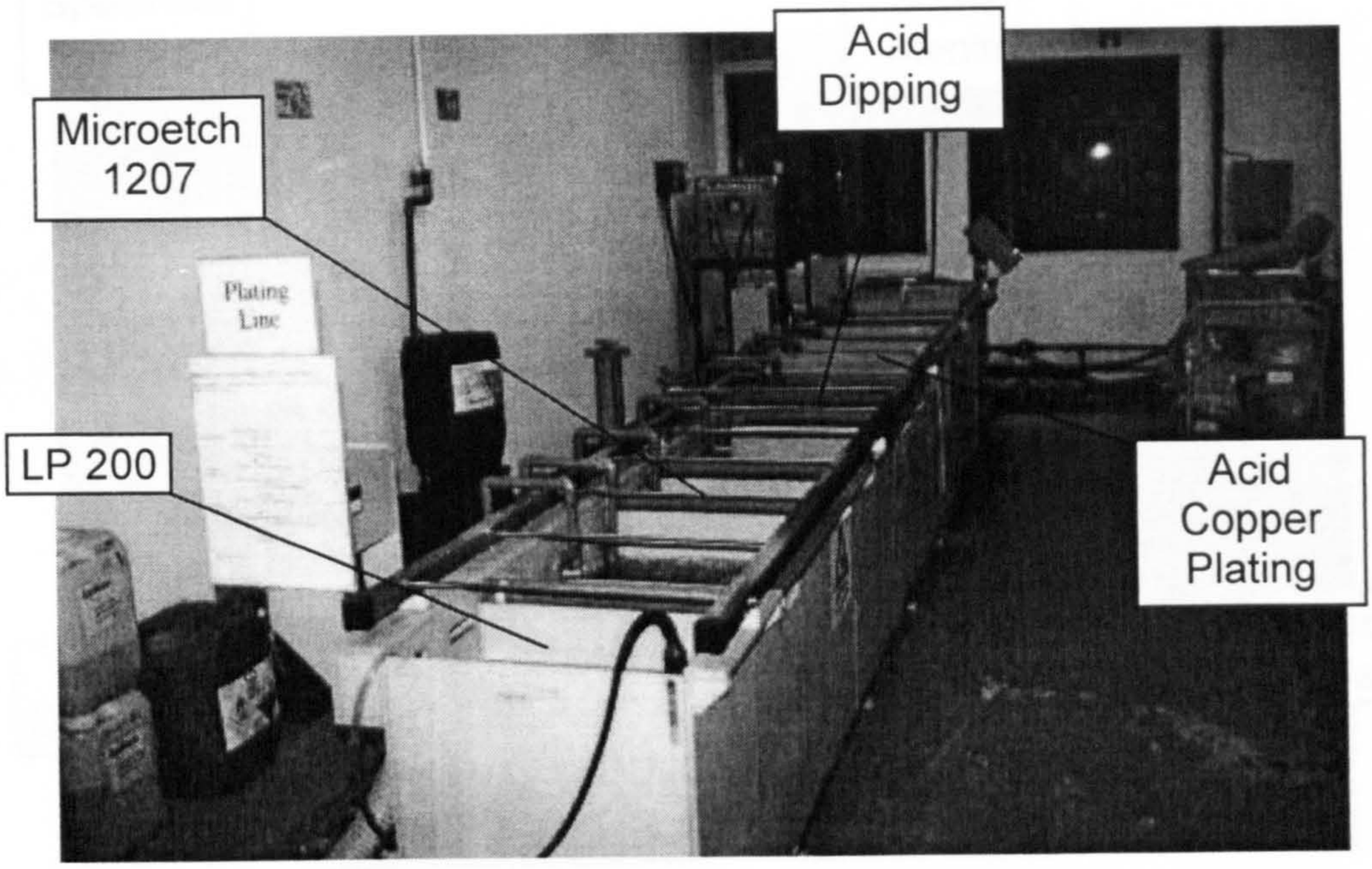

Fig. 3.1 : The 200 Litre Plating Bath

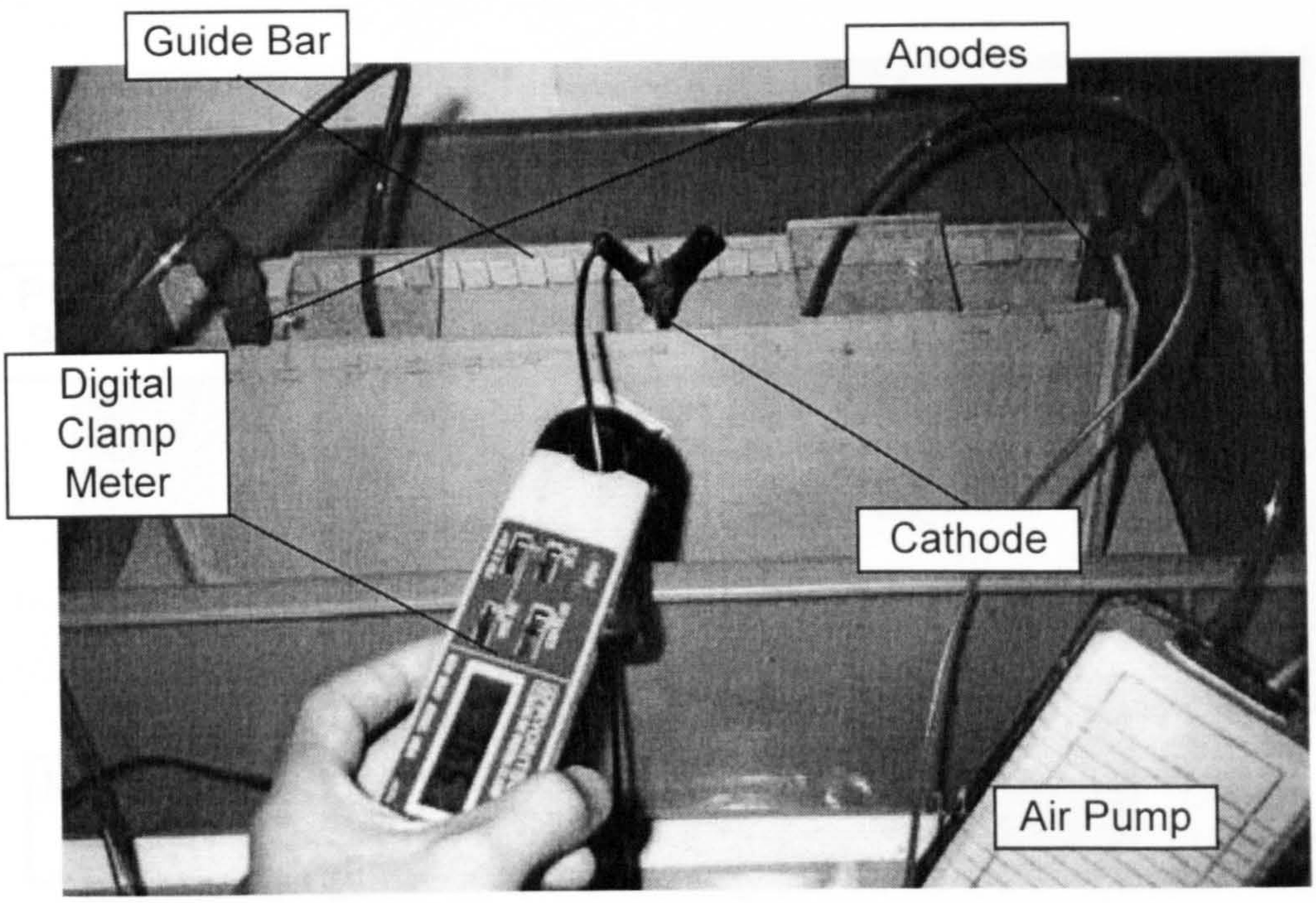

Fig. 3.2 : The Purpose-built Rectangular Testing Cell

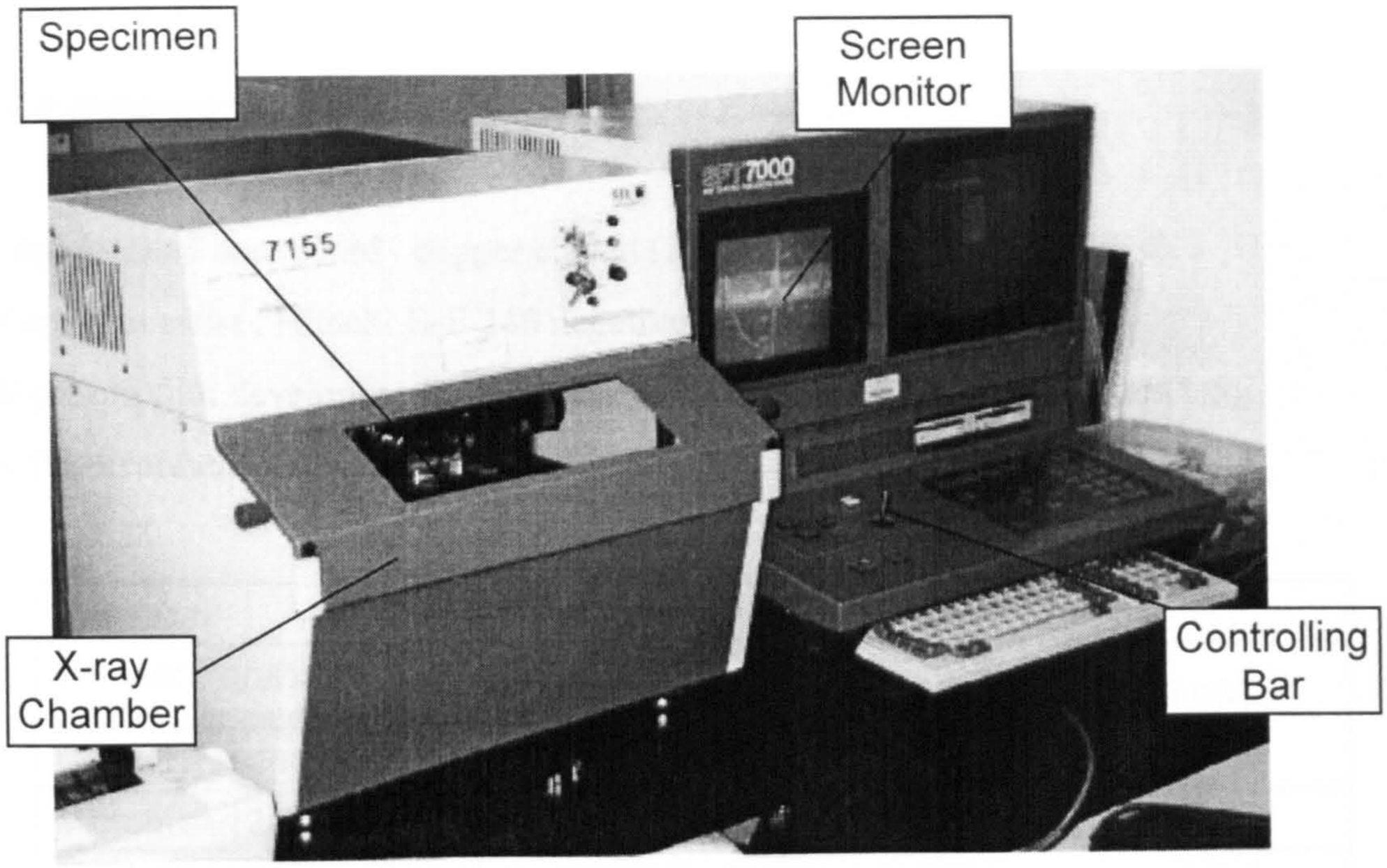

Fig. 3.3 : Sekio SFT 7155 XRF X-ray Coating Thickness Guage

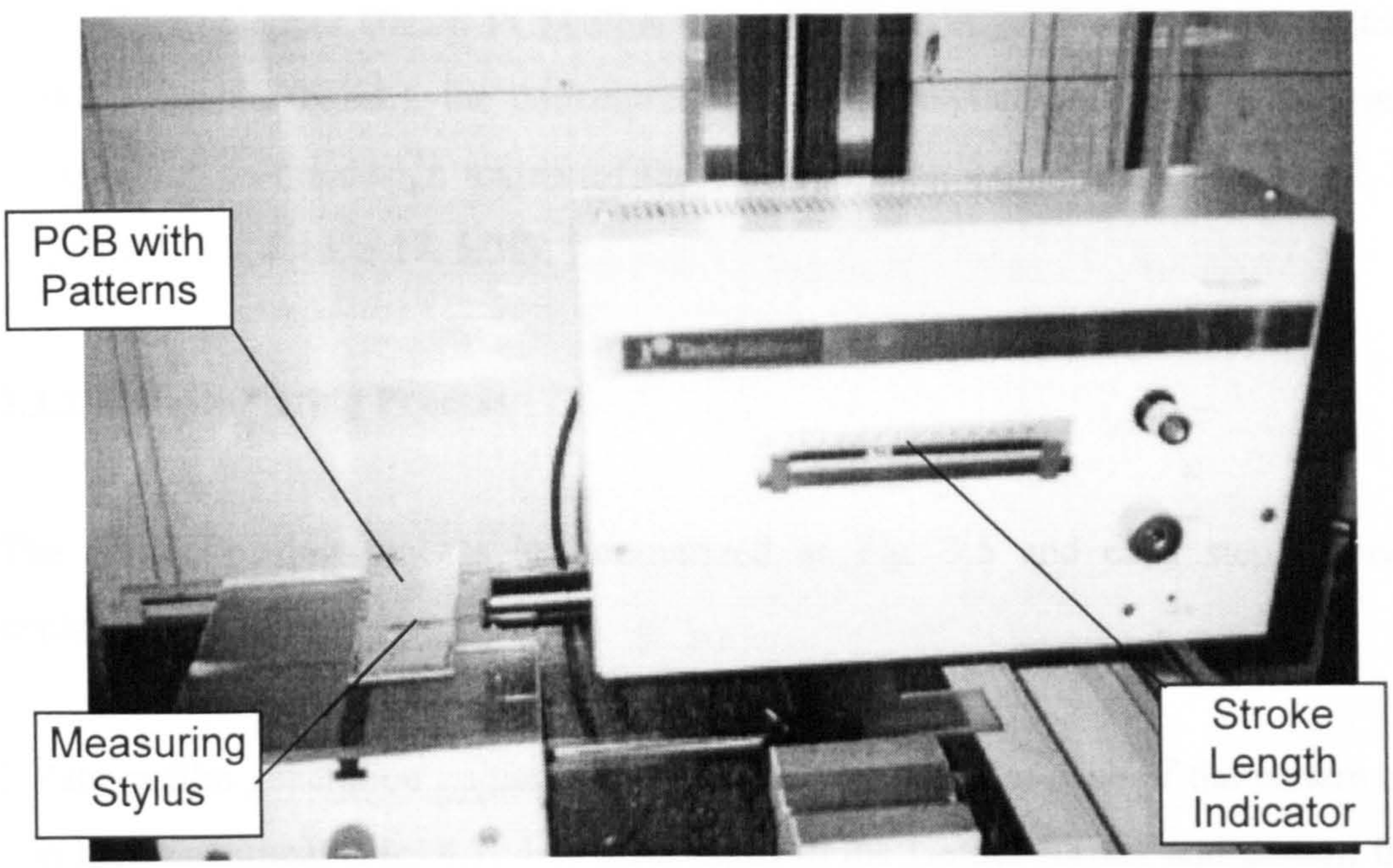

Fig. 3.4 : The Purpose-built Rectangular Testing Cell

3.3 Acid Copper Pattern Plating

3.3.1 Material and Solution

i/ single-sided bare board : copper claded (30 μm) epoxy-glass base (FR4)
ii/ dry film resist : Hitachi H-F 240 negative-working photo film resist
iii/ pattern film developer : Kodak Ultratec developer (1:7 - 10) and fixer (1:5)
iv/ Pre-treatment solution :

Chemical	*Solution Content*
Cleaner Ronaclean LP200 Concentrate or Cuprolite H-81	LP200 or H-81 50 ml/L, Sulphuric acid 50 ml/L, D.I. water to 1 litre
Microetch 1207	1207 (20%), H_2O_2 (10%), D.I. water (70%)
Sulphuric acid	5 - 10% by volume

v/ Acid Copper Plating Solution : copper sulphate ($CuSO_4$), sulphuric acid (H_2SO_4), LeaRonal Copper Gleam PCM Plus (proprietary additive, 5 mL/L 9mL), chloride (Cl^-, 70 ppm 0.3mL), the concentrations of the sulphate and acid are changed according to the design matrix of the corresponding experiments (Table 4.2, 4.5, 5.2, 5.5, 5.9, 5.13, 5.17, 5.20).

3.3.2 Pattern Plating Process

The pattern plating process is summarized as Fig. 3.5 and each step is briefly explained as follows.

i/ Pattern film generation : a part program was developed for each of the pattern used in the experiment (Fig. 4.1, 4.4, 4.18, 4.30) in the Gerber format and pattern films were generated by the photo-plotter using the Gerber file, which were then developed by the developer solutions, rinsed and air-dried.

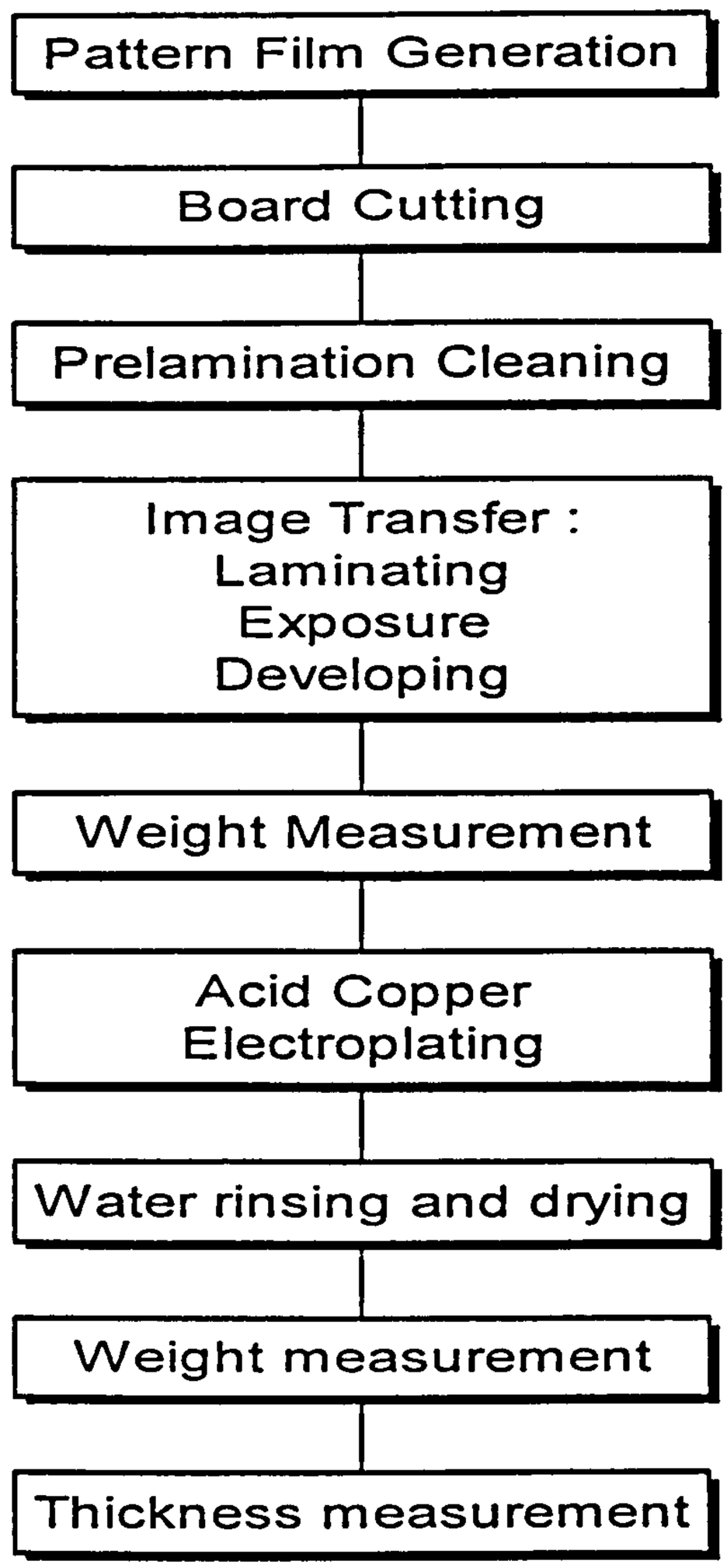

Fig. 3.5 : Flow Chart of the Acid Copper Pattern Plating Process

ii/ Board cutting : the bare boards were cut to suitable sizes by the shearing machine manually. The clearance between the top and bottom blade was set to 0.001" - 0.002" to avoid cracking or deformation of the laminate.

iii/ Prelamination cleaning : the boards were deburred and cleaned by the deburring machine to obtain clean and flat surfaces. They were then dried and preheated in the oven (80°C, 10 minutes) to facilitate the subsequent lamination.

iv/ Image transfer : the dry film image transfer process was performed in three steps :

a/ laminating - dry film resists were laminated by the laminating machine using the hot roll lamination technique, the resist was first heated up to 100 to 120 °C and

the softened resist was then rolled by pressure into the microstructure of the copper surface.

b/ exposure - the circuit pattern (prepared in i/ above) was 'printed' onto the board by the exposure machine using UV light, with an exposure time of 16 - 18 seconds.

c/ developing - the unexposed resist (pattern) areas were removed by the developing solutions in the developing machine to provide the electroactive area for copper plating.

v/ Weight measurement : the weight of the bare boards were measured by the analytical balance (small board) or triple-beam balance (large board) before the copper plating so that the current efficiency could be determined afterward.

vi/ Acid copper electroplating :

a/ the boards were processed in the pretreatment solutions before the actual plating in the following sequence -

Solution	*Duration*	*Purpose*
LP200 or H-81	5 mins.	degreasing, removal of oxide scale, general dirt and chemical residuals left from previous processes
Water Rinsing	2 mins.	general cleaning and avoid carryover of chemicals left from previous process
Microetch 1207	3 - 5 mins.	activate the copper surface with per-oxide etching chemical
Water Rinsing	2 mins.	general cleaning and avoid carryover of chemicals left from previous process
Dilute H_2SO_4	1 - 2 mins.	the acid dipping removes oxide film and residual alkali over the board surface

b/ the anode and cathode were connected to the current source and the plating bath was agitated by the air pump[†]

c/ the required current level was applied to the cathode (board) and monitored regularly with the digital clamp meter and kept constant throughout the entire

[†] The air pump was used only in the purpose-built plating cell, the 200 litre plating bath has a built-in air agitation system.

plating duration. Fig. 3.2 illustrated the plating of board in the purpose-built cell and Fig. A3.12 (Appendix 3.1) shows the board being plated in the 200 litre plating bath

d/ the boards were dried in the oven, air-cooled and weighted before the deposit thickness was measured.

3.4 Plated-Through Hole and Blind Via Plating

Copper Plating of through-holes and vias is similar to that of pattern plating, except that the hole and via is first metallized with a thin film of electroless copper ($\approx 0.5\mu m$) before they can be plated in the acid copper bath.

3.4.1 Solution and Material

Apart from items iv/ and v/ of Sec. 3.3.1 above, additional materials required are :

i/ double-sided bare board : copper claded (30 μm) epoxy-glass base (FR4)

ii/ electroless copper plating solutions :

Chemical	*Solution Content*
Cuprolite X-84 Hyperconcentrate	5 ml/litre, D.I. water to 1 litre
Microincide 1207	1207 20%, H_2O_2 (130 volume 35%) 10%, D.I. water 70%
Uniphase MLX (A)	MLX A salt 200 g/litre, RG(HCl) 20 ml/litre 37%, D.I. water to 1 litre
Uniphase MLX (A+B)	MLX A salt 200 g/litre, RG(HCl) 20 ml/litre 37%, , MLX B 50 ml/litre, D.I. water to 1 litre
Drag-stop 79	drag-stop 70 10%, D.I. water 90%
Cuproflex 1204	A 4%, B 3%, F 10%, NaOH 3%, D.I. water 80%

In the last (Cuproflex) solution, A, B and F are proprietary components and the exact compositions are not released by the manufacturer. A contains copper sulphate and formaldehyde (HCHO), B is sodium hydroxide and F is an chelating agent.

3.4.2 Electroless Copper Plating

The Excellon EX-110 CNC drilling machine (Fig. A3.14, Appendix 3.1) was used to drill the through-holes and vias using part programs (GM codes) developed with a text editor. After drilling the holes/vias and deburring, the electroless copper plating was done in a 2-litre beaker in the following sequence :

Purpose	*Sub-process*	*Chemical*	*Duration (mins.)*
Surface and Hole Preparation	Conditioner	Cuprolite X-84	5
	water rinsing		2
	Microetch	Microincide 1207	5
	water rinsing		2
Hole Catalization	Pre-catalyst	Uniphase MLX (A)	1
	dripping		- -
	Catalyst (activator)	Uniphase MLX (A+B)	5
	water rinsing		2
Flash Electroless Deposition	Accelerator	Drag-stop 79	4
	water rinsing		1
	Electroless copper	Cuproflex 1204	20
	water rinsing		2

i/ Conditioner : an alkaline cleaning step to remove soils (general dirt, oil, oxide scale, chemical residuals) from the copper foil and holes, it ensures the complete coverage of glass fibres and the full adhesion of the electroless copper to the holes' wall, increase the wettability for microetching and facilitate the layer adsorption of activator by providing a surface of uniform polarity.

ii/ Microetch : this slow acid etching is used for removal of copper surface pre-treatments, oxidation and presentation of uniformly active copper surface to maximize the adherence of the subsequent deposit, it increases the surface area of the copper foil and provides anchoring sites for the activator and electroless copper.

iii/ Pre-catalyst (predip) : the boards are immersed into a solution (MLX A) containing ions common to those of the activator so that they are residual with an ion and have a pH common to the catalyst. The boards are then brought directly to the activating bath without an intervening water rinse to avoid surface oxidation.

iv/ Catalyst (activation) : the activating species is held mechanically to both the surface of the copper foil and the epoxy glass, and forms a layer of material between the substrate and the subsequent electroless copper. The catalyst is an acid solution containing palladium held in a reduced state by tin ions.

v/ Accelerator (post-activation) : the accelerator removes part of the colloidal tin on board surfaces and holes, and render the activating species deposited in the activation step as active as possible before the board are immersed into the electroless copper bath.

vi/ Electroless copper : the alkaline chelated copper reducing solution is used to deposit thin copper in the holes and surfaces of the boards. The reaction is autocatalytic in the presence of an activated surface and proper (air) agitation. Fig. A3.13(a) and (b) (Appendix 3.1) show respectively the six electroless copper solutions and the agitated electroless copper bath.

Upon completion of the electroless deposition, the boards were immersed into a dilute (1.5%) sulphuric acid to prevent the freshly produced copper from being oxidised in the air until the acid copper plating was started.

3.4.3 Acid Copper Plating

As the boards were stored in a dilute acid solution, they were water rinsed, oven dried (80 °C, 10 mins.), air cooled to room temperature and weighted before they were plated in the acid copper solution. The acid copper plating procedures are described in Sec. 3.3.2 vi/. and all the plating was performed in the purpose-built testing cell (Fig. 3.2).

3.5 Measurement of Plating Thickness with X-Ray Thickness Gauge/Microscope

For the screening experiment of the uniform pattern plating experiment (Sec. 4.5.1), the deposit thickness was measured under the microscope after microsectioning. For the rest of the uniform pattern plating experiments, the thickness was measured directly by the X-ray thickness gauge after the plating process and no special treatment was needed. For all the PTH/BV experiments, the deposit thickness was measured directly by the X-ray thickness gauge after the PTHs/BVs were cut into upper and lower halves with the shearing machine. Fig. A3.16(a) (Appendix 3.1) shows a board with sectioned PTHs being supported at both ends by two rounded leaf spring before the PTHs are measured by the X-ray thickness gauge, Fig. A3.16(b) (Appendix 3.1) shows the measurement of a plated-through hole being monitored from the screen of the thickness gauge.

3.5.1 Materials

i/ rounded leaf springs
ii/ moulding compound (epoxy 15 ml. : hardener 6 drops : catalyst 6 drops)
iii/ abrasive papers of various grit number
iv/ diamond paste

3.5.2 Microsectioning Procedure

i/ the boards were cut by the shearing machine into suitable size (3 cm × 0.5 cm approx.), with the cutting line perpendicular to the line pattern being measured,
ii/ four to five specimens were clamped together at both ends by rounded leaf springs and put into a rectangular cavity of a mould base
iii/ moulding material was poured into the mould cavity and the air bubbles were removed by vacuum, after which the mould was cured for 24 hours
iv/ the moulded specimens were coarse ground by the polishing machine using abrasive paper of grit number 180, 220, 320, 500 and 1000 sequentially, they were then fine ground with the diamond paste

v/ the specimens were etched in dilute acid and measured under the microscope with 40X magnification.

3.6 Measurement of Plating Thickness with Talysurf Roughness Measuring Machine

Deposit thickness was measured by profilometry using the Talysurf roughness measuring machine (Fig. 3.4) in all the non-uniform pattern plating experiments. The dry film over the board was first removed by dipping in a dilute (5%) sodium hydroxide solution and the stylus of the profilometer was moved across each measurement point to obtain a cross-sectional profile of the line pattern. The length of the transverse motion of the stylus was 3 - 10 mm, depending on the width of the line being measured. Each set of geometric data, consisting of about 1400 pairs of X-Y coordinates, was dumped into a personal computer through a standard RS232 linkage in the ASCII format. A macro program was written in the Microsoft EXCEL to obtain the geometric profile of each measurement point, an example is shown in Fig. A3.18 (Appendix 3.1) . The actual deposit thickness was calculated as the different between the average height of the points between the two critical points and that of the base copper.

3.7 Summary

The experimental setup and procedures were briefly described in the previous sections of this chapter. The apparatus, materials and ingredients of the chemicals employed in the experiments are given. Although the experiments were carried out in a laboratory scale, the setup and procedures were typical of an industrial printed circuit board manufacturing process.

CHAPTER 4
EXPERIMENTAL DESIGN AND ANALYSIS : PATTERN PLATING

4.1 Introduction

The acid copper pattern plating process is usually employed after the electroless copper process of bare PCB fabrication to

i/ form the required circuit pattern over the base copper foil,

ii/ enable sufficient copper buildup over the circuit pattern, especially the plated-through hole (PTH) wall, to meet the minimum required thickness of 0.001" [IPC-A-600E, 95], and

iii/ facilitate copper buildup along the junction of the PTH wall and the base copper foil (and inner layers, if any).

This chapter presents how statistically designed experiments were used to determine the main effects as well as the possible interactions of several major process parameters on the average plating thickness and its variations. It also describes how the levels of these factors can be manipulated to give minimum plating thickness variability within the operability region using simple response surfaces. Planned experiments were performed on the acid copper plating process under the two major categories of

i/ substrate with uniform lithographic patterns over the entire surface, and
ii/ substrate with non-uniform active area densities in different regions of the surface.

4.2 Quality Characteristic

The quality characteristic of interest is the thickness of the copper plating. It is known that the weight of deposited copper is governed by the Faraday's Law [Canning, 82]. Thus, if the metal is deposited uniformly over the entire surface and the cathode efficiency is 100%, the plating thickness can be determined by the equation :

$$T = \frac{I \cdot t \cdot A}{F \cdot n \cdot a \cdot \rho} \qquad [4.1]$$

where T is the thickness of copper deposit (cm), I is the current passed (A), t is the plating duration (second), A is the atomic weight of copper (g), F is the Faraday's constant (coulomb/g eq.), n is the valency of copper, a is the area of circuit pattern (cm^2) and ρ is the density of copper, g/cm^3.

However, unless the cathode is a simple flat surface, it is not possible in practice to produce an electrodeposit of uniform thickness over the whole cathode surface and T gives only the average or nominal thickness of copper. The actual metal distribution over the PCB (cathode) surface is determined by the local current density at each point as well as the cathodic efficiency of the bath at that current density. It is therefore jointly influenced by the cathodic current efficiency-density relationship, the electrode polarization and the current distribution over the surface. In most practical cases, the primary current distribution is the controlling factor in determining the workpiece and pattern scale distribution, although it is the secondary current distribution that actually does the work of depositing copper over the cathodic surface. Areas receiving higher current densities, such as board edges or isolated patterns and through holes, tend to be over-plated while the reverse is true for those recesses, for example, PTH wall, with lower current densities. Inherent thickness variations thus exist and the local metal distribution approximates the secondary distribution. However, the latter is not usually known and therefore the former cannot be predicted explicitly [Pinkerton, 84]. Previous review (Sec. 2.3.2) shows that secondary current distribution, and hence the thickness variation, is affected by a complicated set of interacting process and product variables and statistically designed experiments are employed here to study and

identify their empirical relationship. Finally, it is noted that thickness uniformity is not the only desirable characteristic in electroplating and other properties such as percentage elongation and tensile strength are also important [Coombs, 88]. Since the copper bath used in this study contained commercially available additives and the experimental ranges of all the process parameters fall within normal operability regions, the metallurgical properties of the copper deposits were assumed to meet the industrial standards.

4.3 Process Parameters

While the plating thickness depends obviously on the amount of electricity passed, secondary current distribution is determined by the cathode polarization and the conductivity of the plating bath. Thus, process parameters that might have effects on the quality characteristic concerned include :

- average cathodic current density - as the local current density differs from point to point, the applied current denotes only the average current density over the cathodic surface, it affects directly the plating rate and the thickness variability,
- plating duration - together with the average current density, they determine directly the rate of the local Faradic reaction and hence the nominal plating thickness, but its effect on the thickness variation is not known,
- concentration of brightener - it alters the polarization behaviour of the system and hence the secondary distribution and thickness variability,
- concentration of sulphuric acid - bath acidity has a positive effect on the conductivity of the electrolyte and thus affects the secondary distribution,
- electrode separation - it affects the geometry of the system and the primary distribution over the cathodic surface.

These factors are also the *control factors* of the process as their levels can be specified freely by the process designer to attain the desired level of output. On the other hand, there are certain other product-dependent factors that affect the plating thickness, which include the

- width of the circuit pattern - it is generally observed that thinner lines tend to grow thicker deposits because of the "current crowding" effect [Horkans and Romankiw, 77], a difference in pattern width is thought to be a source of deposit variability,
- ratio of the active area densities among different regions on the cathode.

These are also the *noise factors* of the process as their levels are usually outside the control of the process designer, e.g. the PCB may contain circuit patterns with different active area density and conductor width. Also, in the context of statistical experiments, we distinguish between two different types of parameter effect :

i/ *location effect* - refers to the influence on the average value of the quality characteristic, which is the average plating thickness in this process,

ii/ *dispersion effect* - refers to the influence on the variability of the quality characteristic, i.e. the plating thickness variations over the board surface.

Factors with a strong location effect can be used to control the average thickness while the process variability can be minimized, within the experimental region, by selecting appropriate levels of factors with a strong dispersion effect.

4.4. The Matrix Experiments

The objectives of the experiments are two-fold :

i/ to determine the location and dispersion effects of the process parameters identified above and their relative significance, and
ii/ to identify the appropriate settings of significant parameters to minimize the plating thickness variations over the entire workpiece.

Factorial and response surface designs were employed in the experiments. First developed by Fisher and Yates in the 1920's, factorial designs are one of the major

contributions of statistical insight into experimental design. As [Steinberg and Hunter, 84] pointed out, such designs offer many advantages :

- each experimental run gives information on several factors instead of one-factor-at-a-time,
- the experiment yields as much information about each factor as though it *alone* had been varied, because of the balanced structure of the experiment matrix, and
- valuable additional information is available through the ability to check for possible *interactions* among the factors, which cannot be determined by conventional one-factor-at-a-time experimental design.

For example, a 2^4 full factorial of sixteen runs can be used to investigate all the four main effects of four two-level factors and their eleven possible interactions. Fractional factorial designs were first introduced by [Finney, 45], which allow experimenters to study the main effects and low-order (e.g. two-factors) interactions of several factors in far fewer runs than required to complete the full factorial designs. For example, a one-quarter fraction of a 2^6 full factorial, designated 2^{6-2}, allows study of six factors in sixteen runs. Thus, when the high-order interactions are negligible, as is often the case in industrial processes, fractional designs offer great economy of time and resources. They are usually used to screen out those few important factors out of a large number of potential factors. Normal probability plot is usually used to assess the statistical significance of the effects. In this method, the parameter effects are calculated from the responses and plotted onto a normal probability paper. The effects that are negligible are normally distributed and will tend to fall along a straight line on the plot, whereas significant effects tend to be far away from the line and identifiable as *outliners*.

Once the important parameters are identified, the next step is to determine if the current settings of the important parameters result in a value of the response that is near the optimum. The first-order model and the method of steepest ascent (or descent) are frequently used to determine the path that will move the process toward the optimum. After the approximate region of optimum is identified, a higher order model, such as a second or higher order polynomial, is then built to accurately

approximate the true response function within a relatively small region around the optimum. Response surface designs such as the Box-Behnken spherical design [Box and Behnken, 60] and the central composite design [Box and Wilson, 51],[Box and Hunter, 57] are employed in this stage for the model building. Once an appropriate approximating model has been obtained, it can be analysed to determine the optimum conditions for the process.

4.5 Experimental Study of Copper Plating of Uniform Patterns

Statistical experiments were carried out sequentially in four stages. Firstly, a highly fractionated factorial was used to screen out those significant factors from the six parameters studied in a small number of runs. A full factorial was then employed to determine all the main factors' effects and their interactions. Making use of the insignificant parameters found in the full factorial, the design was projected into a smaller factorial and re-analyzed to establish the most effective path for further experimentation. After locating the approximate optimum region along the path, a nine-run central composite design was then employed to obtain the second-degree model of the response surface within that region. Optimal combination of the parameters yielding minimum variation was then determined from the model. The adequacy of the second-order model in predicting the workpiece level variation was finally verified with a set of sixteen experiments. With the exception of the first stage, which was performed with a Hull cell setup, all the experiments were done in the 200 litre plating bath.

4.5.1 Hull Cell Experiments : Factor Screening

A single replicate of a 2_{IV}^{6-2} fractional factorial was employed to screen out those important factors from six of the parameters identified above, making the reasonable assumption that certain high-order (e.g. three-factors) interactions are negligible. The active area density of the lithographic patterns was not varied in this set of experiment and an uniform pattern was used. Each of the factors was set at two levels : low (-)

and high (+) in such a way that they covered the usual operating ranges of normal production, as summarized as Table 4.1 below.

Factors	*Levels*	
	Low (-)	*High* (+)
A. Brightener (mil/litre)	2	10
B. Electrode Separation (cm)	8.9	11.2
C. Pattern Width (cm)	0.02	0.05
D. Average Current Density (mA/cm^2)	26.9	37.7
E. Sulphuric Acid (g/litre)	160	200
F. Plating Duration (min)	40	60

Table 4.1 - Factor Levels of the Screening Experiment

The experimental matrix was constructed using a 2^4 full factorial for the first four columns and the defining relation $I=ABCE=BCDF$ for the last three columns. The design is a resolution IV design in which no main effect is aliased with any other main effect or with any two-factors interaction. Detailed alias structures are given in Appendix 4.1. The run orders were randomized and all the experiments were conducted with a Hull cell setup. A 4" x 2.75" single-side board was used and the test pattern is shown as Fig. 4.1. The actual plating thickness was measured by a microscope (40X magnification) after microsectioning. The average and the standard deviation of thickness of eight points corresponding to each factor combination were taken as the responses. Table 4.2 summarizes the detailed settings of the sixteen runs and the responses, all raw data are given in Appendix 4.2.

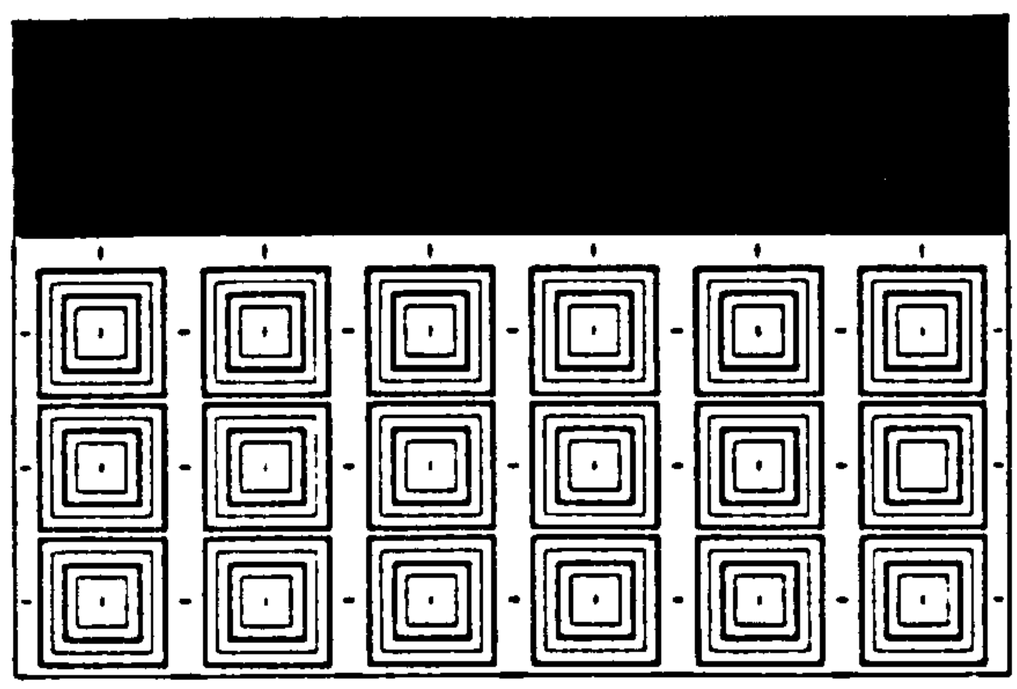

Fig. 4.1 : Test Pattern of the Screening Experiment (Not to Scale)

Run Order	Factors A	B	C	D	E	F	Average Thickness (μm)	Standard Deviation (μm)
11	-	-	-	-	-	-	44.0	3.3
10	+	-	-	-	+	-	40.0	4.6
16	-	+	-	-	+	+	33.4	2.8
1	+	+	-	-	-	+	36.8	4.0
14	-	-	+	-	+	+	59.1	7.0
9	+	-	+	-	-	+	49.9	4.4
15	-	+	+	-	-	-	32.5	3.3
2	+	+	+	-	+	-	33.1	4.9
4	-	-	-	+	-	+	92.8	7.9
8	+	-	-	+	+	+	101.3	7.9
13	-	+	-	+	+	-	35.1	4.4
7	+	+	-	+	-	-	31.6	4.1
6	-	-	+	+	+	-	72.1	4.8
3	+	-	+	+	-	-	63.1	10.2
12	-	+	+	+	-	+	62.9	4.2
5	+	+	+	+	+	+	61.6	7.3

Table 4.2 - Design Matrix and Responses of the Screening Experiment

All the effect calculations and mathematical analyses were done using JMP Release 3.2 while the normal probability and response surface plots were constructed by STATISTICA Release 5.0 and MATLAB Release 4.2. Fig. 4.2(a) and (b) shows respectively the normal probability plot of parameters' effects on the mean plating thickness and the standard deviation. For the mean responses, the outliners found are the factors B, D, F, and the two-factors interactions AE and BD, which are also the important location factors affecting the average plating thickness. Subsequent analysis of variance (ANOVA) confirms that they are all significant at the 0.1% level. For the dispersion effect, Fig. 4.2(b) shows that only the electrode separation (B) and average current density (D) are active in affecting the workpiece level variation. Subsequent ANOVA confirms that they are significant at the 4% and 2% level, respectively. ANOVA tests of the screening experiment are summarized as Table 4.3(a) and (b) below. The normal probability plot of the residuals, given in Fig. 4.3(a) and (b) shows that they are normally distributed for both the mean and standard deviation responses.

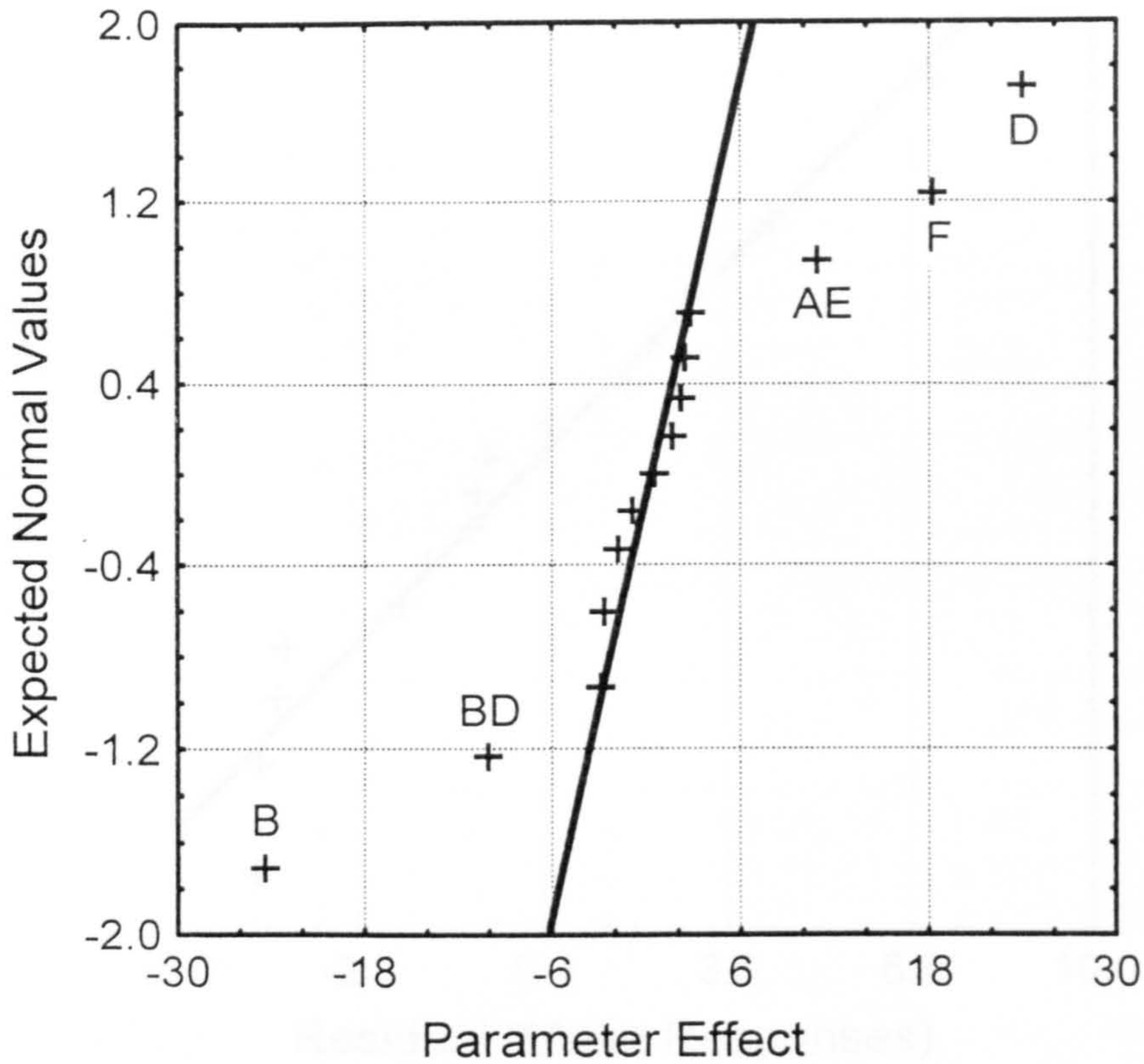

(a) Normal Probability Plot of the Location Effects

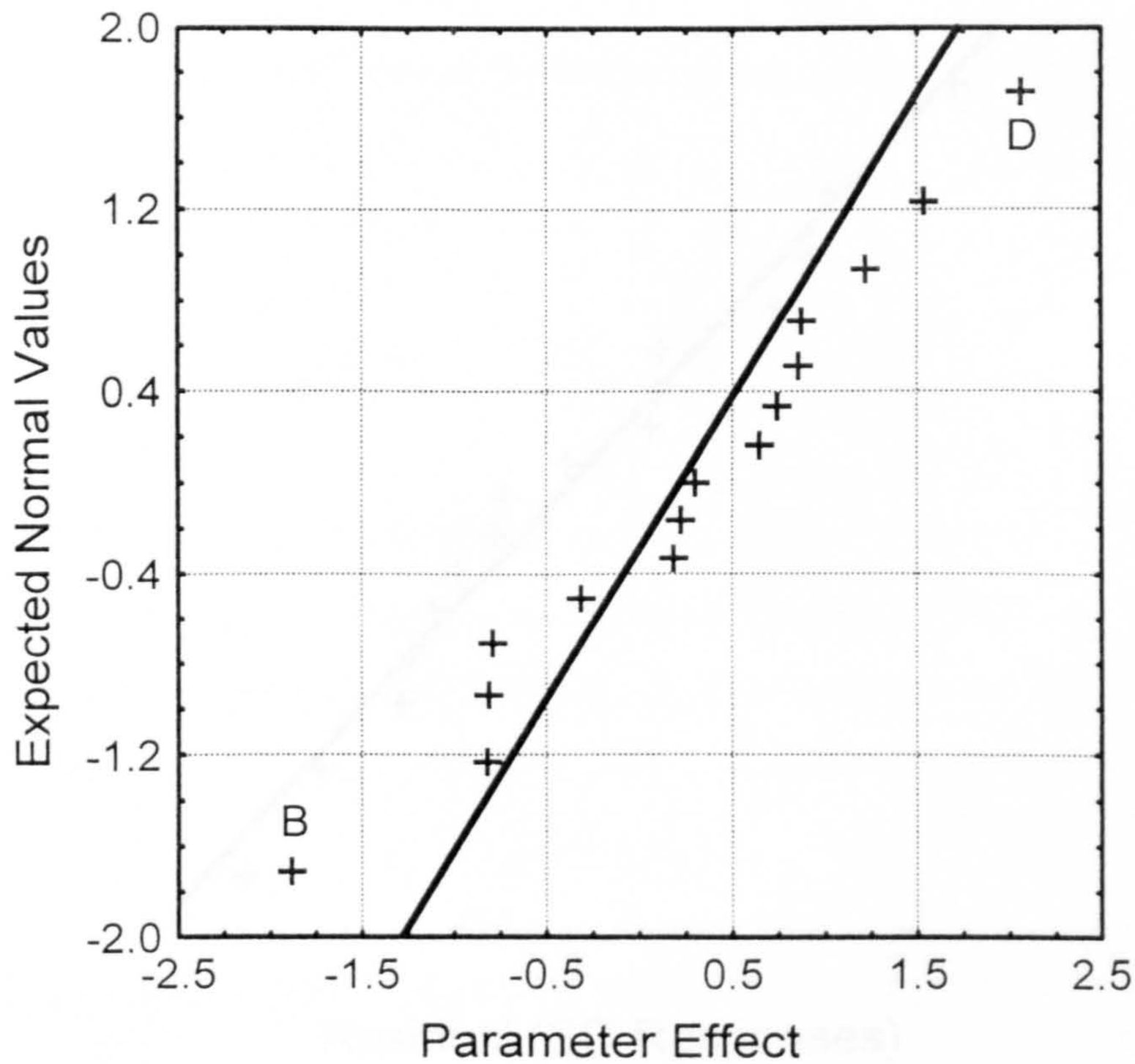

(b) Normal Probability Plot of the Dispersion Effects

Fig. 4.2 : Normal Probability Plots of the Screening Experiment

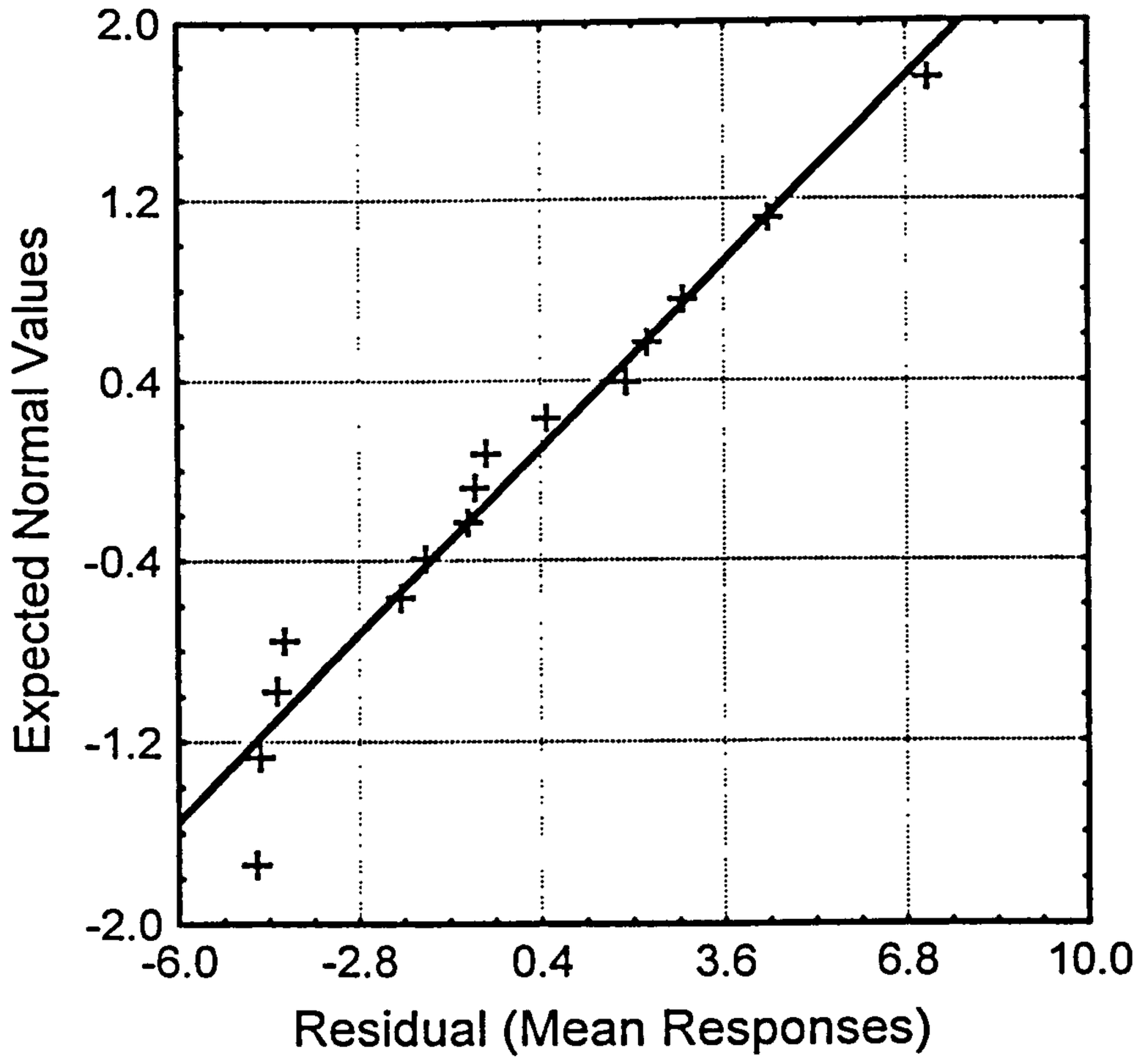

(a) Normal Probability Plot of the Residuals of the Mean Responses

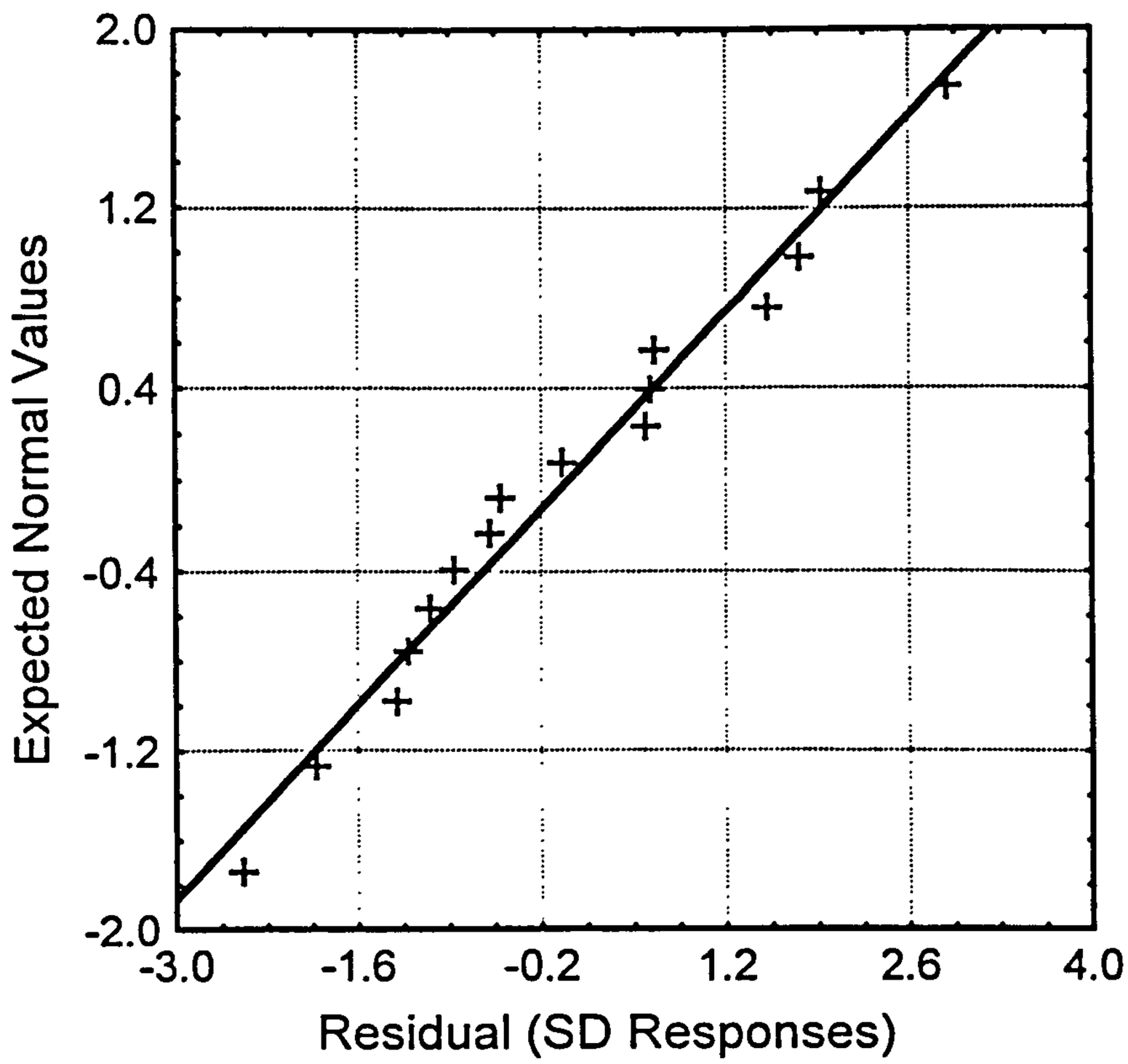

(b) Normal Probability Plot of the Residuals of the Standard Deviation Responses

Fig. 4.3 : Normal Probability Plots of the Residuals of Screening Experiment

Source of Variation	*SS*	*DF*	*MS*	*F*	*Prob. > F*
Model	6893.5	5	1378.7	71.4	< 0.0001
B	2382.6	1	2382.6	123.5	< 0.0001
D	2298.0	1	2298.0	119.1	< 0.0001
F	1332.3	1	1332.3	69.0	< 0.0001
BD	407.5	1	407.5	21.1	0.0099
AE	473.1	1	473.1	24.5	0.0006
Residual	192.9	10	19.3		
Total	70.864	15			

Table 4.3(a) : ANOVA Table of the Screening Experiment (Mean Responses)

Source of Variation	*SS*	*DF*	*MS*	*F*	*Prob. > F*
Model	31.19	2	15.60	5.93	0.0148
B	14.18	1	14.18	5.39	0.0371
D	17.01	1	17.01	6.47	0.0245
Residual	34.13	13	2.63		
Lack of Fit	2.62	1	2.62	1.00	0.3371
Pure Error	31.51	12	2.63		
Total	65.32	15			

Table 4.3(b) : ANOVA Table of the Screening Experiment (SD Responses)

In short, five significant location factors, namely,

- electrode separation (B),
- average current density (D),
- plating duration (F),
- brightener × sulphuric acid interaction (AE), and the
- electrode separation × average current density interaction (BD)

and two significant dispersion factors (B & D) were screened out to be important during the first stage of experimentation and their effects were therefore further investigated.

4.5.2 Plating Bath Experiment : Locating Neighbourhood of Optimum Region

In this stage, the effects of the important factors identified above were experimented in the 200-litre plating bath. The objectives were :

i/ to validate the significance of the location and dispersion effects found in the small scale screening run in the large scale plating bath, and

ii/ to search for the approximate location of the optimum combinations, if any, of the process parameters within the operability region which yields minimum thickness variability.

A replicated full 2^4 factorial was used and the factor levels are summarized as Table 4.4 below. As the two different pattern widths were incorporated into a single test board, only 16 experiments were actually required in this round of investigation.

Factors	*Levels*	
	Low (-)	*High* (+)
A. Pattern Width (cm)	0.02	0.05
B. Plating Duration (min.)	40	60
C. Average Current Density (mA/cm^2)	26.9	37.7
D. Electrode Separation (cm)	12.7	27.9

Table 4.4 : Factor Levels of the Second Experiment

Since our primary concern was the reduction of thickness variation, the concentration of the sulphuric acid and brightener, which have significant location effect only, was not varied in this stage. Given that sulphuric acid has a positive effect on the electrolyte conductivity and thickness uniformity, it was set at a high level of 200 g/litre for all runs. Concentration of brightener, copper sulphate and chloride was set at 8 mil/litre, 70 g/litre and 100 mg/litre, respectively. Although the width of pattern was found to be inactive during the screening run, which is counter-intuitive, it was studied again in this round as its location effect might have been masked by the other three strong location factors. Moreover, as explained in the last paragraph, inclusion of this parameter did not increase the total number of experiments. The experimental matrix and the responses are summarized as Table 4.5. Raw data is given in Appendix 4.3. A 3 x 3 array of similar square patterns was printed onto a 17.8 cm x 17.8 cm board and used as the test board in this round of experiments. The average and standard deviation of the deposit thickness of twenty-four points over the board surface was taken as the response for each run using the X-ray thickness gauge. The

lithographic pattern used and the measuring points are given in Fig. 4.4. It can be seen that each pattern is formed by three pairs of squares of alternating line width (0.02 cm and 0.05 cm) and the 9 patterns are separated by an array of 0.48 cm lines, giving a total electroactive area of 124.39 cm^2 and an average active area density of 0.393. The outside border is treated as an auxiliary electrode. A total of 30 locations were actually measured but the three highest and lowest reading were ignored in the calculation of responses to reduce bias due to extreme data.

Run Order	*Factors*				*Mean Thickness*	*Mean SD*
	A	B	C	D	(μm)	(μm)
3, 23	-	-	-	-	41.488	6.263
6, 31	+	-	-	-	41.191	6.385
16, 18	-	+	-	-	55.059	6.210
9, 27	+	+	-	-	52.125	6.228
11, 19	-	-	+	-	54.005	6.824
5, 28	+	-	+	-	51.090	6.803
7, 32	-	+	+	-	95.748	6.017
8, 26	+	+	+	-	91.083	6.217
13, 24	-	-	-	+	35.360	5.986
14, 21	+	-	-	+	35.712	5.646
10, 29	-	+	-	+	41.886	5.778
1, 30	+	+	-	+	40.132	5.916
2, 20	-	-	+	+	46.420	4.328
15, 17	+	-	+	+	43.114	4.573
4, 22	-	+	+	+	54.238	4.191
12, 25	+	+	+	+	56.105	4.148

Table 4.5 : Design Matrix and Responses of the Plating Bath Experiment

Significant parameters affecting the average plating thickness identified were

- plating duration (B),
- average current density (C),
- electrode separation (D),
- plating duration × average current density interaction (BC),
- plating duration × electrode separation interaction (BD),

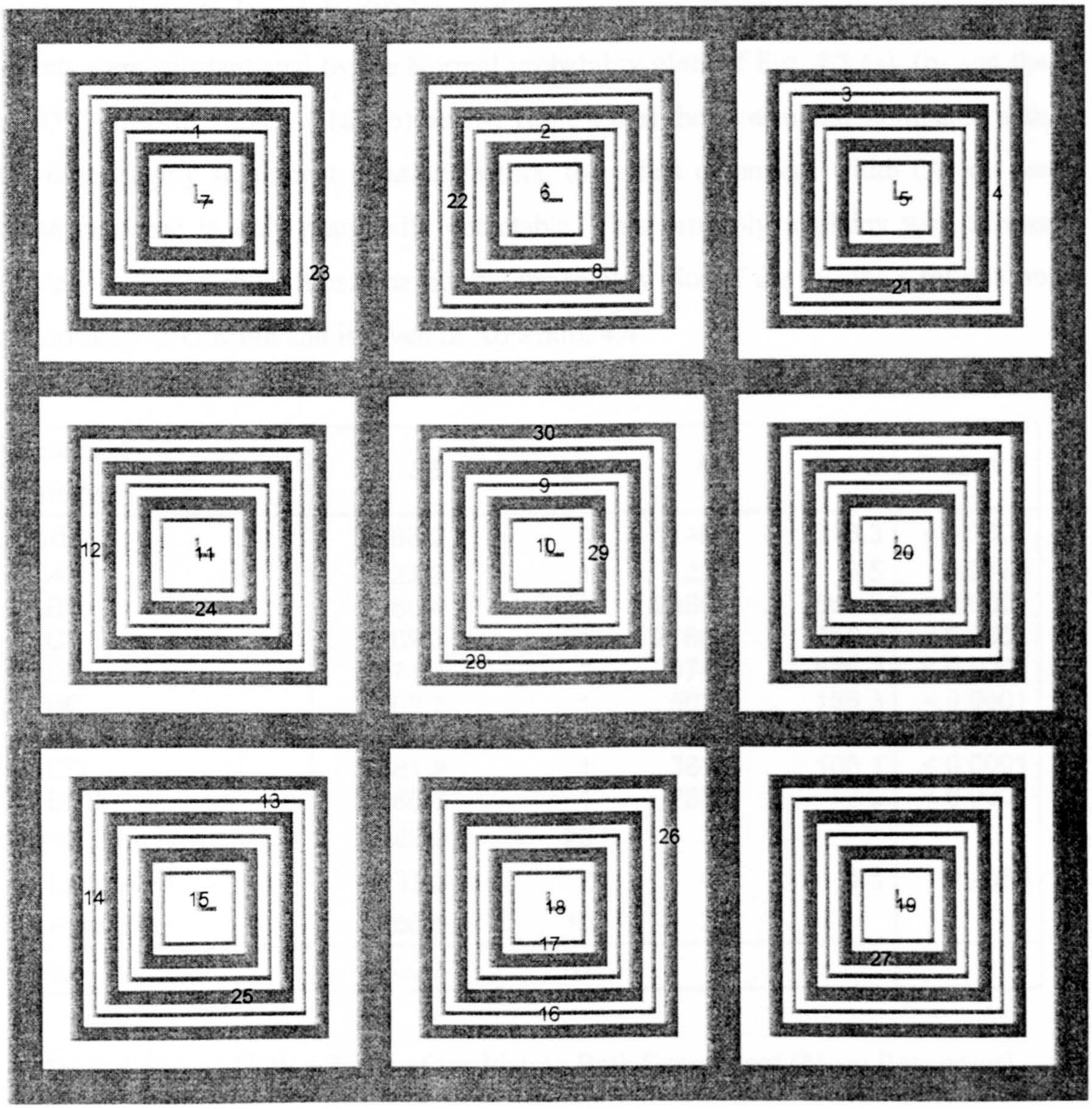

Fig. 4.4 : Lithographic Pattern of the Plating Bath Experiment and the Measuring Points for the Determination of Standard Deviation (Not to Scale)

- average current density × electrode separation interaction (CD) and the
- plating duration × average current density × electrode separation interaction (BCD)

while parameter C, D and the CD interaction were significant dispersion factors. Their effects were substantiated by the Normal probability plots of Fig. 4.5 (a), (b) and the ANOVA tests of Table 4.6 (a), (b) below. Table 4.6(a) shows also that, compared with the other highly significant location factors, the effect of pattern width (A) on the mean response is only marginally detectable. This probably explains why it was hidden in the screening runs. The normal probability plot of the residuals reflects no abnormality of concern and is given in Appendix 4.4.

Source of Variation	*SS*	*DF*	*MS*	*F*	*Prob. > F*
Model	9166.2	8	1145.8	318.3	< 0.0001
A	23.3	1	23.3	6.5	0.0179
B	2380.4	1	2380.4	661.2	< 0.0001
C	2769.5	1	2769.5	769.3	< 0.0001
D	2074.4	1	2074.4	576.2	< 0.0001
BC	562.7	1	562.7	156.3	< 0.0001
BD	693.5	1	693.5	192.6	< 0.0001
CD	381.9	1	381.9	106.1	< 0.0001
BCD	280.5	1	280.5	77.9	< 0.0001
Residual	83.9	23	3.6		
Lack of Fit	33.3	7	4.8	1.5	0.2366
Pure Error	50.6	16	3.2		
Total	9250.1	31			

Table 4.6(a) : ANOVA Table of the Plating Bath Experiment (Mean Responses)

Source of Variation	*SS*	*DF*	*MS*	*F*	*Prob. > F*
Model	22.88	3	7.63	6.94	0.0012
C	3.53	1	3.53	3.21	0.0840
D	13.47	1	13.47	12.25	0.0016
CD	5.88	1	5.88	5.35	0.0283
Residual	30.68	28	1.10		
Total	53.56	31			

Table 4.6(b) : ANOVA Table of the Plating Bath Experiment (SD Responses)

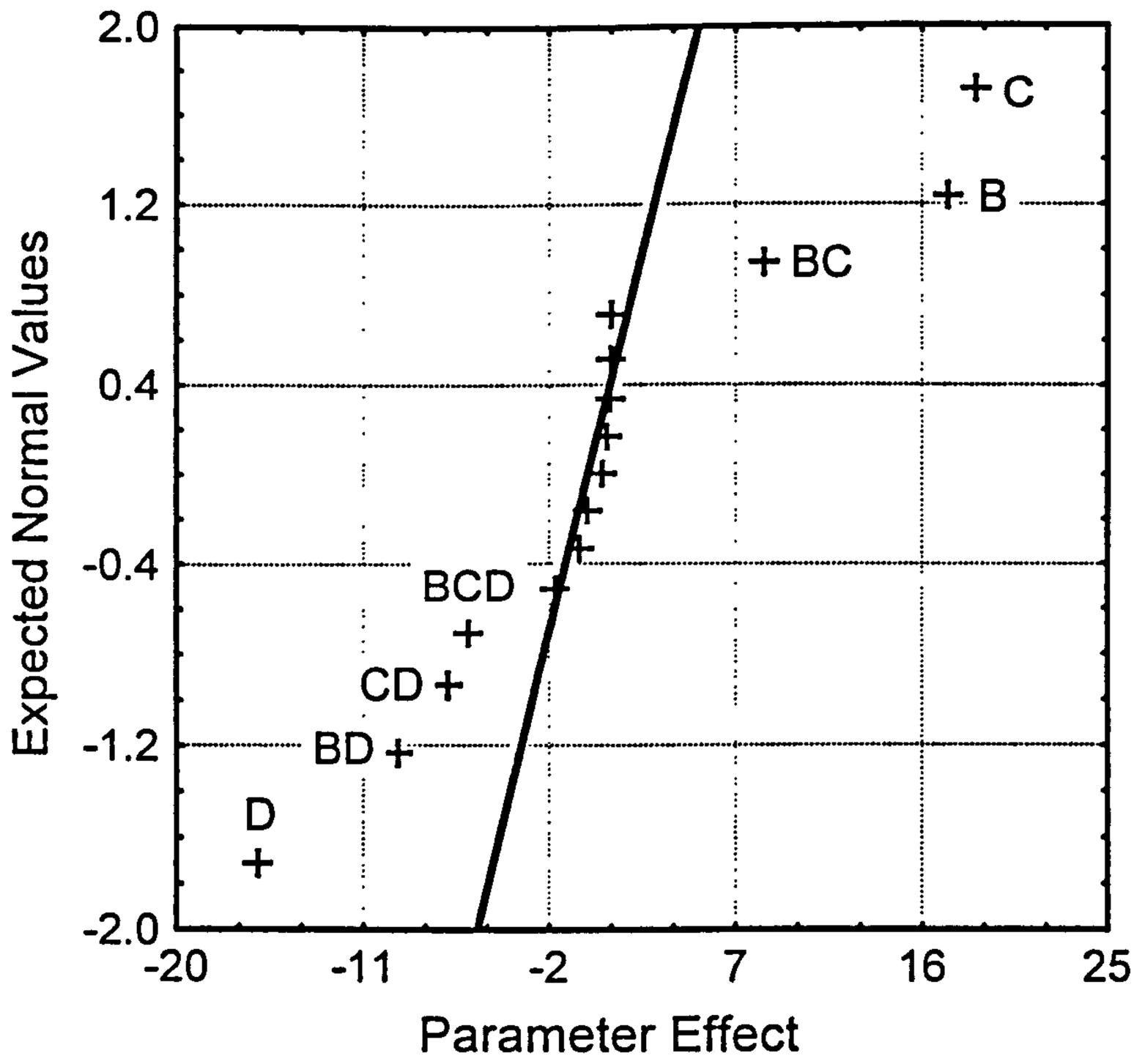

(a) Normal Probability of the Location Effects

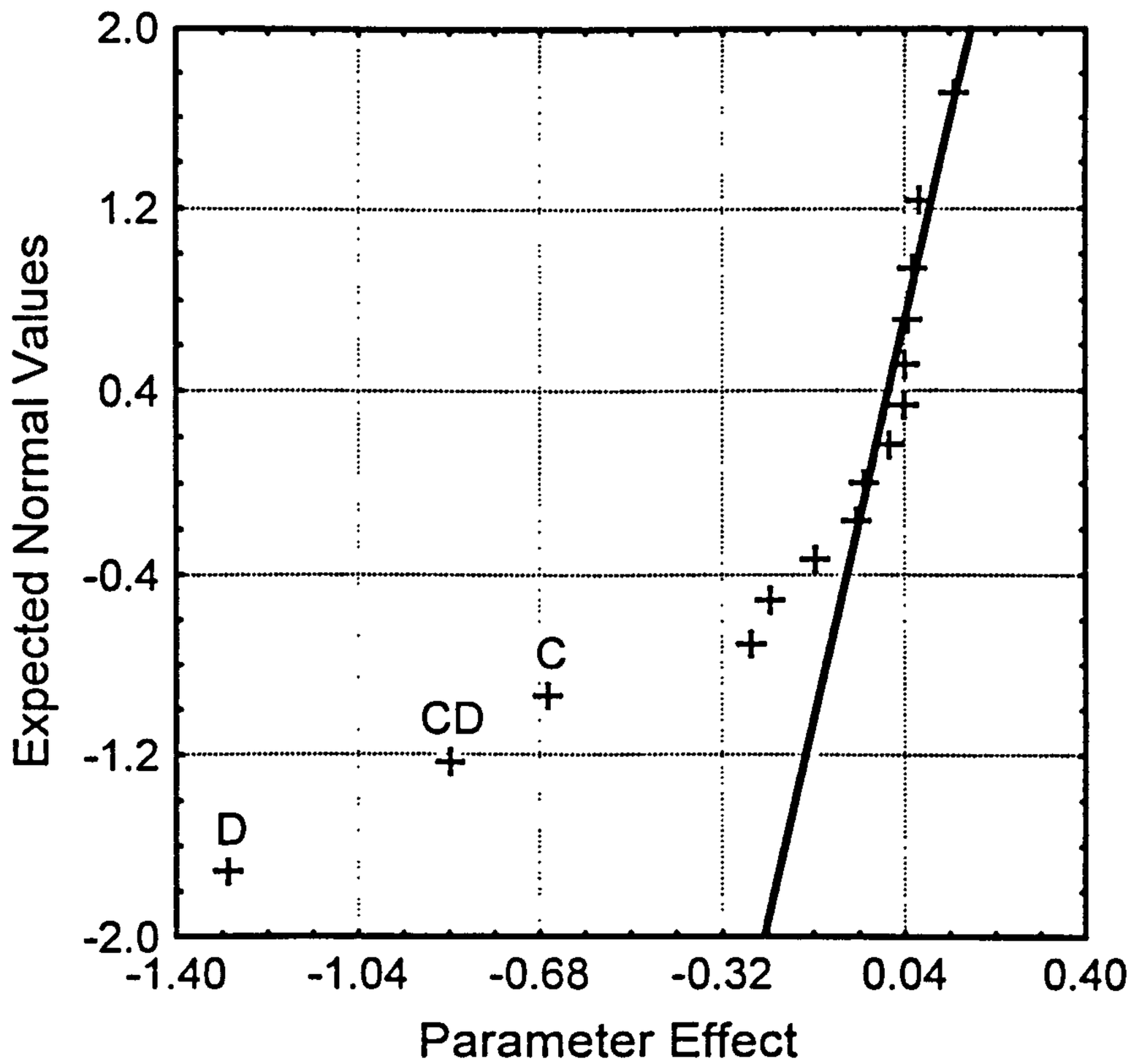

(b) Normal Probability of the Dispersion Effects

Fig. 4.5. Normal Probability Plots of the Plating Bath Experiment

4.5.2.1 Analysis of the Mean Responses

The analysis of mean plot for the significant location factors, which shows the change in the average plating thickness when the parameter is switched from its low (-) to high (+) level, is shown in Fig. 4.6. It can be observed that the plating duration (B) and average current density (C) have strong positive effects on the average thickness while the width of the pattern (A) and the electrode separation (D) have strong negative effects, although the effect of pattern width is much weaker when compared with the other active factors. A thinner deposit results when the pattern width or electrode separation is large. The interaction plot of Fig. 4.7 shows that the combination of low plating duration (B(-), 40 mins) and high average current density (C(+), 37.7 mA/cm^2) gives essentially the same deposit thickness as the B(+)C(-) combination, this is because the total ampere-hour are approximately the same for the two combinations. However, the dispersion effect of both B and C on the run-to-run (between-board) variation is found to be smaller for shorter plating duration. Therefore, for a particular target value of deposit thickness, the use of higher current density and lower plating duration is more desirable.

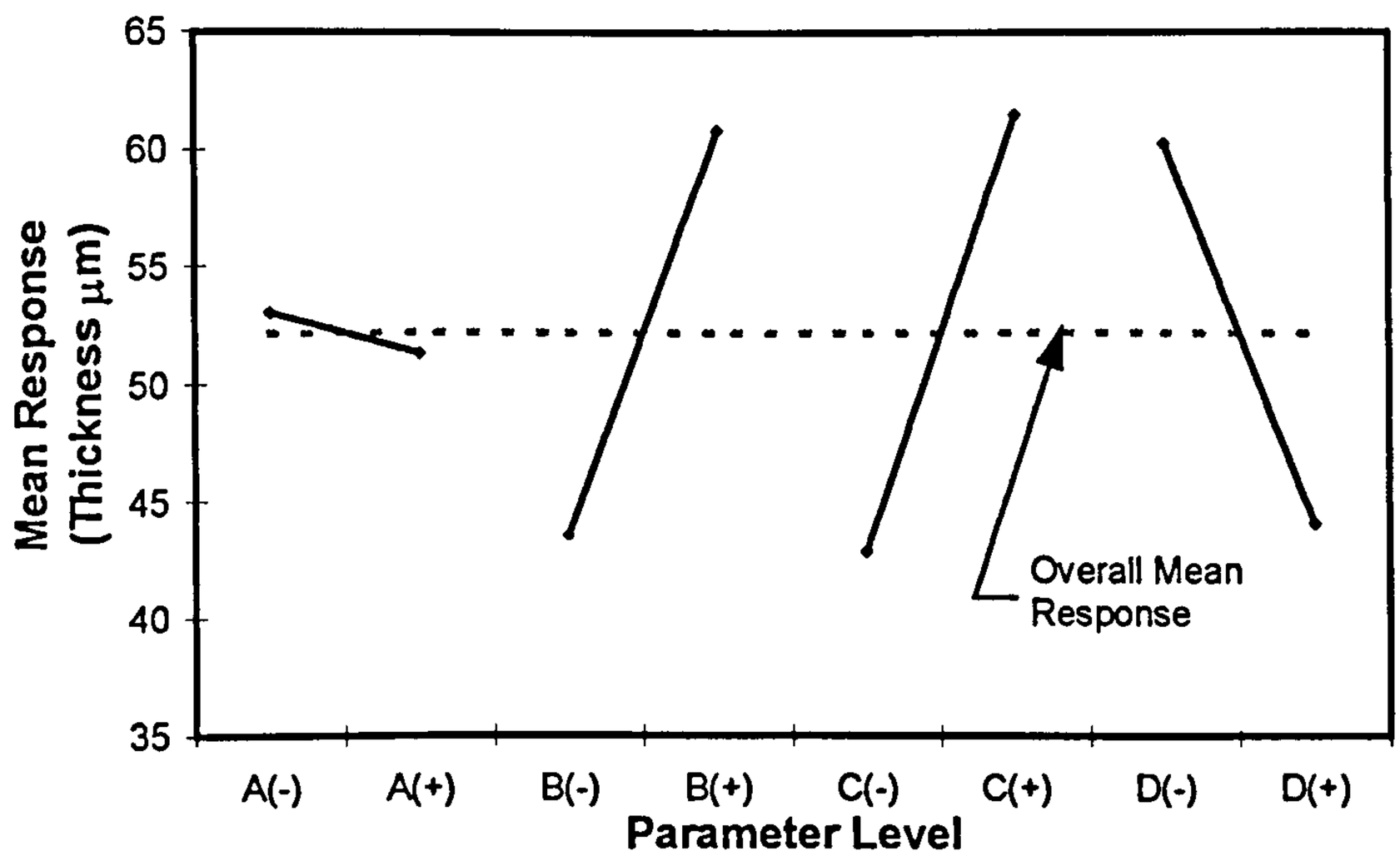

Fig. 4.6 : Analysis of Mean Plot for the Plating Bath Experiment (Mean Responses)

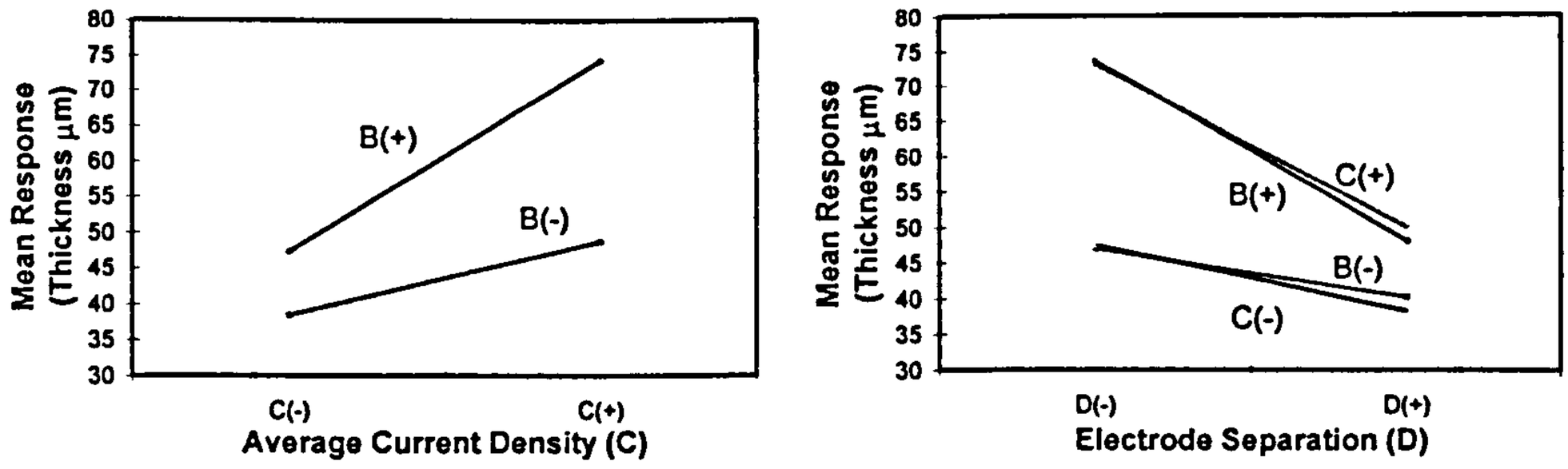

(a) BC Interaction (b) BD and CD Interaction

Fig. 4.7 Interaction Plots for the Parameter B, C and D

4.5.2.2 Analysis of the SD Responses

The analysis of mean plot for the SD responses of Fig. 4.8 shows that both the average current density (C) and electrode separation (D) has strong negative effect on the workpiece level variation. However, their respective effect cannot be considered alone as their interaction is found to be significant. The aggregate effect of the two parameters is shown as the interaction plot of Fig. 4.9(a), which shows that minimum variation results when both of them are at their high levels, i.e. 37.7 mA/cm^2 and 27.9 cm, respectively. The workpiece level uniformity is poor regardless of the level of the average current density when a small electrode separation (12.7 cm) is used. On the other hand, the positive effect of electrode separation on the plating uniformity is attenuated when a large average current density is used, thus minimizing the thickness variability. However, it is found also that the workpiece level variation is highly sensitive to the change of the average current density when a large electrode separation is employed. Combined with the analysis results of the mean responses presented in Sec. 4.5.2.1 above, it can now be concluded that a large average current density and electrode separation coupled with a short plating duration will give better workpiece level uniformity within the operability region. Furthermore, Fig. 4.9(b) shows the mean deposit thickness for the combination of C(+)D(+) under different pattern widths (A) and plating durations (B), and the corresponding Faraday's prediction. It shows that the average plating rating is not sacrificed for reduced variability when a large average current density and electrode separation is used.

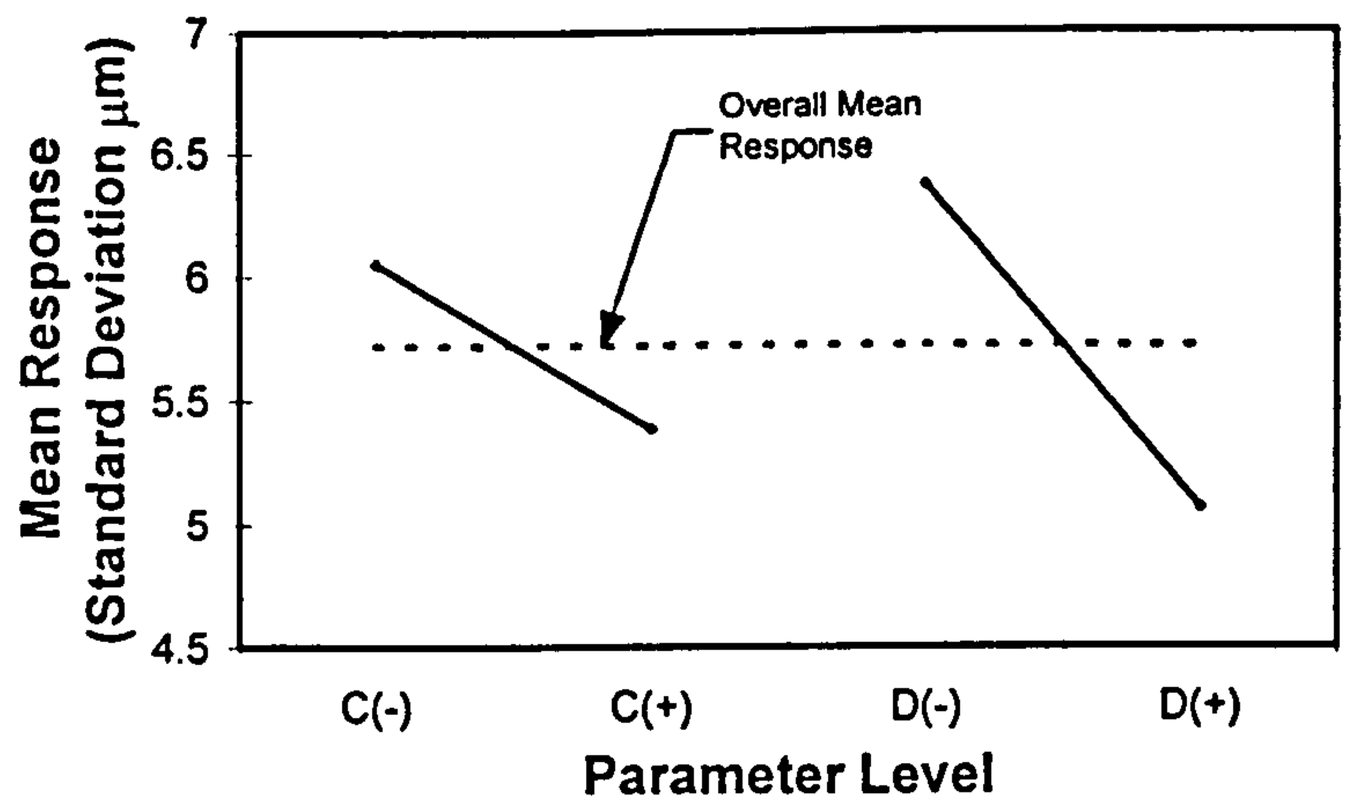

Fig. 4.8 : Analysis of Mean Plot for the Plating Bath Experiment (SD Responses)

4.5.3 Finding the Approximate location of Optimum Region and the First-Order Model

Knowing that the average current density (C) and electrode separation (D) are the two active factors affecting the workpiece level thickness variability, a response surface approach was adopted to identify the local minimum within the process window, i.e., the combination of the two factors giving minimum thickness variation. Firstly, the approximate region within which the optimal point lies is located. As parameters A and B were found to be insignificant in the second round experiment, the 2^4 design was *projected* [Montgomery, 97] into a 2^2 design with eight replicates. The mean standard deviation ($\bar{\sigma}$) of the eight boards in each replicate was then taken as the response, as summarized in Table 4.7 below.

Factors C	*Factors* D	*Standard Deviation*		$\bar{\sigma}$ *(mm)*	*Run* Order*
-	-	6.26 6.39	6.21 6.23	6.27	3, 23, 6, 31, 16, 18, 9, 27
+	-	6.82 6.80	6.02 6.22	6.47	11, 19, 5, 28, 7, 32, 8, 26
-	+	5.99 5.65	5.78 5.92	5.83	13, 24, 14, 21, 10, 29, 1, 30
+	+	4.33 4.57	4.19 4.15	4.31	2, 20, 15, 17, 4, 22, 12, 25

(* second round experiment)

Table 4.7 : Projected 2^2 Design with 8 replicates and the Responses

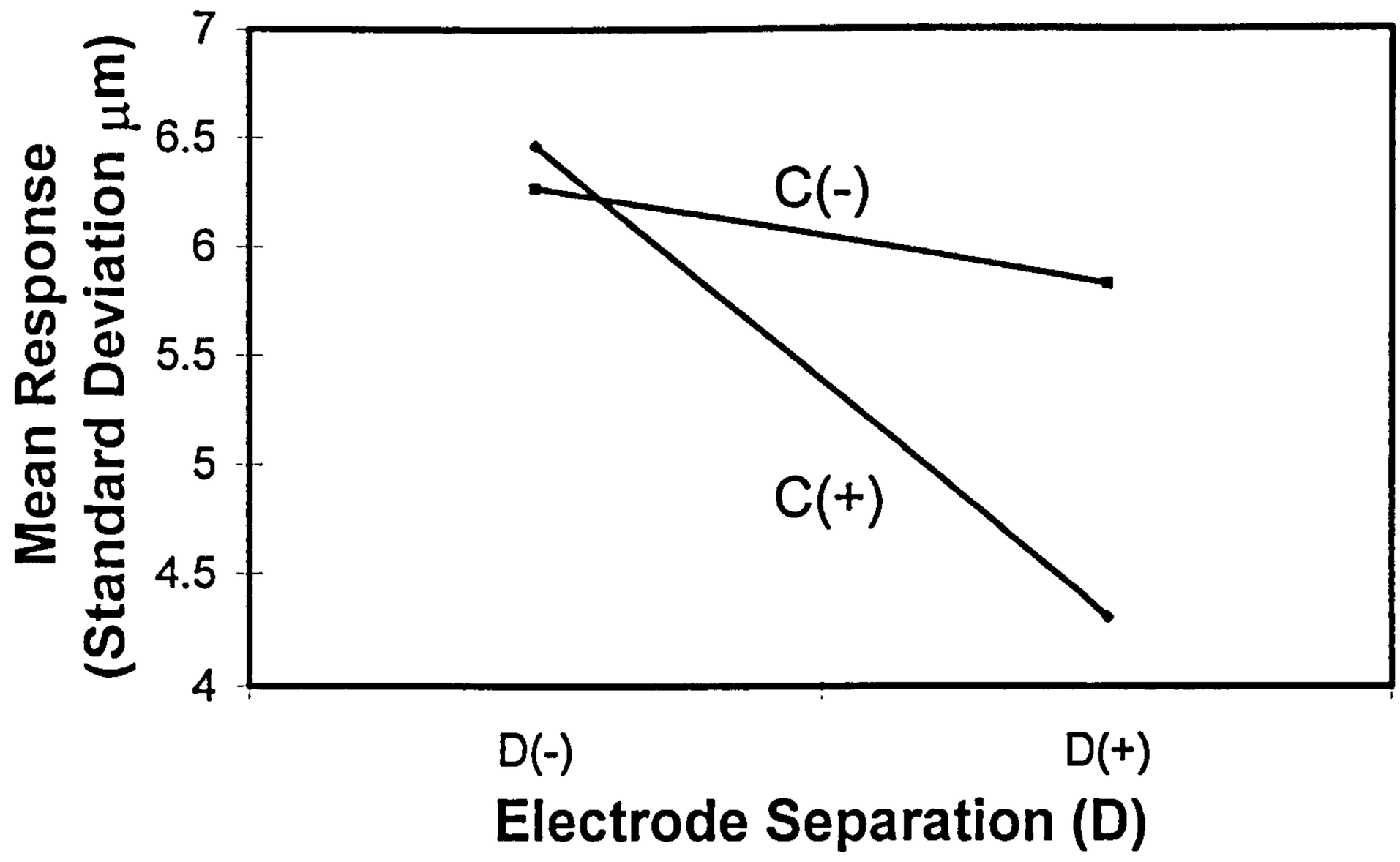

Fig. 4.9(a) : Interaction Plot of CD for the SD Responses

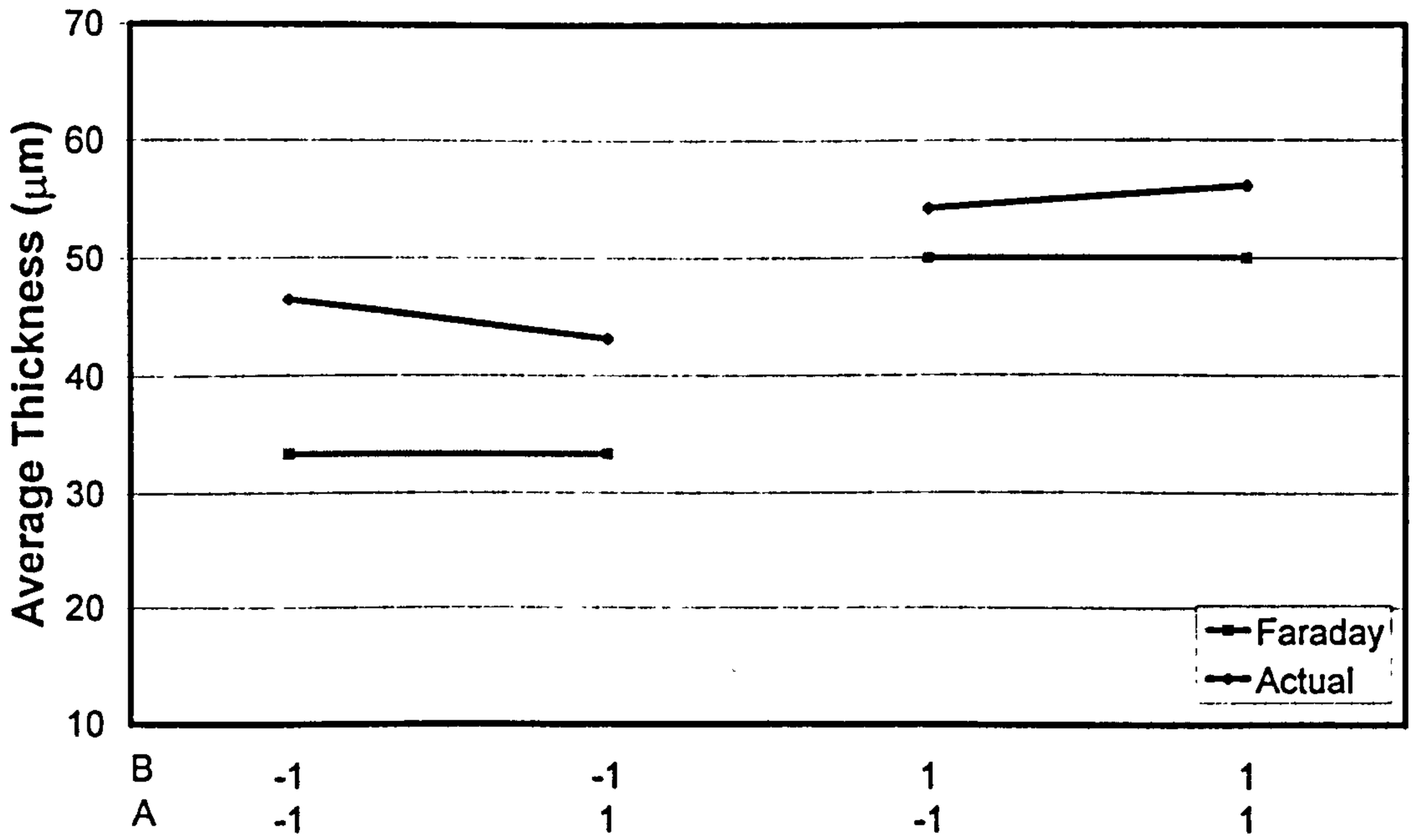

Fig. 4.9(b) : Mean Deposit Thickness compared with Faraday's Prediction for the Combination of C(+), D(+)

Recalling that the CD interaction has significant dispersion effect, a simple steepest descent path based on a first degree model involving factor C and D only is not determinable. This was also confirmed by a very large F value of 793.9 for the lack of fit of the model, which indicates that the response surface is not a plane. However, from the response graph of Fig. 4.10, the top right corner, i.e. 37.7 mA/cm^2 and 27.9 cm separation, is found to give minimum variation and therefore indicates the direction of further experimentation and possible improvement. The first degree model including an interaction term (CD), as given by equation [4.2], suggests also an increment of both C and D levels for reduced thickness variation.

$$\hat{\sigma} = 2.5825 - 0.6525C - 0.3275D - 0.4275CD \qquad [4.2]$$

where $\hat{\sigma}$ is the predicted standard deviation (μm), C and D are the coded variables of the average current density and electrode separation, respectively. For a two-level factor, the coded variable is -1 when the factor is at its low level and +1 when it is at high level. If the factor is a continuous variable, the coded value can be calculated by linear interpolation for level which is in-between the two extremes.

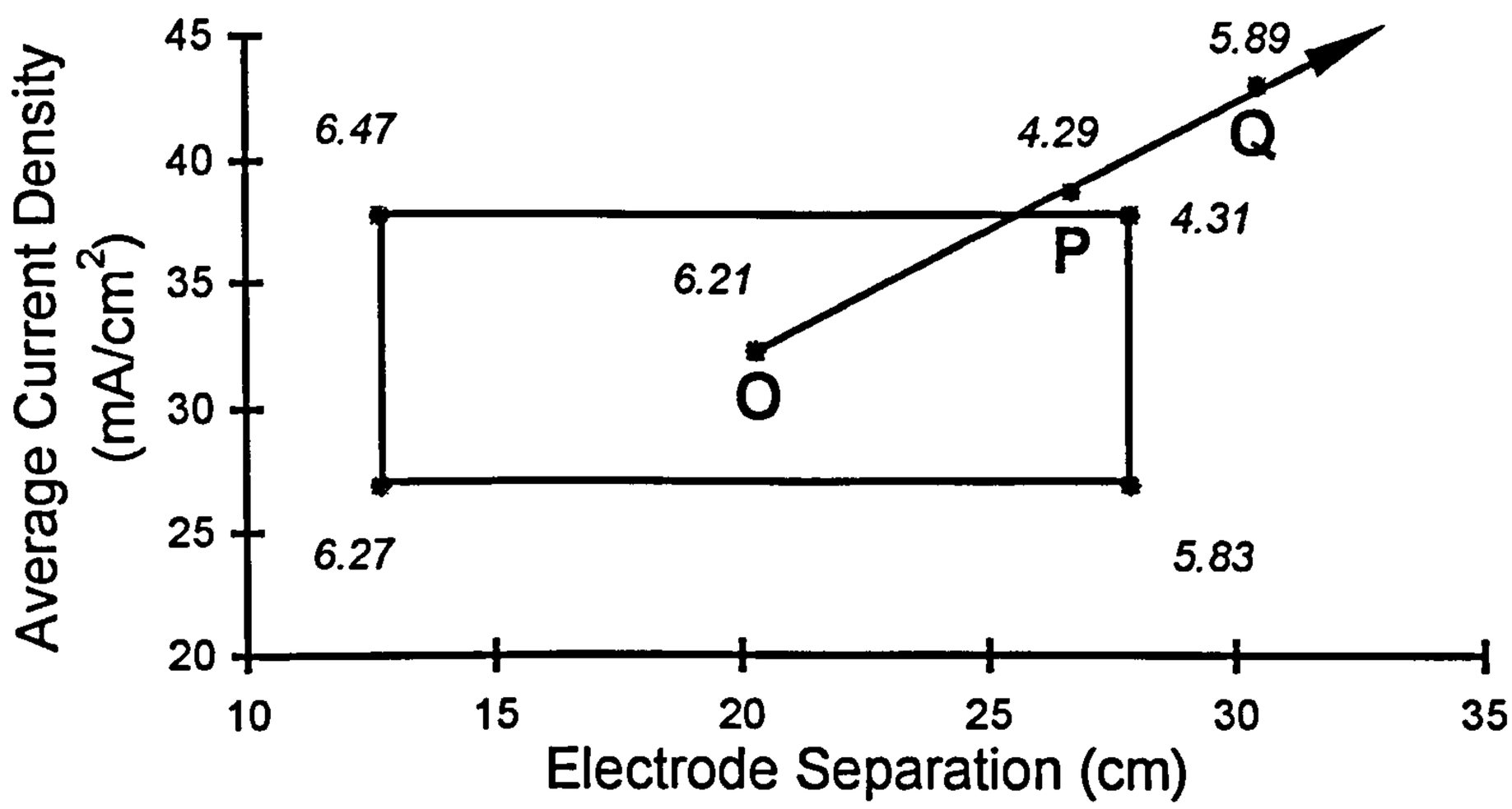

Fig. 4.10 : Response graph of the Projected 2^4 design and the Direction for further Experimentation

Using the center of the 2^2 design, (O), as a starting point, three additional experiments were performed along the approximate steepest descent path of O(20.3,32.3)

P(26.7,38.7)Q(30.5,43). Similarly, the mean standard deviations from two replicates of each point were obtained as the response, which is also shown in Fig. 4.10. The variation was found to be decreasing from point O to P and then increased again at point Q, suggesting strongly that the local minimum might lie within the vicinity of point P. A central composite design (CCD) with four vertices and a replicated center point P was therefore devised to characterize the response surface within the rectangular neighbourhood of P. Table 4.8 summaries the experimental runs and responses. The plating duration was fixed at 20 minutes for all the subsequent experiments. A first degree model was then determined as

$$\hat{\sigma} = 5.1031 + 0.2944C - 0.5020D \qquad [4.3]$$

Average Current Density (mA/cm^2)		*Electrode Separation* (cm)		*Standard Deviation*
coded	uncoded	coded	uncoded	(μm)
-	33.4	-	24.1	5.60
+	44.1	-	24.1	6.45
-	33.4	+	29.2	4.84
+	44.1	+	29.2	5.19
0 *	38.7	0 *	26.7	4.32
0 *	38.7	0*	26.7	4.25

(* using the results of the two replicates of point P)

Table 4.8 : The Central Composite Design and Responses

Subsequent ANOVA rejected the adequacy of the fitted model while single degree of freedom curvature check gave a F value of 763 (> $F_{(1,1,0.025)}$). Both the two figures suggest that a second-degree response surface with higher-degree and crossproduct terms is required.

4.5.4 Second-Order Model Building and Optimization

A *rotatable* CCD with nine runs was therefore employed to determine the additional coefficients of the second-degree polynomial. The design was formulated by simply adding four extra axial points to the design in Table 4.8 with the settings defined by

$(C, D) = (\mp\sqrt{2}, 0)$ and $(C, D) = (0, \mp\sqrt{2})$, in coded form. Table 4.9 summarizes these four additional experiments conducted and the responses.

Average Current Density (mA/cm^2)		*Electrode Separation* (cm)		*Standard Deviation* (μm)
coded	uncoded	coded	uncoded	
0	38.7	$-\sqrt{2}$	22.9	5.76
0	38.7	$\sqrt{2}$	30.5	4.42
$-\sqrt{2}$	31.2	0	26.7	5.46
$\sqrt{2}$	46.3	0	26.7	5.81

Table 4.9 : Four extra axial points of the CCD and the Responses

Based on the ten response values of the CCD, the second-degree model for the response surface was determined as

$$\hat{\sigma} = 4.2871 + 0.3964C - 0.4890D + 0.6754C^2 + 0.4507D^2 - 0.1216CD \qquad [4.4]$$

The significance and adequacy of the model was confirmed by the ANOVA tests shown as Table 4.10. Moreover, the significance of the contribution by the second-degree coefficient estimates was tested with the F statistics,

$$F = \frac{Sum\ of\ Square(2^{nd}\ degree\ terms)\ /\ 3}{Residual\ Mean\ Square\ of\ 2^{nd}\ degree\ model}$$

which gives a value of 18.62 (Prob. > F = 0.0082) and the second-order model was concluded to be necessary and adequate. The model has a good performance of R^2_A (0.93) and PRESS (1.16). The $R^2_{prediction}$ based on *PRESS* for the model is

$$R^2_{prediction} = 1 - \frac{PRESS}{Total\ Sum\ of\ Square}$$
$$= 0.794$$

indicating that the model is able to explain 79.4% of the variability in predicting new observations. Fig. 4.11 shows graphically the two CCDs used and the responses at the nine design points while the response surface of the second-order model is shown in Fig. 4.12.

Source of Variation	*SS*	*DF*	*MS*	*F*	*Prob. > F*
Regression	5.460	5	1.092	26.63	0.0036
Residual	0.164	4	0.041		
Lack of Fit	0.161	3	0.054	18	0.1712
Pure Error	0.003	1	0.003		
Total	5.624	9			

Table 4.10: ANOVA table of the 2nd Degree Model

After identifying the optimum region and the second-degree model, the stationary point of minimum response can now be determined by taking the partial derivatives of Eq. 4.4 with respect to *A* and *B*, respectively, and setting them to zero, i.e.

$$\frac{\partial \hat{\sigma}}{\partial C} = 0, \quad \text{and} \quad \frac{\partial \hat{\sigma}}{\partial B} = 0 \qquad [4.5]$$

Solving the two simultaneous equations of [4.5] gives immediately the optimum solution, in coded form, of C = -0.2477 and D = 0.5083, corresponding to an electrode separation of 28.0 cm. and an average current density of 37.40 mA/cm^2. The estimated minimum thickness variation, $\hat{\sigma}_{min}$, is calculated as 4.11 μm after substituting the coded values of C and D into equation [4.4]. The contour plot of the plating thickness variation and the stationary point is illustrated as Fig. 4.13, which shows clearly that the optimum solution found is the true minimum within the whole experimental region.

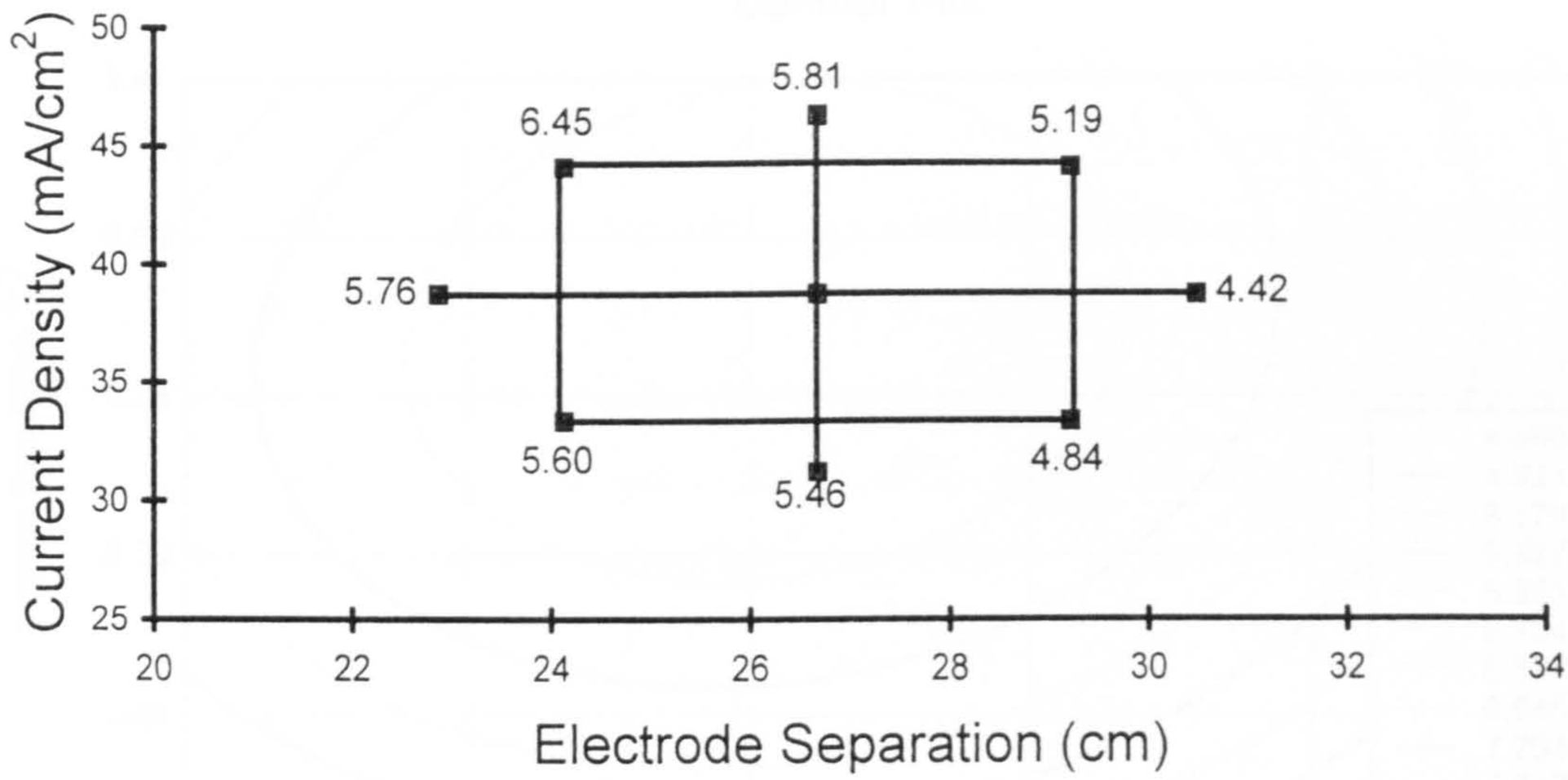

Fig. 4.11 : The Rotatable Central Composite Design and Response Values

Second Order Model : Uniform Pattern Plating

SD =4.2871+0.3964*C-0.4890*D+0.6754*C^2+0.4507*D^2-0.1216*CD

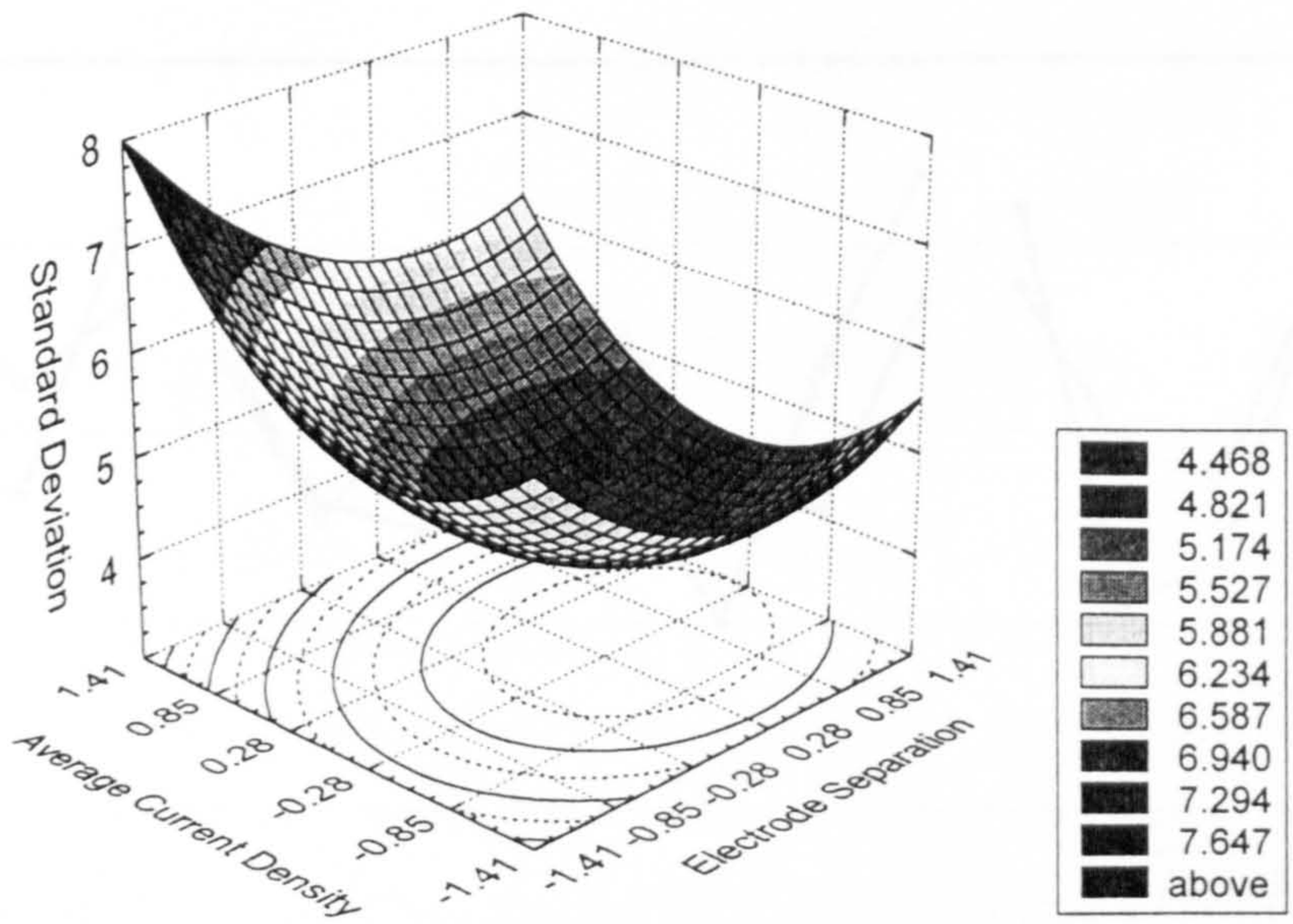

Fig. 4.12 : Response Surface and Contour Plot of the Second Order Model for Uniform Pattern Plating

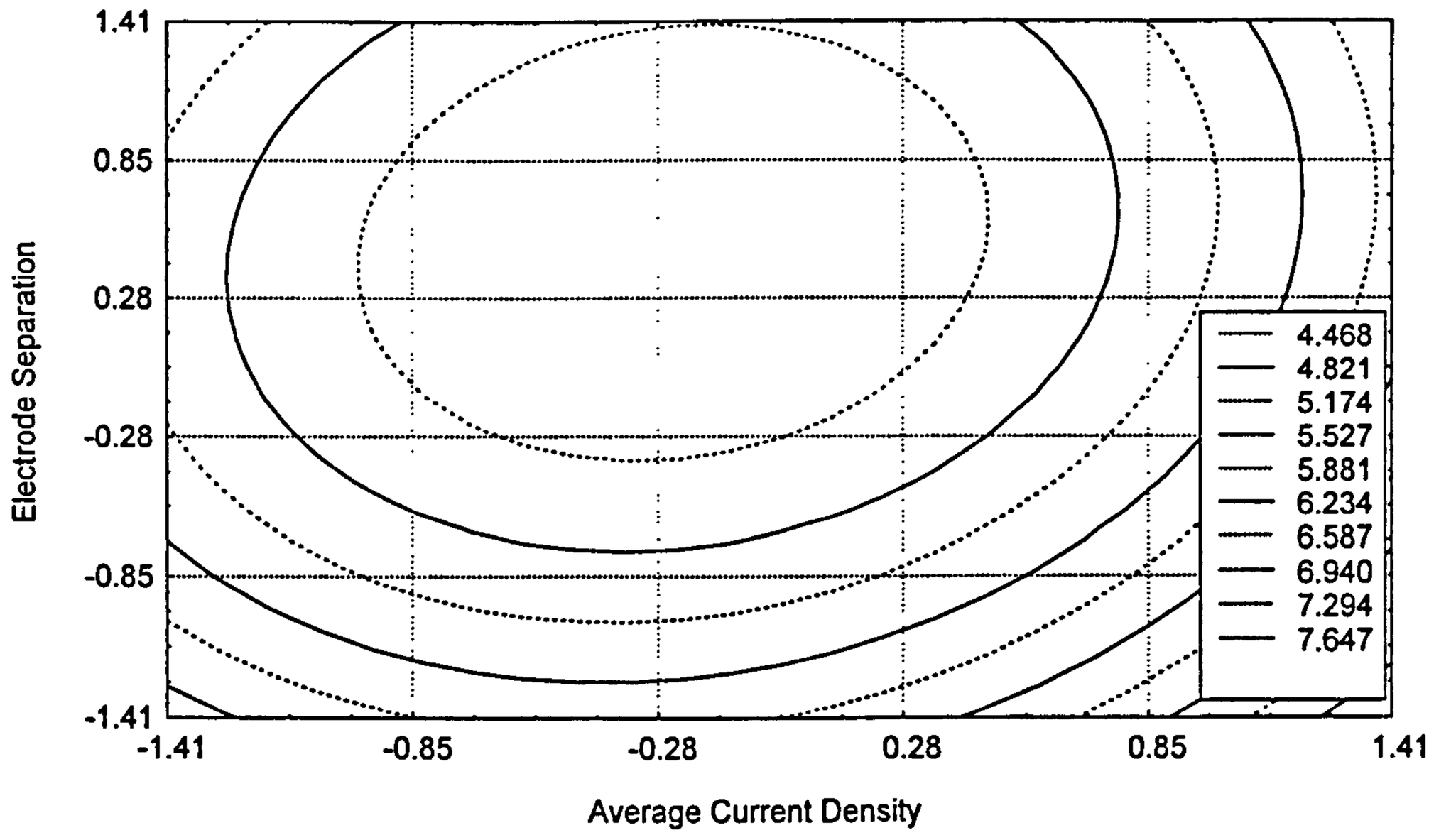

Fig. 4.13 : Contour Plot of the Second Order Model for Uniform Pattern Plating

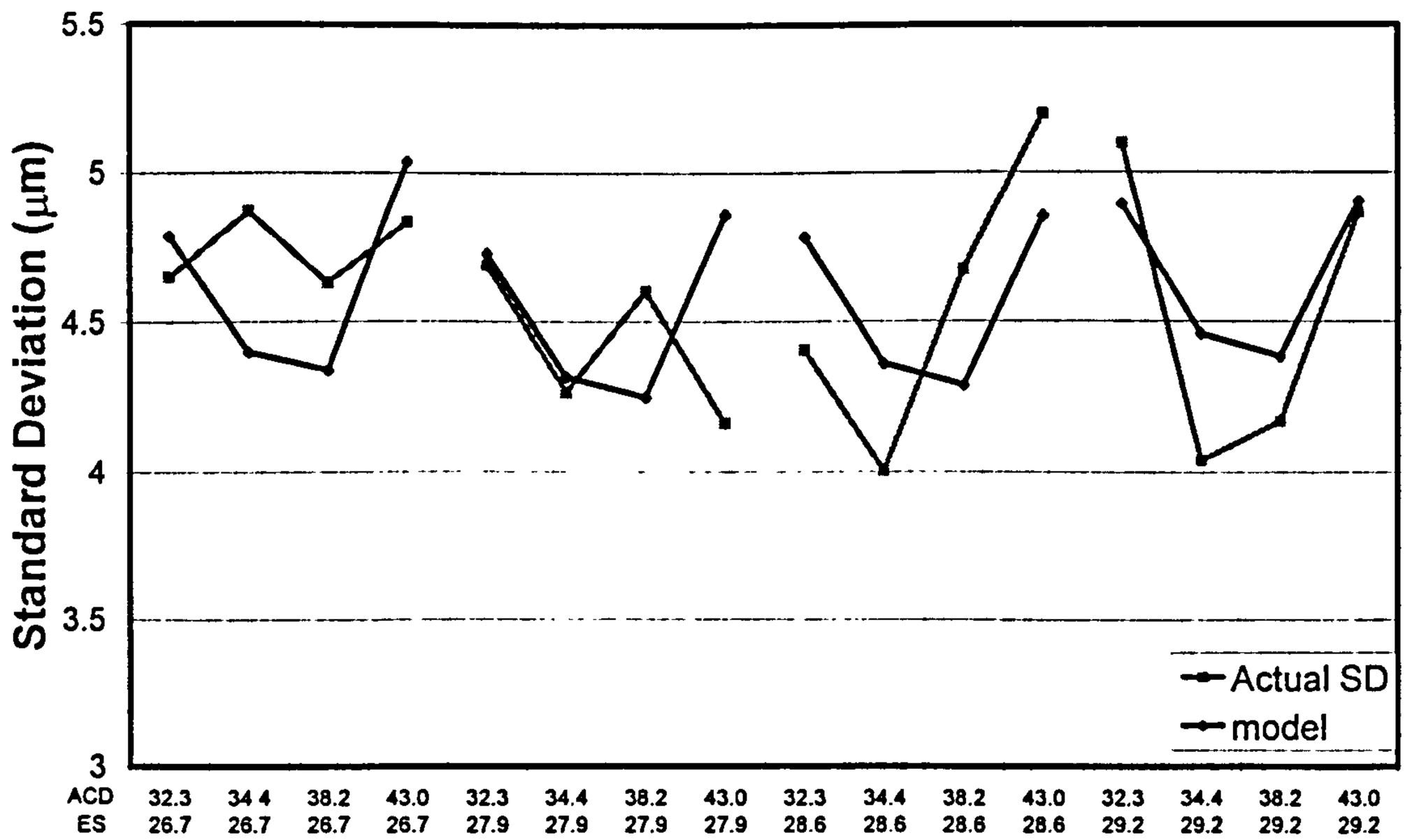

Fig. 4.14 : Verification of the Second Order Model for Uniform Pattern Plating

4.5.5 Model Verification

Verification runs for the second-order model were conducted with 16 combinations of average current density and electrode separation within the operability region. The standard deviation of 16 points over the board surface was taken as the response and the results are summarized as Table 4.11 and graphically in Fig. 4.14. Raw data is given in Appendix 4.5. The bracketed values in Table 4.11 represent the standard deviation predicted by the second-order model of Eq. [4.4]. They show that, except for one case, the model predicts reasonably well within the limits ($R^2_{prediction}$) of its predictive power and the relative error ranges from -10% to +10% of the actual standard deviation observed.

Electrode Separation (cm)	*Average Current Density (mA/cm²)*			
	32.3	34.4	38.2	43.0
26.7	4.649 (4.784)	4.868 (4.402)	4.629 (4.341)	4.831 (5.037)
27.9	4.688 (4.725)	4.269 (4.319)	4.600 (4.251)	4.165 (4.856)
28.6	4.407 (4.780)	4.005 (4.362)	4.673 (4.291)	5.199 (4.850)
29.2	5.100 (4.892)	4.042 (4.461)	4.173 (4.387)	4.863 (4.901)

Table 4.11 : Actual and Predicted Responses of the Verification Run

On the other hand, the average plating thickness is also compared with the Faraday's prediction (Eq. 4.1) assuming uniform distribution in Fig. 4.15. It is found that the actual thickness is always greater than the theoretical prediction by approximately 30%, and the difference increases quadratically with the average current density applied, as shown in Fig. 4.16. This is because only the 0.02 cm and 0.05 cm lines of the square patterns are measured but not the separating lines (0.51 cm), which can be regarded as auxiliary electrodes. The width of these lines (0.48 cm) corresponds to the optimum size of auxiliary electrode for the square pattern (AAD = 0.39) according to the calculation of [Choi and Kang, 96] for uniformly patterned cathode. They found that when the optimum or larger auxiliary electrode was used, the current densities on

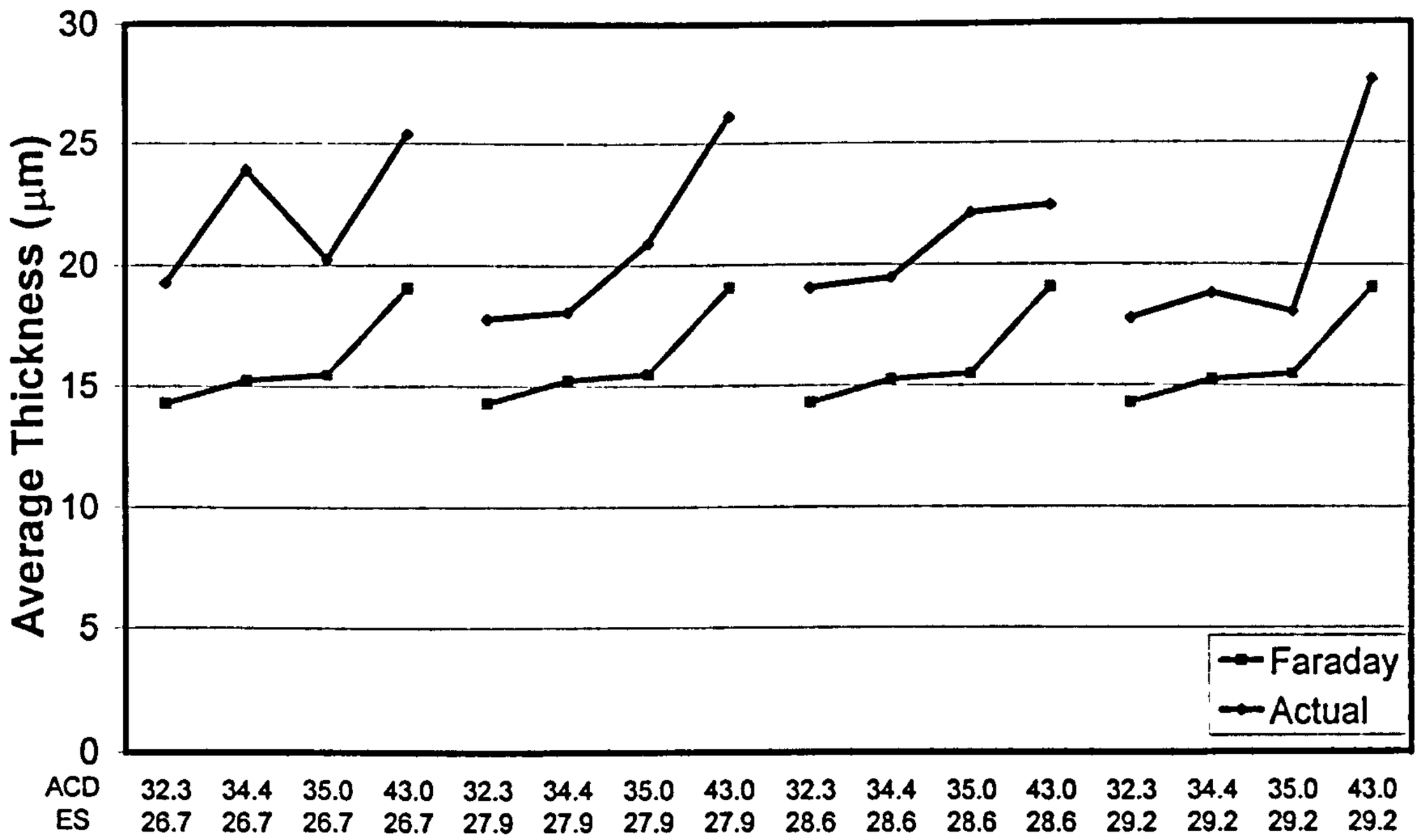

Fig. 4.15 : Actual Average Plating Thickness compared with Faraday's Prediction of the Verification Runs

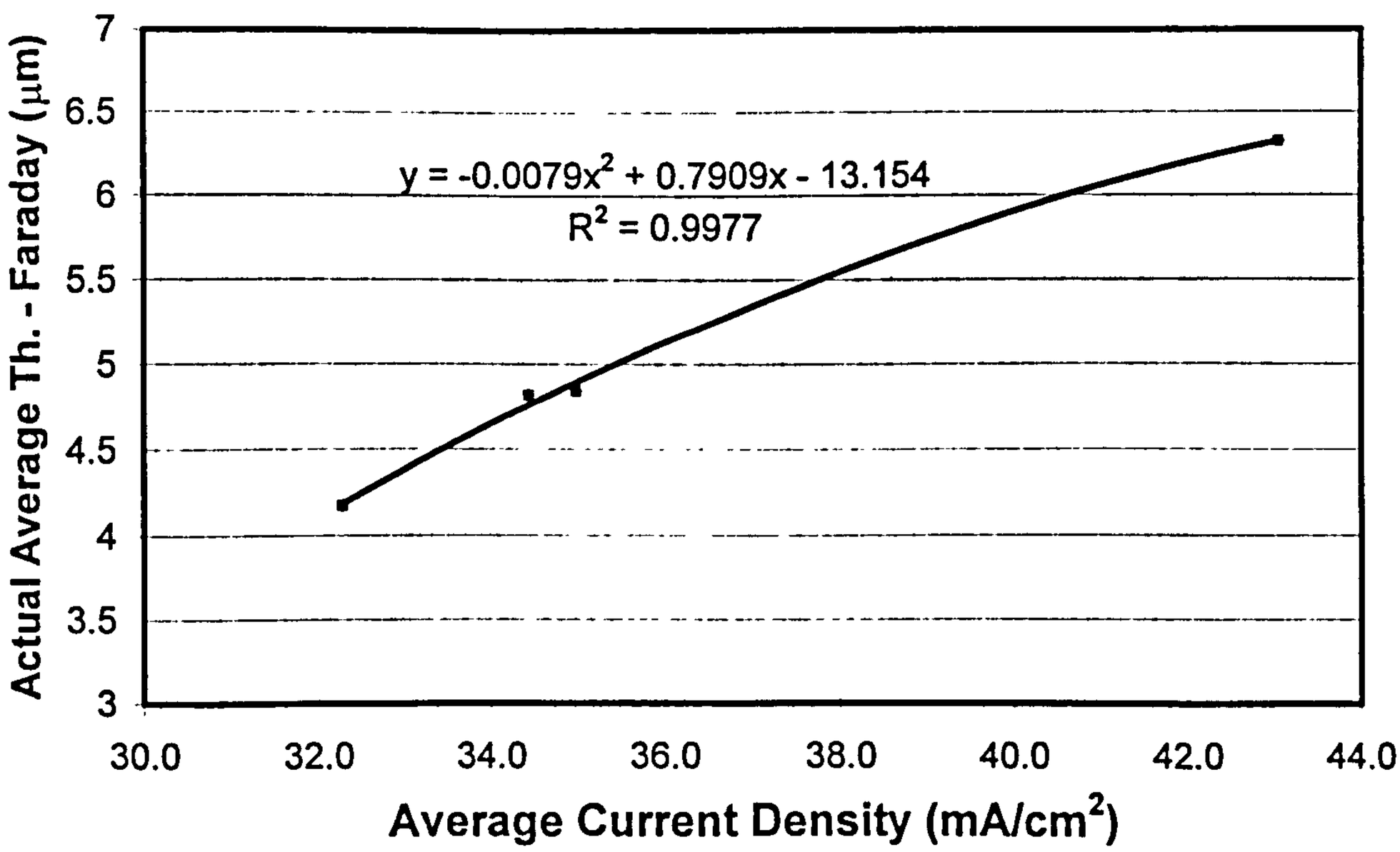

Fig. 4.16 : Difference between Actual Average Plating Thickness and Faraday's Prediction as a function of Average Current Density

the patterned surface became higher than the Faraday's prediction. Furthermore, the normalized difference and the ratio of the actual deposit thickness to the Faraday's prediction was found to be highly correlated with the average current density, as depicted in Fig. 4.17(a) and (b). Both the two graphs show that the deviation from the Faraday's prediction reaches a minimum when the average current density is approximately 38.9 mA/cm[21], which is also very close to the optimum value of 37.40 mA/cm^2 identified above. This suggests the reason why an optimum workpiece level plating uniformity is achievable at a particular combination of average current density and electrode separation, i.e. the thickness variation is minimized when the deviation of the average deposit thickness from the Faraday's prediction is minimized . The effect of the line width can be also viewed as that of the active area density and these two effects were further studied in the next round of investigations.

4.6 Experimental Study of Copper Plating of Non-Uniform Patterns

The active area density (AAD), proposed by [Mehdizadeh *et al.*, 92], is the fractional electroactive area within a particular region of interest (Sec. 2.4.3). It is found that regions with smaller AAD tend to grow thicker deposits than those with larger AAD [Yung *et al.*, 89], [Mehdizadeh *et al.*, 92, 93]. An additional variable, the active area density ratio (AADR), which is defined as the ratio of the AAD of two neighbouring regions, was introduced in this round of experiments to quantify such dispersion effect of the lithographic patterns. Fig. 4.18(a) and (b) show two "zebra" patterns of different AADR, which are also the test boards used in the experiments. The actual dimensions of the test board are 15.3 cm x 5.7 cm and that of the pattern are 10.7 cm x 5.7 cm including the rectangular border.

The patterns of each test board are made up of three regions with two different AADs. The AAD of the left and right region is fixed at 0.1, i.e. the black lines represent 10% of the regional area, while that of the center is 0.9 (Fig. 4.18a) and 0.2 (Fig. 4.18b),

[1] The average current density for which minimum deviation occurs is found from the quadratic relationship as 38.89 mA/cm^2 for the normalized difference and 38.91 mA/cm^2 for the ratio. The two turning points in Fig. 4.17(a) and (b) are the results of the two replicates of Point P in Table 4.8.

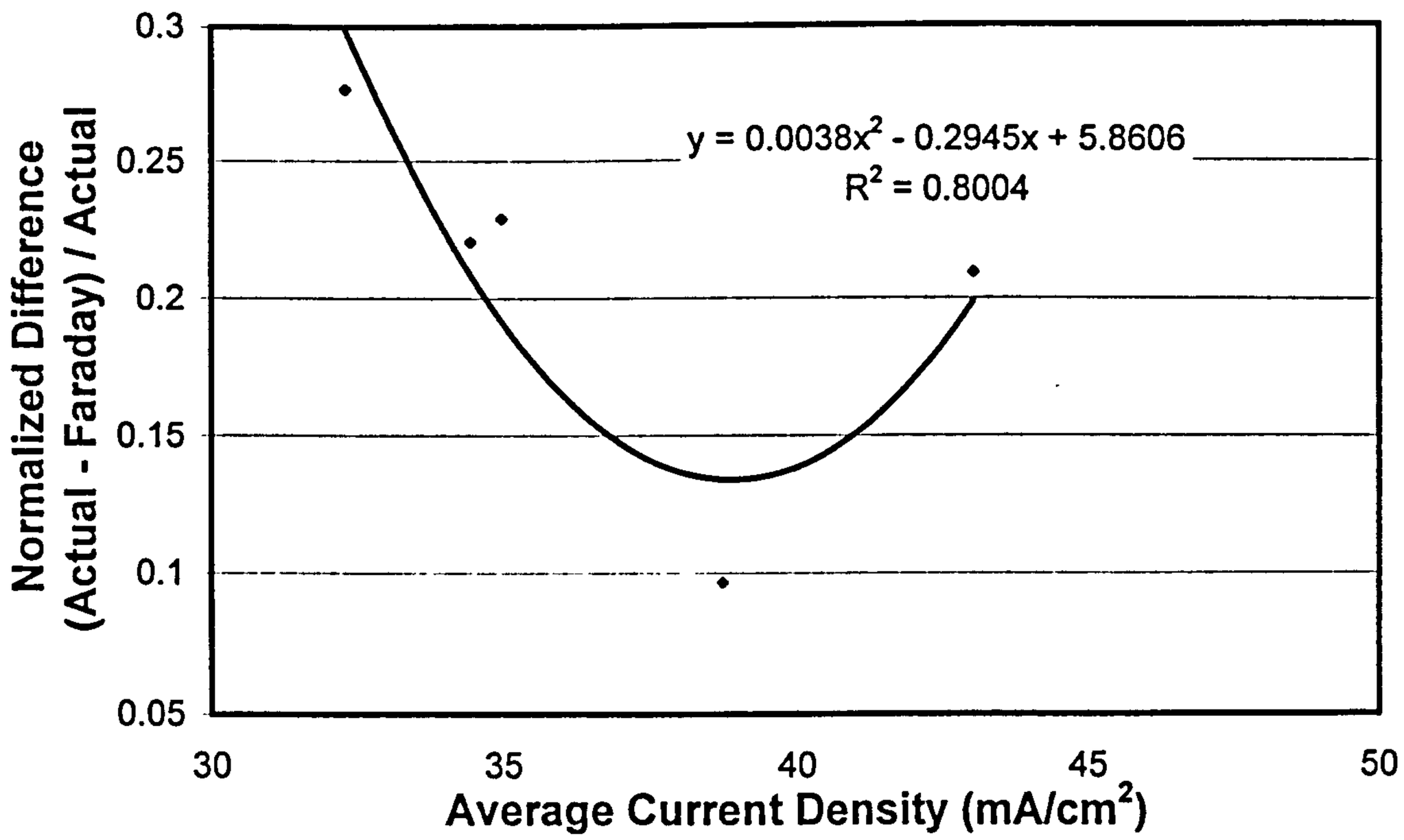

Fig. 4.17(a) : Empirical Relationship between the Normalized Difference and the Average Current Density

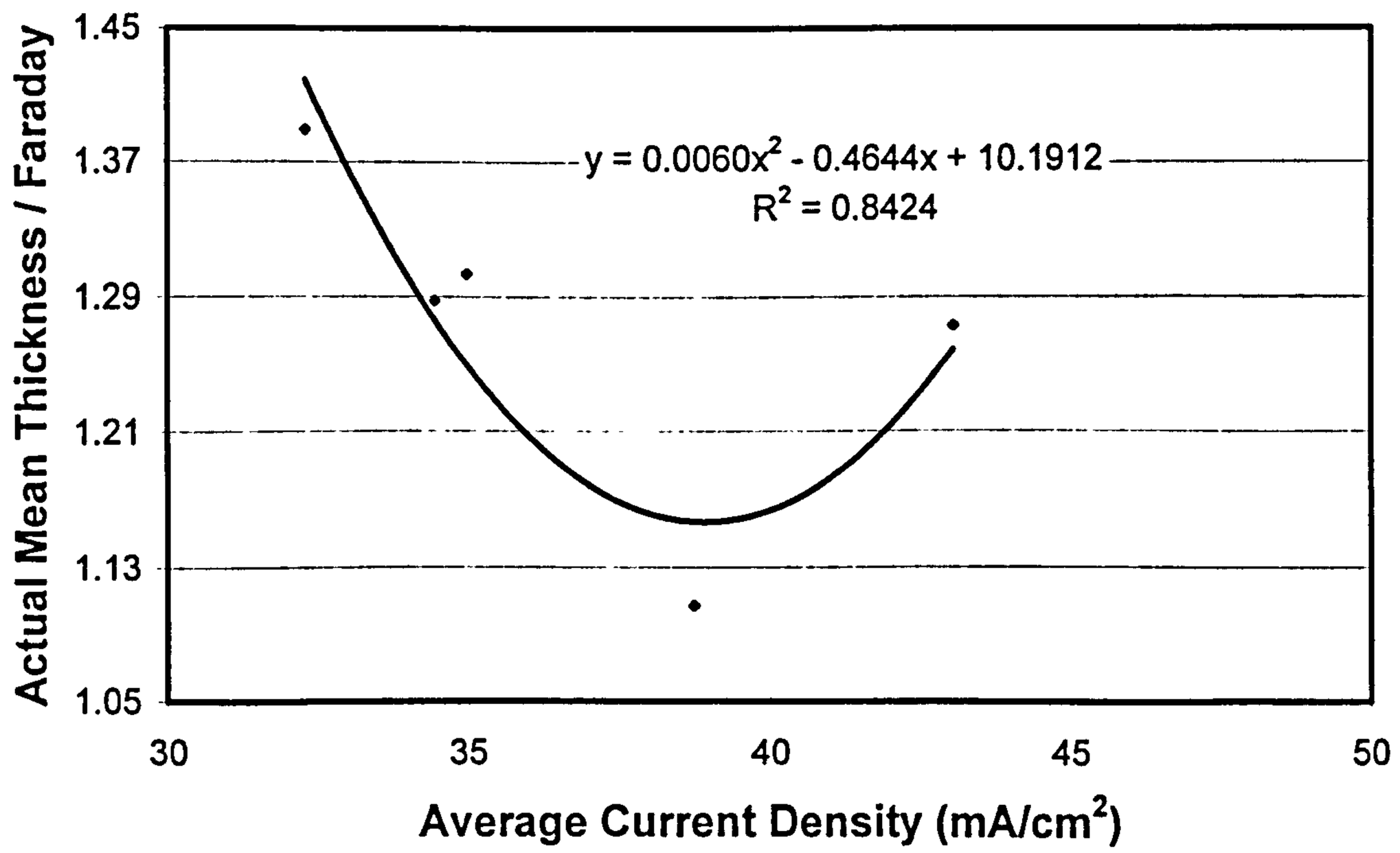

Fig. 4.17(b) : Empirical Relationship between the Ratio of Actual Thickness to Faraday's Prediction and the Average Current Density

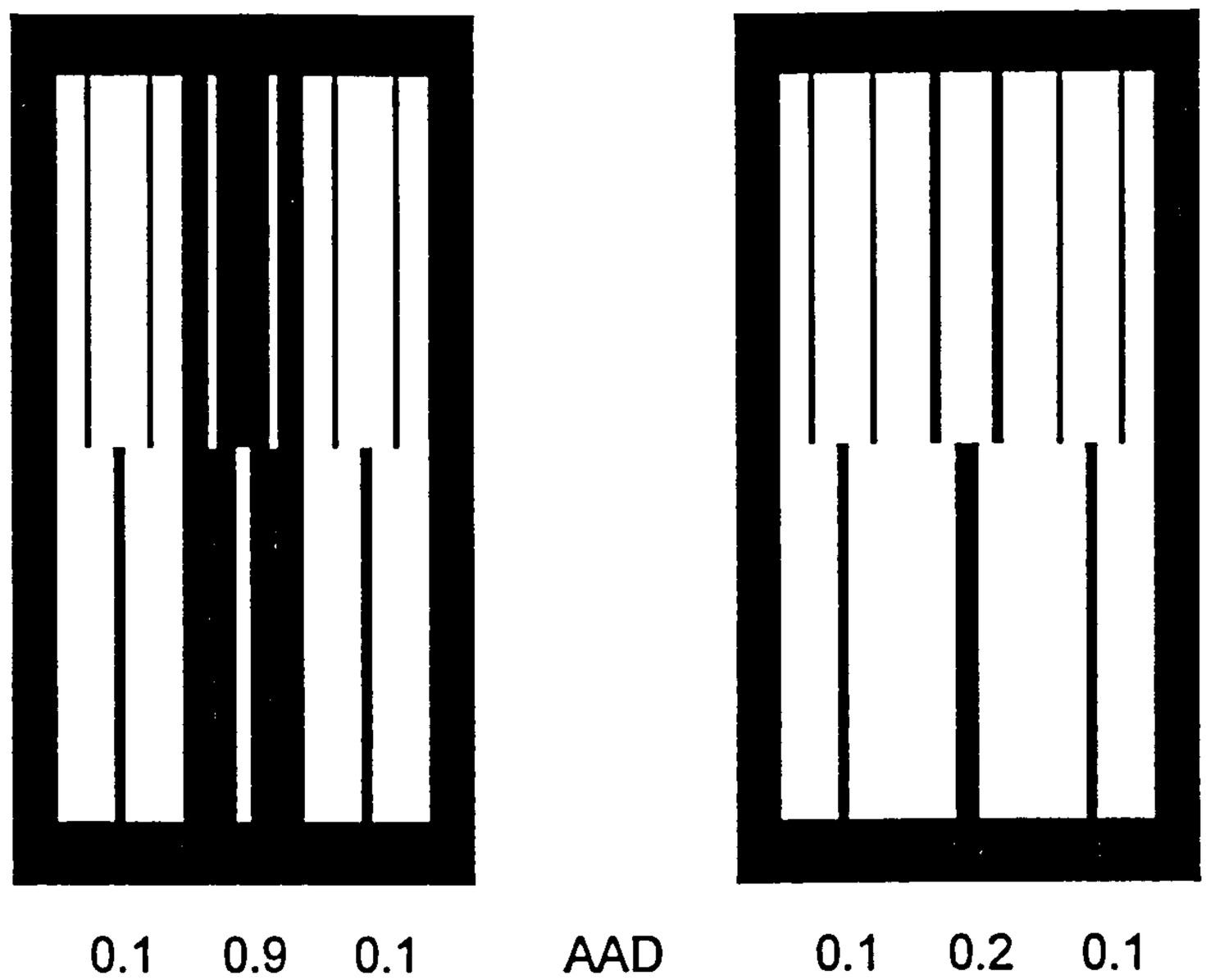

(a) AADR = 9 (b) AADR = 2

Fig. 4.18 : The "Zebra" Pattern used in the Non-uniform Pattern Plating Experiment (Not in Scale)

thus simulating an AADR of 9 and 2, respectively. The average active area density, $\overline{AAD}$, over the cathode is 0.37 for an AADR of 9 and 0.13 for an AADR of 2. The rectangular border serves as an auxiliary electrode and its area is not included in the AAD calculations. The auxiliary electrode is used here to tamper the edge and corner effect [Shih and Pickering, 87], so that practically any remaining nonuniformity could be attributed to non-uniform active area density. Similar method was employed by [Mehdizadeh *et al.*, 93]. The AADR and $\overline{AAD}$ of the upper and lower half of the pattern is the same, but the width of the lines in the lower half region is double that of the upper region so that the effect of line width can also be studied.

The relationship between the average current density, electrode separation, AADR and the workpiece level plating uniformity was first studied with a replicated 2^3 full factorial design of 16 runs. The empirical model obtained was then used to determine the optimum combination of the first two parameters that minimize the thickness variability among patterns of different active area densities. The model was finally verified with a "zebra" pattern and a simple circuit with different AADRs.

4.6.1 The First-Order Model

The parameter settings and the responses of the replicated 2^3 design are summarized in Table 4.12 below. The plating thickness was measured directly with a Talysurf profilometer to eliminate the error induced by the inherent variability of the base copper thickness and the X-ray thickness gauge. A similar approach was also adopted by [Mehdizadeh *et al.*, 93] for measuring the deposit thickness at a pattern level. The standard deviation of 12 thickness readings, 6 from each region of AAD, was taken as the response to reflect the workpiece level plating uniformity. The measurement scheme and a typical thickness profile is given in Appendix 4.6. The background variables of the experiment were kept as : copper sulphate 75 g/litre, sulphuric acid 185 g/litre, chloride 70 ppm, brightener 5 ml/litre, plating duration 20 minutes. Raw data are given in Appendix 4.7. The current efficiency of each experiment was determined by the method of weight gain and summarized as Fig. 4.19 and an average efficiency of 86.4% was found for this round of experiments.

Board no.[1]	*Coded Variables*			*Uncoded Variables*			*SD (μm)*	
	A	*B*	*C*	*ACD (mA/cm²)*	*ES (cm)*	*AADR*	*1st trial*	*2nd trial*
4, 5	-1	-1	-1	30.1	15.2	2	3.288	2.419
2, 9	+1	-1	-1	40.9	15.2	2	5.335	4.274
3, 6	-1	+1	-1	30.1	25.4	2	2.652	2.556
1, 7	+1	+1	-1	40.9	25.4	2	6.369	7.718
15, 19	-1	-1	+1	30.1	15.2	9	7.602	5.614
14, 18	+1	-1	+1	40.9	15.2	9	10.045	7.882
16, 20	-1	+1	+1	30.1	25.4	9	5.458	5.378
13, 17	+1	+1	+1	40.9	25.4	9	10.076	11.839

Table 4.12 : The Replicated 2^3 Design and the SD Responses

The average current density (A), AADR (C) were found to be highly significant in affecting the workpiece level thickness variation, as shown in the ANOVA result of Table 4.13. It was noted that although the AB interaction was still significant at the

[1] A total of 20 boards were actually plated in random order, but four sets of erroneous data from board no. 8, 10, 11 & 12 were discarded.

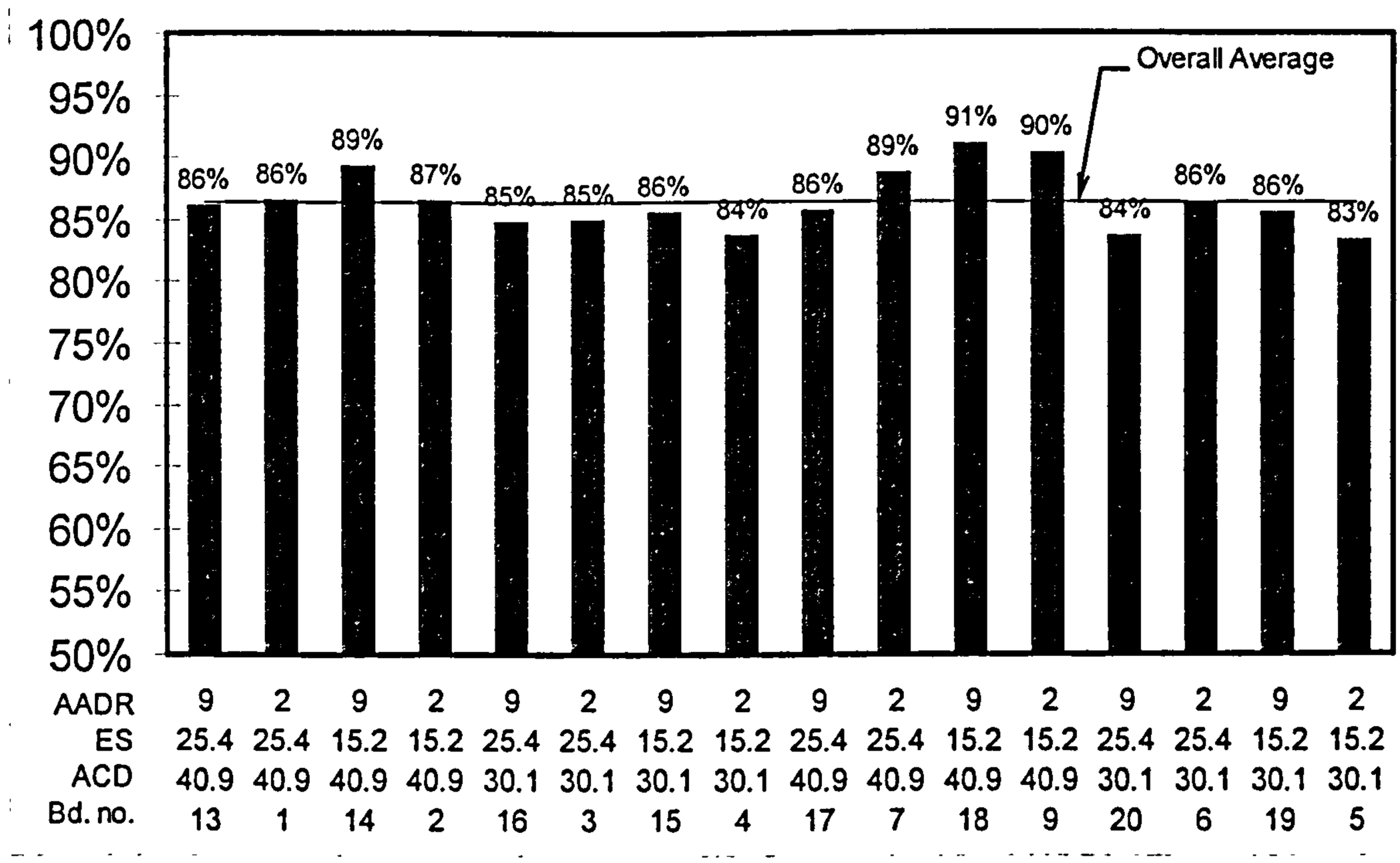

Fig. 4.19 : Current Efficiency of the Non-Uniform Pattern Plating Experiment

Source of Variation	*SS*	*DF*	*MS*	*F*	*Prob. > F*
Model	115.65	7	16.52	17.03	< 0.0001
A	51.02	1	51.02	52.60	< 0.0001
B	1.95	1	1.95	2.01	0.194
C	53.60	1	53.60	55.26	< 0.0001
AB	8.04	1	8.04	8.29	0.021
AC	0.57	1	0.57	0.59	0.464
BC	0.35	1	0.35	0.36	0.565
ABC	0.12	1	0.12	0.12	0.738
Residual	7.73	8	0.97		
Total	123.38	15			

Table 4.13 : ANOVA of the First Order Model for the Non-Uniform Pattern Plating Experiment

2.1% level, its influence was much weaker when compared with A and C, as reflected by the relative magnitudes of their coefficients in the first-order of Eq. 4.6. Besides, it acted differently when compared with the case of uniform pattern (Fig. 4.9(a)), as illustrated in Fig. 4.20 below. It was evident that the plating uniformity was significantly better when a low average current density (30.1 mA/cm^2) was used, irrespective of the levels of the electrode separation. Duncan's test confirmed that the difference between the mean (standard deviation) responses was not significant when the average current density was at the low level. The same interaction effect was observed for both levels of the AADR.

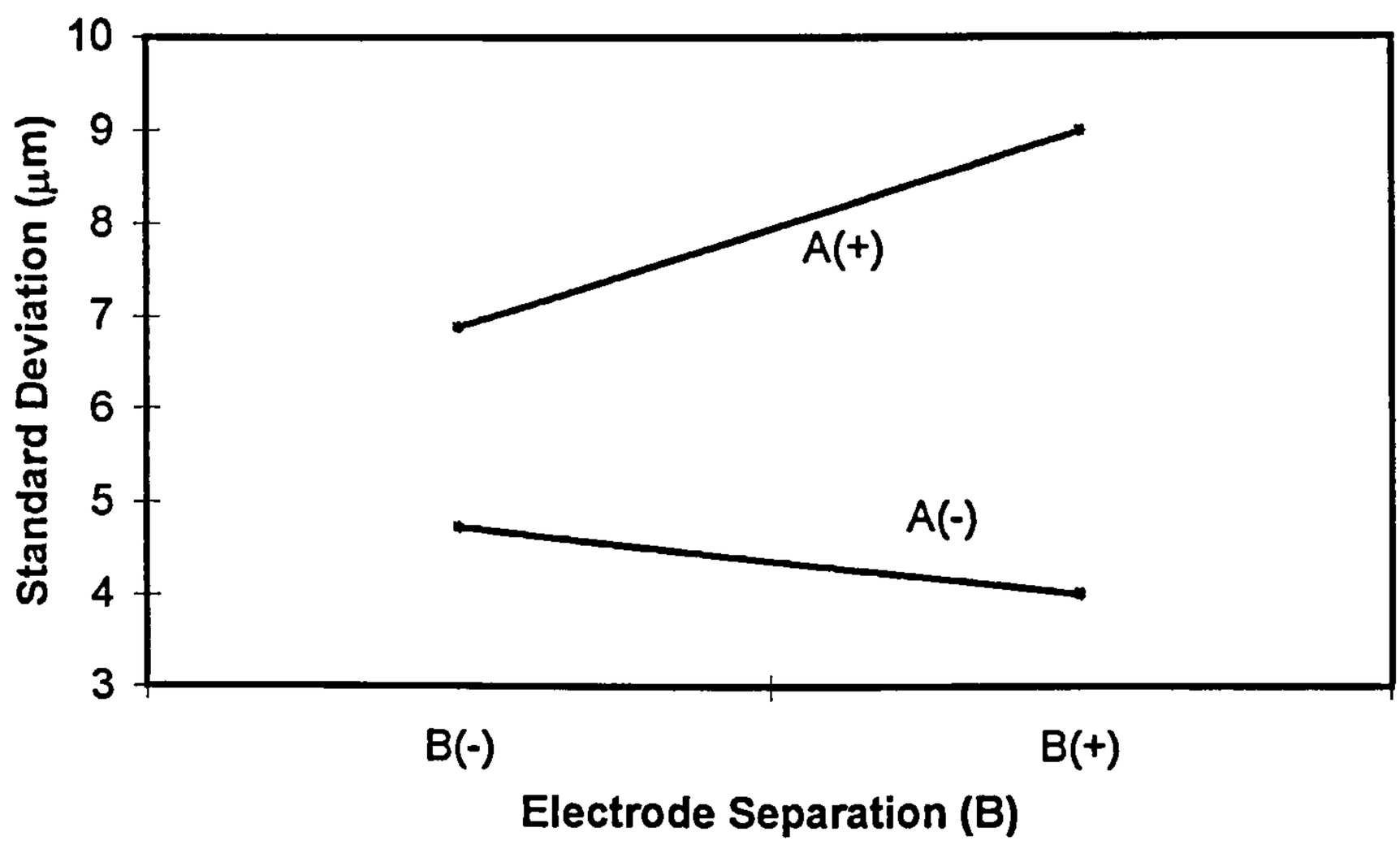

Fig. 4.20 : AB Interaction for the Non-uniform Pattern Plating Experiment

The best model generated by backward elimination suggested a 5-term first-order model of A, B, C and AB (R^2_A 0.90, *PRESS* 18.55, $R^2_{prediction}$ 0.85), but the full model was later found to be more powerful in predicting the actual standard deviation despite of its inferior R^2_A (0.88), *PRESS* (30.91) and $R^2_{prediction}$ (0.75) performance. The first-order model is determined as follows in coded form,

$$\hat{\sigma} = 6.1565 + 1.7857A + 0.3492B + 1.8303C$$
$$+ 0.7091AB + 0.188AC - 0.1483BC + 0.0871ABC \qquad [4.6]$$

where A, B and C are the coded variables of the three parameters ranging from -1 to +1. The response surfaces of the model are shown in Fig. 4.21(a) and (b) for the two

First Order Model for AADR = -1

SD = 4.3262 + 1.5977*A + 0.4974*B + 0.6220*A*B

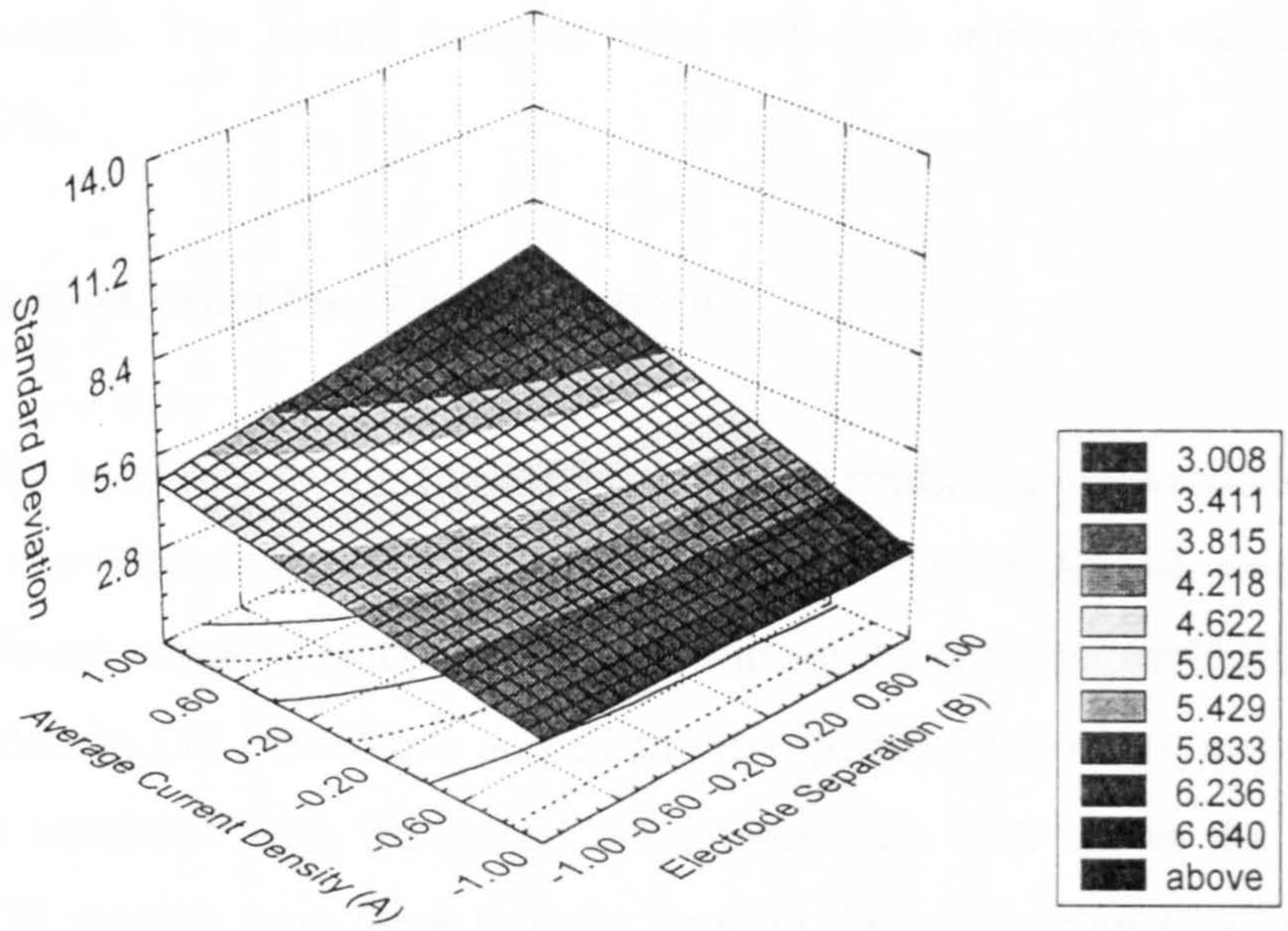

(a) Response Surface of the First Order Model for AADR = -1

First Order Model for AADR = +1

SD = 7.9868 + 1.9734*A + 0.2009*B + 0.7961*A*B

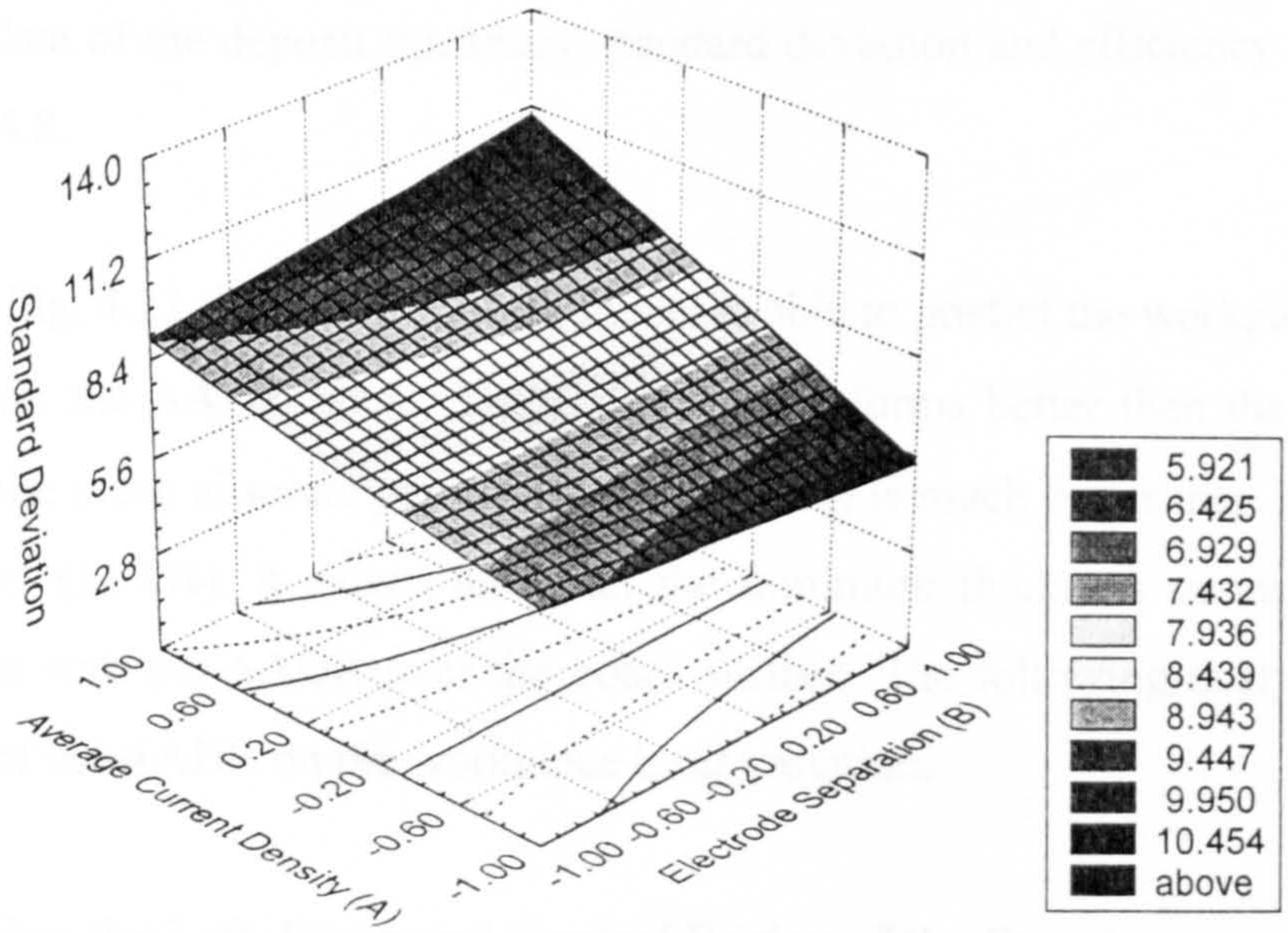

(b) Response Surface of the First Order Model for AADR = +1

Fig. 4.21 : Response Surfaces of the First Order Model for the Non-Uniform Pattern Plating

limits of the AADR. It can be seen that a low average current density of 30.1 mA/cm^2 and a high electrode separation of 25.4 cm give minimum thickness variation for the whole range of AADR. The model suggests also that such minimum variation increases with AADR.

4.6.2 Model Verification Using the "Zebra" Pattern

In order to verify the adequacy of the first-order model in predicting the workpiece level variation and the dependency of the minimum variation on the AADR, twelve boards with six different values of AADR were plated using the optimal combination of average current density (30.1 mA/cm^2) and electrode separation (25.4 cm) and the resulting variations compared with the model predictions. Fig. 4.22 shows the six patterns, with AADR ranging from three to eight, used in the verification runs. The AAD of the left and right region was fixed at 0.1 while that of the centre was varied from 0.3 to 0.8. All the background variables were kept at the same levels as in the Sec. 4.6.1 above and the mean standard deviation of two boards with the same AADR was taken as the responses. The results of the comparison are summarized as Fig. 4.23. An average current efficiency of 91.8% was recorded for the twelve experiments. Raw data of the deposit thickness, standard deviation and efficiency are given in Appendix 4.8.

It can be seen from Fig. 4.23 that the first-order model is able to predict the workpiece level variation within the AADR range. The full model performs better than the 5-term model in that the mean absolute percentage error (6.3%) is much better than that of the 5-term model (11.4%). It shows also that the minimum thickness variation achievable increases with the AADR over the board surface. The following analysis unveiled the effect of the AADR on the workpiece level variation.

4.6.2.1 Analysis Using the Left, Right and Central Region of the Board

When the board is partitioned into its left, right and central regions, the first two regions combined represent the region of small AAD, i.e. 0.1, denoted by SAAD, and

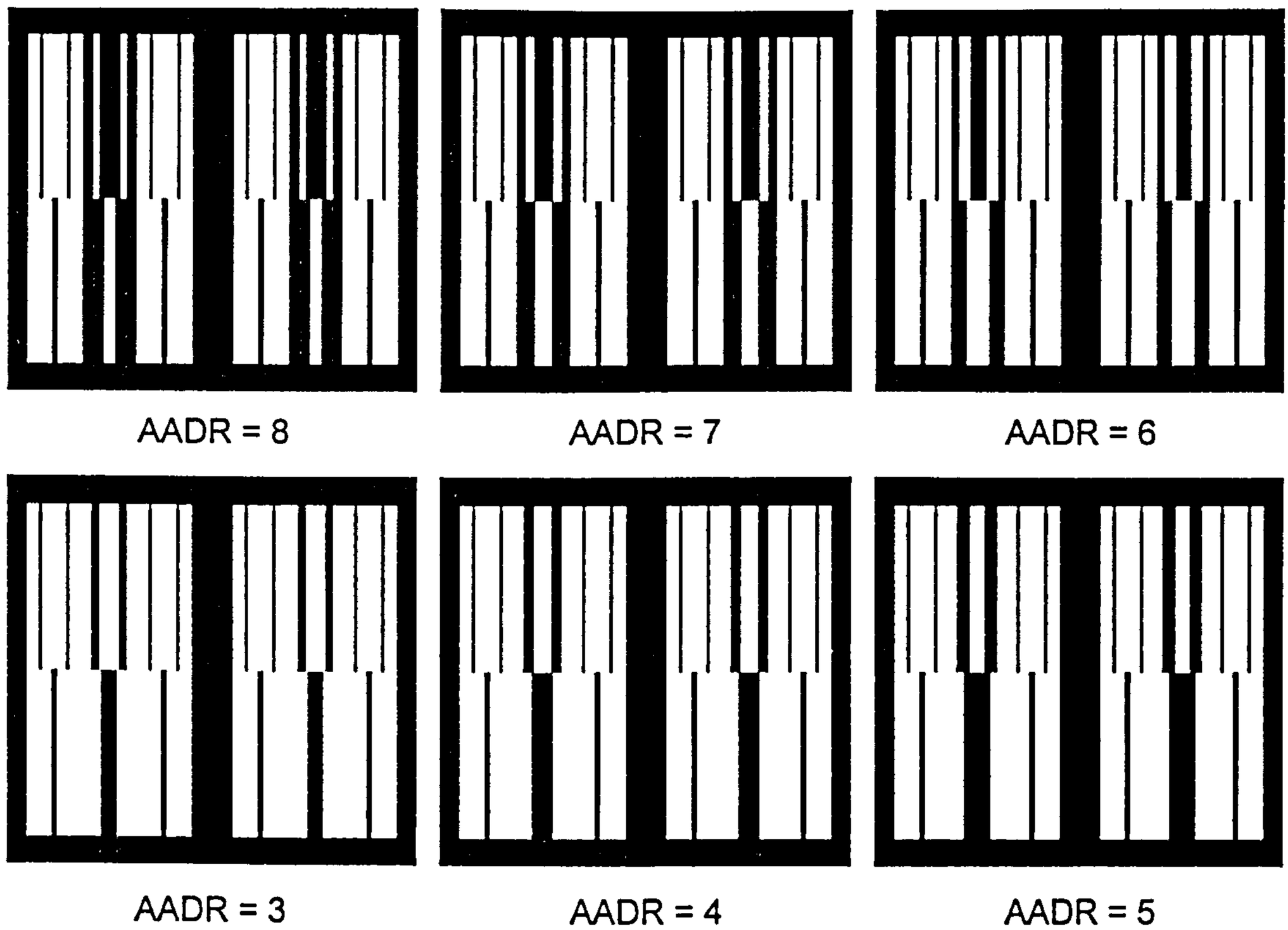

Fig. 4.22 : "Zebra" Patterns Used in the Verification Runs

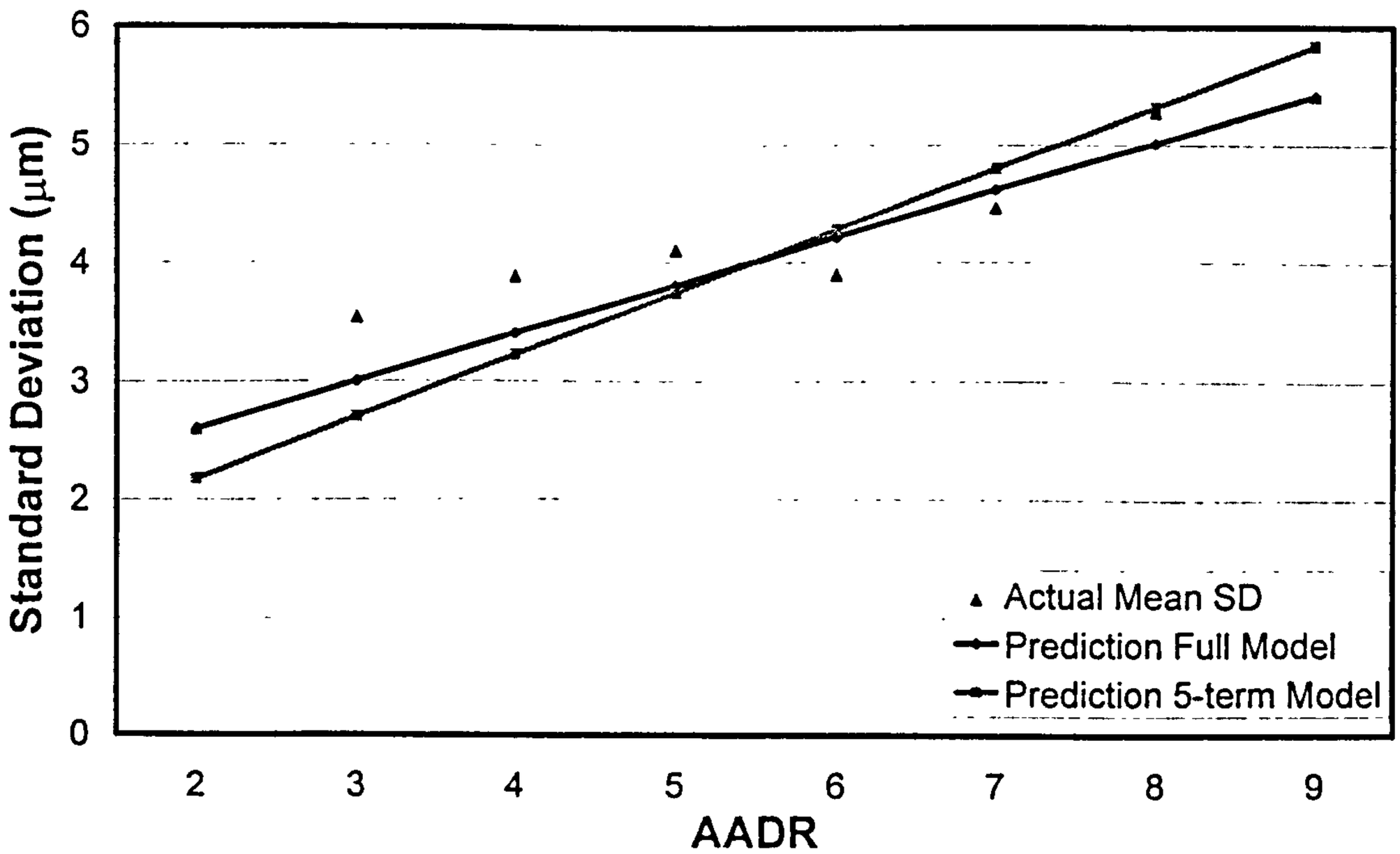

Fig. 4.23 : Comparison of the Actual and Predicted Standard Deviation of the First Order Model

the last region represents the large AAD region, i.e. 0.2-0.9, denoted by LAAD. Fig. 4.24 shows the variation of deposit thickness and its standard deviation with the AADR, with the legends explained in Table 4.14 below.

Legend	*Symbol*	*Explanation*
MS	$\bar{X}_S$	average deposit thickness of the pattern of the SAAD region, (point 1,2,3,4,5,6 in App. V)
ML	$\bar{X}_L$	average deposit thickness of the pattern of the LAAD region, (point 7,8,9,10,11,12 in App. V)
MO	$\bar{X}$	average deposit thickness over the whole board
SDS	s_S	standard deviation of the deposit thickness of the pattern of the SAAD region
SDL	s_L	standard deviation of the deposit thickness of the pattern of the LAAD region
Faraday	--	nominal deposit thickness determined by Faraday's Law (Eq. 4.1)
SDO	s	standard deviation of the deposit thickness over the whole board
SDPF	--	standard deviation of the deposit thickness by the first-order full model (Eq. 4.6)

Table 4.14 : Explanation of the Legends used in Fig. 4.23

The mean value of the results obtained from the two replicates for each AADR is used as the response for all of the above variables. Several distinct features are observable in Fig. 4.24 :

i/ $\bar{X}$ remains nearly constant and unaffected by the increasing AADR, i.e. as long as the average current density and electrode separation are kept unchanged, the average deposit thickness is not significantly affected by the AAD contrast over the board surface,

ii/ $\bar{X}_S > \bar{X}_L$, $\bar{X}_S > \bar{X}$ and $\bar{X}_L < \bar{X}$ for the whole range of AADR, as expected the region with smaller AAD attracts more current and develops thicker deposits than the region with larger AAD,

iii/ both $\bar{X}_S - \bar{X}_L, \bar{X}_S - \bar{X}$ and $\bar{X} - \bar{X}_L$ increase with AADR, which means that the AADR intensifies the difference in deposit thickness between regions with different AAD, such an effect is also observable when the AAD contrast over the

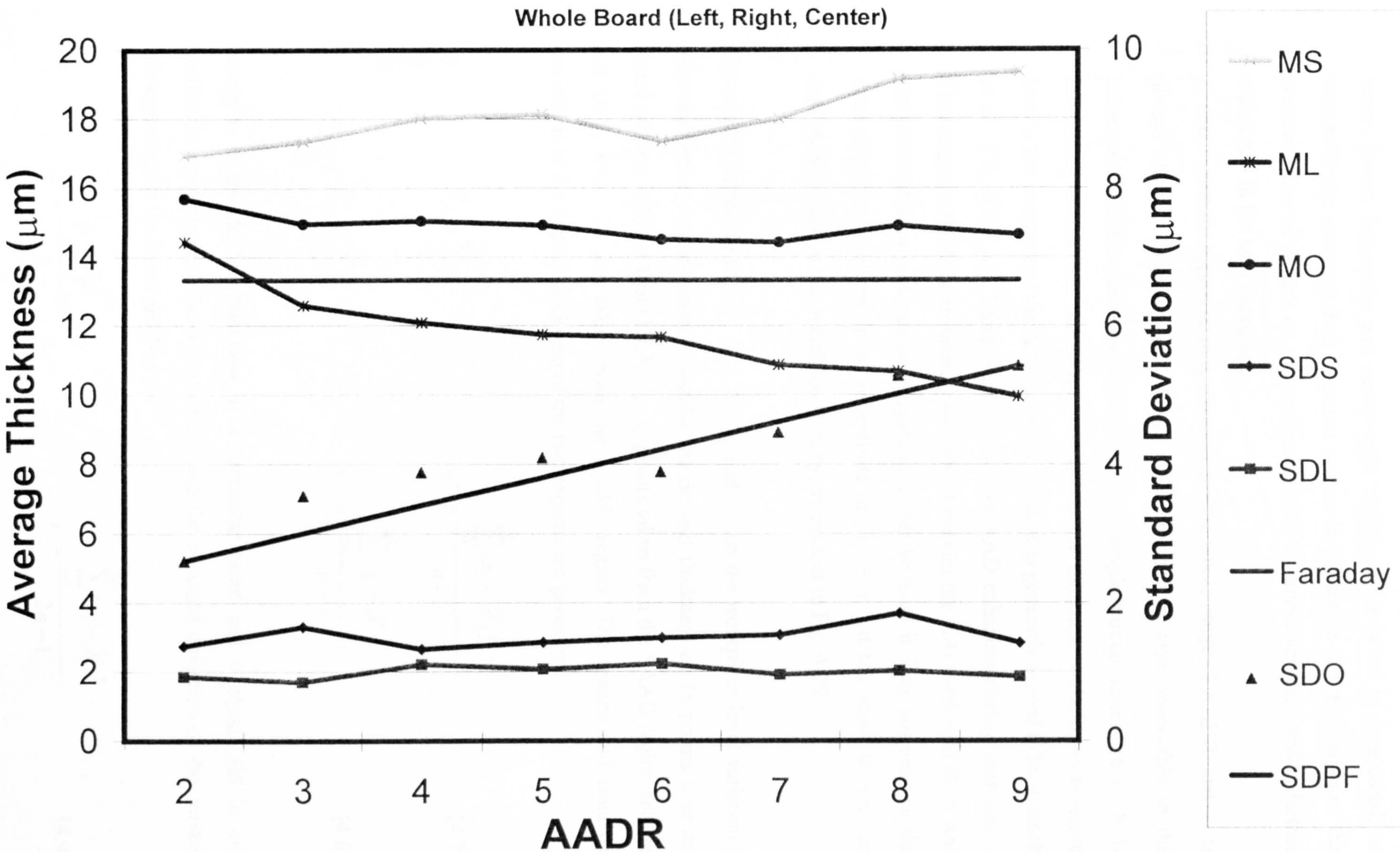

Fig. 4.24 : Variation of the Mean and Standard Deviation of the Deposit Thickness with AADR in the Verification Runs (Board Partitioned into Left, Right and Center Region)

upper, lower, left-centre and centre-right region of the board is considered, as shown by the corresponding response graphs in Appendix 4.9, this explains the positive effect of AADR on the workpiece level thickness variation and is further elaborated in the next paragraph,

iv/ s_S and s_L remain approximately constant for the whole range of AADR, and s_S is always slightly larger than s_L. Such a phenomenon is also observable in the subsequent verification experiments using a simple circuit (Sec. 4.6.3). It is interesting to note that the effect of AAD on the thickness variation is reversed here in the presence of the AAD contrast, while it is generally agreed [Mehdizadeh *et al.*, 92], [Choi and Kang, 96] that smaller AAD enhances plating uniformity. This suggests strongly an interaction effect between the AAD and AADR. It was not observable in previous investigations either because it does not exist in the case of uniform pattern or the magnitude of (s_S + s_L) it too small to have an noticeable effect on the overall uniformity, as evident in Fig. 4.25.

The relative influence of $\bar{X}_S$, $\bar{X}_L$, $\bar{X}$, s_S and s_L on the workpiece level variation s deserves further consideration. Consider the deposit thickness of $2n$ points over the board surface, with the first (1,2,3, ... ,n) points taken from the SAAD region and the last (n+1, n+2, ... ,2n) taken from the LAAD region. The means and standard deviations of the deposit thickness of the two regions are given by

$$\bar{X}_S = \sum_{i=1}^{n} x_i \qquad s_S^{\,2} = \frac{\sum_{i=1}^{n}(x_i - \bar{X}_S)^2}{n-1} \qquad [4.7]$$

$$\bar{X}_L = \sum_{i=n+1}^{2n} x_i \qquad s_L^{\,2} = \frac{\sum_{i=n+1}^{2n}(x_i - \bar{X}_L)^2}{n-1} \qquad [4.8]$$

where x_i is the deposit thickness at a particular point and n equals six in our verification experiment. The overall mean and the standard deviation of the deposit thickness across the board are then

$$\bar{X} = \frac{\bar{X}_S + \bar{X}_L}{2} \qquad s^2 = \frac{\sum_{i=1}^{2n}(x_i - \bar{X})^2}{2n-1} \qquad [4.9]$$

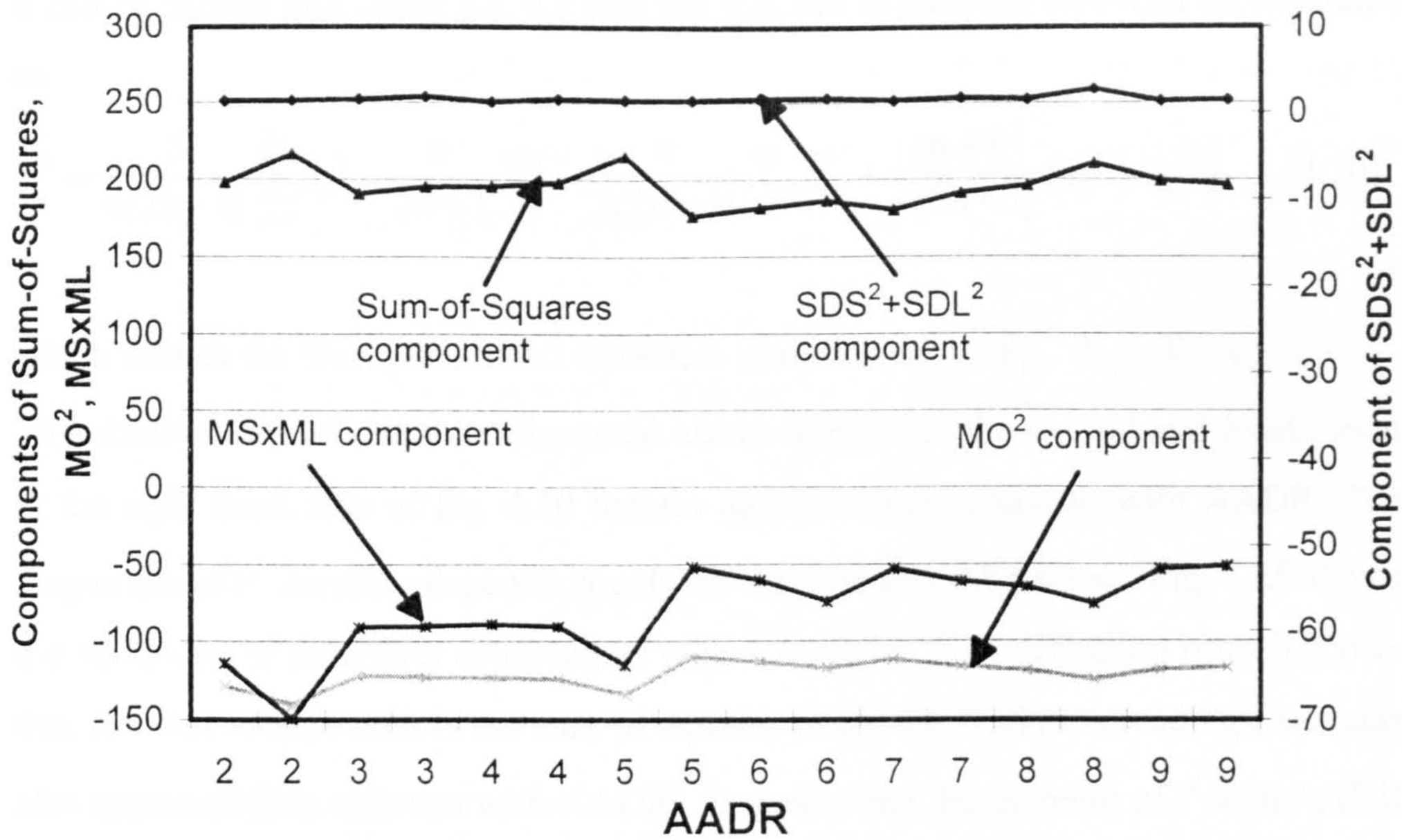

Fig. 4.25 : Variation of the Four Components of s^2 with AADR in the Verification Runs

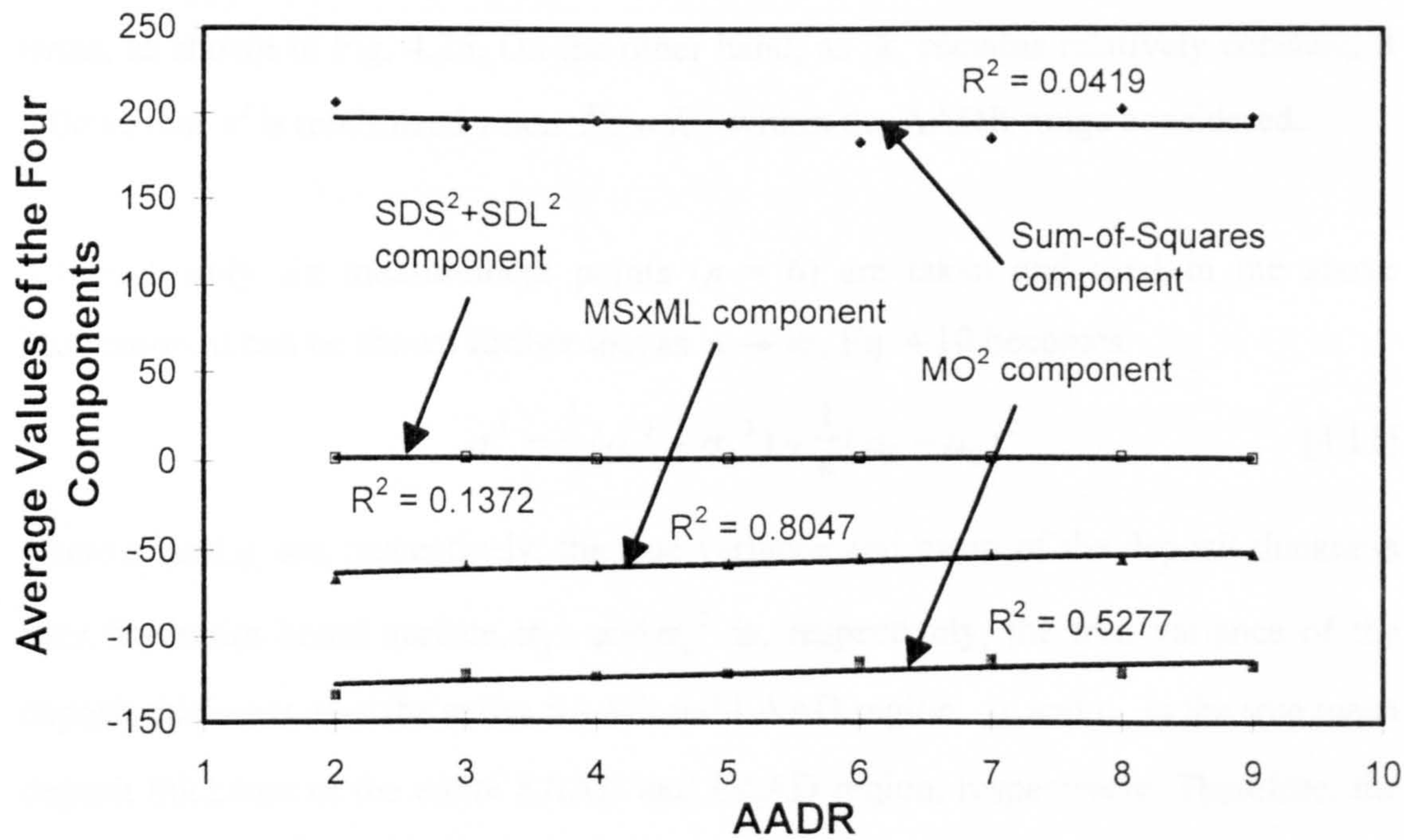

Fig. 4.26 : Correlation of the Four Components of s^2 with AADR in the Verification Runs

It can be shown that, using Eq. 4.7 and Eq. 4.8, the expression for s^2 can be expanded as

$$s^2 = \frac{3}{4(2n-1)}\sum_{i=1}^{2n} x_i^2 - \frac{n}{2n-1}\overline{X}^2 - \frac{n}{2(2n-1)}\overline{X}_S\overline{X}_L + \frac{n-1}{4(2n-1)}(s_S^2 + s_L^2) \qquad [4.10]$$

which relates the workpiece level thickness variation with $\overline{X}_S$, $\overline{X}_L$, $\overline{X}$, s_S and s_L. The observations of i/ and iv/ discussed above imply that the second and fourth term in the right hand side of Eq. 4.10 remain approximately constant with AADR. The magnitude of s^2 therefore depends largely on the first and third terms. Fig. 4.25 shows the variations of these four components with AADR for the verification runs. It shows that the first term, which is the sum of squares of all the thickness readings, remains also approximately constant with AADR[‡]. It means that the increase of s^2 with AADR is mainly the result of the increase of the product term $\overline{X}_S\overline{X}_L$ under the scattering effect of AADR described in iii/ above. This is also supported by the relatively strong correlation of the third term with AADR (.80) when compared with the other three terms, as shown in Fig. 4.26. On the other hand, as $\overline{X}$ remains relatively constant, it follows that s^2 is minimized when $\overline{X}_S = \overline{X}_L$ within the AADR range considered.

Although only six measurement points (n = 6) are taken and used in the above illustration, it can be shown further that as $n \to \infty$, Eq. 4.10 becomes

$$\sigma^2 = \frac{1}{2}(\sigma_s^2 + \sigma_L^2) + \frac{1}{4}(\mu_S - \mu_L)^2 \qquad [4.11]$$

where σ^2 and μ are, respectively, the true variance and mean of the deposit thickness over the entire board surface, σ_S^2 and σ_L^2 is, respectively, the true variance of the deposit thickness over the entire SAAD and LAAD region, μ_S and μ_L is the true mean deposit thickness of the entire SAAD and LAAD region, respectively. Therefore, the sole dependency of σ^2 on μ_S and μ_L remains unchanged if σ_S^2, σ_L^2 and μ^2 do not change with AADR. The workpiece level variation can still be largely attributed to the scattering effect of AADR on μ_S and μ_L under the limiting case. In fact, n = 6 was

‡ In fact, the first term will converge into a linear combination of $\overline{X}_S$, $\overline{X}_L$, s_S and s_L and vanish as n is approaching infinity, as reflected by Eq. [4.11], it means that practically s^2 is independent of the sum of squares of the thickness readings if sufficiently large number of samples are taken.

found to be sufficiently large for the limiting equation of Eq. 4.11 to give an accurate estimate of the actual standard deviation (s), when $\overline{X}_S$, $\overline{X}_L$, s_S and s_L were used in place of their true values. The average absolute percentage error was found to be 1%. This is substantiated by Fig. 4.27 below.

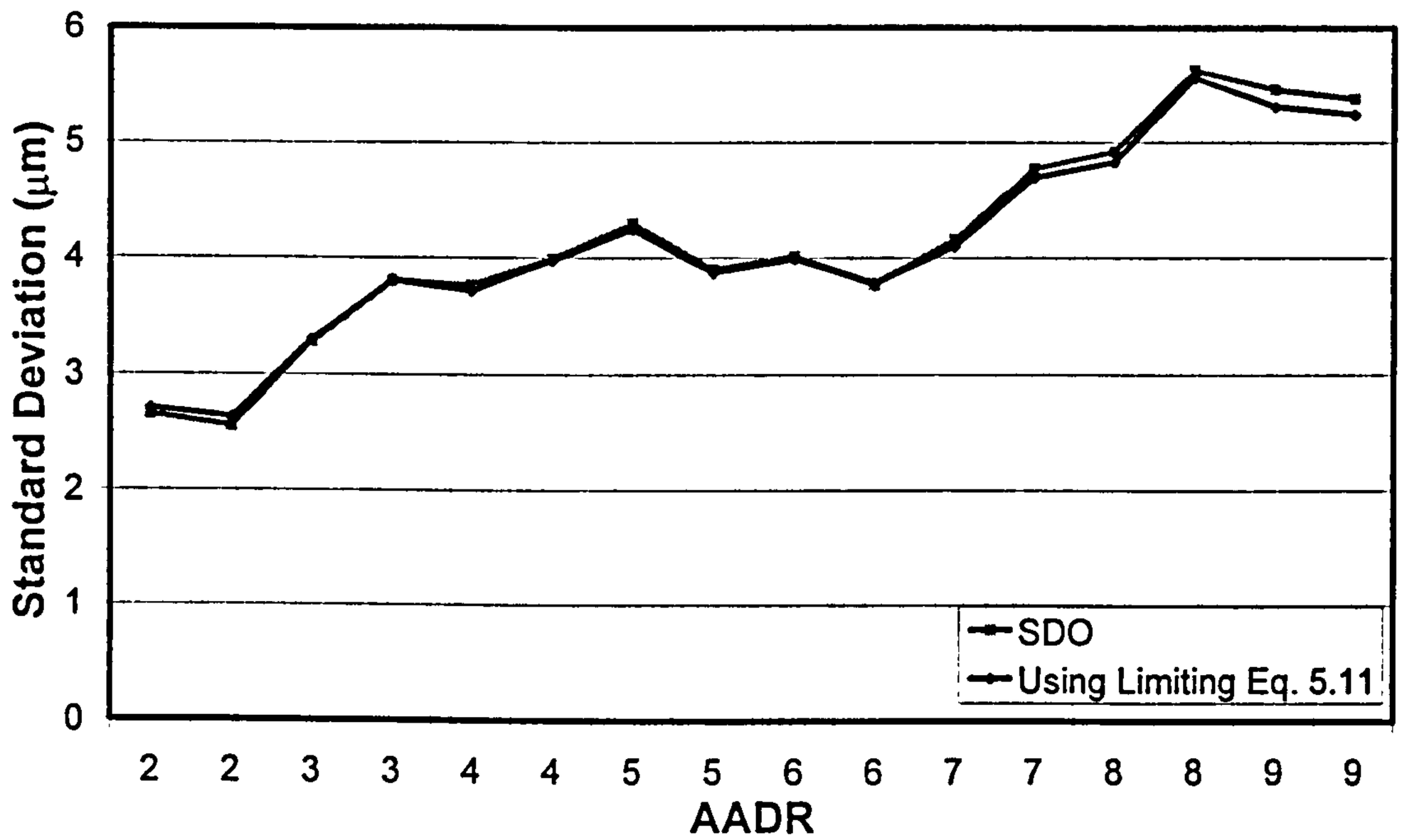

Fig. 4.27 : Comparison of s^2 (SDO) and σ^2 calculated by Eq. 4.11

Furthermore, Eq. 4.11 shows that when $\overline{X}_S = \overline{X}_L$, σ^2 is minimized and is given by the mean of true variances of the deposit thickness over the SAAD and LAAD regions. This happens, theoretically, when AADR = 1 and the mean deposit thickness of the two regions are equal. It means that the workpiece level thickness variation is minimized when the AADs of two neighbouring regions, and hence the average deposit thickness, are the same.

4.6.2.2 Analysis Using the Upper and Lower Region of the Board

The upper and lower half of the board have the same local average active area density, $\overline{\text{AAD}}$ and AADR, but the width of lines in the upper region is only half that of the lower region for AADR 3, 4 and 5. Fig. 4.28 shows the mean responses of the average deposit thickness and the standard deviation when the board is partitioned into its

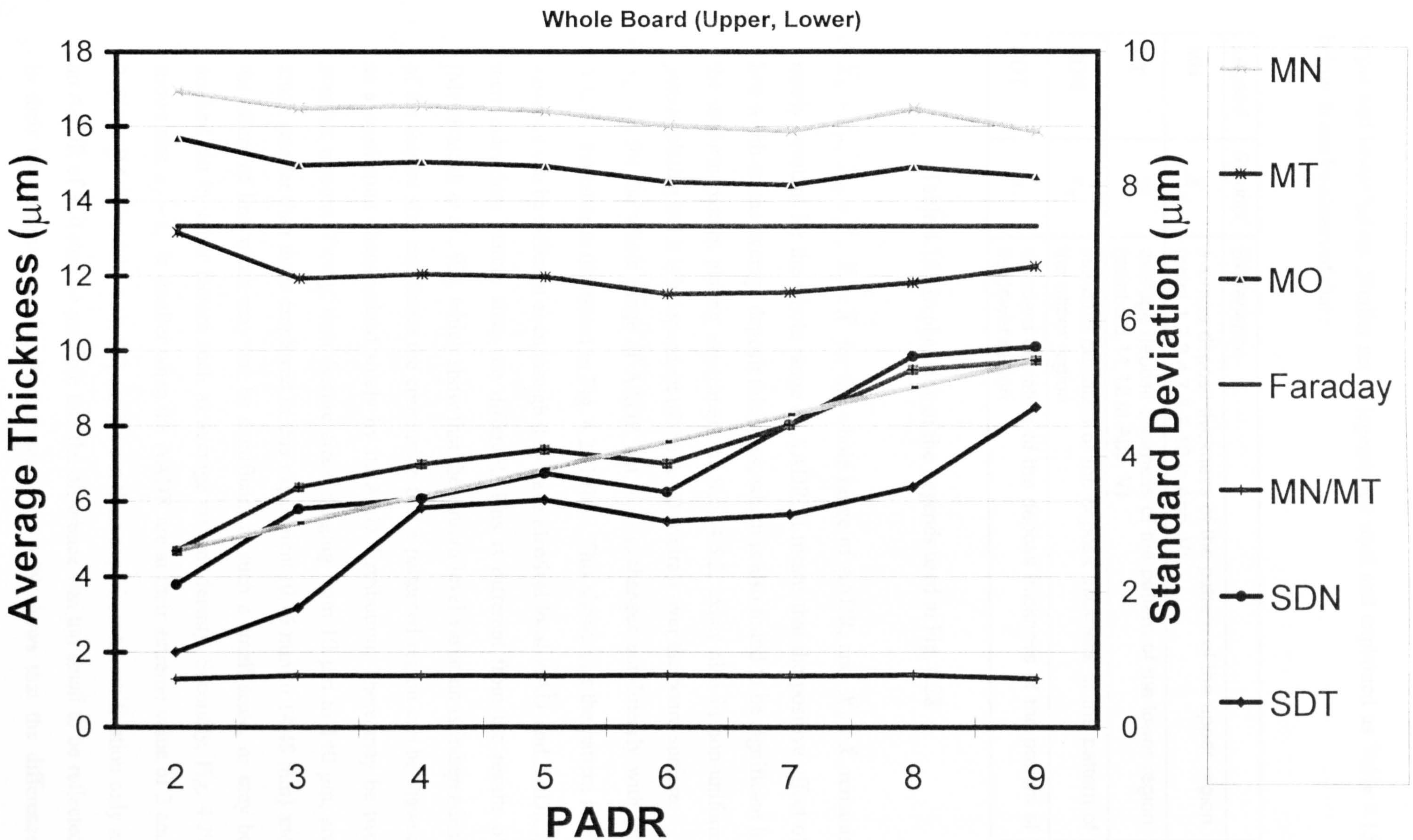

Fig. 4.28 : Variation of the Mean and Standard Deviation of the Deposit Thickness with AADR in the Verification Runs (Board Partitioned into Upper and Lower Region)

upper and lower halves. Similar set of legends are used and explained as Table 4.15 below. It can be observed that :

Legend	*Symbol*	*Explanation*
MN	$\overline{X}_N$	average deposit thickness of the pattern of the upper region, (point 1,2,3,4,7,8,9,10 in App. V)
MT	$\overline{X}_T$	average deposit thickness of the pattern of the lower region, (point 5,6,11,12 in App. V)
SDN	s_N	standard deviation of the deposit thickness of the pattern of the upper region
SDT	s_T	standard deviation of the deposit thickness of the pattern of the lower region

Table 4.15 : Explanation of the Legends used in Fig. 4.28

i/ $\overline{X}_N > \overline{X}_T$, $\overline{X}_N > \overline{X}$, $\overline{X}_T < \overline{X}$ for the whole range of AADR, and $\overline{X}_N / \overline{X}_T$ remains nearly constant for the whole range of AADR. It means that the positive effect of line width on the average deposit thickness, which is also found to be significant in the uniform pattern plating experiment of Sec. 4.5.2, exists also in non-uniform pattern plating but it is independent of the AAD contrast over the board surface.

ii/ $s_N > s_T$ for the whole range of AADR but $s_N - s_T$ changes non-linearly with the AADR, the latter is illustrated in Fig. 4.29 below. This shows that the pattern level variation can be different even though they have identical local $\overline{AAD}$ and AADR *if* their individual feature sizes are different. This is different from the results of [Mehdizadeh *et al.*, 93], which show that the pattern level variation is independent of the feature size and hence the conclusion that a patterned region can be viewed as a continuum characterized solely by its AAD distribution. There may be two possible reasons. Firstly, their feature sizes, ranging from 10 μm to 140 μm, are much smaller than those employed in this experiment (0.76 mm to 14.48 mm) and the effect of line width may not be significant at such a small scale, or may be masked out by other factors such as average current density. Secondly, Fig. 4.29 shows that $s_N - s_T$ is smaller when the AADR are at their extreme value of 2 and 9. Since [Mehdizadeh *et al.*, 93] carried out their experimental verification only at an AADR of 9, it may be possible that the difference was too small to be reflected in their experimental results. Furthermore, Fig. 4.29 shows that the difference

between the pattern level variation caused by the feature size effect is at its minimum when the AADR is around 5, i.e. when the AAD of the center region is approximately 0.5. It suggests an interaction effect of the feature size, AAD and AADR which is worthy of further investigation.

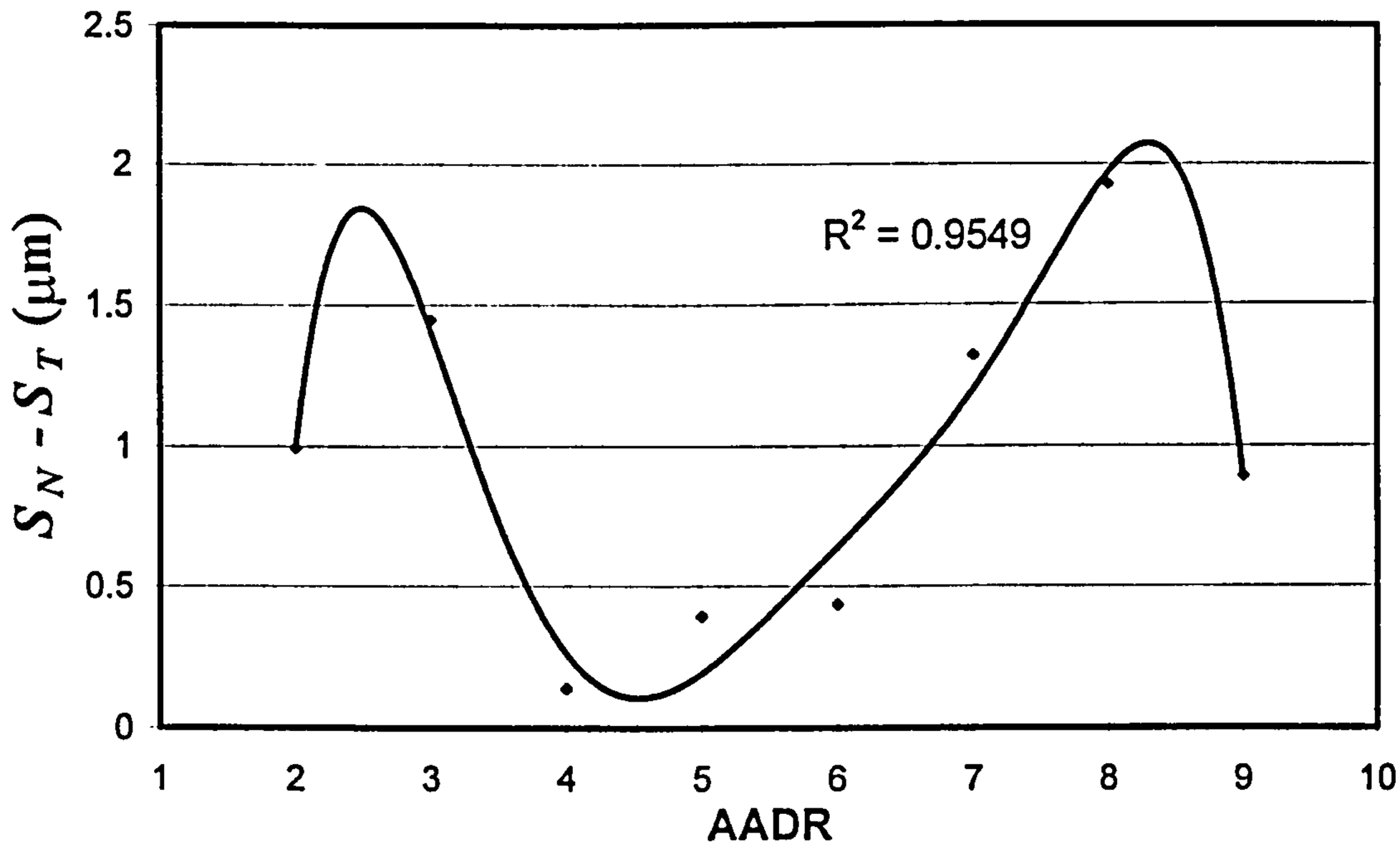

Fig. 4.29 : The Difference in Pattern Level Variation of the Upper and Lower Region

4.6.3 Model Verification Using a Simple Circuit Pattern

The validity of the first-order model was further tested with a simple circuit pattern with AADR ranging from 2 to 6 as shown in Fig. 4.30. The dimensions of the board and the rectangular border were the same as those employed in the previous round of experiments but the circuit consists of two regions of different active area densities only. Table 4.16 summarizes the density values, the difference of the AAD of the two regions, AADD, and the average AAD over the whole board, $\overline{AAD}$, for each AADR. It can be seen that there is a drop of AADD and $\overline{AAD}$ for the AADR of 4 because a smaller AAD is used in the SAAD region. This is different from the previous round in which $\overline{AAD}$ always increases with the AADR.

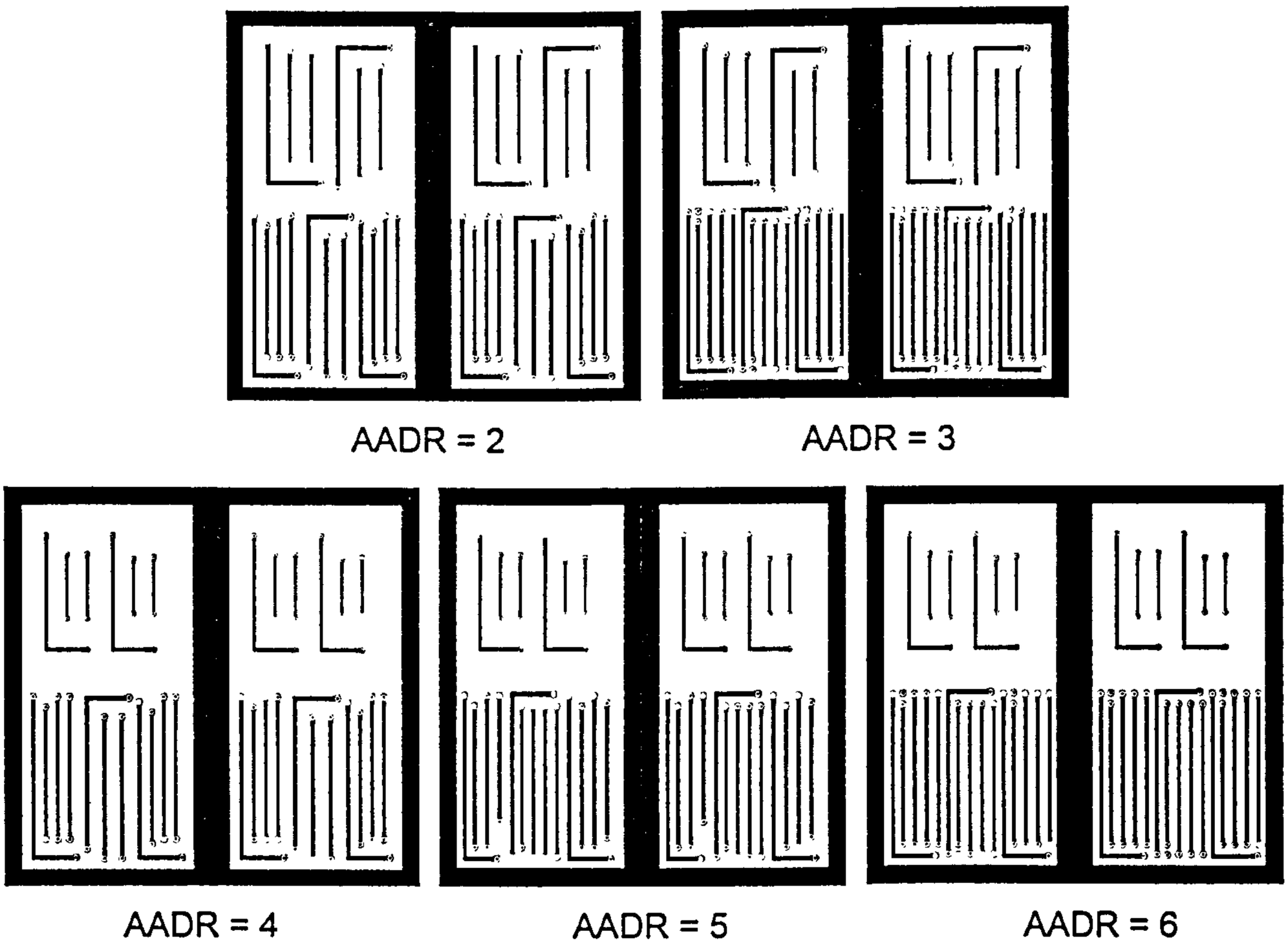

Fig. 4.30 : The Simple Circuit Patterns used in the Second Verification Runs

AAD	*AADR* 2	3	4	5	6
Upper Region (SAAD)	0.1	0.1	0.05	0.05	0.05
Lower Region (LAAD)	0.2	0.3	0.2	0.25	0.3
LAAD-SAAD (AADD)	0.1	0.2	0.15	0.2	0.25
$\overline{AAD}$	0.15	0.2	0.125	0.15	0.175

Table 4.16 : Active Area Densities of the Circuit Patterns

The deposit thicknesses of 12 points (6 from each region) on the pattern were measured for each board. All the process variables were kept at the same levels as in the previous round and the mean standard deviation of two boards with the same AADR was taken as the response. An average current efficiency of 86.4% was recorded for the ten experiments. Raw data of the deposit thickness, standard deviation and efficiency are given in Appendix 4.10. Fig. 4.31 (a) and (b) show the

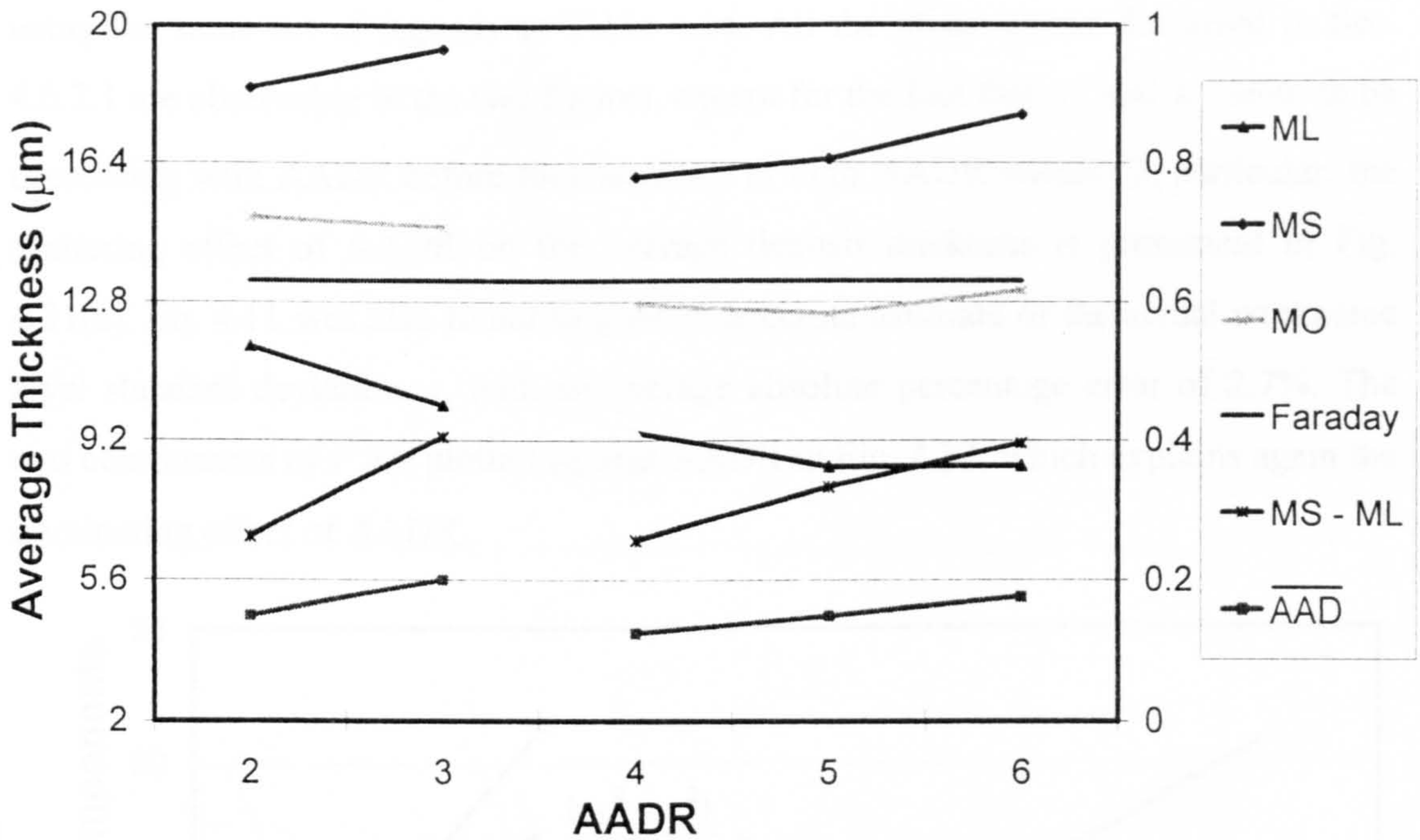

(a) Variation of the Mean Deposit Thickness with AADR

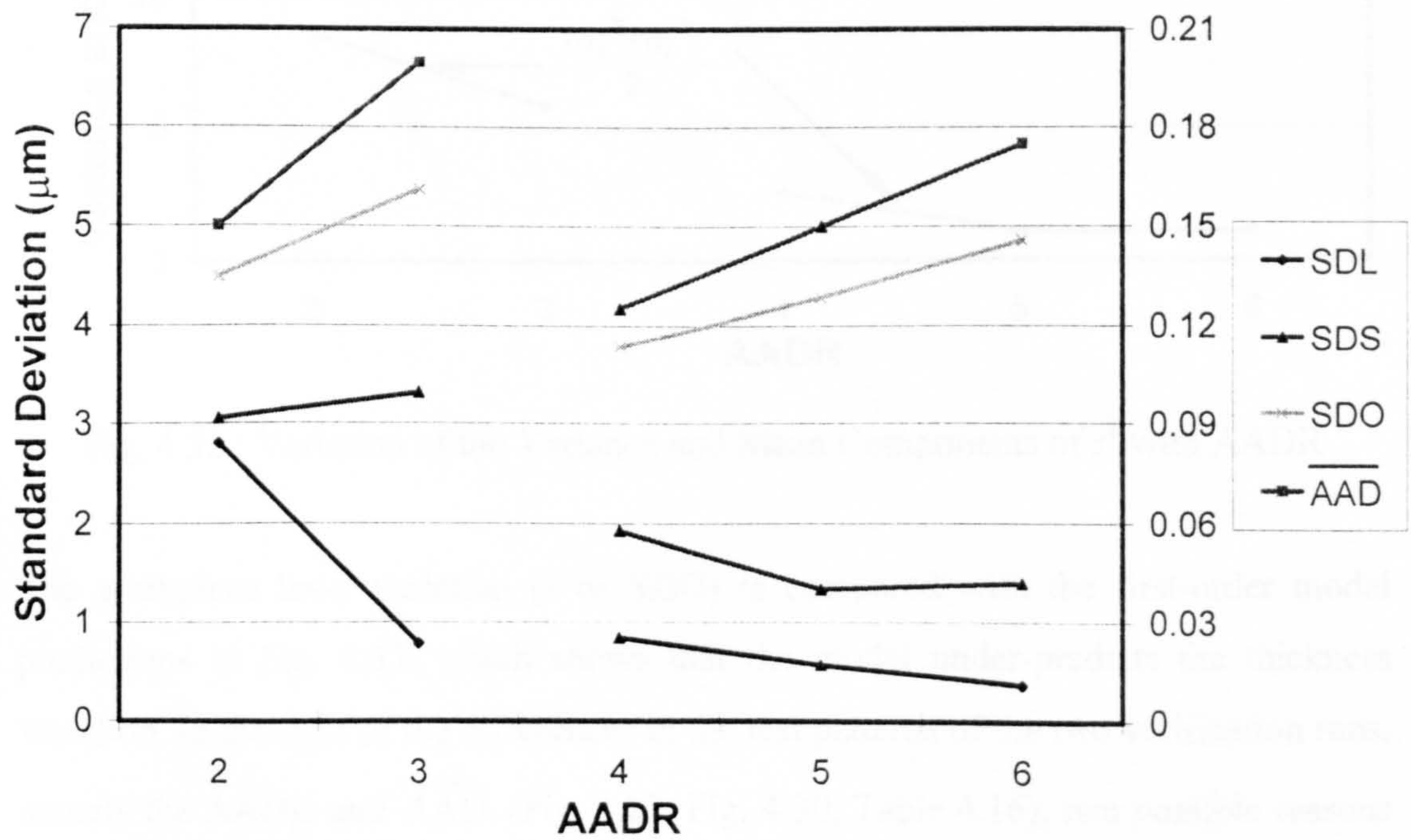

(b) Variation of the Standard Deviation of the Deposit Thickness with AADR

Fig. 4.31 : Mean and SD Responses Graphs of the Second Verification Runs

variation of the mean and standard deviation of the deposit thickness with the AADR, using the same set of legends as Table 4.14. All the observations discussed in Sec. 4.6.2.1 are observable in the two figures, except for the fact that s_S and s_L seem to be decreasing with AADR before they stabilize at high AADR values. In particular, the scattering effect of AADR on the average deposit thickness is prominent in Fig. 4.31(a). Eq. 4.11 was also found to give an accurate estimate of the actual workpiece level standard deviation, s, with an average absolute percentage error of 2.7%. The two components of s^2 are plotted against AADR in Fig. 4.32, which explains again the dominating effect of AADR.

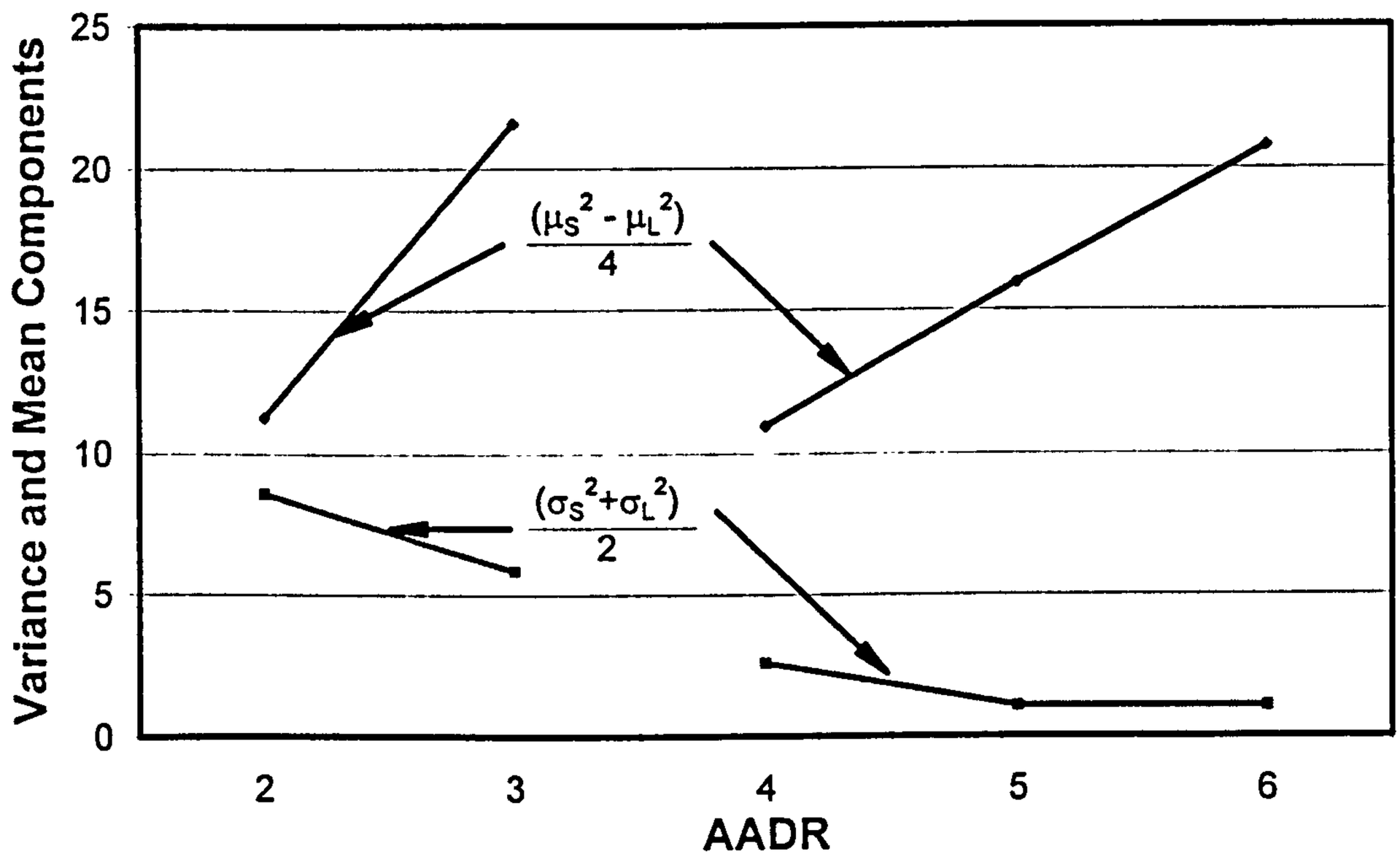

Fig. 4.32 : Variation of the Variance and Mean Components of s^2 with AADR

The workpiece level variation (s or SDO) is compared with the first-order model predictions in Fig. 4.33, which shows that the model under-predicts the thickness variation. In the light of the differences in the test patterns of the two verification runs, namely the AADD and $\overline{\text{AAD}}$ (Fig. 4.22, Fig. 4.30, Table 4.16), two possible reasons are proposed and it is shown that the first-order model can be modified to cater for such effects.

i/ $\overline{\text{AAD}}$ effect : an obvious disruption between the AADR value of 3 and 4 can be observed in the response graph of $\overline{X}$, $\overline{X}_S - \overline{X}_L$ (Fig. 4.31a) and s (Fig. 4.31b), i.e.,

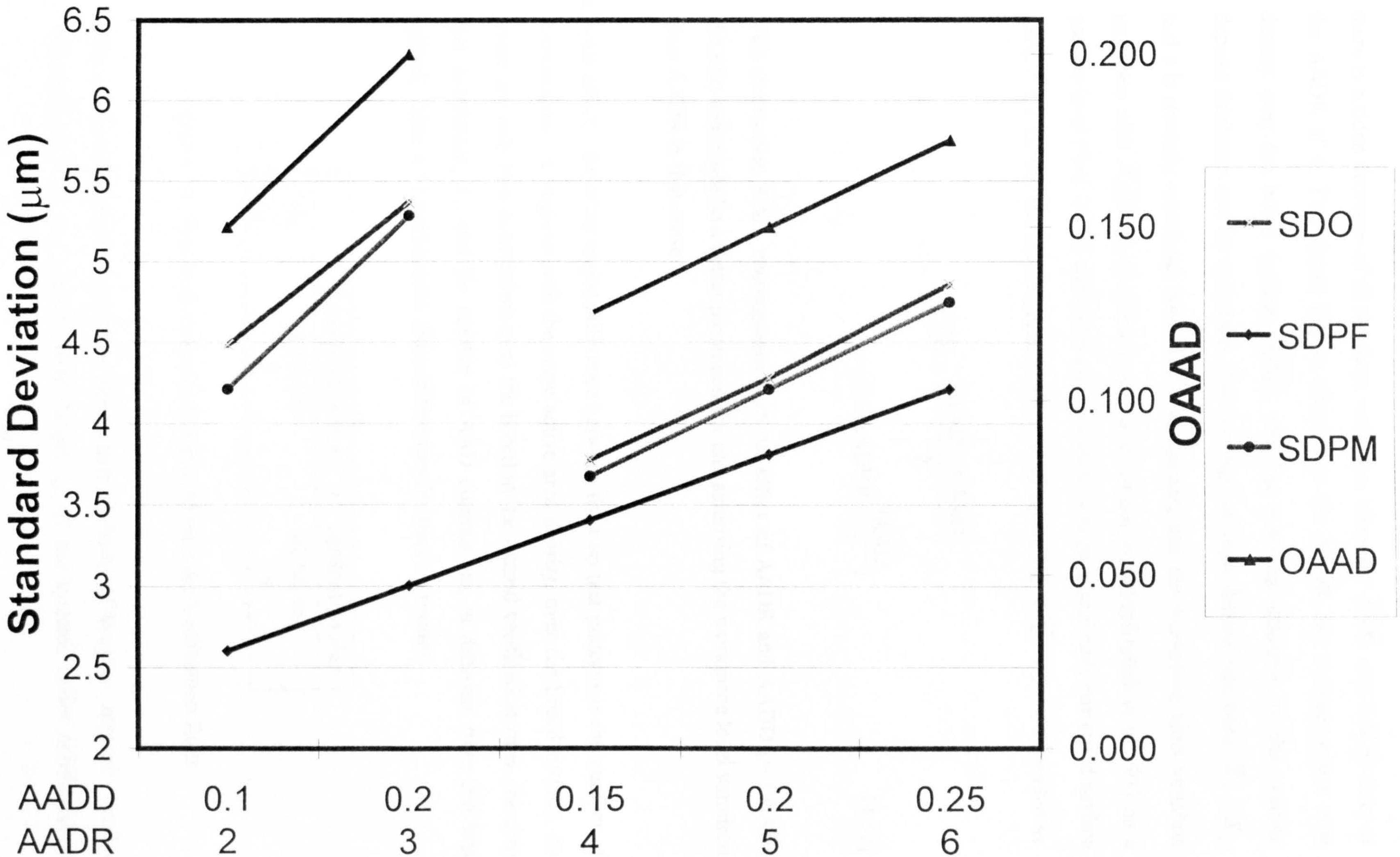

Fig. 4.33 : Comparison of the Actual and Predicted Standard Deviation of the Original and Modified First Order Model

there is sudden decrease of all the three responses when the $\overline{\text{AAD}}$ and AADD drop at the AADR of 4. This shows that in addition to the AADR, the average active area density over the board surface, $\overline{\text{AAD}}$, also has a strong influence on the average deposit thickness and its variations. The two figures show further that both $\bar{X}_s - \bar{X}_L$ and s is strongly correlated with $\overline{\text{AAD}}$, suggesting that the workpiece level variation increases with $\overline{\text{AAD}}$. Such effect is also pointed out by [Mehdizadeh *et al.*, 93] on a pattern-level (Sec. 2.4.3) and [Shih and Pickering, 87] on a uniformly patterned surface (Sec. 2.4.2.2). For the circuit pattern of Fig. 4.30 above, the $\overline{\text{AAD}}$ can be expanded as

$$\overline{\text{AAD}} = \frac{\text{SAAD} + \text{LAAD}}{2}$$

$$= (1 + \text{AADR})(\frac{\text{SAAD}}{2}) \qquad [4.12]$$

This shows that $\overline{\text{AAD}}$ encompasses both the effect of AADR and AADD (= LAAD-SAAD) and might be a better parameter for characterizing the workpiece level variation than AADR in that sense.

ii/ scale effect : the other major difference between the two test patterns is the number of continuums, i.e. regions with the same active area density, over the board surface. As there are only two continuums over the board in the second verification runs, the area per continuum, A_c, and the number of AAD contrast, n_c, is different from the first round. Table 4.17 summarizes these differences for the two rounds.

	1st Verification Run	*2nd Verification Run*
A_c	13.93 cm^2	22.08 cm^2
n_c	2	1

Table 4.17 : The Differences in A_c and n_c of the Two Verification Runs

The review of previous researches shows that all forms of Wagner number involve the reciprocal of the characteristic length, L, of the systems under consideration

(both one and two-dimensional), and the deposit uniformity is inversely proportional to the Wagner number. It seems logical to suggest that the three-dimensional workpiece level variation can be characterized by the area under consideration, with the former being proportional to the latter. It follows that reducing the area of the zone over which the AAD contrast occurs, i.e. A_c, will reduce also the workpiece level variation. For the purpose of simplicity, it is assumed here that the whole board surface is divided into continuums of equal area A_c, which is also the case of the two verification runs. On the other hand, while A_c reflects the scale of the problem, one additional parameter, n_c, is needed to reflect the degree of non-uniformity of the surface patterns. Since the workpiece level variation increases with A_c, it will be inversely proportional to n_c if the total area of the board is kept constant.

After considering the above two effects, the modified parameter for the active area density effect, AADP, should take the form

$$\text{AADP} = f(\overline{\text{AAD}}, A_c, \frac{1}{n_c}) \qquad [4.13]$$

To preserve the linearity between the low (-) and high (+) levels of the parameter, which is required by the first-order model of Eq. 4.6, AADP should be a linear function of AADR also. After a number of trials, it was found that

$$\text{AADP} = \overline{\text{AAD}}\sqrt{\frac{A_c}{n_c}} \qquad [4.14]$$

was found to be the best transformation. After substituting the corresponding values of $\overline{\text{AAD}}$, A_c and n_c into Eq. 4.14, the coded and uncoded parameters of AADR and AADP is recalculated as Table 4.18 for the two verification runs. The first-order model is modified by simply using the coded parameter of AADP instead of AADR. As coded parameters are used in Eq. 4.6 and the coded AADR and AADP are the same for the first verification run, the standard deviation predicted by the modified model remains unchanged. For the second verification run, the workpiece level

variation, denoted by SDPM in Fig. 4.33, is calculated using the modified first-order model and the average percentage error is found to be 2.8%. The modified model is considered highly accurate, given the major difference between the test patterns used in the two rounds of experiments.

AADP		AADR							
		2	3	4	5	6	7	8	9
1st Verification	uncoded	0.14	0.17	0.21	0.24	0.28	0.31	0.35	0.38
	coded	-1	-0.71	-0.43	-0.14	+0.14	+0.43	+0.71	+1
2nd Verification	uncoded	0.28	0.37	0.23	0.28	0.32	N/A	N/A	N/A
	coded	+0.14	+0.91	-0.24	+0.14	+0.53	N/A	N/A	N/A

Table 4.18 : Recalculated Parameter Levels of AADR and AADP for the Two Verification Runs

4.7 Summary

In short, six sets of statistically designed experiment were conducted sequentially to study the effects of the average current density, electrode separation and active area density on the workpiece level plating uniformity of patterned substrates. Statistical models were established to predict the plating thickness variability of both uniformly and non-uniformly patterned substrate in the operability space and verified experimentally. Optimum combinations of the two process parameters giving minimum thickness variability were determined from the model. The verification run of the uniform-pattern model showed that the optimum average current density yielded also minimum deviation of deposit thickness from Faraday's prediction. The scattering effect of the AAD contrast in the average deposit thickness was unveiled in the first verification run of the nonuniform-pattern model and elaborated from a statistical viewpoint. The first-order prediction model was further modified to cater for the effects of the average active area density and scaling, which were uncovered by the second verification runs using a simple circuit pattern.

CHAPTER 5

EXPERIMENTAL DESIGN AND ANALYSIS : PLATED-THROUGH HOLE AND BLIND VIA PLATING

5.1 Introduction

The previous sets of matrix experiments showed that the workpiece level plating uniformity of patterned substrates was significantly affected by the average current density, electrode separation and their interaction. It seems that the thickness variation is predictable within the operability region and can be minimized using an empirical second-order model. The objective of this set of experiment is to investigate, among the others, the effect of these two parameters on the workpiece level uniformity of PTH and BV plating. This differs from the previous investigations where plating uniformity was modelled at the feature level, as reflected in the review of Sec. 3.3.4.1.

5.2 Plated-Through Hole (PTH) Plating Workpiece Level Modelling

The objectives of the PTH experiments can be summarized as

i/ to identify the significant process and product parameters that affect the plating thickness distribution of plated-through holes at a workpiece level,

ii/ to determine the effects of these significant parameters, and their interactions,

ii/ to construct an empirical model for the relationship between the workpiece level thickness variation and the significant process parameters, and

iii/ to identify the optimum combination of parameters settings so as to minimize the thickness variability within the experimental range.

5.2.1 Factors Screening and the First Order Model

Six process and product parameters were studied in the first stage of experimentation, and their levels are summarized in Table 5.1 below. Concentration of sulphuric acid

and copper sulphate are known to affect the feature-level tertiary current distribution, especially in the high current density regime (30-40 mA/cm^2) when the mass transfer limit is approached [Lanzi and Landau, 88], [Hazlebeck and Talbot, 90]. Anode-cathode separation is geometry-dependent, hole separation and aspect ratio are product-dependent parameters. The ranges of A, B and C cover the usual operating window while that of D, E and F represent the limits of the configuration of the first (smaller) purpose-built testing cell and the PCB thickness.

Factors	*Levels*	
	(-1)	(+1)
A. Concentration of sulphuric acid (g/L)	165	200
B. Concentration of copper sulphate (g/L)	65	90
C. Average current density (mA/cm^2)	32.28	43.04
D. Electrode separation (cm)	12.7	17.78
E. Inter-holes distance (cm)	0.45	2.2
F. Corrected aspect ratio* (mm)	2.56	6.40

Table 5.1 : Factors Settings of the 2_{VI}^{6-1} PTH Screening Experiment

A 2_{VI}^{6-1} FFD with 32 runs was used to screen out those important factors to be included in subsequent model building and the direction of further experimentation. This allows the studying of the main effect of each parameter and the interactions between the six process and product parameters. This resolution VI design was constructed using a 2^5 full factorial as the first five columns and the sixth column was generated by the defining relationship $I = ABCDEF$, i.e. $F = ABCDE$. Such a high resolution ensures that each main effect is aliased only with a single 5-factor interaction and each 2-factor interaction is aliased only with a single 4-factor interaction. Therefore, all the main effects and 2-factor interactions obtained are clear from all low-order interactions, which are assumed to be negligible. The Full alias structure is given in Appendix 5.1. Four layouts of the test boards are shown in Fig. 5.1 to illustrate the combinations of the various levels of inter-hole distance (E) and the corrected aspect ratio (F). Depending on the dimension of the inter-holes distance

* The adjusted aspect ratio, L^2/R_0, as suggested by [Kessler and Alkire, 76b], [Alkire and Mirarefi, 77a, 77b] and [Yung *et al*, 89], is used here instead of the conventional L/R_0.

(E), a maximum of thirty and a minimum of eight through holes and blind vias were drilled on the test boards using a CNC drilling machine.

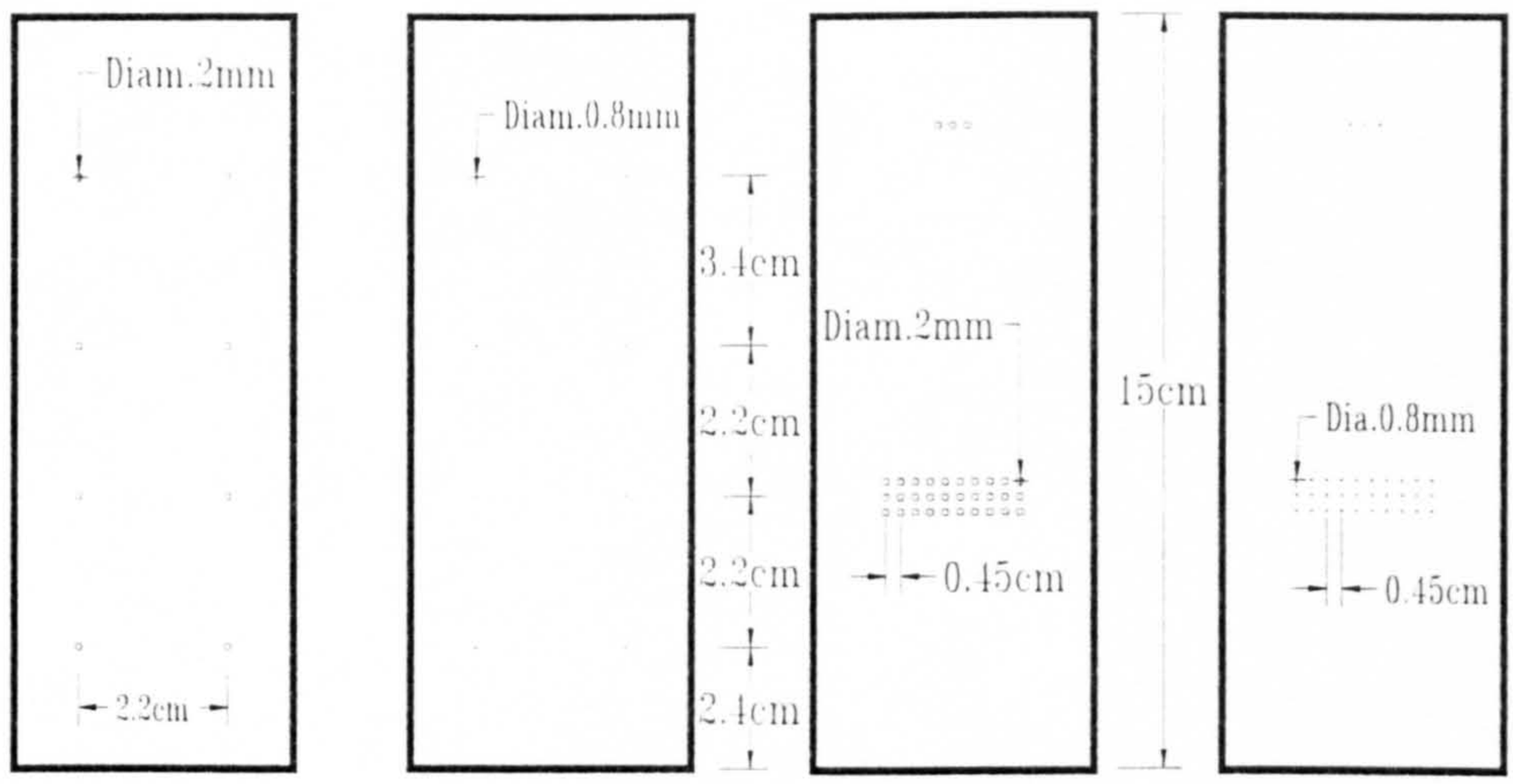

Fig. 5.1 : Test Boards of the PTH Screening Experiment (Not to Scale)

The mean and standard deviation of the plating thickness on the walls of the through-holes measured by the X-ray thickness gauge were determined and taken as the responses. All the hole walls were measured but the largest and smallest thickness values were excluded from the calculations to reduce the bias caused by extreme data. The parameter settings and the responses of the screening experiment are summarized as Table 5.2 below. The experiments were conducted in a randomized order. Raw data of the thickness readings are given in Appendix 5.2. The plating efficiency of all the experimental runs, as determined by the method of weight gain, is charted as Fig. 5.2. All the effect calculations and mathematical analysis were done using JMP Release 3.2 while the normal probability and response surface plots were constructed by STATISTICA Release 5.0 and MATLAB Release 4.2.

5.2.1.1 Analysis of the Mean Responses :

To identify the significant parameters affecting the mean plating thickness, a normal probability plot of the mean responses is constructed as Fig. 5.3, which shows that the average current density (C), electrode separation (D), the corrected aspect ratio (F) and the sulphuric acid × copper sulphate (AB) have strong effects on the average plating rate. ANOVA is performed after pooling all the residual sum of squares and

Run No.	Run order	A	B	C	D	E	F	Mean (μm)	SD (μm)
1	29	-	-	-	-	-	+	12.121	3.012
2	20	+	-	-	-	-	-	13.717	3.293
3	11	-	+	-	-	-	-	13.280	1.703
4	1	+	+	-	-	-	+	9.4470	1.422
5	30	-	-	+	-	-	-	13.011	3.377
6	21	+	-	+	-	-	+	14.093	2.597
7	15	-	+	+	-	-	+	14.795	1.941
8	8	+	+	+	-	-	-	14.232	3.232
9	32	-	-	-	+	-	-	13.054	2.530
10	18	+	-	-	+	-	+	12.551	2.130
11	13	-	+	-	+	-	+	14.256	3.053
12	7	+	+	-	+	-	-	13.654	2.262
13	25	-	-	+	+	-	+	14.022	2.383
14	19	+	-	+	+	-	-	16.285	5.194
15	12	-	+	+	+	-	-	14.538	4.191
16	6	+	+	+	+	-	+	12.908	2.601

Run No.	Run order	A	B	C	D	E	F	Mean (μm)	SD (μm)
17	31	-	-	-	-	+	-	12.506	1.939
18	17	+	-	-	-	+	+	11.502	3.453
19	10	-	+	-	-	+	+	11.465	1.655
20	3	+	+	-	-	+	-	10.523	1.771
21	27	-	-	+	-	+	+	12.778	2.085
22	24	+	-	+	-	+	-	15.121	2.521
23	16	-	+	+	-	+	-	15.722	1.974
24	5	+	+	+	-	+	+	10.573	3.179
25	28	-	-	-	+	+	+	13.676	1.848
26	22	+	-	-	+	+	-	13.111	1.166
27	9	-	+	-	+	+	-	13.331	1.528
28	2	+	+	-	+	+	+	9.970	1.714
29	26	-	-	+	+	+	-	16.960	3.830
30	23	+	-	+	+	+	+	16.275	3.168
31	14	-	+	+	+	+	+	13.870	3.081
32	4	+	+	+	+	+	-	16.308	5.081

Table 5.2 : Parameter Settings and the Responses of the PTH Screening Experiment

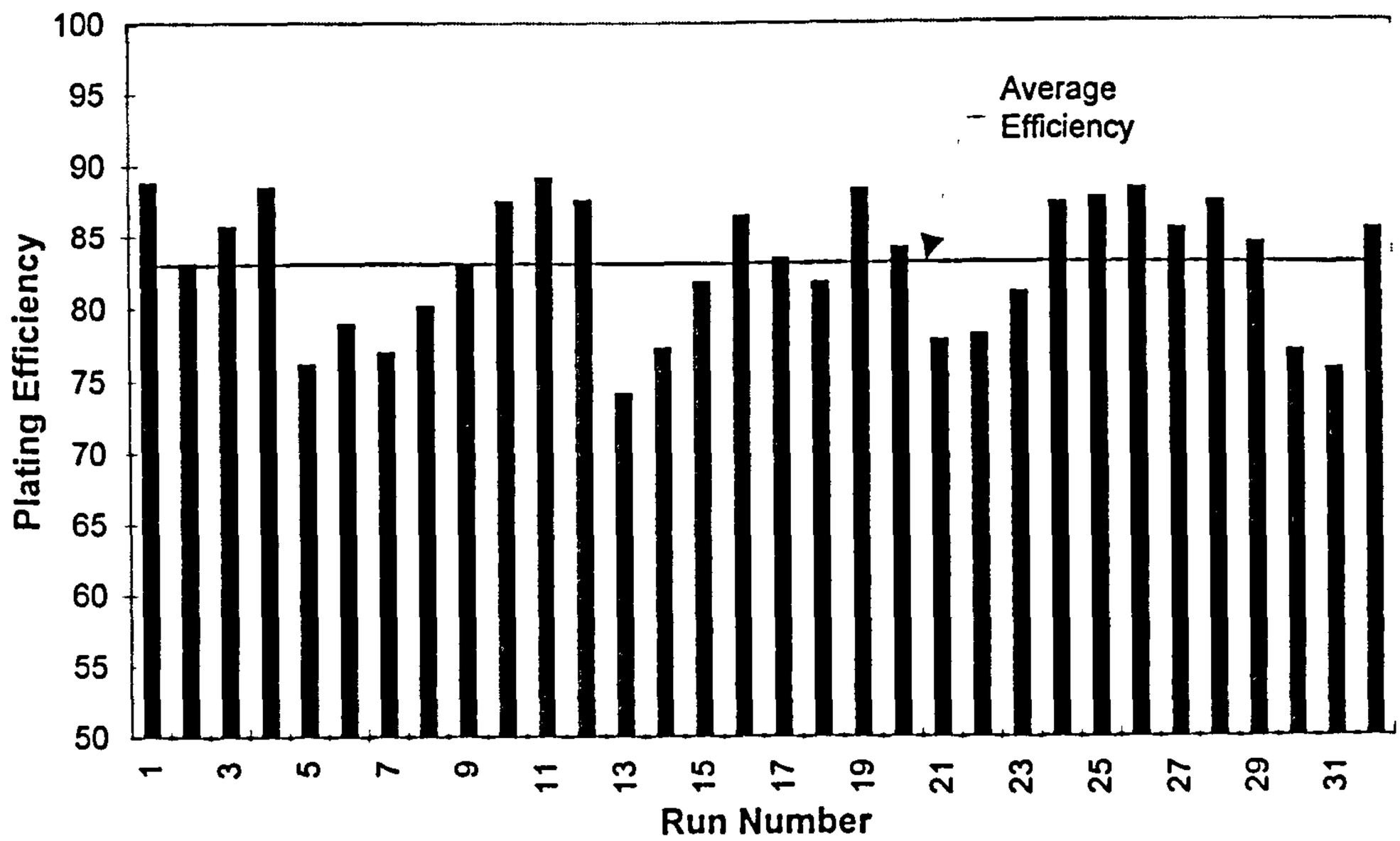

Fig. 5.2 : Plating Efficiency of the PTH Screening Experiment

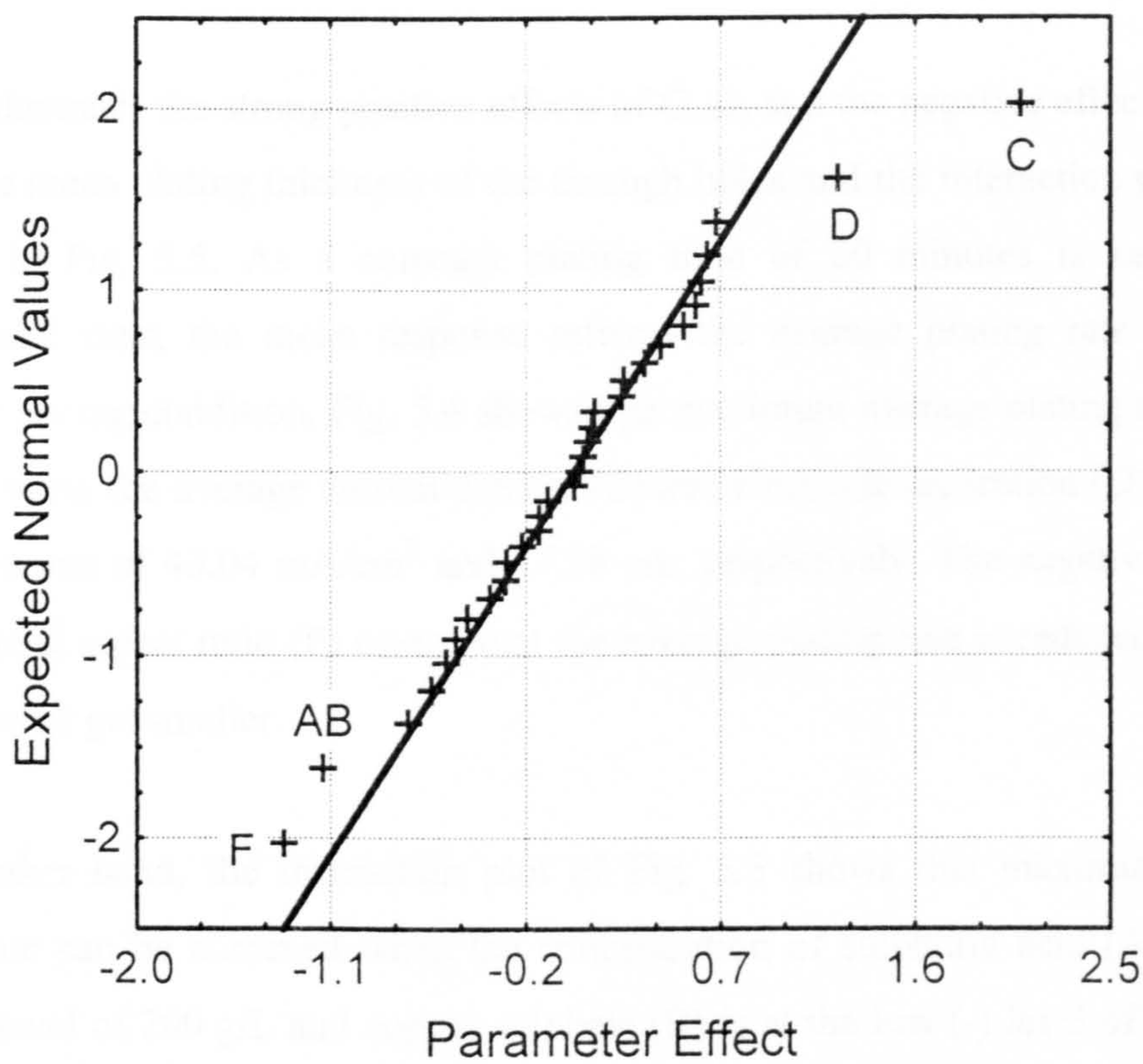

Fig. 5.3 : Normal Plot of the PTH Screening Experiment (Mean Responses)

Source	*SS*	*DF*	*MS*	*F*	*Prob. > F*
Model	78.266	6	20.307	17.54	< 0.0001
A	2.596	1	2.596	2.24	0.1469
B	4.434	1	4.434	3.83	0.0617
C	34.708	1	34.708	29.97	< 0.0001
D	12.358	1	12.358	10.67	0.0032
F	13.854	1	13.854	11.96	0.0020
AB	10.316	1	10.316	8.91	0.0063
Residual	28.959	25	1.158		
Total	107.226	31			

Table 5.3 : ANOVA Table of the PTH Screening Experiment (Mean Responses)

summarized as Table 5.3, which confirms the significance of the model and the four parameters.

Fig. 5.4 illustrates the strong positive effects of C, D, and the negative effects of F and AB on the mean plating thickness of the through holes and the interaction plot of AB is given in Fig. 5.5. As a constant plating time of 20 minutes is kept for all experimental runs, the mean response reflects the average plating rate under the particular plating condition. Fig. 5.4 shows that maximum average plating rate can be achieved when the average current density (C) and electrode separation (D) are at the high (+) levels of 43.04 mA/cm^2 and 17.78 cm, respectively. The negative effect of the corrected aspect ratio (F) means that the average plating rate is reduced when the through holes get smaller.

On the other hand, the interaction plot of Fig. 5.5 shows that maximum average plating rate can be achieved when the concentration of sulphuric acid (A) is at the high (+) level of 200 g/L and copper sulphate (B) is at the low (-) level of 90 g/L, *or vice versa*. Duncan's multiple range test [Duncan, 55] for the mean responses shows that, at an α-risk of 0.01,

- the positive effect of sulphuric acid on the average plating rate is not significant when the copper sulphate is at its low (-) level, and
- the positive effect of copper sulphate on the average plating rate is not significant when the sulphuric acid is at its low (-) level.

This interacting effect can also be observed in the interaction plot of Fig. 5.5. It means that maximum average plating rate would be resulted regardless of the concentration of the sulphuric acid or copper sulphate when either one, but not both, of the parameters is kept at a low (-) level. On the contrary, if either one of the parameter is at its high (+) level, maximum average plating rate can only be maintained when the other one is kept at its low (-) level. The strong negative effect of copper sulphate on the average plating rate at the high acid level can be explained by its negative effect on the conductivity of the electrolyte [Newman, 1991b]. The overall current efficiency is reduced when the ohmic resistance of the electrolyte is increased.

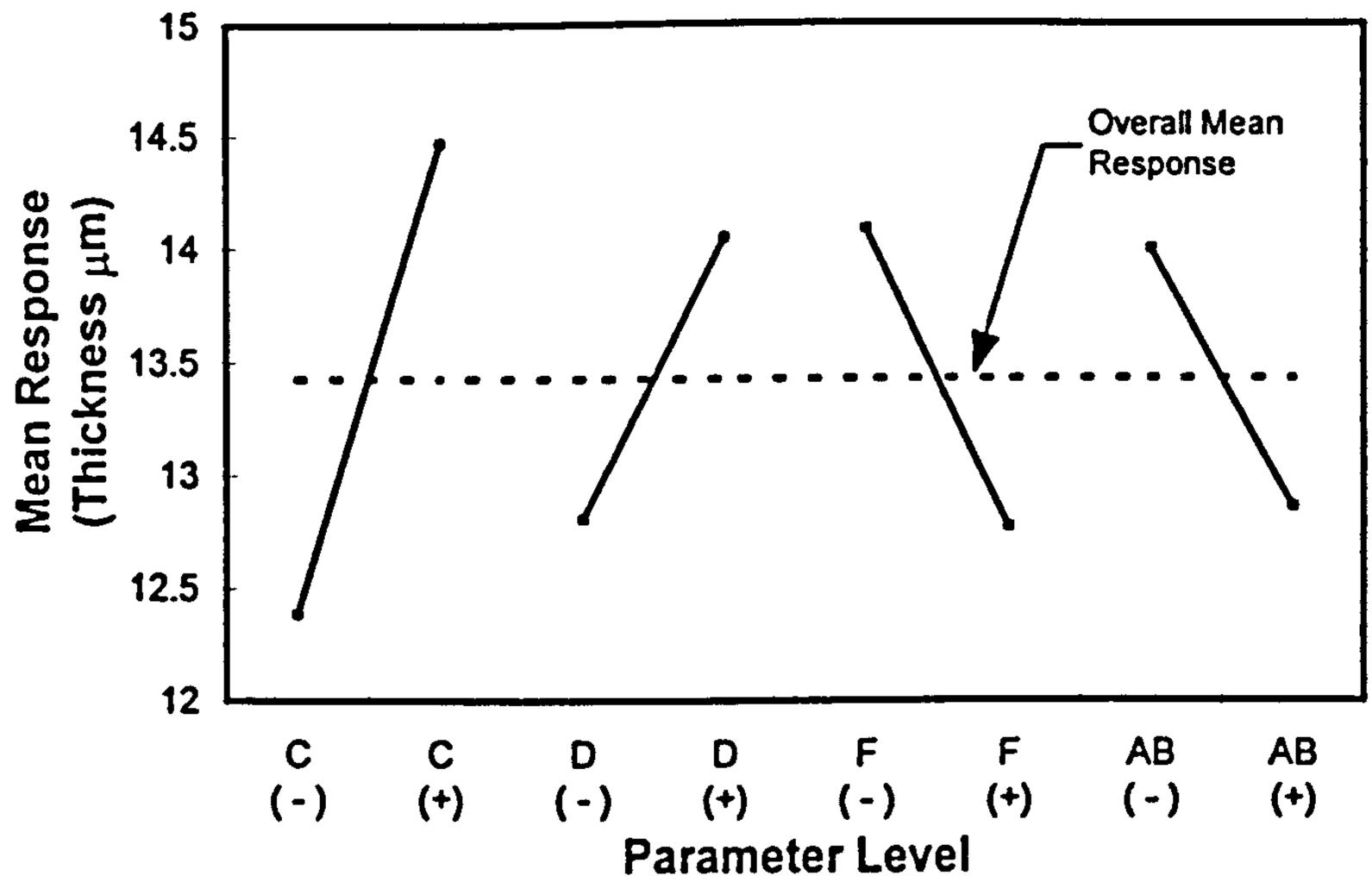

Fig. 5.4 : Analysis of Mean Plot of the Significant Location Parameters

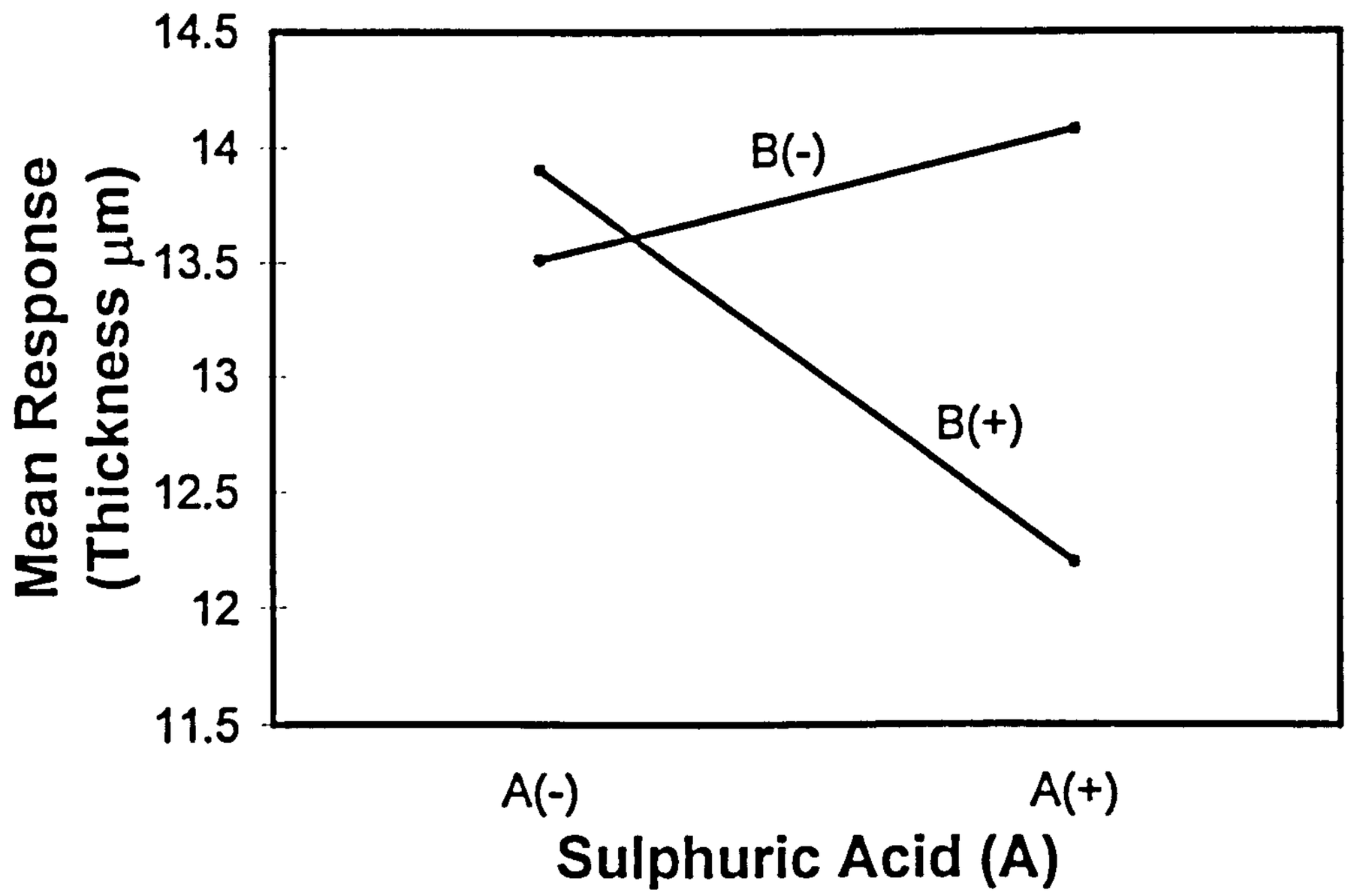

Fig. 5.5 : Interaction Plot of AB for the Mean Responses

5.2.1.2 Analysis of the SD Responses

The normal probability plot of the SD responses is shown as Fig. 5.6, which shows that average current density (C), the average current density × electrode separation (CD) interaction and the average current density × corrected aspect ratio (CF)

interaction are the significant parameters affecting the workpiece level plating uniformity of the through holes.

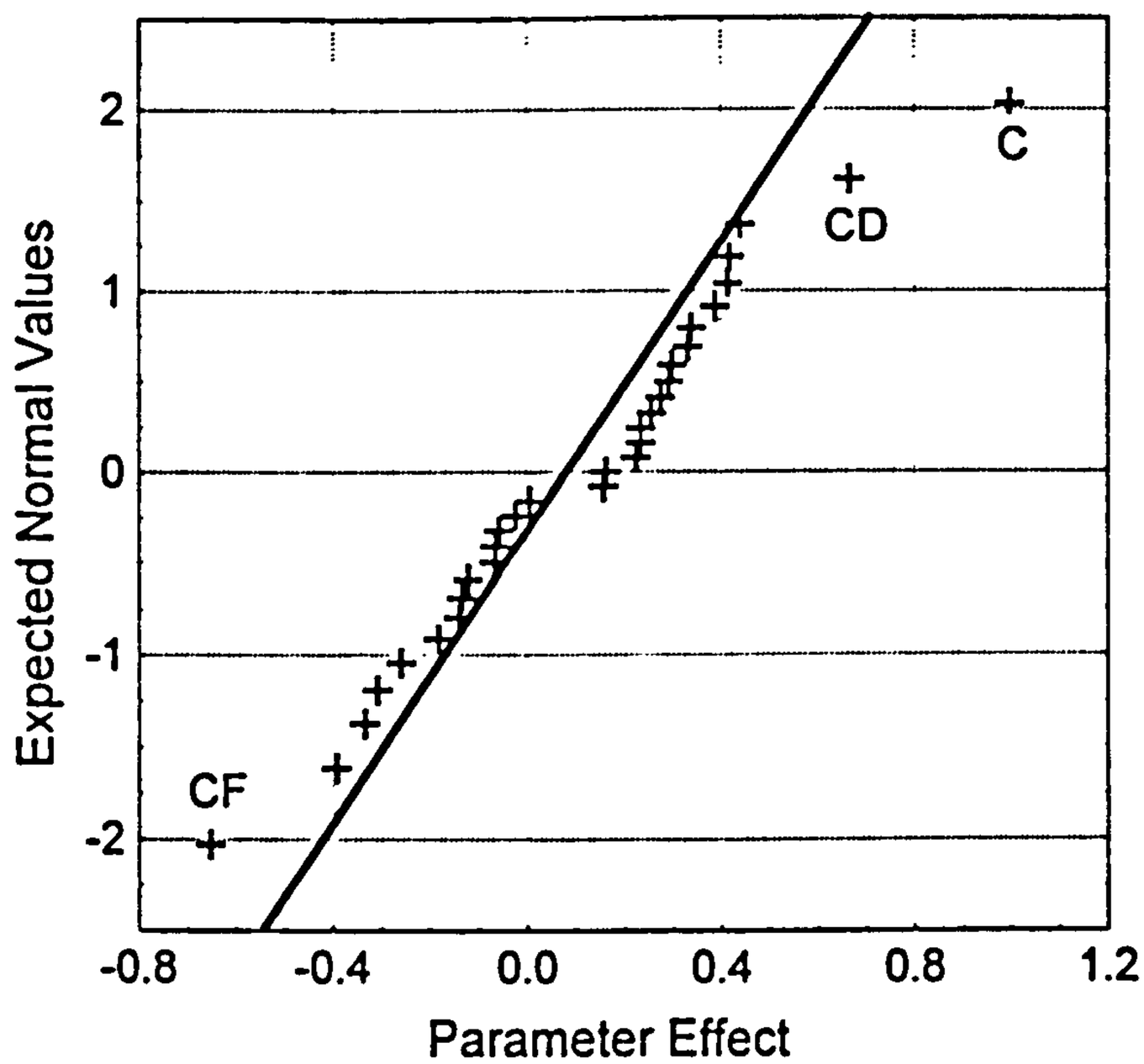

Fig. 5.6 : Normal Plot of the PTH Screening Experiment (SD Responses)

Fig. 5.7 shows the analysis of mean plot for the effects of significant factors C, the interaction CD and CF, which is also defined as the change in the mean response, i.e. mean standard deviation, when the factor is switched from its low (-) to the high (+) level. It shows that parameters C and CD have strong positive effects on the workpiece level thickness variation while CF has strong negative effect.

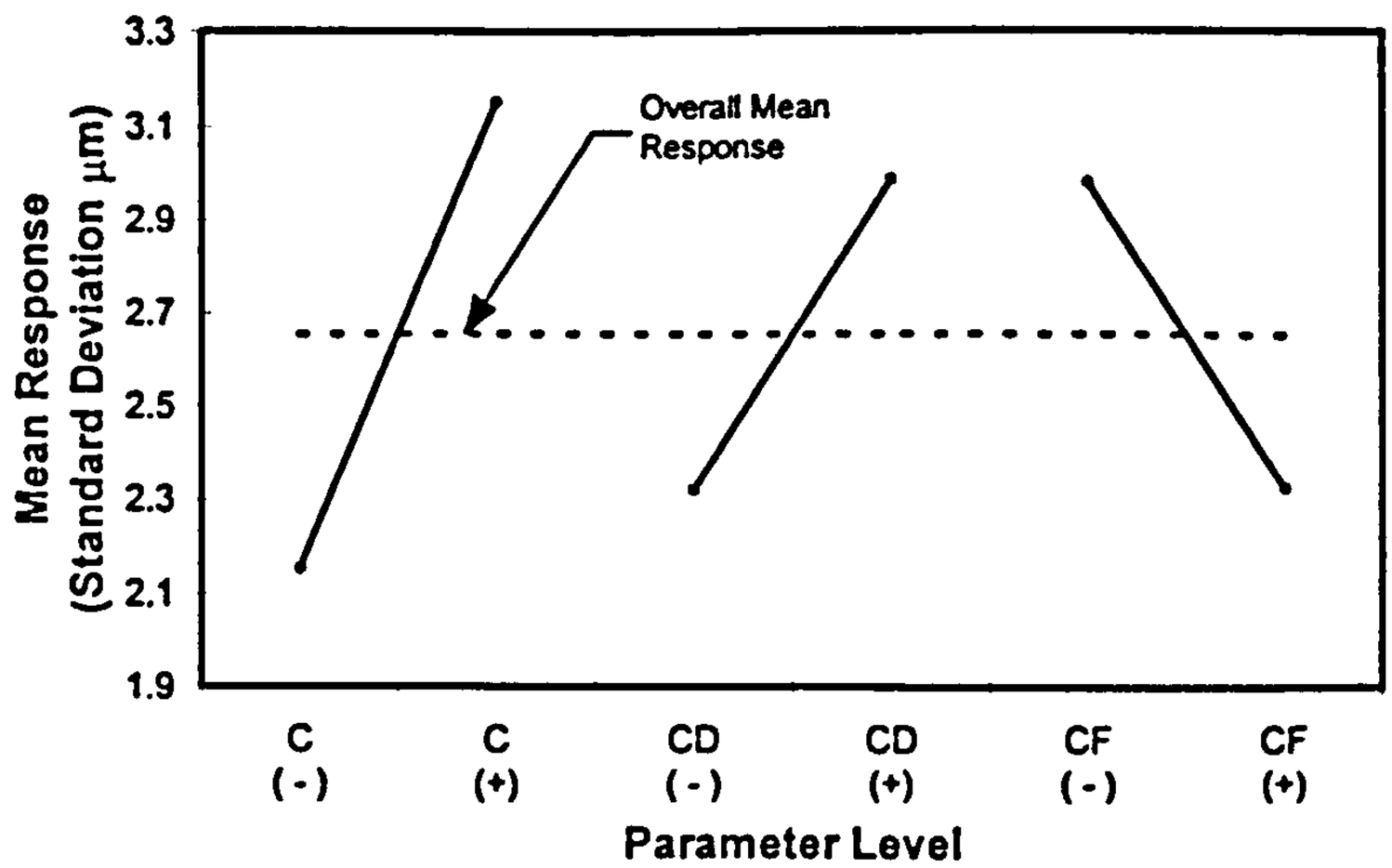

Fig. 5.7 : Analysis of Means Plot for the SD Responses

As the two interaction factors are significant, desirable parameter settings can only be determined from the interaction plots, which are shown as Fig. 5.8(a) and (b). The intersecting lines indicate strong interaction between the three parameters. If the objective is to minimize the thickness variation within the experimental range, Fig. 5.8(a) shows that the low average current density, C(-), of 32.28 mA/cm^2 and a large electrode separation, D(+), of 17.78 cm should be selected. Fig. 5.8(b) shows also that a low level of average current density gives better uniformity regardless of the level of the corrected aspect ratio F. Moreover, both the two interaction plots show that a low level of average current density can reduce the dispersion effect of the D and F, i.e. the variability induced by D and F from run to run can be reduced when an average current density of 32.28 mA/cm^2 is used.

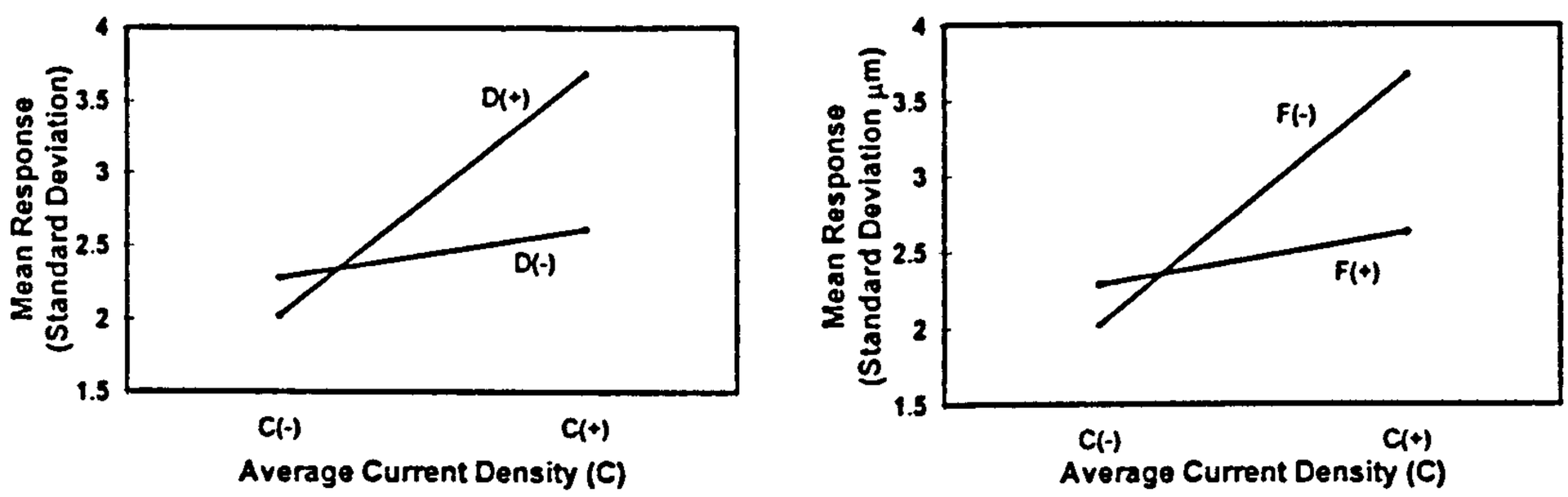

(a) CD Interaction (b) CF Interaction

Fig. 5.8 Interaction Plots for the Parameters C, D and F

5.2.1.3 Building the First-Order Model of the SD Responses

By pooling the sum of squares of all the insignificant parameters to give an estimate of the random error, an ANOVA is performed and the 4-term first-order model is found to be highly significant (α = 0.0003). The principal of hierarchy [Myers and Montgomery, 95] requires also the inclusion of the parameter D (electrode separation) and F (corrected aspect ratio) into the model, which yields the ANOVA table of Table 5.4. The 6-term first-order model, which can also be obtained by the projected 2^3 full factorial design of C, D, F and selecting the same set of parameters, is given by the equation below in coded form :

$$SD = 2.6536 + 0.4986C + 0.2064D + 0.1959F + 0.3325CD + 0.3269CF \qquad [5.1]$$

where SD is the predicted standard deviation.

Source	*SS*	*DF*	*MS*	*F*	*Prob. > F*
Model	17.505	5	3.501	6.97	0.0003
C	7.956	1	7.956	15.85	0.0005
D	1.363	1	1.363	2.72	0.1111
F	1.229	1	1.229	2.45	0.1296
CD	3.538	1	3.538	7.05	0.0134
CF	3.419	1	3.419	6.81	0.0148
Residual	13.057	26	0.502		
Lack of Fit	2.086	2	1.043	2.28	0.124
Pure Error	10.971	24	0.457		
Total	30.562	31			

Table 5.4 : ANOVA Table of the PTH Screening Experiment (SD Responses)

Although the model was found to be significant in the ANOVA test, the R^2_A (0.4906) and *PRESS* (19.78) performance, however, are unsatisfactory, indicating the limited predictive power ($R^2_{prediction}$ = 0.35) of the fitted model. The lack of fit, which is insignificant, of the model shows that the first-order model accurately describes the response surface and can be used to search for levels of the parameters that would produce more optimal values of the response, i.e. smaller thickness variation (SD).

As the first-order model contains two interaction effects (CD, CF), the response surface is a twisted plane and the path of steepest descent is not determinable. An approximate direction of steepest descent, however, can be identified from the response cube-plot of the projected 2^3 full factorial shown as Fig. 5.9.

In Fig. 5.9(a), the values at the corners of the cube are the average responses of the four replicates of the eight design points of the full factorial, while in Fig. 5.9(b), they refer to the predicted responses using first-order model of Eq. 5.1. It shows that minimum variation results at low average current density (C) and high electrode separation (D) for the whole range of the corrected aspect ratio (F). Therefore, in the coded variable coordinate system of (C,D,F), the line joining (0,0,0) and (-1,1,-1) represents the direction for minimizing the workpiece level variation and hence the path of further experimentation.

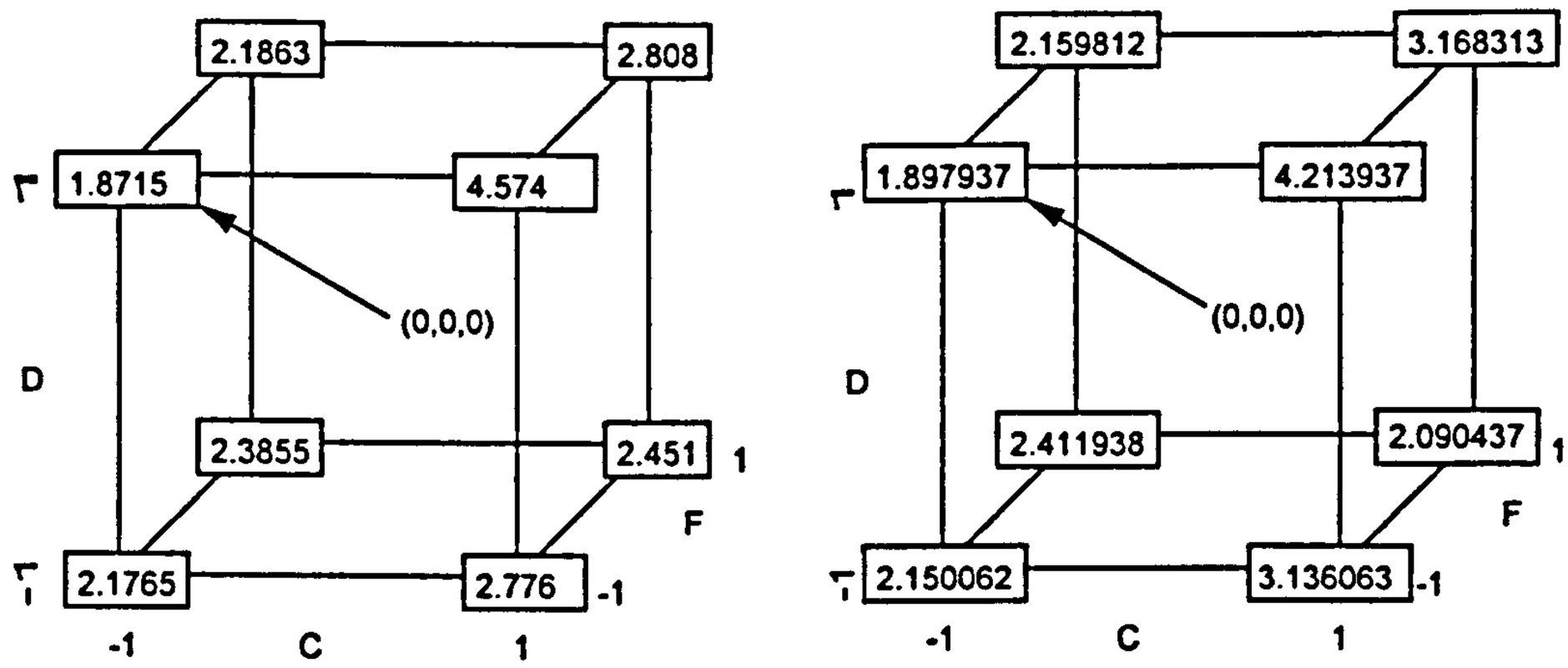

(a) Actual SD Responses (b) Predicted SD Responses

Fig. 5.9 : Cube-plot of the Projected 2^3 full factorial of the PTH Screening Experiment (SD Responses)

5.2.1.4 Residual Analysis

Analysis of the residuals of the first-order model revealed no abnormality of concern. Normal probability plot is given in Appendix 5.3.

5.2.2 Second-Order Model Building and Optimization of Workpiece Level Variation

Using the corner (-1,1,-1) in the (C,D,F) space as the centre point, a 16-run rotatable CCD involving the three factors C, D and F was designed and conducted to build a second-order model for the workpiece level variation and examine the possibility of minimizing such variation within the experimental space. Factor levels and settings are summarized in Table 5.5 below. As the factors A, B and E were found to be insignificant in the first-order model, they were not included in the second-order model and were held constant in this round of experiments.

Factors		Fixed Level	Factor Levels (-1.682)	(-1)	(0)	(+1)	(1.682)
A.	Sulphuric acid (g/L)	180	--	--	--	--	--
B.	Copper Sulphate (g/L)	75	--	--	--	--	--
C.	Average current Density (mA/cm^2)	--	27.8	29.6	32.3	35.0	36.8
D.	Electrode Separation (cm)	--	15.6	16.5	17.8	19.1	20.0
E.	Inter-hole Distance (cm)	0.45	--	--	--	--	--
F.	Corrected Aspect Ratio (mm)	--	2.048	2.226	2.560	3.012	3.413

Table 5.5 : Factor levels and setting of the PTH CCD Experiment

Similar to the first round experiment, the standard deviations of the hole-wall plating thickness were taken as the responses and summarized in Table 5.6. Twenty thickness readings were taken from the ten holes of each test board and the two largest and smallest readings were discarded in the calculation, raw data are given in Appendix 5.4. An average plating efficiency of 86.7% was recorded in this round.

Observation no.	Run order	C	D	F	SD (μm)
1	2	-1	-1	-1	0.3673
2	15	1	-1	-1	1.8830
3	10	-1	1	-1	0.9132
4	6	1	1	-1	2.2348
5	11	-1	-1	1	2.5430
6	8	1	-1	1	2.7993
7	3	-1	1	1	1.9653
8	9	1	1	1	1.8670
9	12	-1.682	0	0	1.7033
10	1	1.682	0	0	3.4312
11	4	0	-1.682	0	1.9151
12	7	0	1.682	0	1.4272
13	16	0	0	-1.682	0.7296
14	13	0	0	1.682	1.3834
15	5	0	0	0	1.1404
16	14	0	0	0	1.3805

Table 5.6 : Factor levels and Responses of the PTH CCD Experiment

The 10-term full second-order model in coded form is determined as

$$SD = 1.2579 + 0.4321C - 0.1049D + 0.357F + 0.4681C^2 + 0.1513D^2 - 0.066F^2$$
$$- 0.0686CD - 0.3349CF - 0.301DF \qquad [5.2]$$

The R^2_A, *PRESS* and $R^2_{prediction}$ values of the model are 0.90, 2.71 and 0.71, respectively, which shows that the second-order model is better than the first-order model of Eq. 5.1. Using the method of backward elimination [Miller, 90], the best fitted model is found to be the 8-term model of Eq. [5.3] with a R^2_A of 0.91, *PRESS* of 1.74 and $R^2_{prediction}$ of 0.81. This is also the model where the Mallow's C_p statistic [Mallow, 73] (7.23) first approaches the number of model parameters (8). Table 5.7 shows the ANOVA test of the model and its significance.

$$SD = 1.1541 + 0.4321C - 0.1049D + 0.357F + 0.4959C^2 + 0.1791D^2$$
$$- 0.3349CF - 0.301DF \qquad [5.3]$$

Source	*SS*	*DF*	*MS*	*F*	*Prob. > F*
Model	8.845	7	1.264	22.57	0.0001
Residual	0.448	8	0.056		
Lack of Fit	0.419	7	0.060	2.07	0.4906
Pure Error	0.029	1	0.029		
Total	9.293	15			

Table 5.7 : ANOVA of the PTH 8-term Second-order Model (SD Responses)

5.2.2.1 Response Surfaces and Optimization

As the second-order model (Eq. 5.3) contains three independent variables, the response surface can only be conveniently visualized by fixing the level of one of the variables. Two response surfaces are shown in Fig. 5.10(a) and (b) for the cases of low (-1) and high (+) level of the corrected aspect ratio (F). The response surfaces show that minimum variability can be obtained for different values of F. The optimum

PTH 8-term Second-order Model, F = -1

$SD = 0.7971+0.767C+0.1961D+0.4959C^2+0.1791D^2$

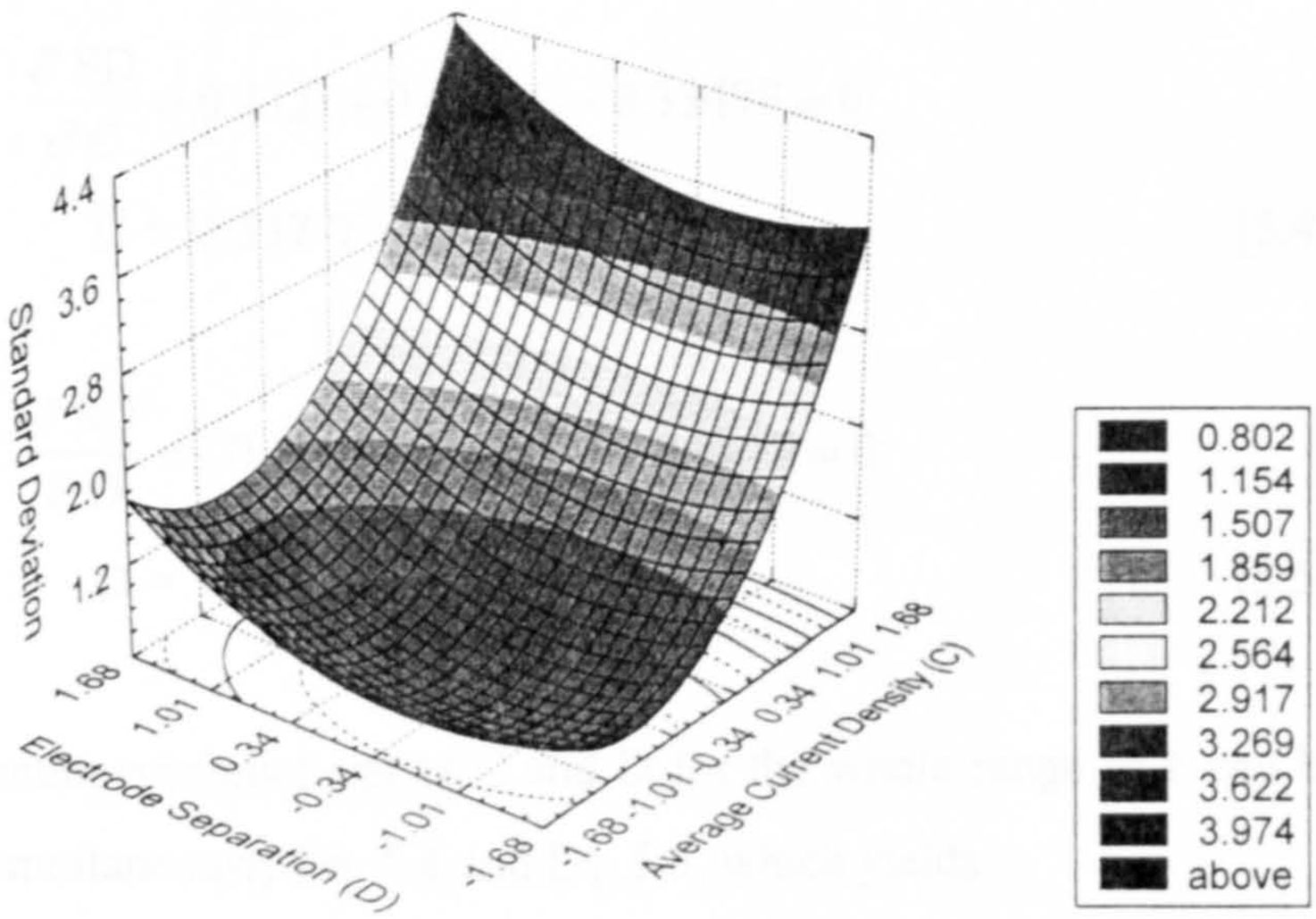

Fig. 5.10a : Response Surface and Contour Plot of the PTH 8-term Second-order Model for the case of F = -1

PTH 8-term Second-order Model, F = 1

$SD = 1.5111+0.0972C-0.4059D+0.4959C^2+0.1791D^2$

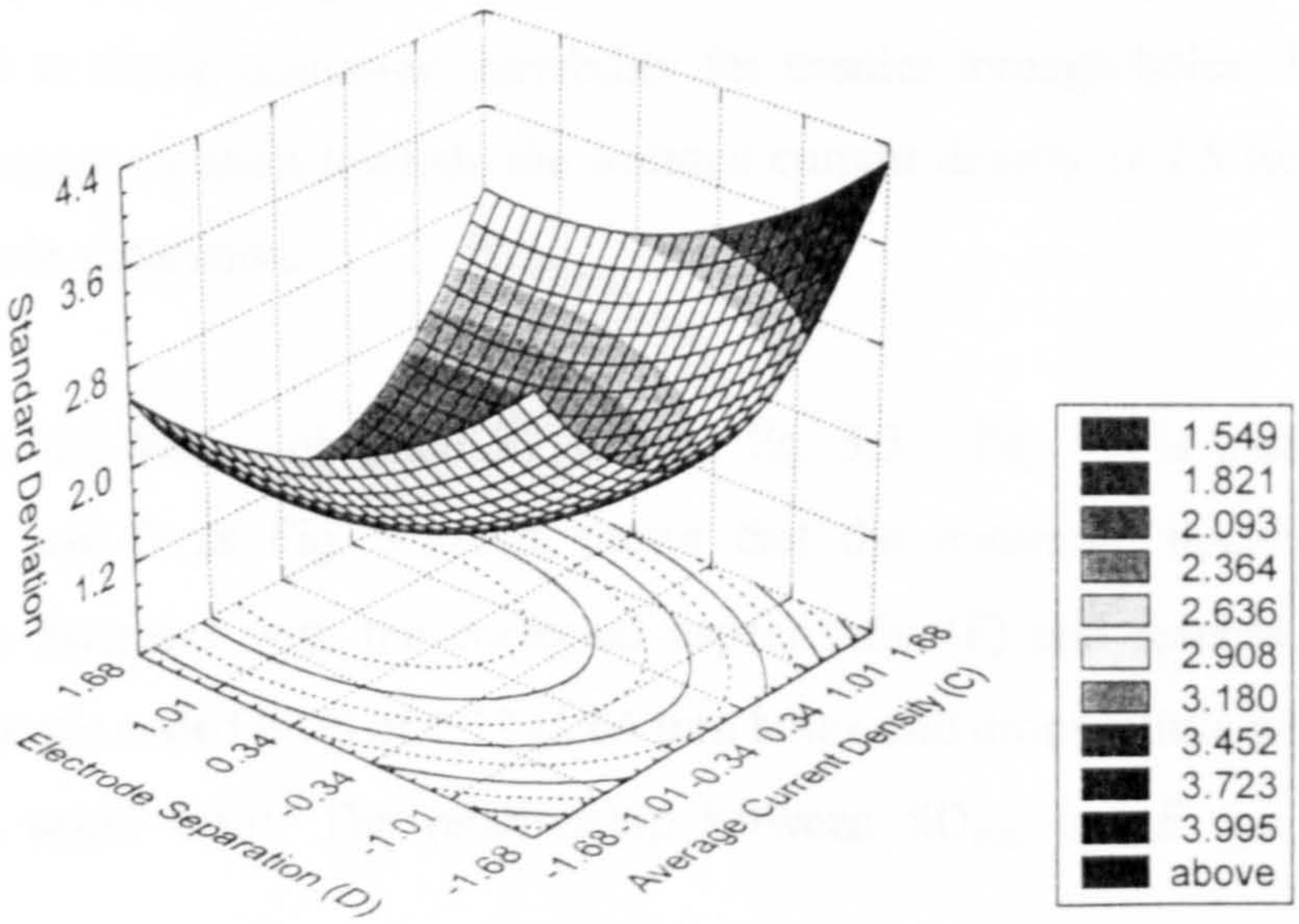

Fig. 5.10b : Response Surface and Contour Plot of the PTH 8-term Second-order Model for the case of F = 1

values of average current density (C) and electrode separation (D), which depend on the value of F, can be determined by simple differentiation as follows.

$$\frac{\partial SD}{\partial C} = 0.4321 + 0.9918C - 0.3349F = 0$$

i.e. $$C = 0.3377F - 0.4357 \qquad [5.4]$$

$$\frac{\partial SD}{\partial D} = -0.1049 + 0.3582D - 0.301F = 0$$

i.e. $$D = 0.8403F + 0.2929 \qquad [5.5]$$

The locus of the optimum combinations of C and D for the whole range of F can be obtained by solving simultaneously Eq. 5.4 and Eq. 5.5, which yields

$$D = 2.4883C + 1.3771 \qquad [5.6]$$

The resulting locus, illustrated in Fig. 5.11, shows that optimum values of average current density (C) and electrode separation (D) increase with the corrected aspect ratio (F) within the experimental range. Therefore, larger current density and electrode separation is required to obtain minimum variability for smaller through-holes. The sensitivity of the optimum solution towards the average current density is 2.5 times higher than the electrode separation.

The minimum variability, SD_{min}, obtained by solving Eq. 5.3 - Eq. 5.5 is plotted against parameter C and D as Fig. 5.12. It shows that the minimum thickness variability achievable increases with the corrected aspect ratio (F) and reaches its maximum when F is at the coded level of 1.13 (1.66 mm hole), and drops a little when F is approaching its upper limit. The relationship between SD_{min} and F can be determined as

$$SD_{min} = -0.183F^2 + 0.4148F + 1.0446 \qquad [5.7]$$

Eq. 5.7 is graphed as Fig. 5.13, which shows that although the workpiece level

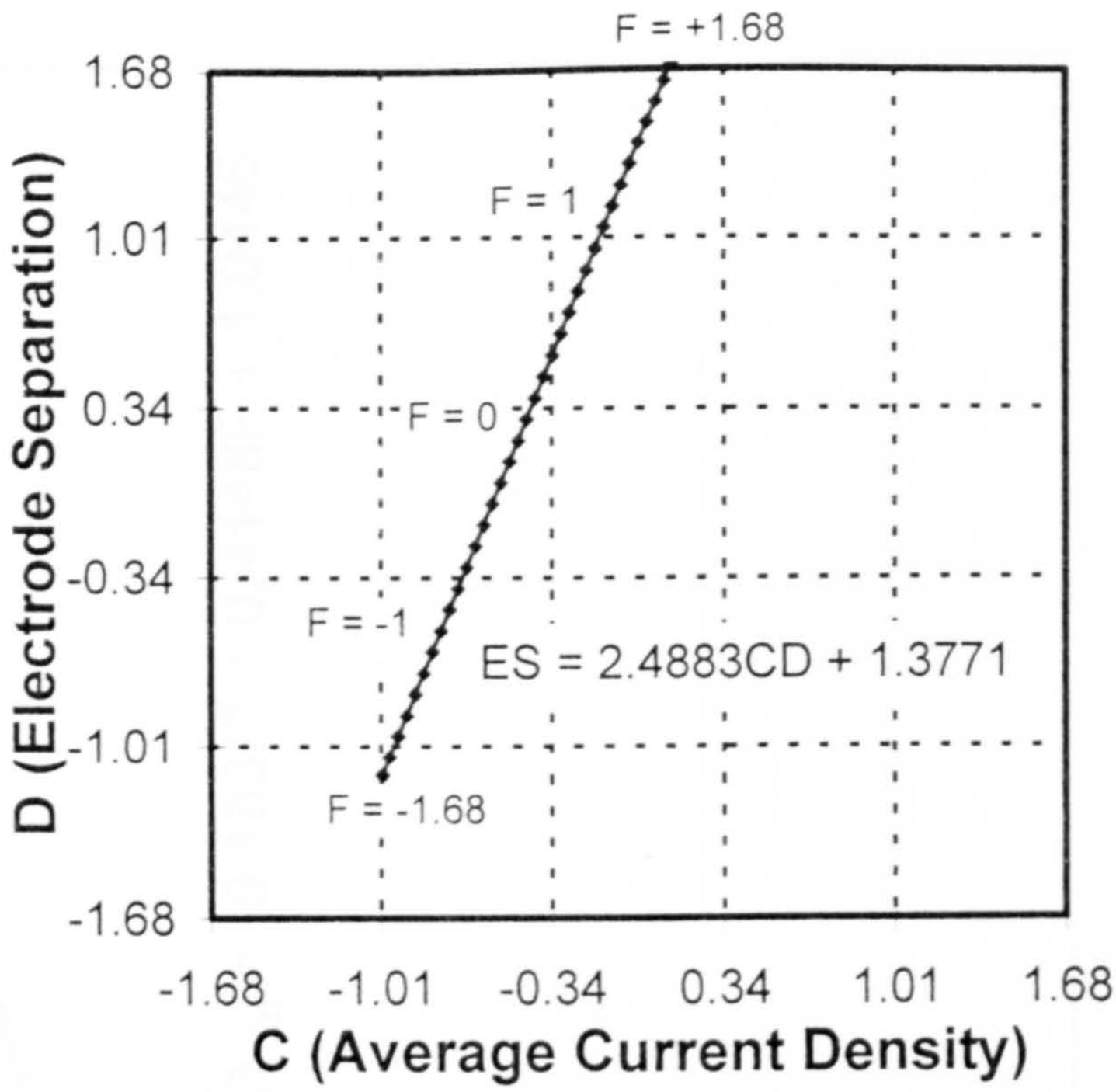

Fig. 5.11 : The Locus of the Optimum Combinations of parameter C and D for the whole range of F

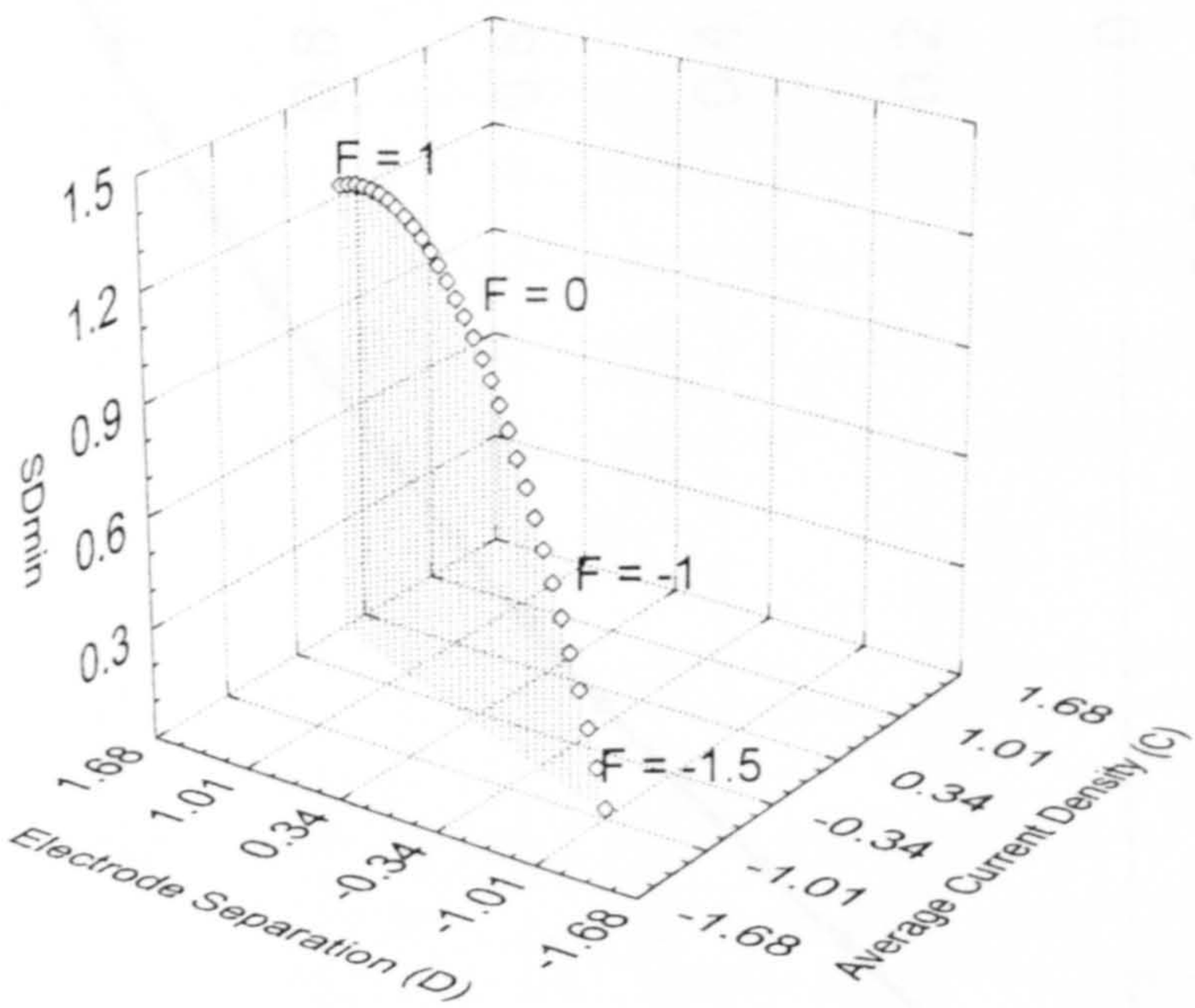

Fig. 5.12 : Predicted Minimum Standard Deviation of Plating Thickness at different levels of Corrected Aspect Ratio (F)

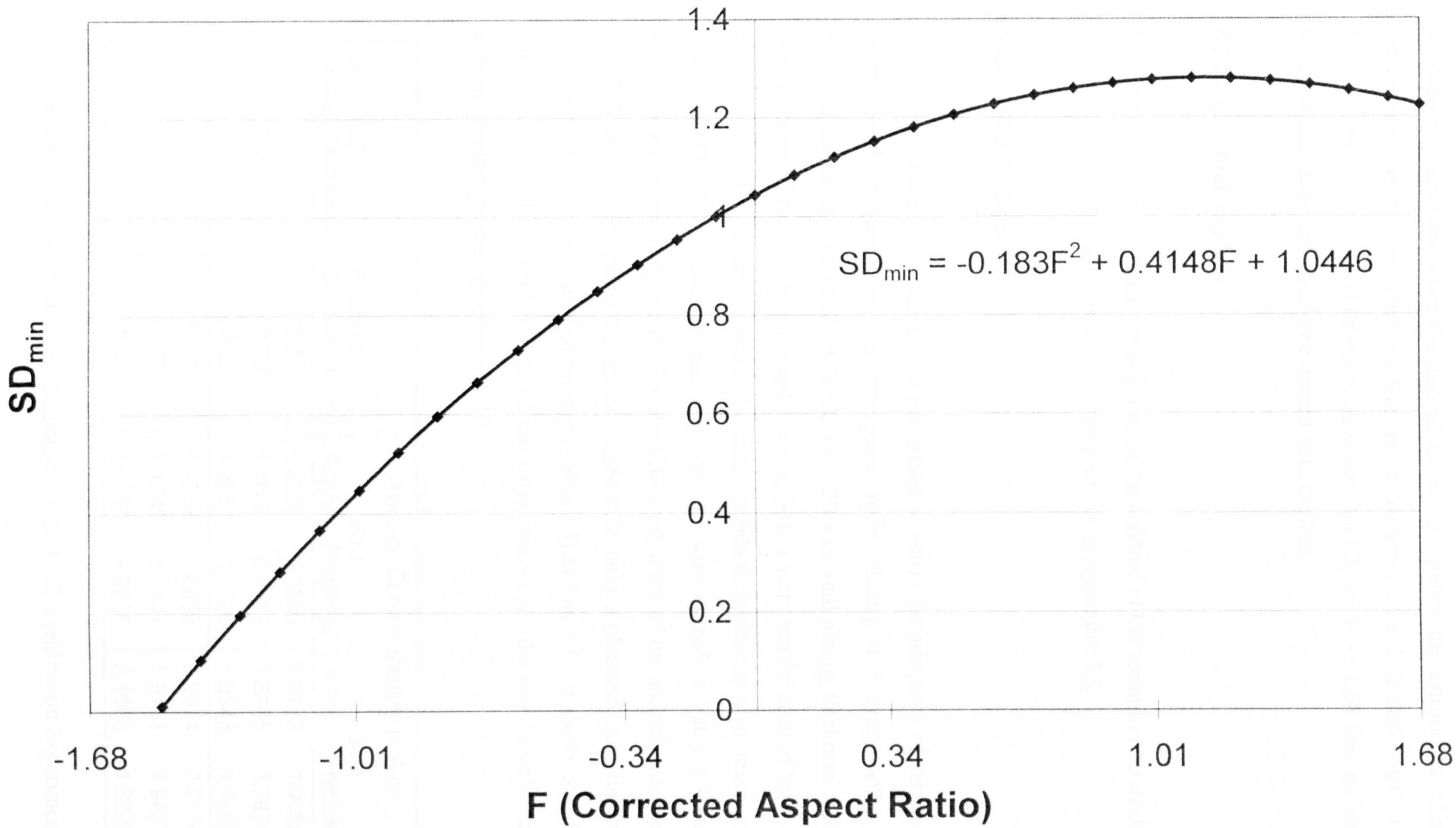

Fig. 5.13 : The Dependence of the Minimum Variability on the Corrected Aspect Ratio

uniformity deteriorates when the through-holes get smaller, the detrimental effect of the corrected aspect ratio tends to decrease at the same time. It is also noted in Fig. 5.11 that the optimum level of electrode separation (D) for F = +1.68 lies outside the experimental range and should be treated with caution.

5.2.2.2 Residual Analysis

Normality and independence assumptions of the residual of the second-order model were verified by the normal probability plot set out in Appendix 5.5.

5.2.3 Model Verification

Twenty four more experiments were performed to verify the adequacy of the second-order model in predicting the workpiece level plating uniformity within the experimental range. The standard deviation of 20 hole wall plating thickness readings were determined from each test board. Two replicates were run for each of the twelve combinations of C, D and F, while the mean standard deviations were taken as the responses. The factors settings and responses are summarized in Table 5.8 below. Raw data are given in Appendix 5.6. Predicted responses of the second-order model (Eq. 5.3) are plotted against the actual standard deviations obtained from the model building (Table 5.6) and verification runs (Table 5.8) as Fig. 5.14. It shows that the 8-term model is able to predict 90% of the variations within the experimental range, with an absolute percentage error of 0.10.

		Average Current Density (mA/cm²)			
Corrected	*Electrode*	30.1		34.4	
Aspect Ratio (mm)	*Separation (cm)*	Actual	Predicted	Actual	Predicted
2.44	16.51	1.2265	1.1600	1.9763	1.9960
	17.78	1.1000	0.9572	1.6685	1.7931
	19.05	1.2057	1.1126	1.6946	1.9485
2.69	16.51	1.4288	1.6858	2.2874	2.2174
	17.78	1.1735	1.3121	1.5144	1.8437
	19.05	1.2347	1.2965	2.1808	1.8282

Table 5.8 : Factors Settings and Responses of the PTH Verification Experiment

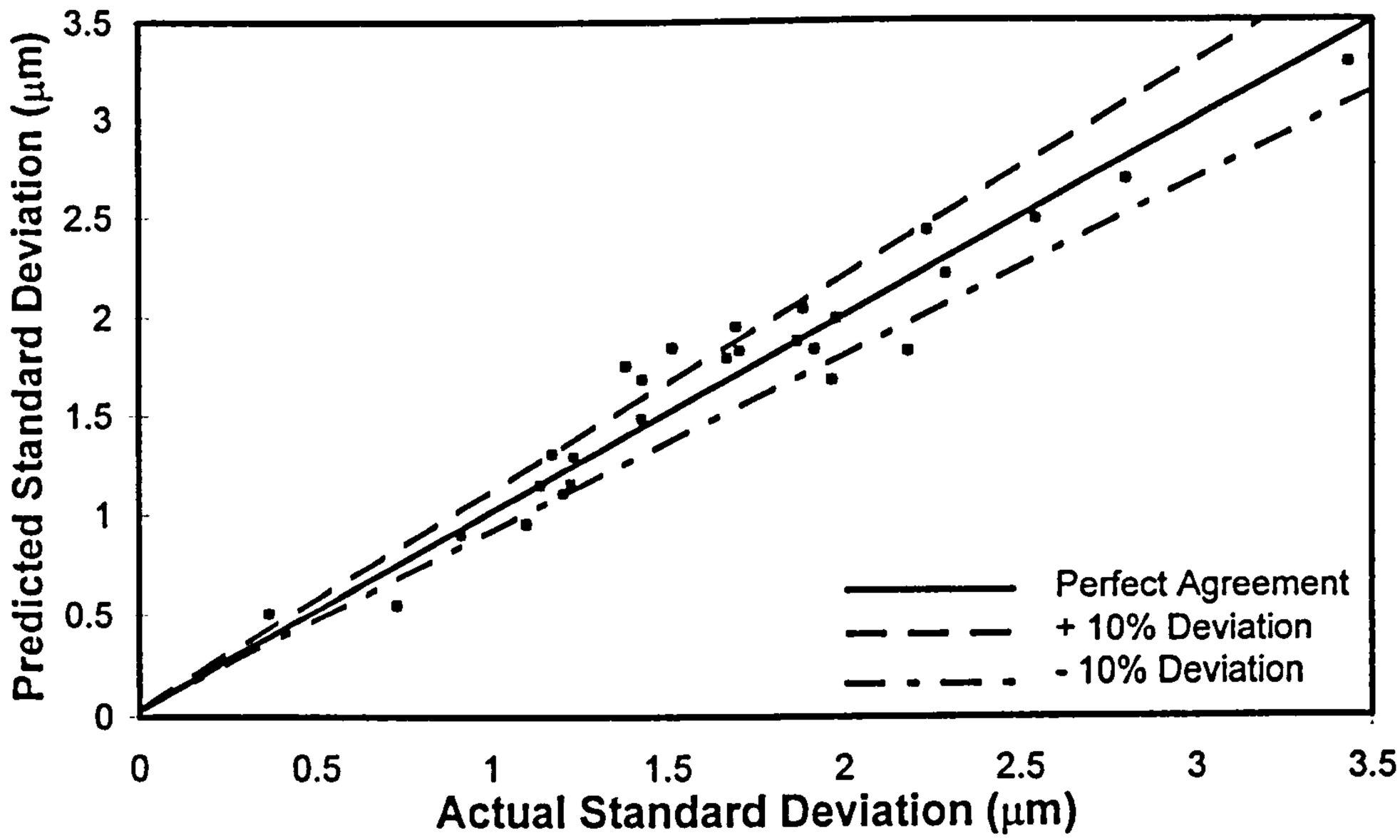

Fig. 5.14 : Verification Results of the PTH 8-term Second-order Model

5.3 Blind Via (BV) Plating Workpiece Level Modelling

5.3.1 Factors Screening and the First-Order Model

The parameter set of the screening runs is similar to that of the PTH experiment, except for the fact that an extra parameter of the depth ratio is added. The depth ratio is defined as the ratio of the depth of the blind via to the thickness of the PCB and is dimensionless. A 32-run 2_{IV}^{7-2} FFD was employed to study the effects of the seven parameters on the mean and variation of the plating thickness on the wall of the blind via. The experiments and test boards were so designed that part of the experiments could be conducted in parallel with the PTH screening runs, thus reducing the total number of runs. Parameters settings and results are summarized as Table 5.9. The resolution IV design was constructed using a 2^5 full factorial as the first five columns and the defining relationship $I = ABCDF = ABDEG$ for the last two columns. The full alias structure is given in Appendix 5.7. The plating thicknesses on the wall of the blind vias were measured by the X-ray thickness gauge, while their means and

standard deviations were determined as the responses. Raw data are tabulated in Appendix 5.8.

Run No.	A	B	C	D	E	F	G	Mean (μm)	SD (μm)
1	-	-	-	-	-	-	+	8.583	1.129
2	+	-	-	-	-	+	-	6.800	0.985
3	-	+	-	-	-	+	-	7.278	1.347
4	+	+	-	-	-	-	+	8.743	1.151
5	-	-	+	-	-	+	+	10.750	2.197
6	+	-	+	-	-	-	-	10.230	1.838
7	-	+	+	-	-	-	-	7.912	1.744
8	+	+	+	-	-	+	+	10.660	2.101
9	-	-	-	+	-	+	-	9.292	1.760
10	+	-	-	+	-	-	+	7.784	1.684
11	-	+	-	+	-	-	+	8.553	1.957
12	+	+	-	+	-	+	-	9.082	1.656
13	-	-	+	+	-	-	-	11.200	2.472
14	+	-	+	+	-	+	+	10.920	2.147
15	-	+	+	+	-	+	+	11.910	2.142
16	+	+	+	+	-	-	-	11.240	2.423

Run No.	A	B	C	D	E	F	G	Mean (μm)	SD (μm)
17	-	-	-	-	+	-	-	8.067	1.224
18	+	-	-	-	+	+	+	6.699	1.092
19	-	+	-	-	+	+	+	7.569	1.280
20	+	+	-	-	+	-	-	7.884	1.381
21	-	-	+	-	+	+	-	8.595	1.859
22	+	-	+	-	+	-	+	8.472	1.865
23	-	+	+	-	+	-	+	9.914	1.867
24	+	+	+	-	+	+	-	8.742	2.005
25	-	-	-	+	+	+	+	8.478	1.674
26	+	-	-	+	+	-	-	6.843	1.215
27	-	+	-	+	+	-	-	7.464	1.275
28	+	+	-	+	+	+	+	8.278	1.446
29	-	-	+	+	+	-	+	12.050	2.585
30	+	-	+	+	+	+	-	10.900	2.587
31	-	+	+	+	+	+	-	11.470	2.339
32	+	+	+	+	+	-	+	13.050	2.629

Table 5.9 : Parameter settings and the Responses of the BV Screening Experiment

5.3.1.1 Analysis of the Mean Response

The normal probability plot of the mean responses, shown as Fig. 5.15, shows that the significant parameters are the average current density (C), electrode separation (D) and the two two-factor interaction : sulphuric acid × copper sulphate (AB) and average current density × electrode separation (CD). The ANOVA table of Table 5.10 confirms also their significance.

Fig. 5.16 illustrates the strong positive effects of C, D, AB and CD on the mean plating thickness of the blind-vias and their respective interaction plots are given in Fig. 5.17(a) and (b). As in the case of the PTH screening experiment, the mean response reflects the average plating rate under the particular plating condition. Fig. 5.17(a) shows that maximum average plating rate can be achieved when both the concentration of sulphuric acid (A) and copper sulphate (B) are at the high (+) level, i.e. 200 g/L and 90 g/L, respectively. However, such maximum plating rate is found to

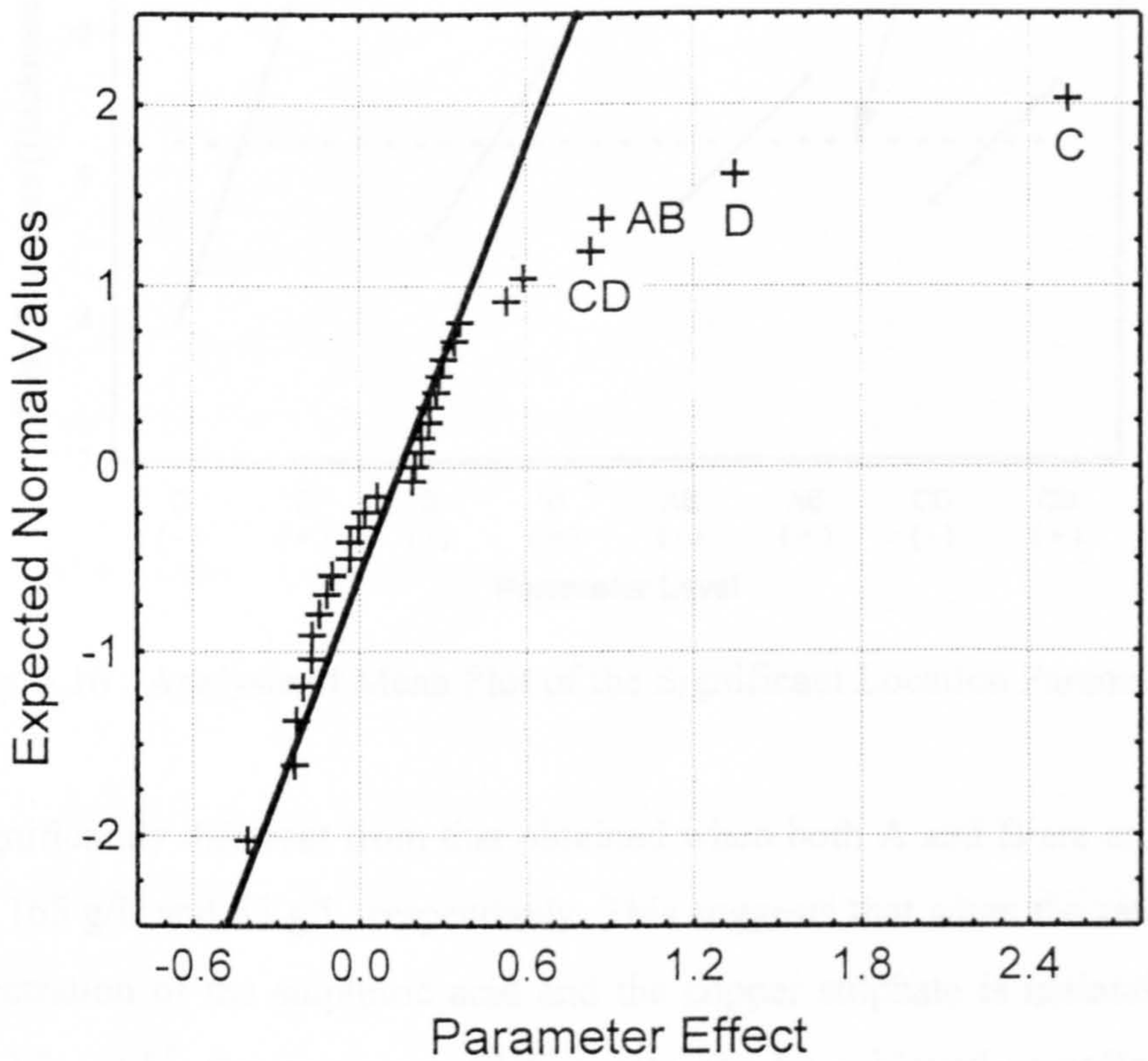

Fig. 5.15 : Normal Plot the of the BV Screening Experiment (Mean Responses)

Source	*SS*	*DF*	*MS*	*F*	*Prob. > F*
Model	77.777	4	19.444	35.29	< 0.0001
C	51.559	1	51.559	93.57	< 0.0001
D	14.586	1	14.586	26.47	< 0.0001
AB	6.103	1	6.103	11.08	0.0025
CD	5.529	1	5.529	10.03	0.0038
Residual	14.866	27	0.551		
Lack of Fit	2.801	11	0.255	0.34	0.9624
Pure Error	12.065	16	0.754		
Total	30.562	31			

Table 5.10 : ANOVA Table of the BV Screening Experiment (Mean Responses)

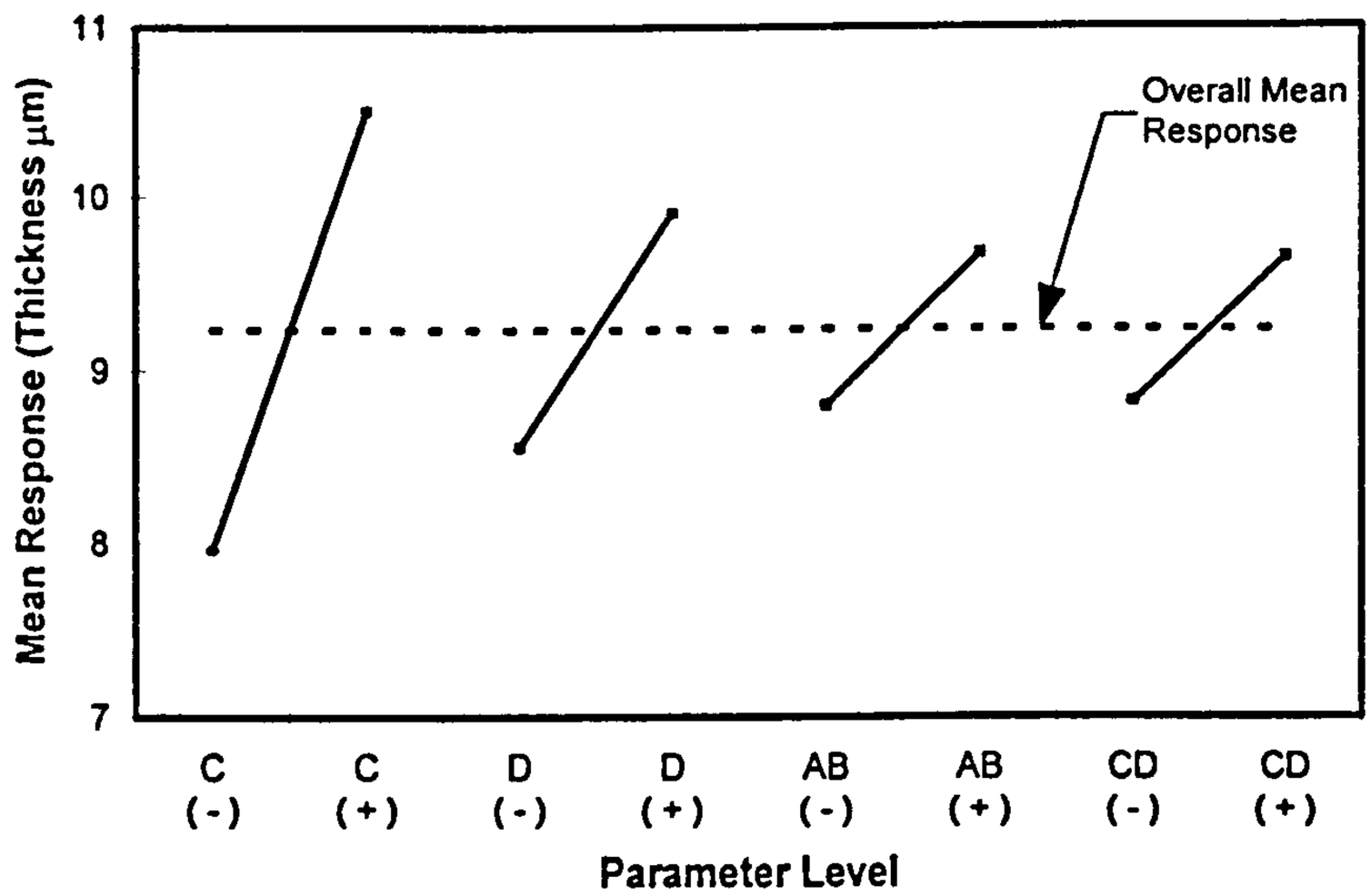

Fig. 5.16 : Analysis of Mean Plot of the Significant Location Parameters

be not significantly different from that obtained when both A and B are at the low (-) level, i.e. 165 g/L and 65 g/L, respectively. This suggests that when the ratio between the concentration of the sulphuric acid and the copper sulphate is maintained in the range of 2.2 - 2.5[†], the maximum plating rate can be achieved regardless of their absolute concentration levels provided, of course, that they are within their respective operating ranges. This is explained by the strong interacting effects between the two parameters illustrated also on the same plot. It means that the concentration of sulphuric acid has a positive effect on the average plating rate when the copper sulphate concentration is high (B+), but its effect is reversed when it is at a low level (B-). Therefore, alternating the levels of either one of the parameters without a proportional change of the other one will result in a lower average plating rate.

On the other hand, Fig. 5.17(b) shows that maximum average plating rate is resulted when high average current density (43.04 mA/cm^2) and large electrode separation (17.78 cm) is employed. While the first condition is common to all Faradaic reactions, the interaction plot shows that this Faradaic effect is attenuated by the magnitude of the electrode separation, which manifests itself as the strong interaction between the two parameters.

[†] The value 2.2 represents the ratio of the concentration of sulphuric acid to that of the copper sulphate when both of them are at the high (+) level, i.e. 200/90, while the value 2.5 represents the same ratio when both of them are at the low (-) level, i.e. 165/65.

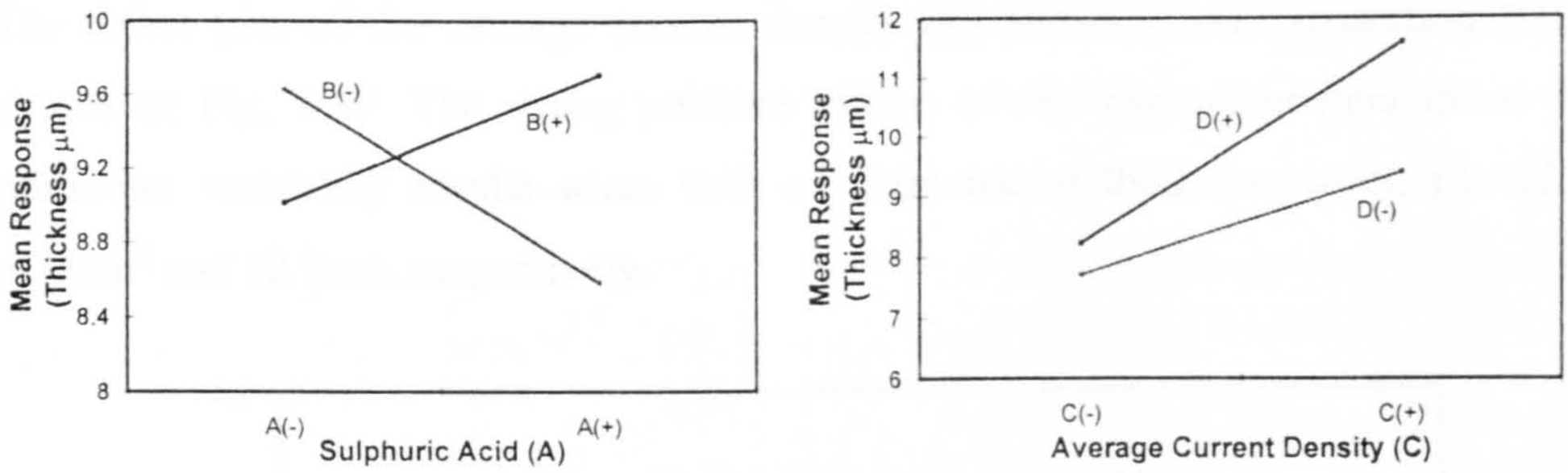

(a) AB Interaction (b) CD Interaction

Fig. 5.17 Interaction Plots for the Parameters A, B, C, and D for the Mean Responses

5.3.1.2 Analysis of the SD Responses

Normal probability of Fig. 5.18 shows that the average current density (C) and the electrode separation are the only two active parameters affecting the workpiece level uniformity of the blind vias. Both of the two parameters have strong positive effect on the thickness variation[‡].

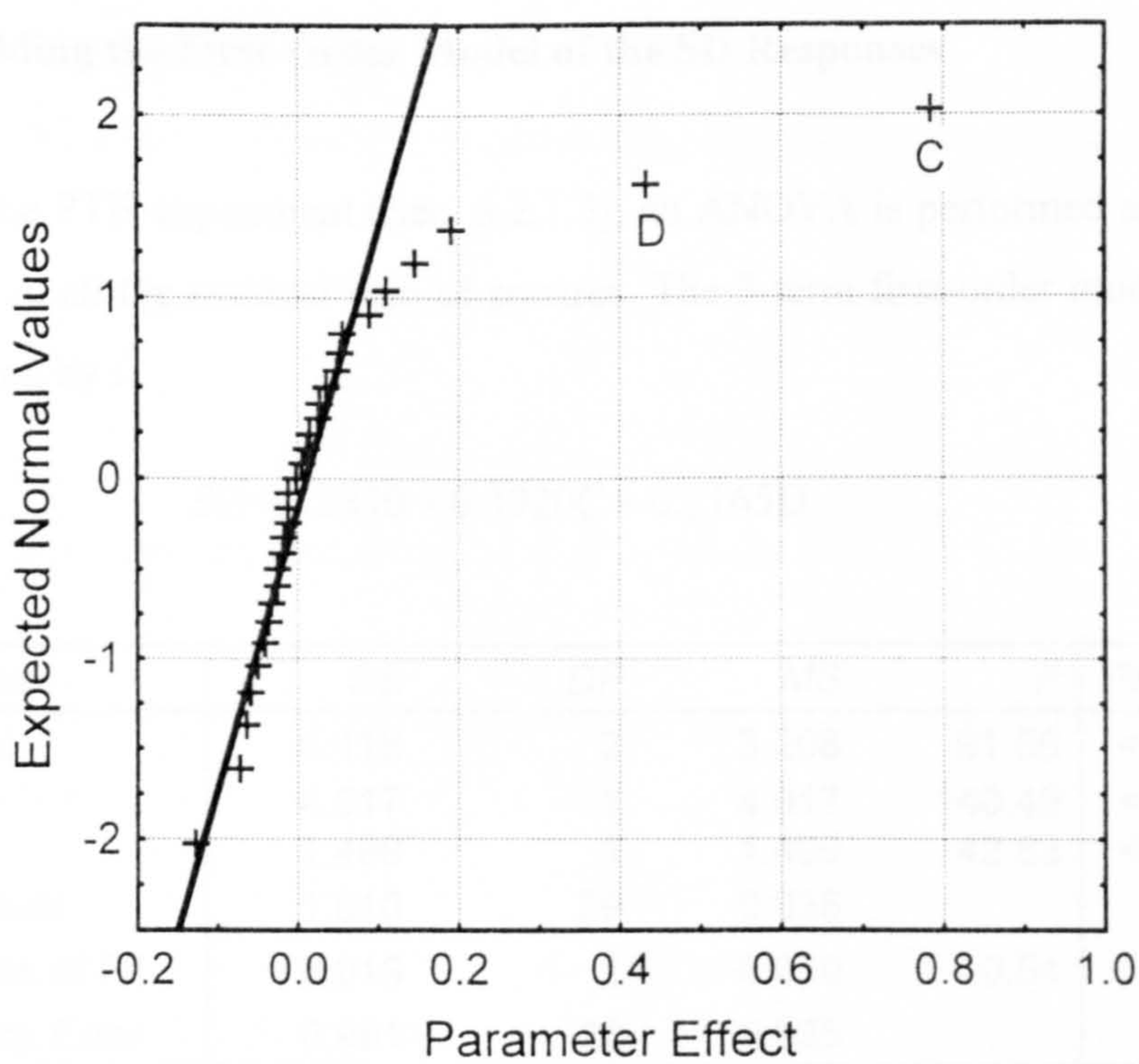

Fig. 5.18 : Normal Probability Plot of the BV Screening Experiment (SD Responses)

‡ In contrast to the findings of the PTH experiments (Sec. 6.2.1.2), the CD interaction and the corrected aspect ratio of the blind via were no longer significant in affecting the thickness variability.

The effect plot of the average current density (C) and electrode separation (D) is shown as Fig. 5.19. The strong positive effects of the two parameters mean that minimum variability results when both of them are at their low level, i.e. 32.28 mA/cm^2 and 12.7 cm, respectively.

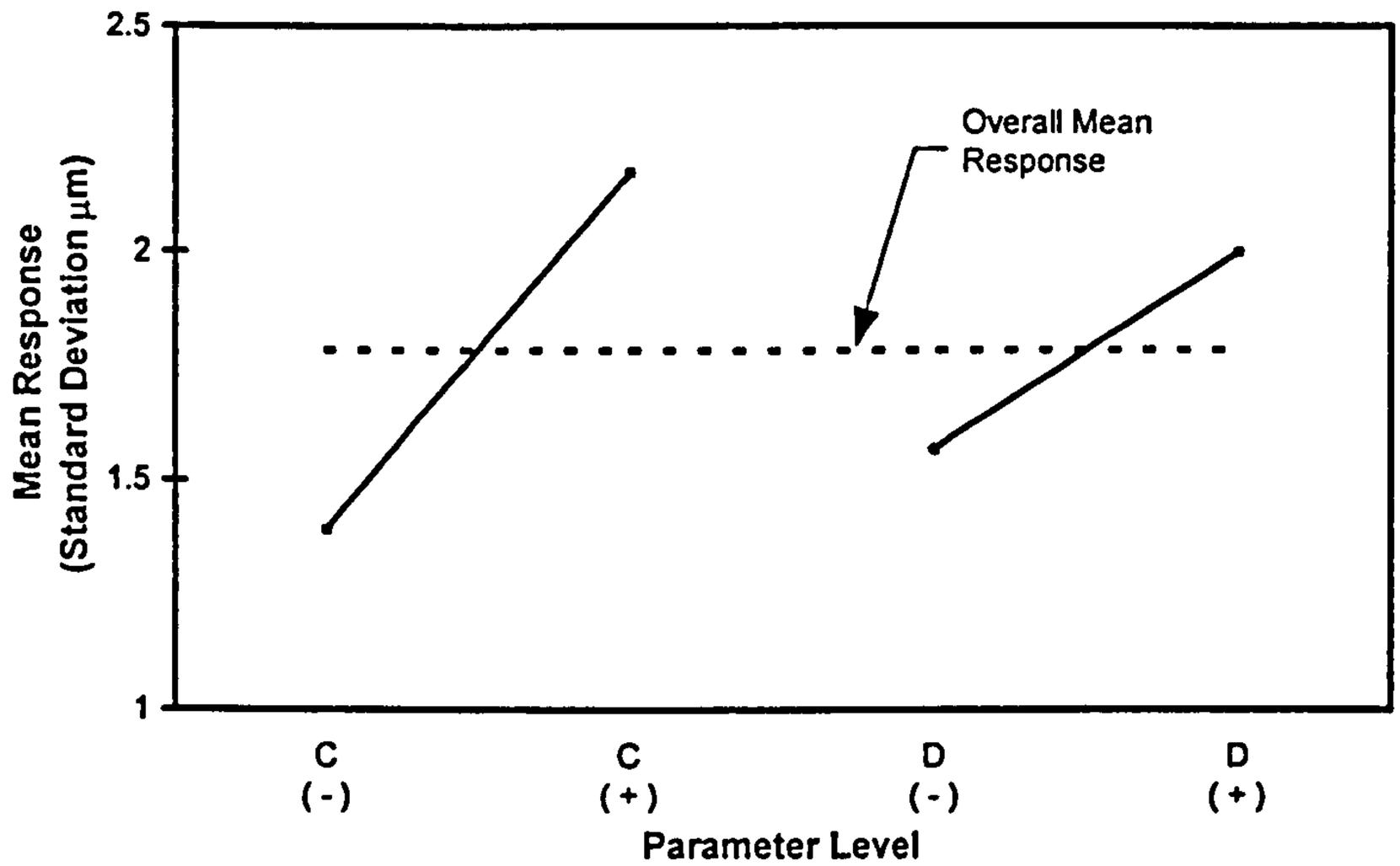

Fig. 5.19 : Analysis of Mean Plot for the SD Responses

5.3.1.3 Building the First-Order Model of the SD Responses

Similar to the PTH experiment (Sec. 5.2.1.3), an ANOVA is performed as Table 5.11 by pooling up all the residual sum of squares. The 3-term first-order model, in coded form, is given by :

$$SD = 1.7830 + 0.3920C + 0.2165D \qquad [5.8]$$

Source	*SS*	*DF*	*MS*	*F*	*Prob. > F*
Model	6.416	2	3.208	91.66	< 0.0001
C	4.917	1	4.917	140.49	< 0.0001
D	1.499	1	1.499	42.83	< 0.0001
Residual	1.010	29	0.035		
Lack of Fit	0.019	1	0.019	0.54	0.4685
Pure Error	0.991	28	0.035		
Total	7.427	31			

Table 5.11 : ANOVA Table of the BV Screening Experiment (SD Responses)

The model is highly significant, with a R^2_A of 0.8546, a *PRESS* of 1.23 and a $R^2_{prediction}$ of 0.8344. The response surface of the first-order model is shown as Fig. 5.20, which indicates clearly the location of minimum variability, [C(-), D(-)], within the experimental range. It is noted that this location is different from that of the PTH system, which is found to be [C(-), D(+)] in Sec. 5.2.1.3 above.

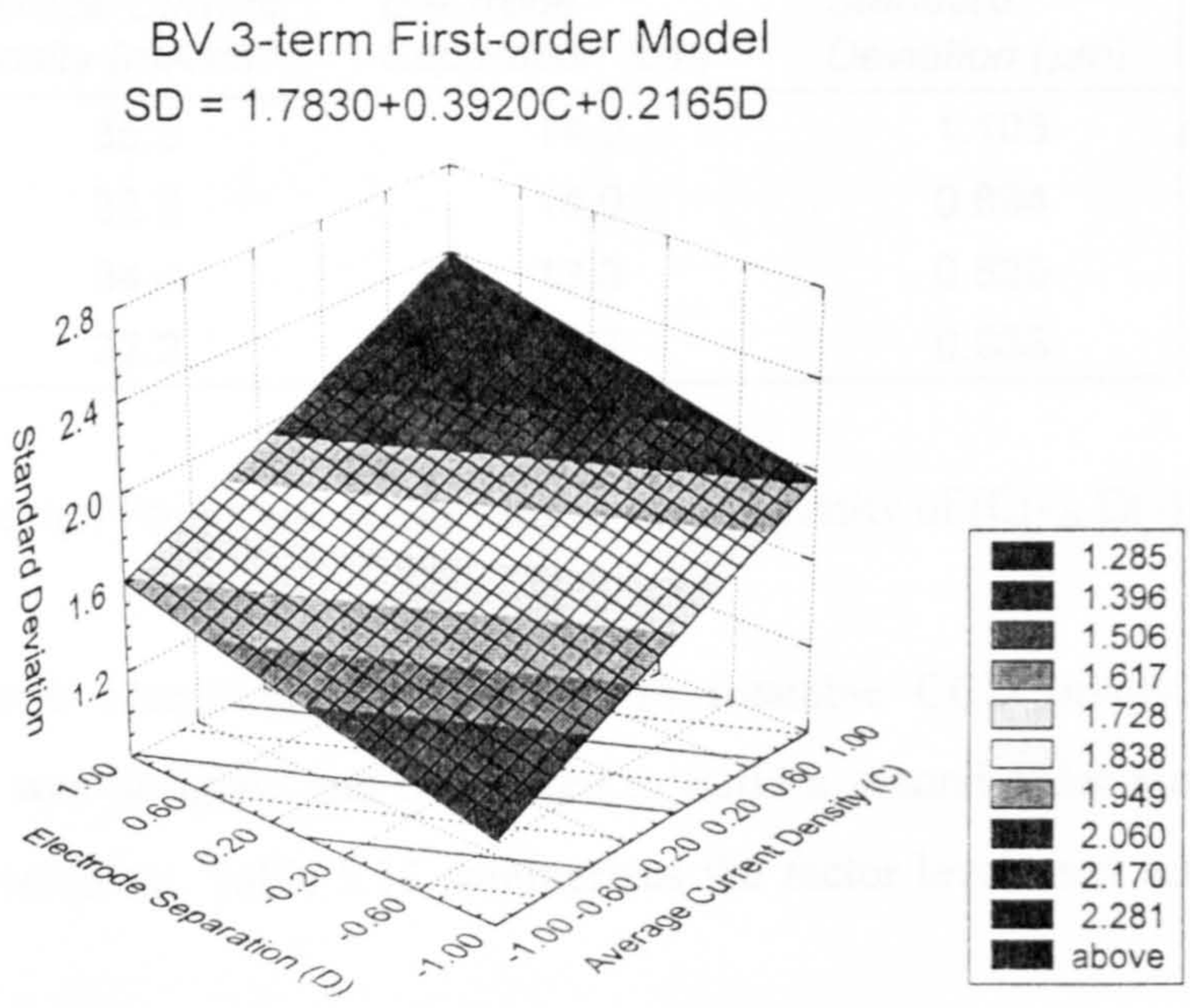

Fig. 5.20 : Response Surface and Contour Plot of the BV 3-term First-order Model

5.3.1.4 Residual Analysis

Analysis of the residuals of the first-order model revealed no abnormality of concern, as reflected by the normal probability plot of Appendix 5.9.

5.3.2 Second Order-Model Building and Optimization of Workpiece Level Variation

Four more experiments were performed in the proximity of the minimum variability, [C(-), D(-)], identified in the first-order model above. The factors settings and responses are summarized in Table 5.12 and the raw data given in Appendix 5.10. All the other insignificant parameters were held constant at their low (-) levels. The same measurement and response scheme was adopted in this round of experiments and the

average plating efficiency was found to be 87.3%. The results shows that further reduction of thickness variation can be achieved within the region and the combination of C = 35.0 mA/cm^2 and D = 14.0 cm represents a good candidate of the centre point of the CCD design for second-order model building.

Board No.	*Average Current Density (mA/cm^2)*	*Electrode Separation (cm)*	*Standard Deviation (μm)*
1	35.5	14.0	1.103
2	32.3	14.0	0.894
3	34.4	13.3	0.820
4	32.3	12.7	0.953

Table 5.12 : Design Points and Responses in the Proximity of [C(-), D(-)]

Using the centre point identified above, a 10-run rotatable CCD involving the parameters C and D was designed and conducted to build a second-order model for the workpiece level variation. Table 5.13 summarizes the factor levels and setting of the CCD employed.

Factors		*Fixed Level*	*Factor Levels* (-1.414)	(-1)	(0)	(+1)	(1.414)
A.	Sulphuric acid (g/L)	180	--	--	--	--	--
B.	Copper Sulphate (g/L)	75	--	--	--	--	--
C.	Average current Density (mA/cm^2)	--	31.2	32.3	35.0	37.7	38.8
D.	Electrode Separation (cm)	--	12.2	12.7	14.0	15.2	15.8
E.	Inter-hole Distance (cm)	0.45	--	--	--	--	--
F.	Corrected Aspect Ratio (mm)	--	--	--	--	--	--
G.	Depth Ratio	0.875	--	--	--	--	--

Table 5.13 : Factor levels and setting of the BV CCD Experiment

The standard deviations of the hole-wall plating thickness were taken as the responses and summarized in Table 5.14. Twenty thickness readings were taken from the ten

holes of each test board and the largest and smallest readings were discarded in the calculation, raw data are given in Appendix 5.11. An average plating efficiency of 84.5% was recorded in this round.

Observation no.	*Run order*	*C*	*D*	*SD (μm)*
1	2	-1	-1	2.3858
2	15	1	-1	1.0223
3	10	-1	1	2.3140
4	6	1	1	3.1654
5	3	-1.414	0	1.3620
6	9	1.414	0	1.1683
7	12	0	-1.414	2.8150
8	1	0	1.414	3.4248
9	11	0	0	1.5544
10	8	0	0	1.7602

Table 5.14 : Factor Levels and Responses of the BV CCD Experiment

The 6-term full second order model in coded form is determined as

$$SD = 1.6573 - 0.0982C + 0.3667D - 0.1887C^2 + 0.7386D^2 + 0.5537CD \qquad [5.9]$$

The ANOVA test of Table 5.15 confirms the significance of the model, its R^2_A (0.9266) performance is better than that of the first-order model derived above (Sec. 5.3.1.3) although its $R^2_{prediction}$ (0.7781) is slightly lower. The full model is also the best fitted model under the backward elimination process [Miller, 90] and the Mallow's criteria [Mallow, 73].

Source	*SS*	*DF*	*MS*	*F*	*Prob. > F*
Model	6.303	5	1.261	23.79	0.0045
Residual	0.213	4	0.053		
Lack of Fit	0.192	3	0.064	3.05	0.3930
Pure Error	0.021	1	0.021		
Total	6.516	9			

Table 5.15 : ANOVA of the BV Second-order Full Model (SD Responses)

5.3.2.1 Response Surface and Optimization

Fig. 5.21 shows that the response surface of the second-order mode (Eq. 5.9) is a saddle system [Montgomery, 97], in which the stationary point is neither a maximum nor a minimum point.

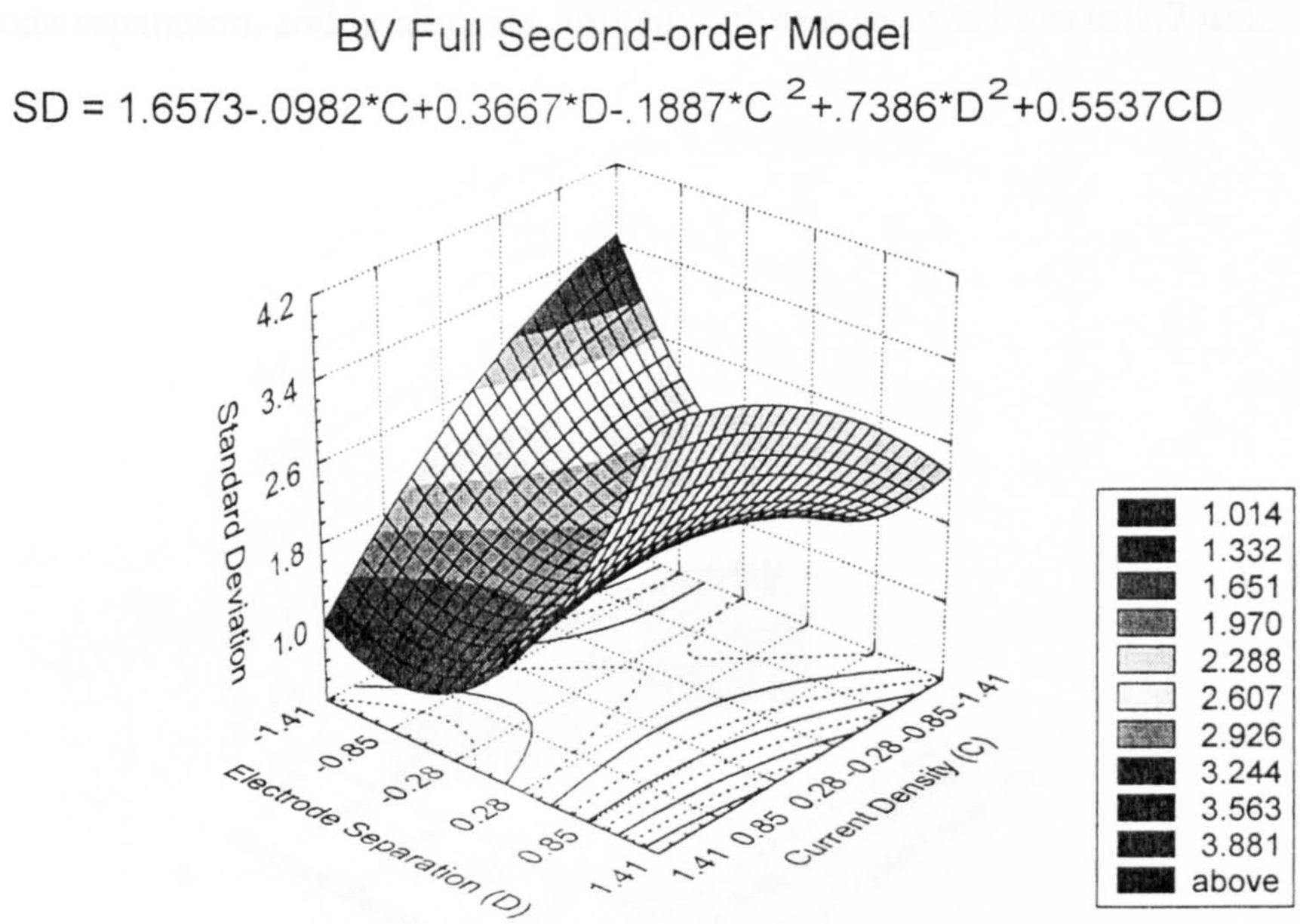

Fig. 5.21 : Response Surface and Contour Plot of the BV Full Second-order Model (SD Responses)

The location of the minimum variation within the experimental space can be found on the plane of C = 1.414, on which the second-order model becomes

$$SD = 0.7386D^2 1.1496D + 1.1410 \qquad [5.10]$$

Differentiating Eq. 5.10 with respect to D yields the stationary point of C = 1.414 (36 mA/cm^2) and D = -0.7782 (12.98 cm), which gives a minimum standard deviation, SD_{min}, of 0.6934 μm. The locus of the minimum standard deviation is given in Fig. 5.22 while Fig. 5.23(a) and (b) shows respectively the quadratic relationship between SD_{min} and C, and the linear relationship between the optimum values of C and D. The

first two graphs show that SD_{min} is smaller at the two extreme values of C. Fig. 5.23(b) shows that, contrary to the case of PTH (Fig. 5.11, Sec. 5.2.2.1), the sensitivity of the optimum solution towards the electrode separation is 2.7 times higher than the average current density. Physically, it means that as long as the process is operating along the path shown in Fig. 5.23(b), the workpiece level variability of the BVs will be minimized with respect to that particular combination of average current density and electrode separation, and in all cases limited to the range of 0.7 μm to 1.7 μm.

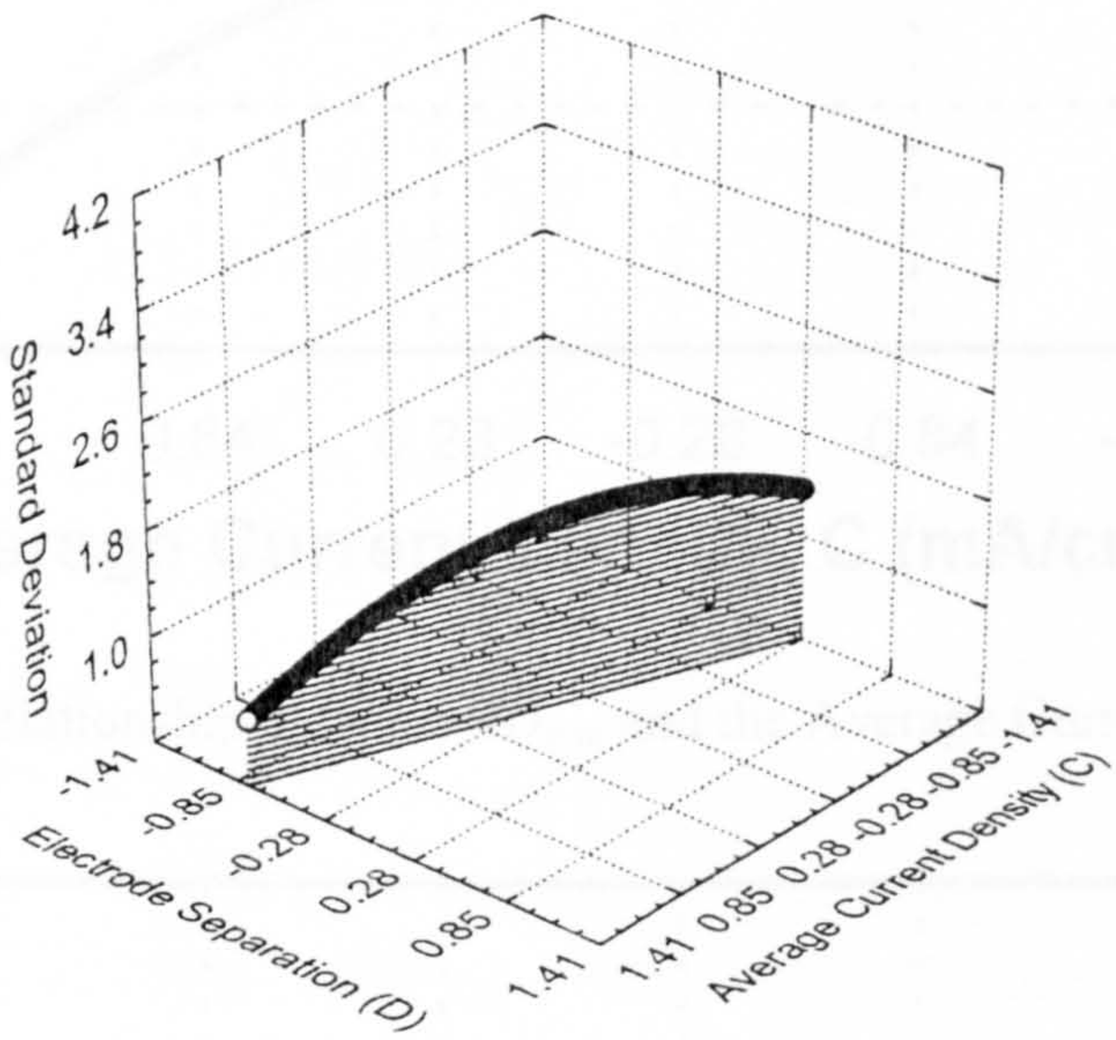

Fig. 5.22 : Locus of the SD_{min} within the Optimum Region

5.3.2.2 Residual Analysis

Analysis of the residuals of the first-order model revealed no abnormality of concern. Normal probability plot of residuals is given in Appendix 5.12.

5.3.3 Model Verification

Twelve four more experiments were performed to verify the adequacy of the second-order model in predicting the workpiece level plating uniformity within the experimental range. The standard deviation of 20 hole wall plating thickness readings

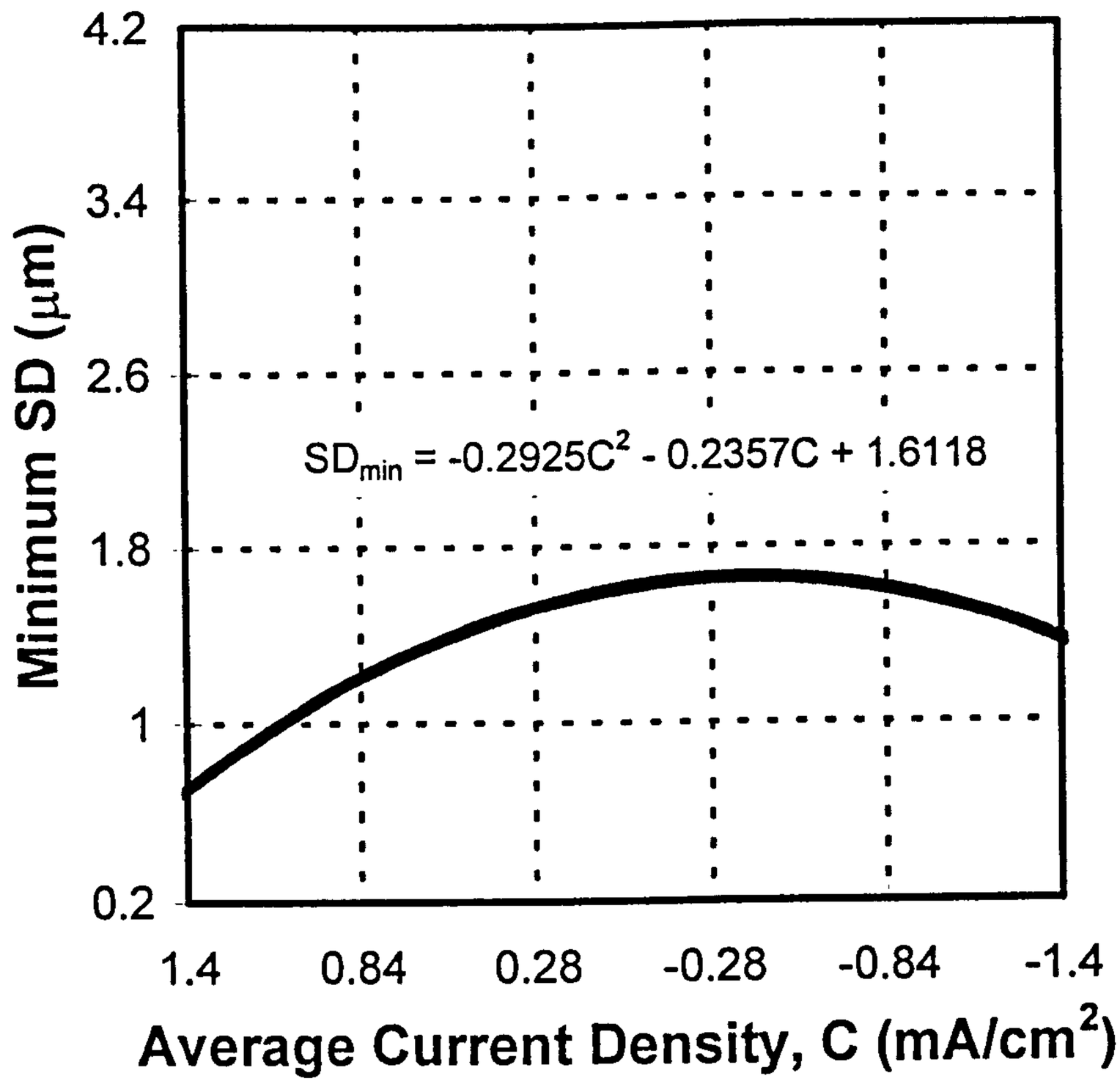

Fig. 5.23(a) : Relationship between SD_{min} and the Average Current Density

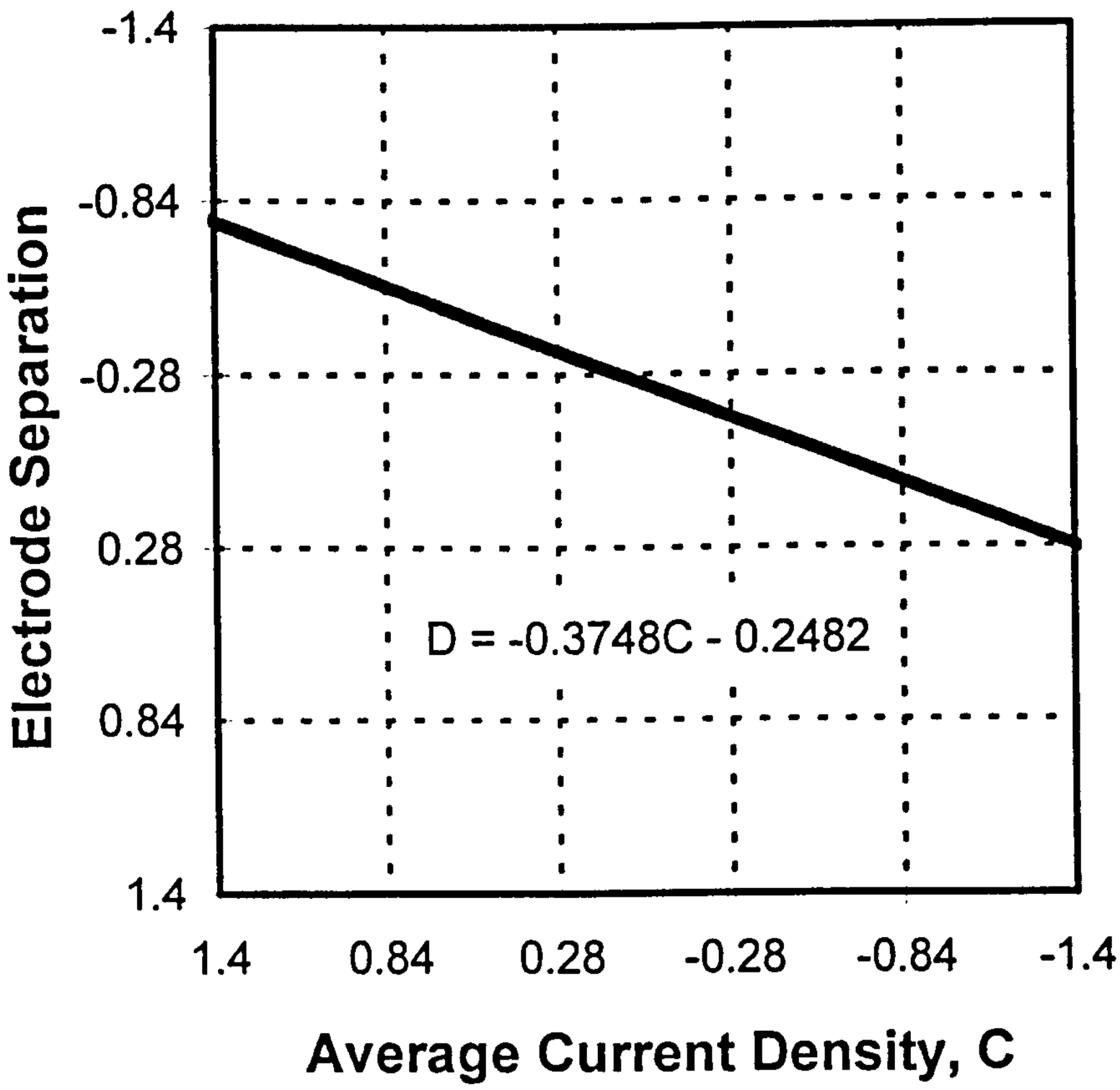

Fig. 5.23(b) : Locus of the Optimum Combination of parameter C and D

were determined from each test board. Two replicates were run for each of the twelve combinations of C and D, while the mean standard deviations were taken as the responses. The factors settings and responses are summarized in Table 5.16 below, and raw data are given in Appendix 5.13. Predicted responses of the second-order model (Eq. 5.9) are plotted against the actual standard deviations obtained from the model building (Table 5.14) and verification runs (Table 5.16) as Fig. 5.24. It shows that the full second-order model is able to predict 92.6% of the variations, which is much higher than the expected performance of 77.81% hinted by the $R^2_{prediction}$ of the model determined in Sec. 5.3.2 above.

5.4 Combined Models for PTH and BV

The response surfaces calculated above for the PTH and BV plating can be used to determine which of the two features is limiting the workpiece level variation when they coexist on the same board. This can be done by overlapping the two response surfaces if their corresponding CCDs are within the same experimental space. However, it is shown in the above that the centre points of the PTH CCD (C(-),D(+)) and the BV CCD (C(-),D(-)) are different. Extrapolation of response surface of one CCD to another is difficult for fixed effect models as the behaviour of the response outside the original CCD space may be different. Therefore, two additional sets of experiments were performed to obtained the required response surface as follows.

5.4.1 PTH Crossed with the BV Model at the BV CCD Space

In order to obtain a response surface of the PTH process in the BV CCD space, a new CCD was constructed with the corner and centre points of the BV CCD (Table 5.13) and summarized in Table 5.17. The design is the same as that of Table 5.13 except that the levels of (-1.682) and (+1.682) are used for C and D for the axial runs. The responses are summarized as Table 5.18 and raw data are given in Appendix 5.14.

		Standard Deviation (μm)	
Electrode Separation (cm)	*Average Current Density (mA/cm^2)*	*Actual*	*Predicted*
12.7	31.0	2.3699	2.3525
	32.0	2.0194	2.1521
	35.5	1.2117	0.9751
14.0	30.0	1.2637	1.5668
	33.0	1.7062	1.6301
	34.0	1.4435	1.5304
	35.0	1.1713	1.3703
15.2	30.5	2.3076	2.2775
	31.5	2.5554	2.5503
	34.0	2.8616	2.9680
	37.0	3.1164	2.9710
	39.0	2.8862	2.6710

Table 5.16 : Factors Settings and Responses of the BV Verification Experiment

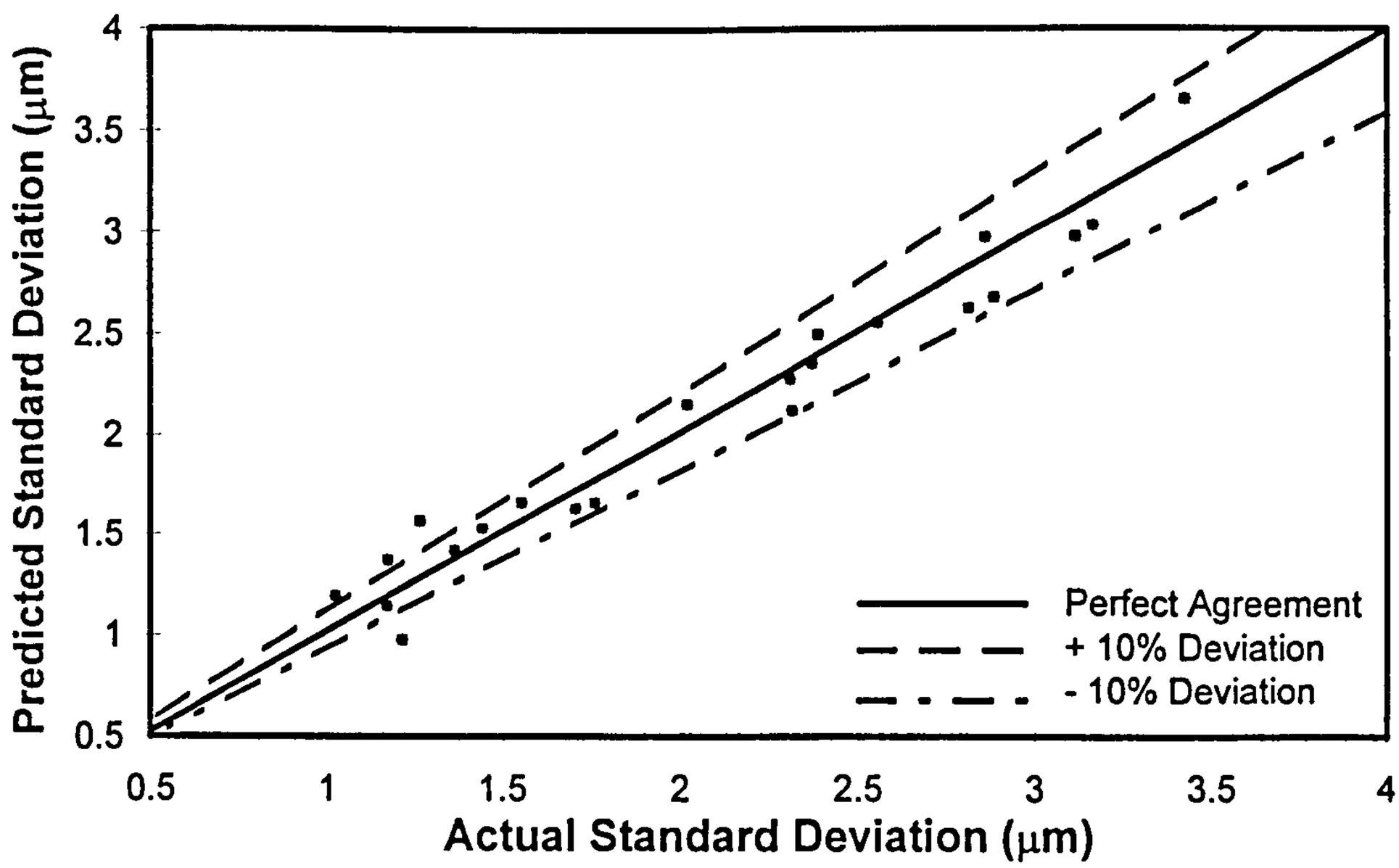

Fig. 5.24 : Verification Results of the BV Full Second-order Model

Factors		Fixed Level	Factor Levels (-1.682)	(-1)	(0)	(+1)	(1.682)
A.	Sulphuric acid (g/L)	180	--	--	--	--	--
B.	Copper Sulphate (g/L)	75	--	--	--	--	--
C.	Average current Density (mA/cm^2)	--	30.4	32.3	35.0	37.7	39.5
D.	Electrode Separation (cm)	--	11.7	12.7	14.0	15.2	16.3
E.	Inter-hole Distance (cm)	0.45	--	--	--	--	--
F.	Corrected Aspect Ratio (mm)	--	2.048	2.226	2.560	3.012	3.413

Table 5.17 : Factor levels and setting of the Second PTH CCD Experiment in the BV CCD Space

Observation no.	Run order	C	D	F	SD (μm)
1	7	-1	-1	-1	2.3266
2	3	1	-1	-1	1.8190
3	9	-1	1	-1	0.6517
4	12	1	1	-1	1.8527
5	10	-1	-1	1	1.8898
6	1	1	-1	1	1.7336
7	8	-1	1	1	1.7021
8	6	1	1	1	0.4844
9	5	-1.682	0	0	2.1800
10	15	1.682	0	0	1.8909
11	13	0	-1.682	0	1.4335
12	2	0	1.682	0	2.1884
13	4	0	0	-1.682	1.2533
14	16	0	0	1.682	1.2389
15	11	0	0	0	1.5402
16	14	0	0	0	1.5219

Table 5.18 : Responses of the Second PTH CCD Experiment in the BV CCD Space

The ANOVA test conducted afterwards shows that the second-order model was not significant (Prob. > F = 0.84), meaning that there was no evidence of second-order curvature in the response over the BV CCD space. On the other hand, the first-order model constructed using the 2^3 full factorial, i.e. the eight corner points, and the two

centre points was found to be highly significant. Table 5.19 shows the ANOVA of the model, the R^2_A and $R^2_{prediction}$ values were found to be 0.9980 and 0.8756, respectively. The insignificant lack of fit of the model re-confirmed the fact that second-order model was not necessary. The first-order model is given by the equation

$$SD = 1.5522 - 0.0851C - 0.3848D - 0.105F + 0.0809CD - 0.2584CF + 0.0256DF - 0.3463CDF \quad [5.11]$$

Source	*SS*	*DF*	*MS*	*F*	*Prob. > F*
Model	2.8814	7	0.4116	588	0.0017
Residual	0.0013	2	0.0007		
Lack of Fit	0.0011	1	0.0011	5.5	0.2566
Pure Error	0.0002	1	0.0002		
Total	2.8827	9			

Table 5.19 : ANOVA of the PTH First-order Model in the BV CCD Space

The intersection of the response surfaces of Eq. 5.11 and that of the BV second-order model (Eq. 5.9) are shown in Fig. 5.25(a), (b), (c) for the (coded) corrected aspect ratio (F) values of -1, 0, +1, respectively. They show which of the two features, i.e. PTH and BV, is limiting the workpiece level plating uniformity within the operability space of average current density and electrode separation. Fig 5.25(a) and (b) show that for medium to large through-hole size (2mm to 2.4 mm diameter), the BV deposit variability is larger than that of the PTH in the upper half and lower left corner of the operability space. Therefore, it is the BV instead of the PTH that limits the workpiece level plating uniformity in these regions. The opposite is true in the PTH limiting region where the PTH plating variability is larger. For the case of small through-hole size (1.6 mm diameter), the central portion of the operability space becomes BV limiting also as a result of the 'twisting' of the PTH response surface, i.e. lowering of PTH plating variability in that region. These figures can be used to aid the advantageous deployment of improvement effort in reducing workpiece level plating variation of PTHs and BVs. For example, in the BV limiting region, effort should be directed towards the reduction of BV plating variability. On the other hand, the intersecting lines of the three figures represents the situations when the PTHs and BVs have equal variances.

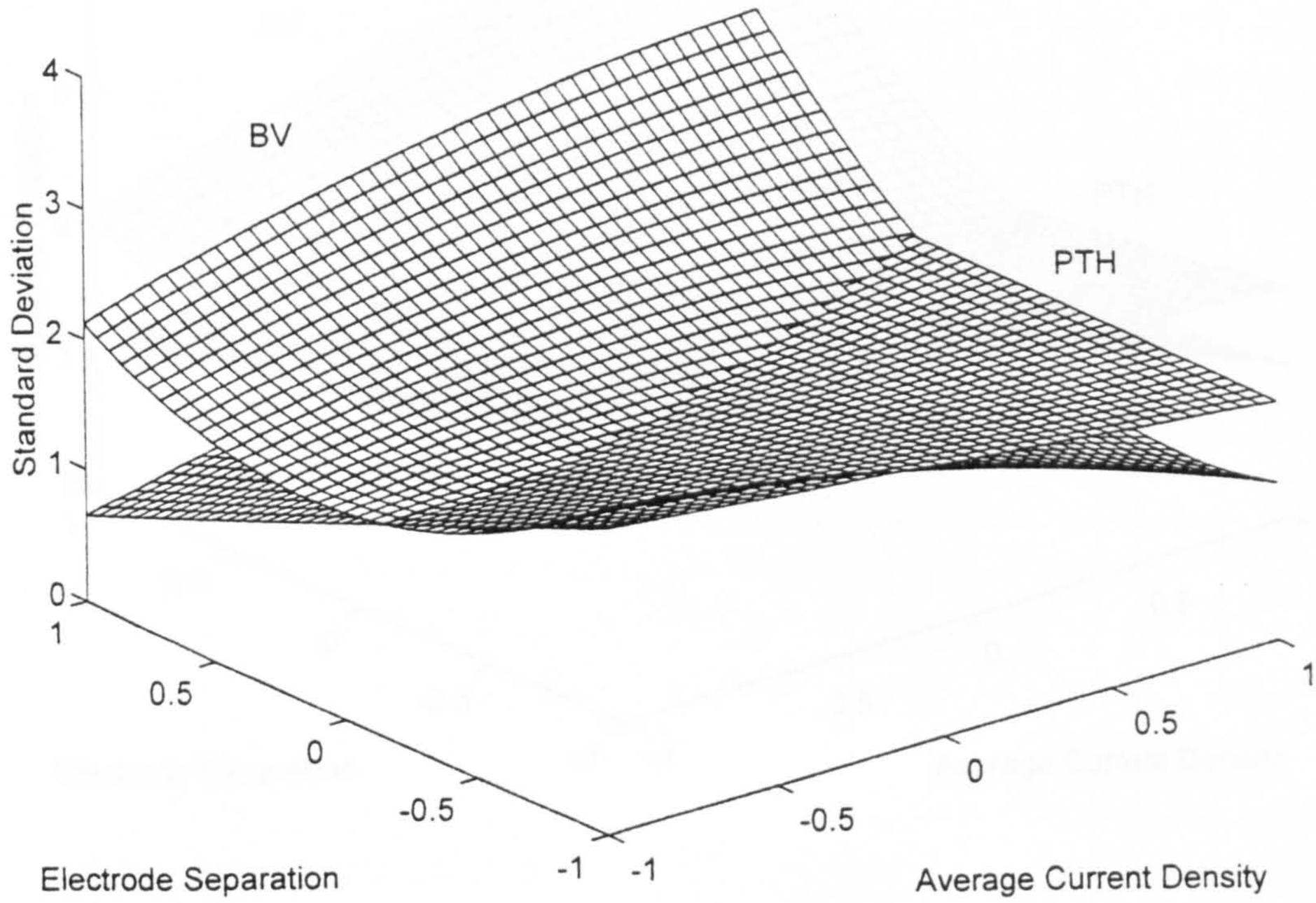

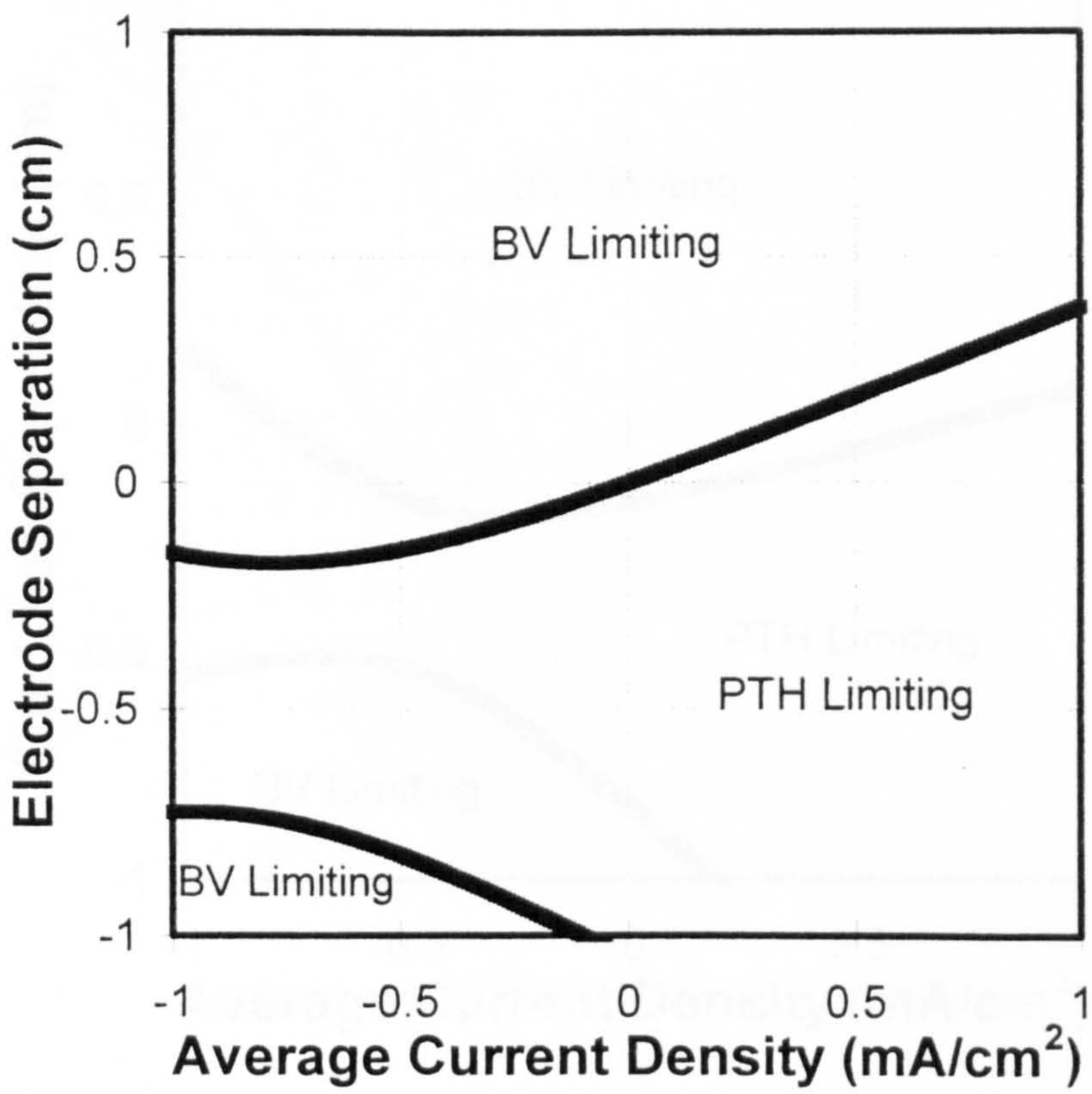

Fig. 5.25(a) : Intersection of the PTH and BV Response Surfaces in the BV CCD Space for F = -1

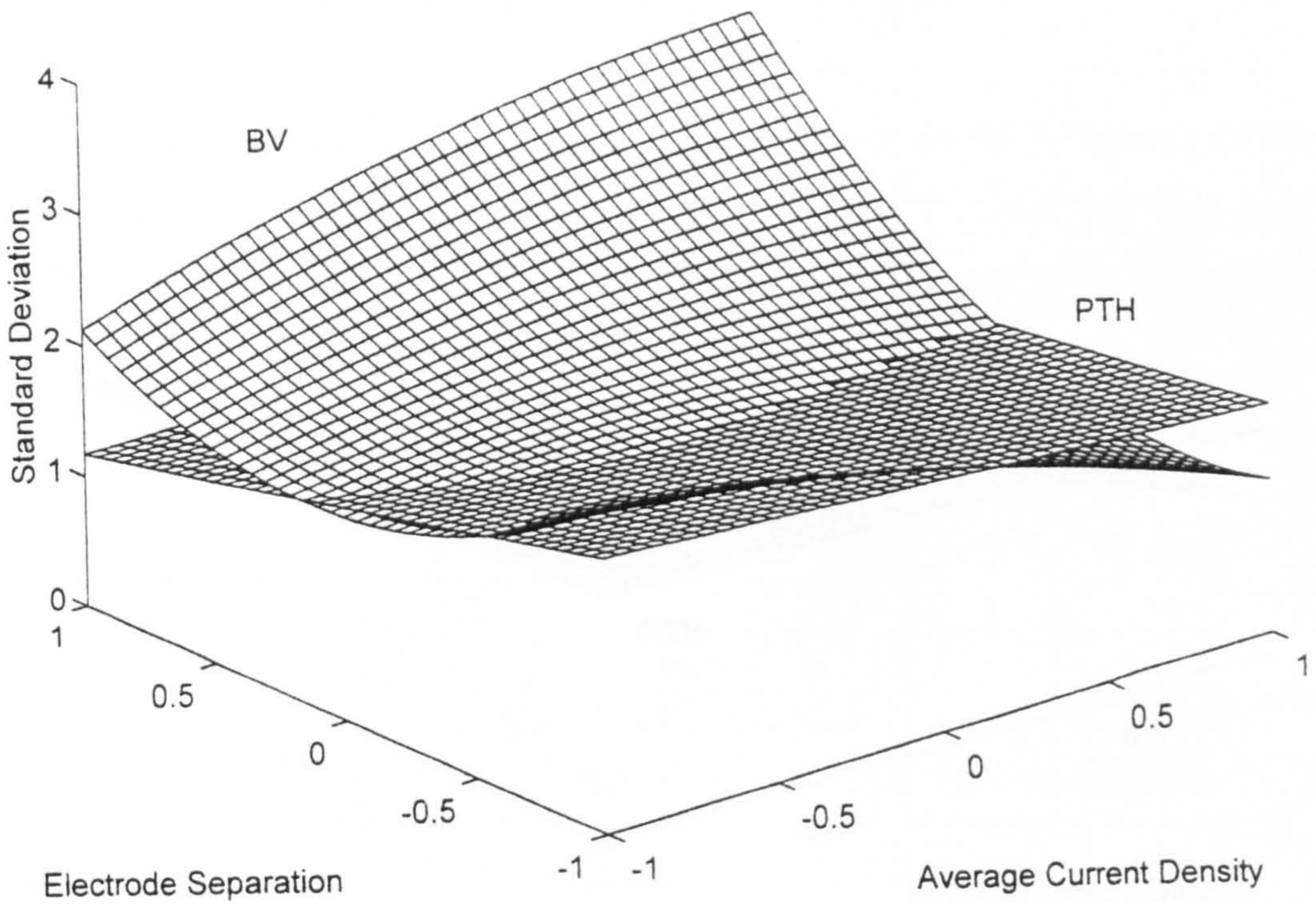

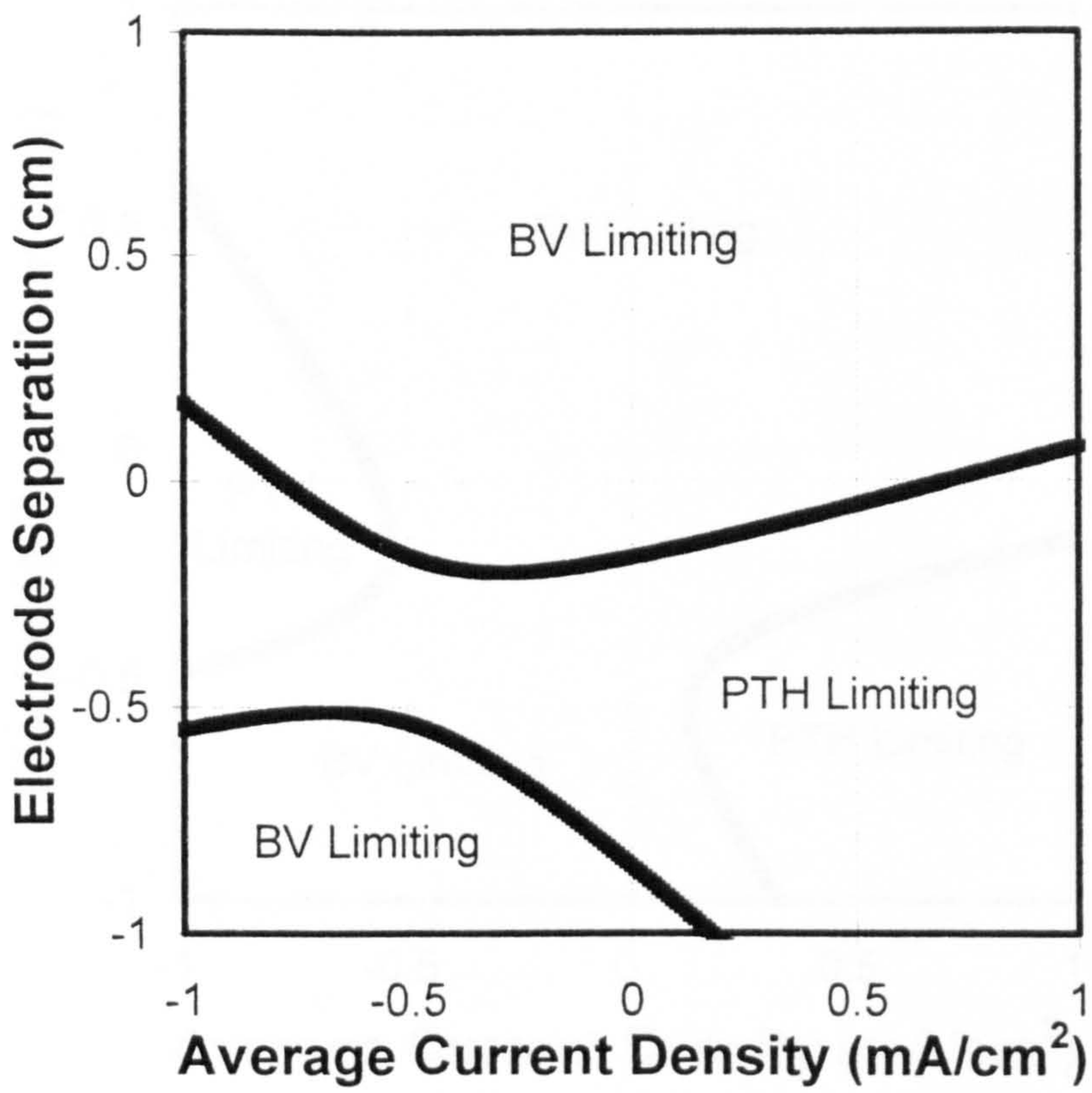

Fig. 5.25(b) : Intersection of the PTH and BV Response Surfaces in the BV CCD Space for F = 0

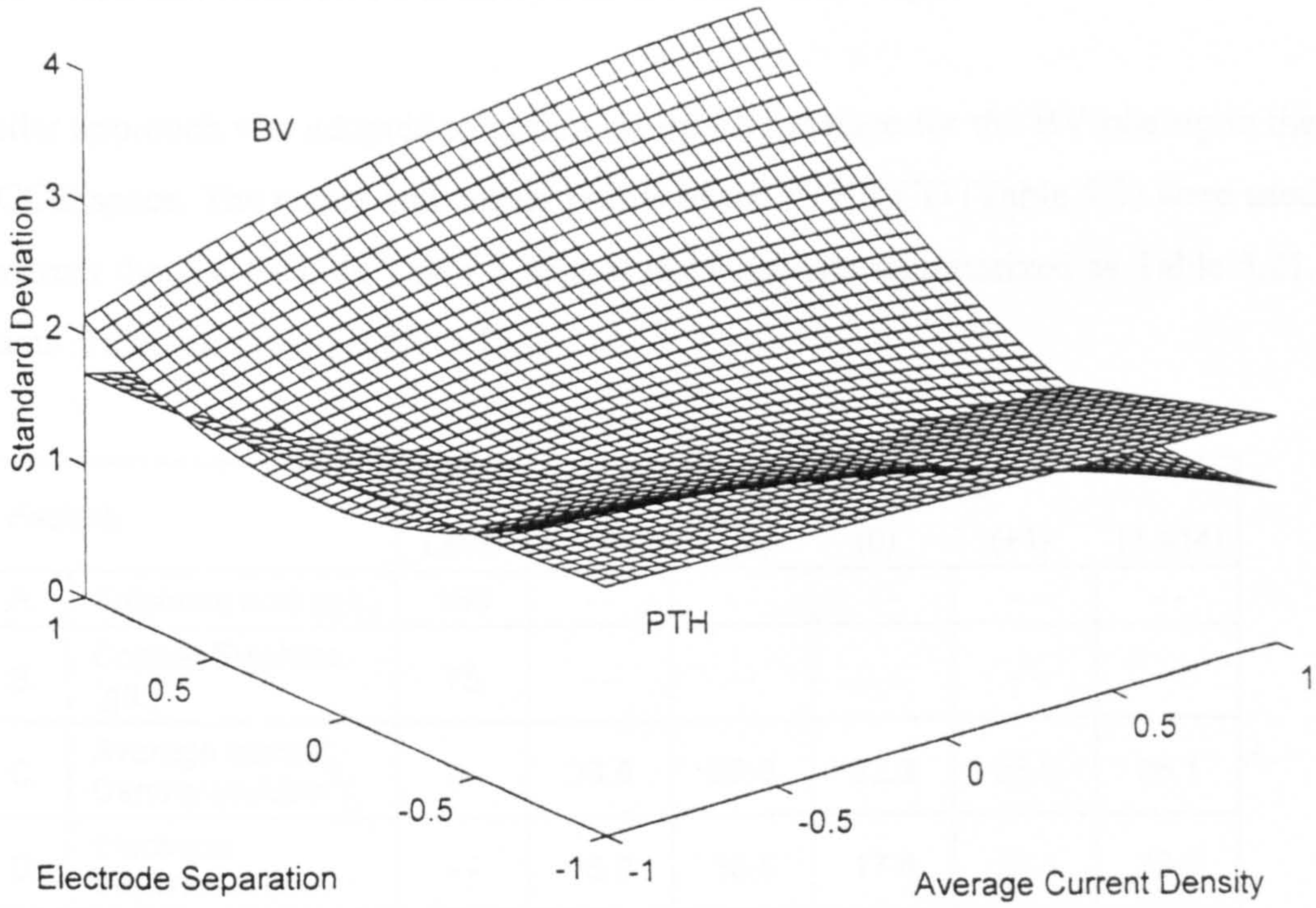

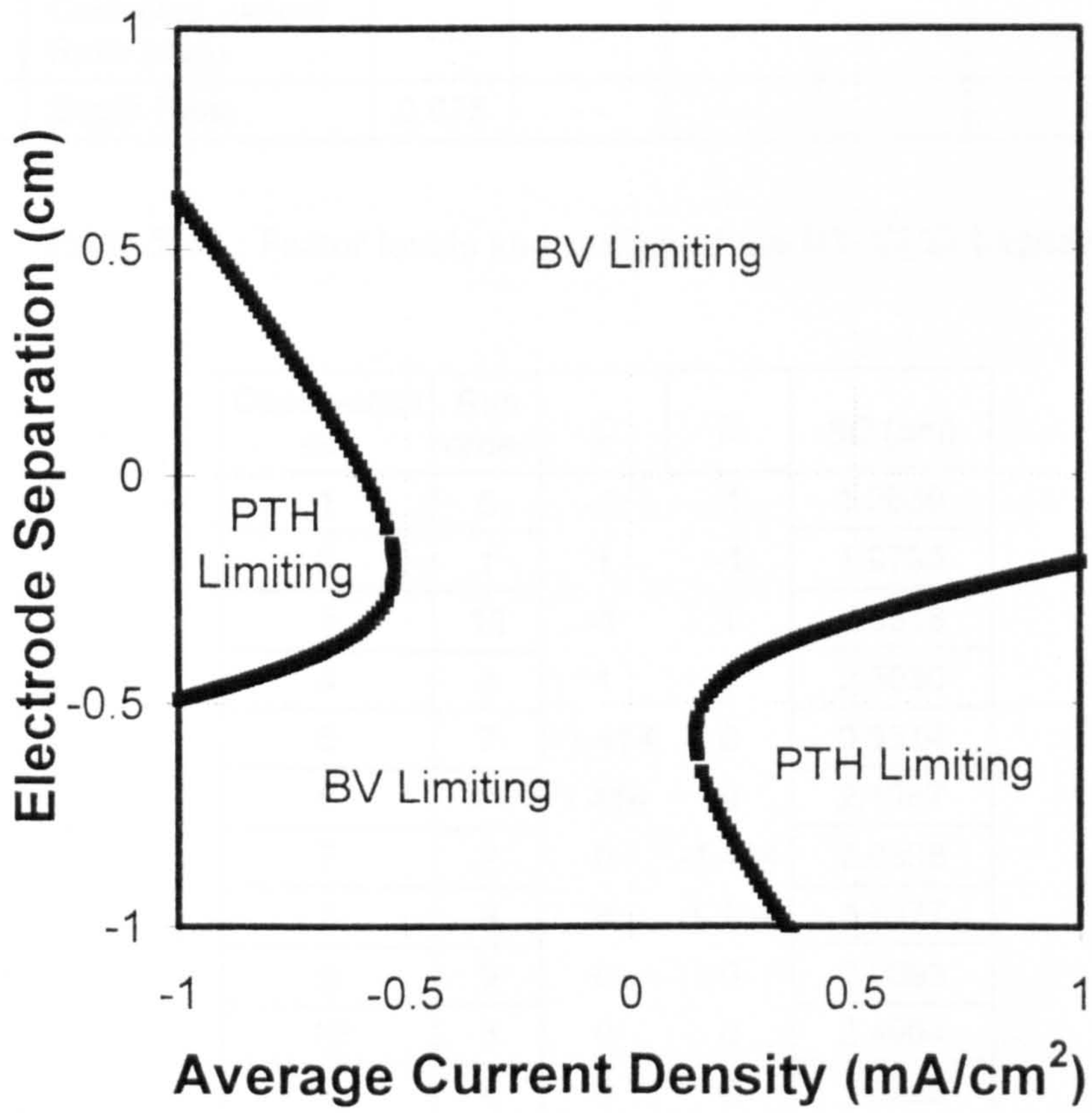

Fig. 5.25(c) : Intersection of the PTH and BV Response Surfaces in the BV CCD Space for F = +1

5.4.2 BV Crossed with the PTH Model at the PTH CCD Space

A similar approach was adopted to obtain a response surface for the BV plating in the PTH CCD space. The centre and corner points of the PTH CCD (Table 5.5) were used to construct the BV CCD in Table 5.20 and the responses summarized as Table 5.21. Raw data are given in Appendix 5.15.

Factors		*Fixed Level*	*Factor Levels*				
			(-1.414)	(-1)	(0)	(+1)	(1.414)
A.	Sulphuric acid (g/L)	180	--	--	--	--	--
B.	Copper Sulphate (g/L)	75	--	--	--	--	--
C.	Average current Density (mA/cm^2)	--	28.5	29.6	32.3	35.0	36.1
D.	Electrode Separation (cm)	--	16.0	16.5	17.8	19.1	19.6
E.	Inter-hole Distance (cm)	0.45	--	--	--	--	--
F.	Corrected Aspect Ratio (mm)	--	--	--	--	--	--
G.	Depth Ratio	0.875	--	--	--	--	--

Table 5.20 : Factor levels and setting of the BV CCD Experiment

Observation no.	*Run order*	*C*	*D*	*SD (μm)*
1	6	-1	-1	1.2630
2	1	1	-1	1.9795
3	10	-1	1	2.8518
4	5	1	1	2.3030
5	7	-1.414	0	0.9514
6	11	1.414	0	2.1987
7	2	0	-1.414	2.0808
8	8	0	1.414	1.5377
9	9	0	0	2.0093
10	3	0	0	2.4964
11	4	0	0	1.8659

Table 5.21 : Responses of the Second BV CCD Experiment in the PTH CCD Space

Similar to the case of PTH, the second-order model was found to be insignificant and the first-order model was sufficient to describe the responses, as indicated by the ANOVA test of Table 5.22. The first-order model constructed with the corner and centre points is given by

$$SD = 2.1098 + 0.4781C - 0.3163CD \qquad [5.12]$$

Source	*SS*	*DF*	*MS*	*F*	*Prob. > F*
Model	1.3145	2	0.6573	11.61	0.0216
Residual	0.2265	4	0.0566		
Lack of Fit	0.0081	2	0.0041	0.04	0.9615
Pure Error	0.2184	2	0.1092		
Total	1.5410	6			

Table 5.22 : ANOVA of the PTH First-order Model in the BV CCD Space

The R^2_A and $R^2_{prediction}$ values were found to be 0.7795 and 0.7685, respectively. The intersection of the response surfaces of Eq. 5.12 and that of the PTH second-order model (Eq. 5.3) are shown in Fig. 5.26(a), (b), (c) for the corrected aspect ratio (F) values of -1, 0, +1, respectively. They show that for medium to large through-hole sizes, the BV plating variability is greater than that of the PTH for almost the entire operability space. For small through-holes, the PTH plating variability is the limiting factor of the workpiece level uniformity in the lower left corner of the space, i.e. the combination of small average current density and electrode separation.

5.5 Summary

This chapter summaries the sequential experimental studies of the PTH and BV copper plating process. Significant process parameters affecting the workpiece level uniformity were identified as the average current density and the electrode separation, which were also found to be significant in the pattern plating experiments. The corrected aspect ratio was found to be significant for PTH plating only. Second-order response surfaces were constructed for both processes and their predictive power

verified. Two more sets of experiment were conducted to obtain the response surface of the PTH process at the optimum region of the BV process and vice versa. The intersection of these response surfaces showed that in most cases the BV plating variation is greater than that of the PTH and thus limiting the workpiece level uniformity.

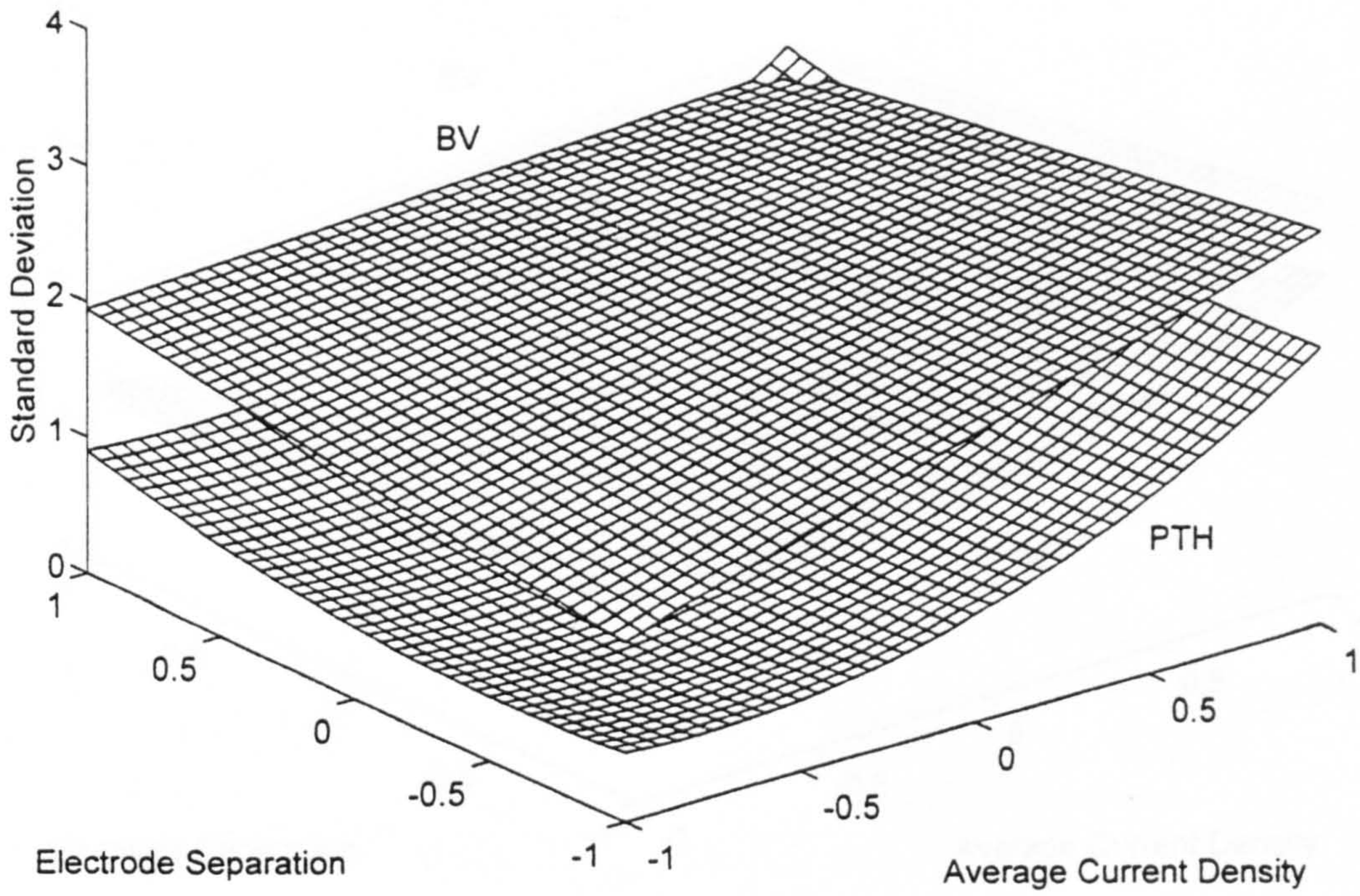

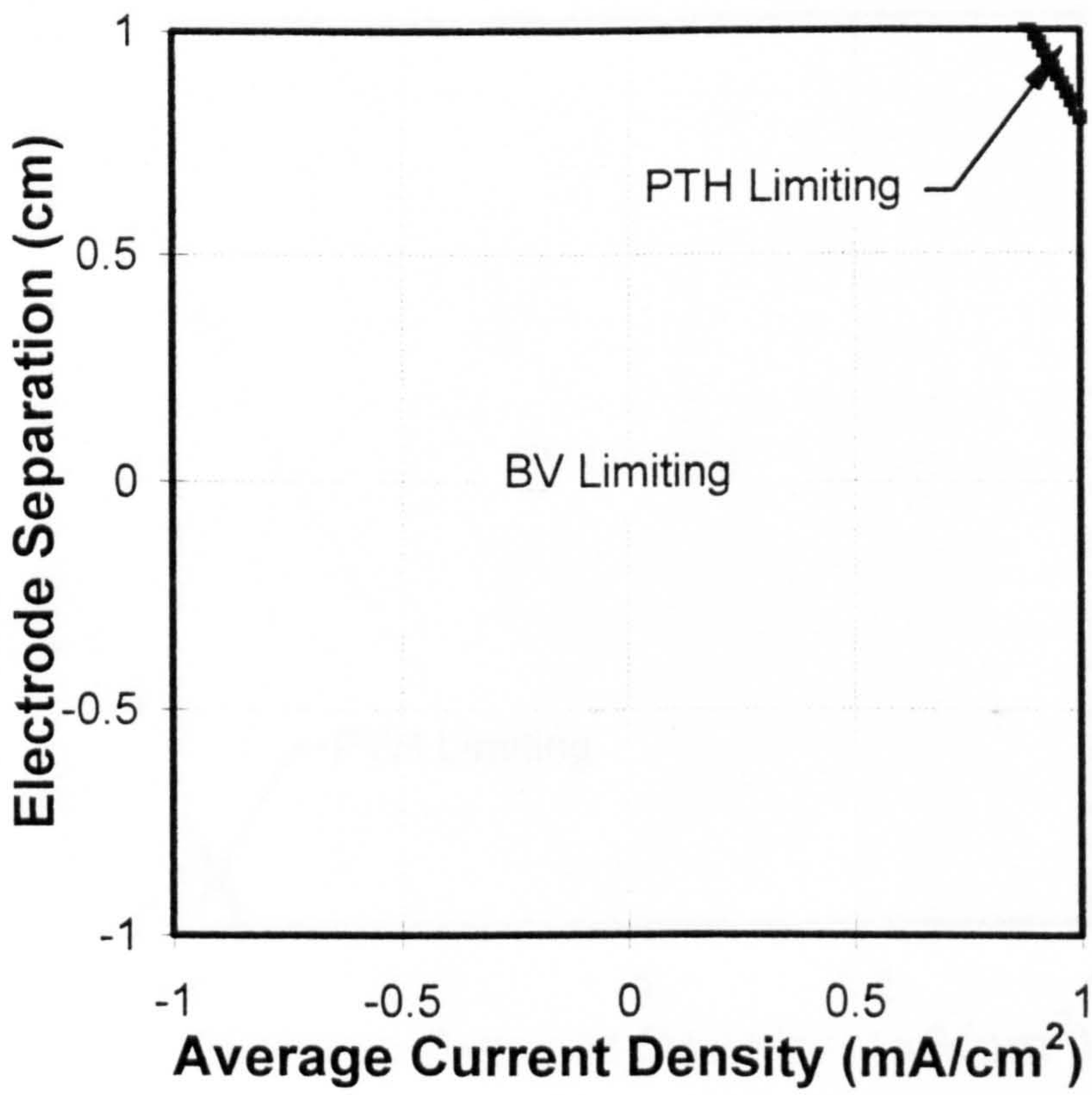

Fig. 5.26(a) : Intersection of the PTH and BV Response Surfaces in the PTH CCD Space for F = -1

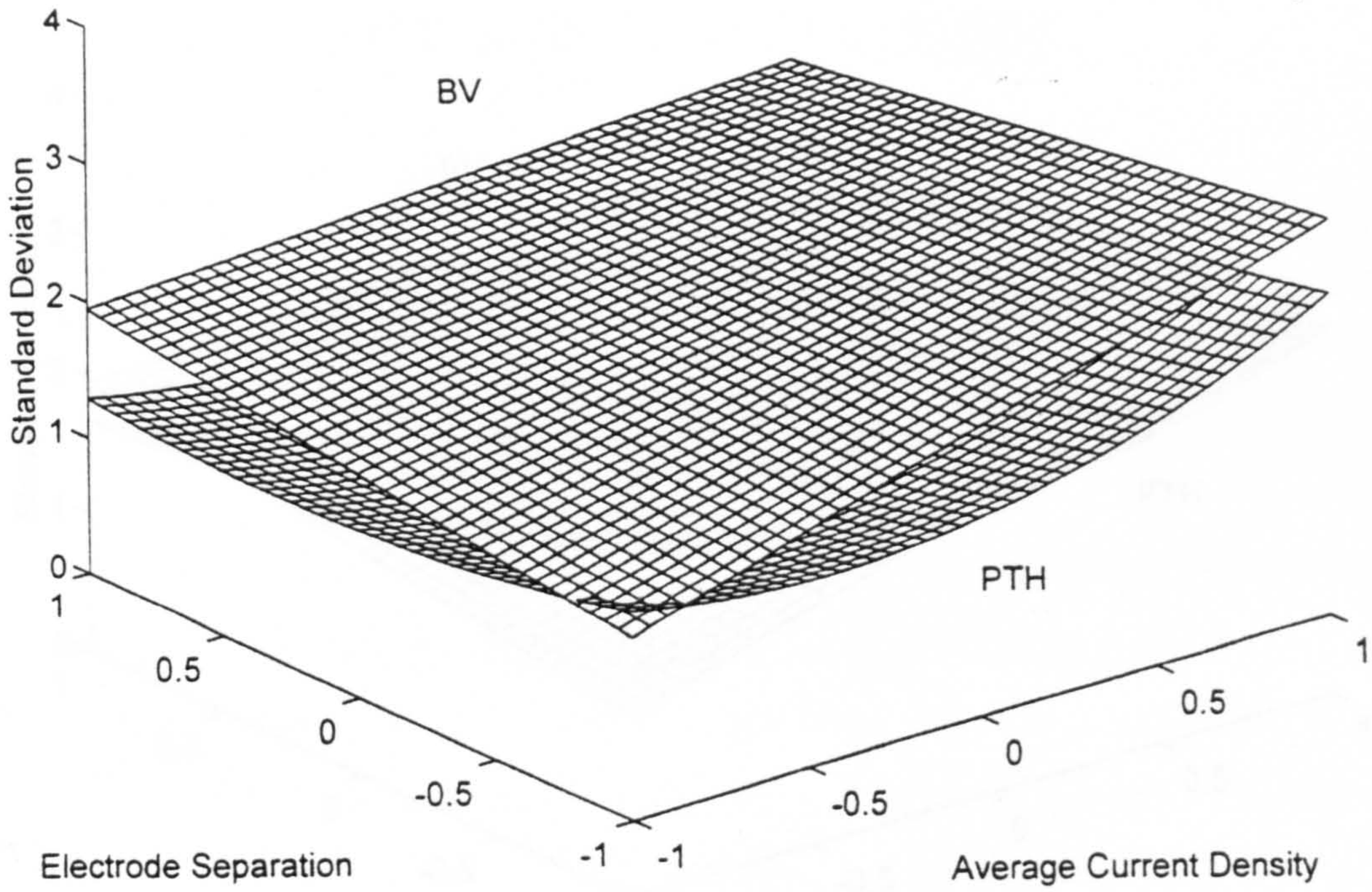

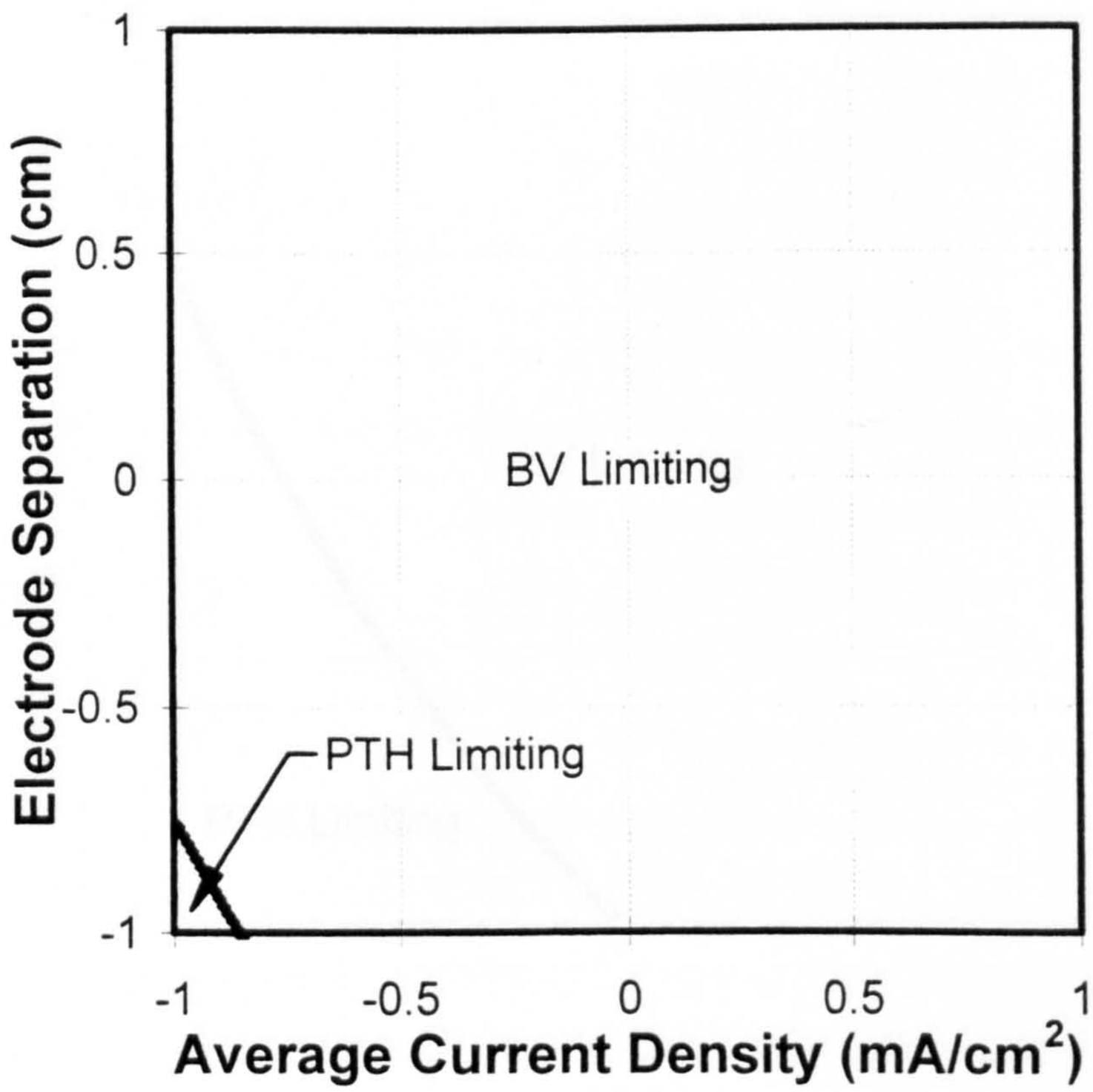

Fig. 5.26(b) : Intersection of the PTH and BV Response Surfaces in the PTH CCD Space for F = 0

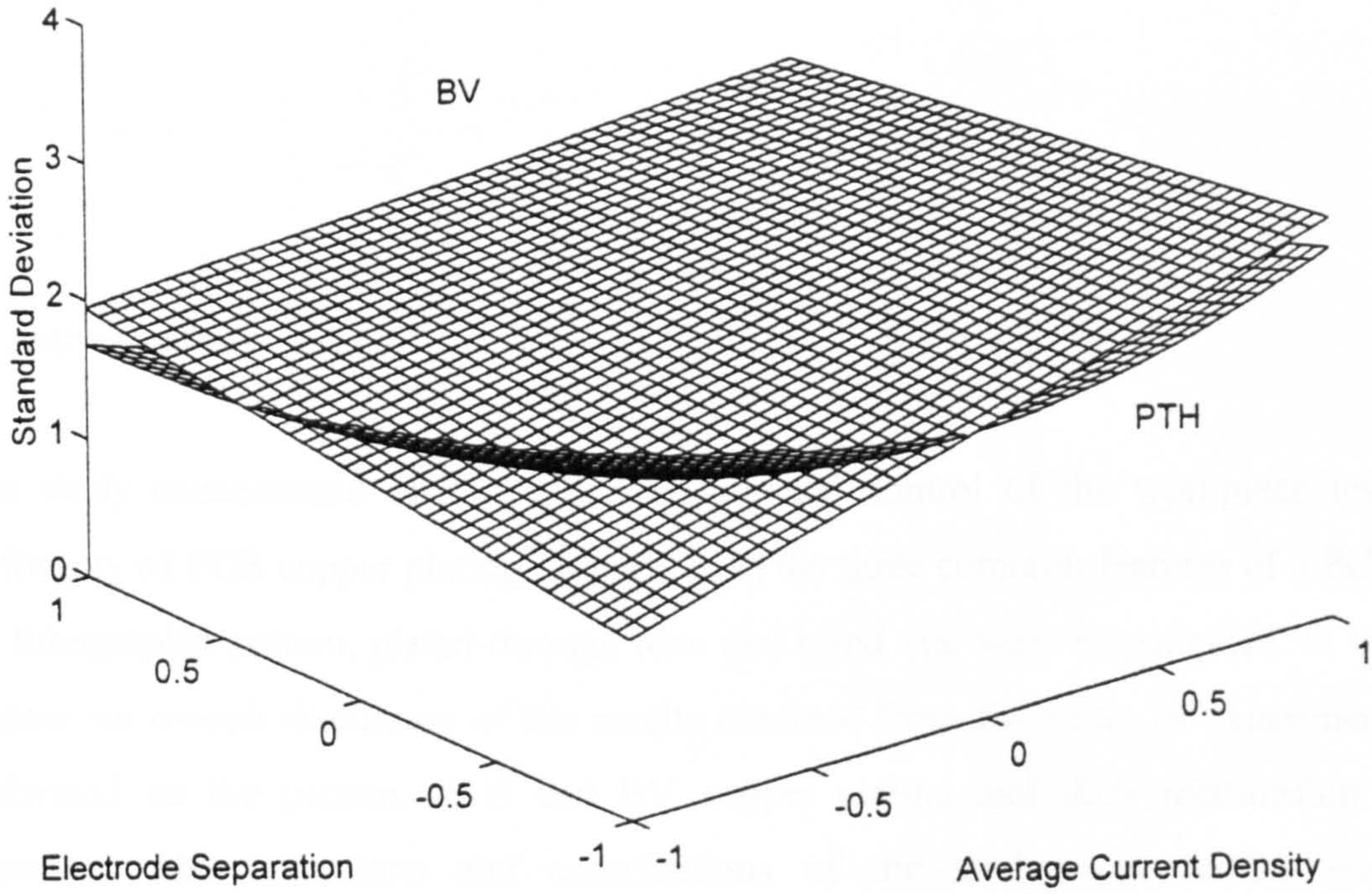

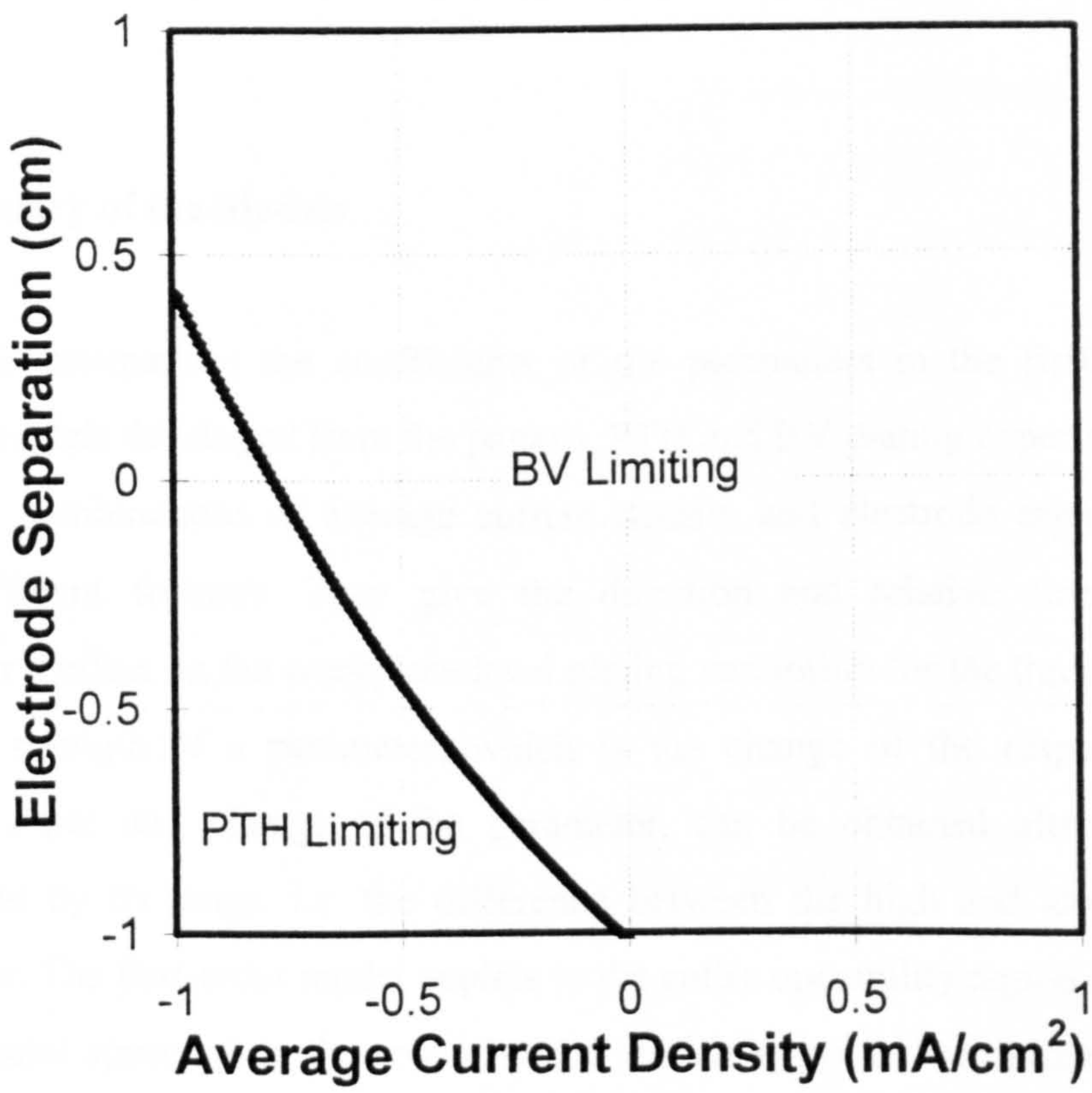

Fig. 5.26(c) : Intersection of the PTH and BV Response Surfaces in the PTH CCD Space for F = +1

CHAPTER 6
DISCUSSION AND CONCLUSION

6.1 Introduction

This study concentrated on the understanding and control of the workpiece level uniformity of PCB copper plating. In particular, the three common features of a PCB, i.e. lithographic pattern, plated-through hole and blind via, were investigated. In this chapter, an overall discussion of the results obtained from the series of experiments performed on the pattern, PTH and BV copper plating and their relationship is presented. The limitations and contributions of the study, and further work recommended to be performed in this area are also discussed.

6.2 Summary of the Models

Table 6.1 summarizes the coefficients of the parameters in the first/second order (coded) models developed from the pattern, PTH and BV plating experiments, and the optimum combinations of average current density and electrode separation for the three different features. They give the direction and relative strength of each parameter's effect on the workpiece level plating variability for the three features. The absolute strength of a parameter, which is the change of the response (standard deviation) per unit change of the parameter, can be obtained after dividing the coefficient by its range, i.e. the difference between the high and low level of the parameter. The first-order model applies to the entire operability region defined by the experimental space while the second-order models apply to the optimum regions of the particular process only.

	Uniform Pattern (*2nd Order*)	*Non-Uniform Pattern* (*1st Order*)	*P T H* (*2nd Order*)	*B V* (*2nd Order*)
Equation No.	4.4	4.6	5.2	5.9
Constant	4.2871	6.1565	1.2579	1.6573
Average Current Density	+ 0.3964 (10 mA/cm^2)	+ 1.7857 (10 mA/cm^2)	+ 0.4321 (5 mA/cm^2)	- 0.0982 (5 mA/cm^2)
Electrode Separation	- 0.4890 (5.1 cm)	+ 0.3492 (10.2 cm)	- 0.1049 (2.5 cm)	+ 0.3667 (2.5 cm)
Active Area Density Ratio	N / A	+ 1.8303	N / A	N / A
Corrected Aspect Ratio	N / A	N / A	+ 0.3570	N / A
(Average Current Density)^2	+ 0.6754	N / A	+ 0.4681	- 0.1887
(Electrode Separation)^2	+ 0.4507	N / A	+ 0.1513	+ 0.7386
(Corrected Aspect Ratio)^2	N / A	N / A	- 0.0660	N / A
Average Current Density x Electrode Separation	- 0.1216	+ 0.7091	- 0.0686	+ 0.5537
Average Current Density x Active Area Density Ratio	N / A	+ 0.1880	N / A	N / A
Average Current Density x Corrected Aspect Ratio	N / A	N / A	- 0.3349	N / A
Electrode Separation x Corrected Aspect Ratio	N / A	N / A	- 0.3010	N / A
Electrode Separation x Active Area Density Ratio	N / A	- 0.1483	N / A	N / A
Average Current Density x Electrode Separation x Active Area Density Ratio	N / A	+ 0.0871	N / A	N / A
Optimum Avg. Current Density Electrode Separation	 37.4 mA/cm^2 27.9 cm	 30.1 mA/cm^2 25.4 cm	* 28.1 - 29.8 mA/cm^2 17.0 - 19.3 cm	 36 mA/cm^2 13 cm

☐ The parameter effect is either insignificant or non-applicable (N/A)
* Depends on the corrected aspect ratio of the through-holes
Bracketed value show the range of the parameter's level

Table 6.1 : Summary of Coefficients of the Parameters in the Pattern, PTH & BV Models

6.3 Discussion on the Pattern Plating Experiments

It has been shown in the review (Sec. 2.4.3) that workpiece level current distribution studies before 1988 were primarily concerned with non-patterned surfaces. [Blue, 80] calculated that, when the plating current was small (a quarter of the limiting current density), the workpiece level thickness distribution could be well approximated by the primary current distribution, which was in turn determined by the bath geometry only. This is the rationale behind studying the effects of the average current density and electrode separation in the pattern plating experiments. The first screening experiment (Sec. 4.5.1) showed that the concentration of the brightener and sulphuric acid did not have a significant effect on the thickness variability. [Goodenough and Whitlaw, 89] reported a similar phenomenon on a non-patterned copper disc and showed that the effect of these two components on the Wagner number, i.e. throwing power, was negligible when the average current density exceeded 14 mA/cm^2.

The first-order (Eq. 5.2, 5.6), and second-order (Eq. 5.4), models developed in the subsequent experiments quantified the significant effects of the average current density and electrode separation on the workpiece level deposit uniformity. The results are in qualitative agreement with the conclusion of previous investigations [Koseki, 68], [Shin and Pickering, 87], and show that the workpiece level plating variability can be effectively controlled and minimized by careful manipulation of bath geometry, i.e. the electrode separation. This result reflects also the dominating influence of the primary distribution on the workpiece level uniformity in the high current density regime; as the average current density chosen for these experiments (26.9 mA/cm^2 - 37.7 mA/cm^2) represents a high fraction of the limiting current density, which is estimated to be approximately 50 mA/cm^2*.

Analysis of the verification results of the first-order model for the uniform pattern plating (Sec. 4.5.5) suggests that the workpiece level variation is minimized when the deviation of the average deposit thickness from the Faraday's prediction (Eq. 4.1) is

* The limiting current density was deduced from experimental observation of the occurrence of burned deposits on the cathode surface, and is found to be agree with the estimated value for a similar solution (0.3M $CuSO_4$, 2M H_2SO_4) used in [Yung and Romankiw, 89].

minimized. This reiterates the fact that Faraday's prediction gives only nominal deposit thickness under the assumption of uniform thickness distribution. However, the average deposit thickness is larger than the Faraday's prediction even through the variability is minimized. This phenomenon is explained as the effect of the auxiliary electrode surrounding the pattern by [Choi and Kang, 96]. Also, such a deviation is found to bear a quadratic relationship with the average current density around the optimum region (Fig. 4.17 (a), (b)). Practically, this means that the deviation from the Faraday's prediction might be used as an indicator of the workpiece level plating uniformity.

The interacting effects between the average current density and the electrode separation, so far not reported in the literature, have been effectively identified and modelled using statistical experiments. The practical significance of this interaction effect is discussed below.

i/ For plating of uniformly-patterned PCBs, such as an array of repeating circuit patterns, high average current density coupled with large electrode separation and short plating duration is advantageous as reduced plating variation can be achieved without sacrificing plating rate. However, tighter control of the electrode separation is required as the thickness variation is highly sensitive to the inter-electrode distance when a high average current density is used (Fig. 4.9).

ii/ Conventional definitions of the Wagner number (Eq. 2.9, 2.13, 2.16, 2.22) show that the workpiece level uniformity can be improved by using smaller average current density in the Tafel regime. It is postulated here that the combined effect of a large average current density and electrode separation is equivalent to a reduced average current density over the substrate. However, the significant interaction means that the effect of the average current density cannot be considered alone, i.e. minimization of thickness variation does not necessarily result from reduction of the current density or proximity of the electrodes alone. The second-order model (Eq. 4.4) showed that there exists an optimal combination of the two parameters so that the workpiece level variation is minimized.

iii/ This interaction effect is different in the case of non-uniform pattern plating. The first-order model (Eq. 4.6) showed that the plating uniformity was better when a low average current density was used for all levels of electrode separation and AADR, which was indicative of a secondary current distribution characterized by the Wagner number. The electrode separation itself was no longer significant to the workpiece level variation.

The relative influence of the average current density, electrode separation and AADR is reflected by their corresponding coefficients in the first-order model of Eq. 4.6. It shows that the AADR, which is known to affect the pattern-scale secondary current distribution [Mehdizadeh, 92], and the average current density dominate. Together with the discussion in iii/ above, it seems apparent that the workpiece level thickness variability of a non-uniformly patterned surface is jointly determined by the primary and secondary current distribution, with the latter being more influential than the former. However, this does not undermine the effectiveness of altering the bath geometry to obtain desirable workpiece level uniformity, especially in the high current density regime where the effect of the bath chemistry on its polarization characteristic is weak.

Apart from the above interaction effect, several other peculiar features of non-uniform pattern plating derived from the experiments are discussed as follows. The first-order model of Eq. 4.6 and the subsequent revised model show that the workpiece level uniformity is jointly controlled by the average current density and average active area density ($\overline{\mathrm{AAD}}$) of the substrate. Although exact values of Wa_T and Wa_L were not determined for the pattern plating experiments in Sec. 4.6, approximate solutions are obtained in Appendix 6.1 using the empirical formula of [Caban and Chapman, 77], [Turner and Johnson, 62] and the physiochemical properties of similar solutions given in [Goodenough and Whitlaw, 89] and [Mehdizadeh *et al.*, 93]. The calculation shows that Wa_T (0.65 - 0.86) is much smaller than Wa_L(4.1 - 11.4), indicating that the electrodeposition is performed in the Tafel (high overpotential) regime [Mehdizadeh *et al.*, 92]. Therefore, the workpiece level behaviour is different from the pattern level model of [Mehdizadeh, 92], which predicts a sole dependence of current distribution on Wa_T (average current density

effect) in the Tafel regime (Sec. 2.4.3). The workpiece level variability depends not only on the average current density but also on the average active area density of the patterns, and is reduced when either or both of them are smaller. Such a behaviour was evident in the two verification runs (Sec. 4.6.2 and 4.6.3), in which the average current density was held constant at 30.2 mA/cm^2 and the $\overline{AAD}$ was varied from 0.17 to 0.33. [Choi and Kang, 96] observed this dual-dependence on a uniformly patterned substrate. It might be explained by the fact that the amount of current, rather than current density, passing through the system is reduced when $\overline{AAD}$ is smaller.

Apart from demonstrating the adequacy of the first-order model, the two verification runs unveiled the possible interaction between AADR and $\overline{AAD}$, which has not been recognized in previous investigations [Mehdizadeh, 92, 93], [Choi and Kang, 96]. In the first verification run using the zebra pattern, the effects of AADR and $\overline{AAD}$ are confounded because they increase simultaneously across the runs, i.e. $\overline{AAD}$ increases linearly with AADR. Eq. 5.12 shows clearly the confounding nature of these two parameters. The original first-order model (Eq. 4.6) does not distinguish between these two effects and $\overline{AAD}$ is therefore used in the modified model to reflect the combined effect of these two parameters. However, the results of the second verification run (Sec. 4.6.3) show that the workpiece level variability can be remarkably small when $\overline{AAD}$ is smaller, even though the AADR is kept constant or increased. The cases of AADR = 3 and 4 in Fig. 4.33 illustrate a good example, in which the thickness variation drops significantly even though the AADR is increased. This suggests two possibilities. Firstly, the positive effect of $\overline{AAD}$ is overriding at the workpiece level and the negative effect of the AADR is suppressed. Secondary, there is an interaction effect between AADR and AAD and the variability is smaller for a particular combination of AADR and $\overline{AAD}$. In either case, it means that the negative effect of AADR on the workpiece level variability can be counteracted by reducing the $\overline{AAD}$ over the substrate surface at the same time.

6.4 Discussion on the PTH and BV Plating Experiments

Previous work on the modelling of PTH plating showed that the feature scale uniformity is limited by the ohmic resistance (secondary current density effect) rather than the mass transfer resistance (cupric ion concentration, agitation effect) of the system [Lanzi and Landau, 88], [Yung *et al.*, 89], [Yung and Romankiw, 89]. Similar results are not found in the literature for BV plating. The statistical models developed here show that ohmic limitation applies also to the workpiece level thickness variation for both PTH and BV plating, although mass transfer limitation has more influence on optimum BV plating.

The plating rate was found to be maximized for both PTH and BV when large average current density (43.04 mA/cm^2) and electrode separation (17.8 cm) were used, but it leaded also to a poor workpiece level uniformity according to the first-order model of Eq. 6.1 (PTH) and Eq. 6.8 (BV). The interaction effect between the sulphuric acid and copper sulphate, which was found to be significant in affecting the plating rate but not the thickness variation in both cases, could be used to obtain a compromise between the two conflicting requirements. Such an effect, however, was found to be acting differently for PTH and BV plating. While a high acid concentration (165 g/L) was desirable for both features, a low sulphate concentration (65 g/L) for PTH and a high sulphate concentration (90 g/L) for BV was desirable. This is evident from the interaction plots of Fig. 5.5 and Fig. 5.17 for PTH and BV, respectively. Addition of copper sulphate is known to have a negative effect on the acidity and conductivity of a acid-sulphate system [Newman, 1991b] while conductivity is found to have the opposite effect on the reaction rate of plating with convection (positive effect) and without convection (negative effect) [Hazlebeck and Talbot, 90]. The above difference in the interaction effect might be explained by the fact that convection of electrolyte within the through-holes is usually assured for the PTH plating to be effective, but mass transport inside the vias is restricted and the situation is comparable to plating without convection. As the positive effect of copper sulphate on the plating rate is insignificant at a low acid concentration (Sec. 5.2.1.1), a combination of low acid and sulphate concentration seems to be desirable for both PTH and BV for maximum plating rate.

On the other hand, the electrode separation was found to be significant in affecting the workpiece level variation of the BVs but not the PTHs, and the uniformity deteriorated with the electrode separation in the former case. This is evident from both the first-order (Eq. 6.1 (PTH), Eq. 6.8 (BV)) and second-order model (Eq. 5.2 (PTH), Eq. 5.9 (BV)) of the two processes. It is believed that, under the same agitation scheme, the convective flow of electrolyte into the blind-vias is enhanced when the electrode separation is reduced and hence the deposit uniformity is improved also. However, the flow of electrolyte in the PTH is unrestricted and therefore not affected by the inter-electrode distance as long as the minimum electrolyte velocity [Kessler and Alkire, 76a] is maintained within the through-holes.

In contrast, the average current density was found to be significant in affecting the workpiece level variation of the PTHs but not the BVs in the second-order model. Together with the difference in the effect of electrode separation discussed above, this affects the parametric dependence of the optimum solution for the two processes. The second-order model of the PTH plating predicts that larger average current density and electrode separation is required to obtain minimum workpiece level variability for smaller through-holes, while the optimum combination is 2.5 times more sensitive to the average current density than to the electrode separation (Fig. 5.11). The BV second-order model predicts that the optimum combination is 2.7 times more sensitive to the electrode separation than to the average current density (Fig. 5.23).

The second-order models developed for the two processes show also that, while the workpiece level variation of each of them can be minimized within their respective optimum region, simultaneous optimization of both processes is not possible. This is because the average current density × electrode separation interaction, which is found to be significant in PTH but not BV plating, necessitates two different optimum regions for the processes (Fig. 5.9 and Fig. 5.20). This is also reflected by the significant lack of fit during the trials of fitting a second-order response surface for the PTH plating in the BV optimum region (Sec. 5.4.1) and vice versa (Sec. 5.4.2). The combined models developed for the PTH and BV plating in Sec. 5.4 aid the understanding of which of the two features is limiting the workpiece level uniformity at a particular combination of average current density and electrode separation.

Having said this, the first order models for the PTH and BV plating do indicate that there exists a compromise solution when the whole operability region is considered. Fig. 5.8(a) and Fig. 5.20 show that a combination of low average current density (32.3 mA/cm^2) and small electrode separation (12.7 cm) gives a standard deviation of 2.3 μm for PTH and 1.2 μm for BV, which are close to the minimum variability achievable within the operability region. However, the validity of such a solution diminishes as the through-holes get smaller as the optimum value for the electrode separation increases rapidly with the corrected aspect ratio (Fig. 5.11). It will also be noted that the standard deviation obtained for the PTH plating (2.3 μm) in the compromise solution is higher than the minimum standard deviation achievable with the second-order model (Fig. 5.13).

Sec. 4.6.1 shows that an average current density of 30.1 mA/cm^2 and an electrode separation of 25.4 cm gives minimum thickness variability for a non-uniformly patterned substrate. It can be seen that the electrode separation, which has an opposite effect on the thickness variability of non-uniform patterns (positive) and PTHs (negative), prohibits the simultaneous minimization of the workpiece level variability of the two features

.

6.5 Limitations of the Study

This research work has its limitations and discussion of these limitations provides insight into both the contribution and generality of the findings reported here. One limitation is the scale of the experimental setup, which is relatively small compared with actual production environment. Such a limitation is commonly found in the experimental studies of electrodeposition processes because most of the physio-chemical and polarization properties are highly system dependent. The models developed in this work, which are not defined by these parameters, are believed to be relatively robust to the scale of the system. Moreover, the orthogonality of the factorial and response surface designs employed enhances also the robustness of the parameters' effects [Steinberg and Hunter, 84]. Another limitation originates from the relative simplicity of the lithographic pattern used in the non-uniform pattern plating

experiments, i.e. substrates with only two different active area densities were considered. One may also criticise that the number of sample points taken from each board for the deposit thickness measurement were too small to represent the workpiece level variability. However, it has been shown in Sec. 4.6.2.1 and Sec. 4.6.3 that a sample size of six is sufficiently large to arrive at a solution as if the true mean and standard deviation of the thickness distribution were used. Finally, the relatively low aspect ratio of the through-holes and blind vias (0.8 - 2) used in the experiments limits the applicability of the results to higher aspect ratio holes, although the general trend of the parameters' effects should not be limited.

6.6 Contributions of the Study

The importance of deposit thickness uniformity has long been understood and recognised in the current distribution modelling of electrochemical processes. The results obtained in this series of experiments make several contributions to the understanding and control of workpiece level variability in the acid copper plating of printed circuit boards. Firstly, statistically proven and electrochemically informed models were developed for the copper plating of uniform/non-uniform patterns, plated-through holes and blind vias. They were able to predict, within the operability range and experimental accuracy, the workpiece level thickness variability for the three features. Secondly, the work furnishes specific knowledge of the effects of important process and product parameters, in particular the interaction between the average current density and electrode separation, on the plating uniformity and how they can be manipulated to optimise the three sub-processes with respect to minimized workpiece level variability.

Thirdly, the verification runs of the non-uniform pattern plating experiments explained the scattering effect of the active area density contrast on the deposit thickness of regions with different active area densities. Moreover, they provide empirical indications for the promising solution of reducing simultaneously the overall active area density to reduce the workpiece level variability when the active area density contrast over the board surface is increased.

Finally, these models unveiled the limitations hindering the simultaneous optimization of the electroplating of all the three features. The results should provide insights to researchers and practitioners of copper electroplating in understanding and controlling the plating thickness variation at a workpiece level.

6.7 Suggestions for Future Work

Further research work in this area should try to overcome the limitations discussed in Sec. 6.5 above and to further examine the relevant issues which have arisen from the experimental results in this study. The validity of the models developed in this thesis, and the predicted parameters' effects, may be tested in baths of different sizes with the same length-to-breadth ratio to evaluate the effect of scaling. The results may provide insight into the possibility and limitations of generalizing the results of small scale studies. The non-uniform pattern plating experiments confirmed the significance of the overall active area density, active area density ratio, number of density contrasts and the area of continuum over the substrate on the workpiece level variability. A further set of experiment could be designed to investigate the effects and possible interactions between these product-dependent parameters. The results of such experiments may give us better knowledge of the influence of lithographic patterning in a complex circuit and possible means of counteracting its undesirable effects with proper combination of process parameters. Furthermore, the first verification run of the non-uniform pattern plating models shows that the pattern level variation across two regions can be different even through they have the same local average active area density and active area density ratio if their individual feature sizes are different. It is suspected that the size and spatial arrangement of the features within the region are affecting the current and thickness distribution. This calls for a new parameter that can better characterize the non-uniform distribution of lithographic patterns than the concept of active area density ratio and the experimental investigation of its parametric dependence on the various process parameters.

6.8 Conclusions

This thesis has presented experimental studies of acid copper electroplating of patterned substate, plated-through holes and blind vias. Statistical models have been developed to aid the understanding of the effects of various process and product parameters on the workpiece level plating thickness uniformity. Although the results of previous theoretical analyses are not readily applicable to the industrial type electroplating investigated in this study, primarily because of the practical difficulty of achieving 100% current efficiency, they help the explanation of some of the behaviours observed in the experiments and predicted by the models. These electrochemically informed models indicate also the optimum combinations of the process parameters resulting in minimum variability within the experimental range, and the behaviour of the optimum solutions. In summary, key contributions made by the experimental investigations reported here are :

- statistical models of the pattern, through-hole and blind-via copper plating processes are established using designed experiments for the control and minimization of workpiece level deposit variability
- these models are statistically proven and electrochemically informed
- they are able to predict, within a known operability space and experimental accuracy, the workpiece level plating variability for the three sub-processes
- they provide specific knowledge of the effects of key process and product parameters, particularly the current density and electrode separation interaction, on the workpiece level plating uniformity
- the work uncovered the potential interaction between the active area density, density contrast and overall active area density over the board surface, which has practical significance for designing the layout of the printed circuit
- limitations to the simultaneous optimization of all the three features are unveiled by these models, the intersections of the response surfaces for the combined models of plated-through holes and blind-vias indicate the feature that limits the workpiece level uniformity within the operability space of the average current density and electrode separation.

REFERENCES

Agar J.N., Hoar T.P., 1947, Factors in Throwing Power Illustrated by Potential-Current Diagrams, *Discussions of the Faraday Society*, No. 1, pp. 162 - 168.

Alkire R. and Ju J.B., 1987, The Effect of an Impinging Fluid Jet on Mass Transfer and Current Distribution of a Circular Through-hole, *Journal of the Electrochemical Society*, Vol. 134, No. 11, pp. 1172 - 1180.

Alkire R. and Mirarefi A.A., 1973, The Current Distribution Within Tubular Electrodes under Laminar Flow, *Journal of the Electrochemical Society*, Vol. 120, No. 11, pp. 1507 - 1515.

Alkire R. and Mirarefi A.A., 1977a, Current Distribution in a Tubular Electrodes under Laminar Flow : Two Electrode Reactions, *Journal of the Electrochemical Society*, Vol. 124, No. 8, pp. 1214 - 1220.

Alkire R. and Mirarefi A.A., 1977b, Current Distribution in a Tubular Electrodes under Laminar Flow : One Electrode Reaction, *Journal of the Electrochemical Society*, Vol. 124, No. 7, , pp. 1043 - 1049.

Barringer T. and Carano M., 1986, Optimization of an Acid Copper Plating Bath for Through-hole Plating, *Plating and Surface Finishing*, Vol. 73, No. 3, pp. 36 - 37.

Berger L., Boeckl R., Kronemann R. and Meyer D., 1980, *IBM Technical Digest Bulletin*, Vol. 23, pp. 201.

Bialecki R., Nahlik R., Lapkowski M., 1984, Applying the Boundary Element Method to Electrochemical Calculations of Primary Current Distribution, *Electrochimica Acta.*, Vol. 29, No. 7, pp. 905 - 910.

Blue J. L., 1980, Efficient Calculation of Current Flow in Electroplating Cells, *The Bell System Technical Journal*, Vol. 59, No. 2, pp. 169 - 182.

Bokisa G.S. and McFarland C.W., 1993, Statistical Modelling of Printed Circuit Hole Plating, *Proceedings of the 80th AESF Annual Technical Conference*, pp. 1033 - 1045.

Box G.P.E., Behnken D.W., 1960, Some New Three Level Designs for the Study of Quantitative Variables, *Technometrics*, Vol. 2, pp. 455 - 476.

Box G.P.E., Hunter W.G., Hunter J.S., 1978, *Statistics for Experimenters*, Wiley, pp. 306 - 342, 510 - 539.

Box G.P.E., Hunter J.S., 1957, Multi-factor Designs for Exploring Response Surfaces, *Annals of Mathematical Statistics*, Vol. 28, pp. 195 - 242.

Box G.P.E., Wilson K.B., 1951, On the Experimental Attainment of Optimum Conditions, *Journal of the Royal Statistical Society*, Ser. B, Vol. 13, pp. 1 - 45.

Caban R., Chapman T.W., 1977, Statistical Analysis of Electrode Kinetics Measurements - Copper Disposition from $CuSO_4$-H_2SO_4 Solutions, *Journal of the Electrochemical Society*, Vol. 124, No. 9, pp. 1371 - 1379.

Canning W. plc., 1982, *The Canning Handbook - Surface Finishing Technology*, W. Canning plc., pp. 546 - 549, 780 -791.

Chern J.W.E., Cheh H.Y., 1996a, Modeling of Plated Through-Hole Processes. I. Current Distribution, *Journal of the Electrochemical Society*, Vol. 143, No. 10, pp. 3139 - 3144.

Chern J.W.E., Cheh H.Y., 1996b, Modeling of Plated Through-Hole Processes. II. Effect of Leveling Agents on Current Distribution, *Journal of the Electrochemical Society*, Vol. 143, No. 10, pp. 3144 - 3148.

Choi Y.S. and Kang T., 1996, Three-Dimensional Calculation of Current Distribution in Electrodeposition on Patterned Cathode with Auxiliary Electrode, *Journal of the Electrochemical Society*, Vol. 143, No. 2, pp. 480 - 485.

Coombs C. F., 1988, *Printed Circuits Handbook*, 3rd ed., McGraw-Hill, pp. 6.1 - 6.38, 11.1 - 12.47.

Couch R.W., Bikales R.G., 1961, Plating of Printed Circuits with Pyrophosphate Copper and a Cyanide Bath, *Proc. Am. Electroplaters Soc.*, Vol. 48, pp. 176 - 181.

Dalby S., Nickelsen J. and Alting L., 1975, Metal Distribution in Electroplating, *Electroplating and Metal Finishing*, Vol. 28, pp. 18 - 23.

DeBecker B., West A. C., 1996, Workpiece, Pattern, and Feature Scale Current Distributions, *Journal of the Electrochemical Society*, Vol. 143, No. 2, pp. 486 - 492.

Deconinck J., 1992, *Current Distributions and Electrode Shape Changes in Electrochemical Systems*, Springer-Verlag.

Deconinck J., Maggetto G., 1985, Calculation of Current Distribution and Electrode Shape Change by the Boundary Element Method, *Journal of the Electrochemical Society*, Vol. 132, No. 12, pp. 2960 - 2965.

Dini J.W., 1964, Plating Through Holes in Printed Circuit Boards : Evaluation of Some Copper Baths, *Plating*, Vol. 51, pp. 119 - 124.

Dini J.W., 1989, Strategy of Experimentation, *Plating and Surface Finishing*, Vol. 76, No. 9, pp. 64 - 70.

Duffek E.F., 1988, Plating, in *Printed Circuits Handbook*, 3rd ed., Coombs C.F., Editor-in-Chief, McGraw-Hill, pp. 12.44.

Dukovic J.O., Tobias C.W., 1990, Simulation of Leveling in Electrodeposition, *Journal of the Electrochemical Society*, Vol. 137, No. 12, pp. 3748 - 3755.

Dukovic J.O., 1993, Feature-scale simulation of resist-patterned electrodeposition, *IBM J. Res. Develop.*, Vol. 37, No. 2, pp. 125 - 141.

Dukovic J.O., 1990, Computation of current distribution in electrodeposition, a review, *IBM J. Res. Develop.*, Vol. 34, No. 5, pp. 693 - 705.

Duncan A.J., 1955, Multiple Range and Multiple F Tests, *Biometrics*, Vol. 11, pp. 1 - 42.

Engelmaier W. and Kessler Thomas, 1978, Investigation of Agitation Effects on Electroplated Copper in Multilayer Board Plated-Through Holes in a Forced-Flow Plating Cell, *Journal of the Electrochemical Society*, Vol. 125, No. 1, pp. 36 - 43.

Evans U.R., 1960, *The Corrosion and Oxidation of Metals : Principles and Practical Applications*, Edward Arnold, pp. 862.

Finney D.J., 1945, Fractional Replication of Factorial Arrangements, *Annals Eugenics*, Vol. 12, pp. 291 - 301.

Fomichev V.G., 1968, Current Distribution at a Nonequipotential Electrode, *Soviet Electrochem.*, Vol. 4, pp. 708 - 713.0

Forrest G. and Reed D., 1993, Current Density Effect, *Printed Circuit Fabrication*, Vol. 16, No. 8, pp. 26 - 30.

Gabe D.R., Robinson D.J., 1971, Dendritic Formation and the Effects of Addition Agents in the Electrodeposition of Copper from Acid Sulphate Solutions, *Trans. Inst. Metal Finishing*, Vol. 49, pp. 17 - 21.

Gauvin W.H., Winkler C.A., 1955, The Effect of Chloride Ions on Copper Electrodeposition, *Journal of the Electrochemical Society*, Vol. 99, No. 1, pp. 71 - 77.

Gnusin N.P., Poddubnyi N.P., Rudenko E.N., Formin A.G., 1965, Distribution of the Current on the Cathode in the form of a Band in the Half-Space of an Electrolyte with a Polarization Curve expressed by the Tafel Formula, *Elektrokhimiya*, Vol. 1, No. 4, pp. 452 - 459.

Goh T.N., Roy S.K., 1989, Application of Taguchi's Orthogonal Array in a Material Screening Experiment, *Quality Assurance*, Vol. 15 No. 1, pp. 10 - 13.

Goodenough M, Whitlaw K.J., 1989, Studies of copper deposition for high aspect ratio printed circuit boards, *Trans. Inst. Metal Fin.*, Vol. 67, pp. 57 - 62.

Haak R., Ogden C., Tench D., 1981, Evaluation of Agitation Within Circuit Board Through-holes, *J. Appl. Electrochem.*, Vol. 11, pp. 771 - 780.

Haluzan I., Reichenbach D., 1991, Investigation of Copper Deposition on Printed Circuit Boards Using Taguchi Methods, *Circuit World*, Vol. 17, No. 4, pp. 24 - 26.

Harry M.J., 1989, PCB Plated Through Hole Optimisation : A Case Study in SPC, *Circuit World*, Vol. 16, No. 1, pp. 33 - 43.

Hazlebeck D.A., Talbot J.B., 1991a, Modelling of the Electroplating of a Through-Hole Considering Additive Effects and Convection, *Journal of the Electrochemical Society*, Vol. 138, No. 7, pp. 1985 - 1997.

Hazlebeck D.A., Talbot J.B., 1991b, Modelling of the Electroplating of a Through-Hole with Flow Reversal and Downstream Counterelectrode Configurations, *Journal of the Electrochemical Society*, Vol. 138, No. 7, pp. 1998 - 2002.

Hazlebeck D.A., Talbot J. B., 1990, Modeling of Additive Effects on the Electroplating of a Through-Hole, *AIChE Journal*, Vol. 36, No. 8, pp. 1145 - 1155.

Hine F., Yoshizawa S., Okada S., 1956, Effect of the Walls of Electrolytic Cells on Current Distribution, *Journal of the Electrochemical Society*, Vol. 103, No. 3, pp. 186 - 193.

Horkans J. and Romankiw L.T., 1977, Pulsed Potentiostatic Deposition of Gold from Solutions of the Au(I) Sulfite Complex, *Journal of the Electrochemical Society*, Vol. 124, No. 10, pp. 1499 - 1505.

Howe D., McCormick, Yonnet C., Glossop G., 1979, , *Finishing Industry*, Vol. 1, pp. 34 - 44.

Huffman D., Witkowski M., 1991, Assessing Small Hole Plating Capabilities, *Trans. Inst. Metal Finish.*, Vol. 69, No. 3, pp. 96 - 99.

Hull R.O., 1939, Current Density Range Characteristics - Their Determination and Application, *Am. Electroplat. Soc.*, Vol. 27, pp. 52 - 59.

Hume E. C., Deen W. M., Brown R. A., 1984, Mass Transfer Analysis of Electrodeposition Through Polymeric Masks, *Journal of the Electrochemical Society*, Vol. 131, No. 6, pp. 1251 - 1258.

Lynne B. Hare, Perspectives on the Taguchi Controversy, *Annual Quality Congress Transactions*, 1990, Vol. 44, ASQC, Milwaukee, pp. 381 - 384.

Ibl N., 1981, Nomenclature for Transport Phenomena in Electrolytic Systems, *Pure and Appl. Chem.*, Vol. 53, pp. 1829 - 1840.

IPC-A-600E, 1995, Acceptability of Printed Boards, Institute for Interconnecting and Packaging of Electronic Circuits, USA.

Kardos O. and Foulke D.G., 1962, in *Advances in Electrochemistry and Electrochemical Engineering*, Vol.2, Delahay P. and Tobias C., Editors, Wiley Interscience, New York.

Kasper C., The Theory of the Potential and the Technical Practice of Electrodeposition, *Transactions of the Electrochemical Society*, Vol. 77 (1940), pp. 353 - 384, Vol. 78 (1940), pp. 131 - 160, Vol. 82 (1942), pp. 153 - 184.

Kessler T. and Alkire R., 1976a, Copper Plating of Multilayer Printed Wiring Boards, *Plating and Surface Finishing*, Vol. 63, No. 9, pp. 22 - 27.

Kessler T. and Alkire R., 1976b, A Model for Copper Electroplating of Multilayer Printed Wiring Boards, *Journal of the Electrochemical Society*, Vol. 123, No. 7, pp. 990 - 999.

Klingert J.A., Lynn S., Tobias C.W., 1964, Evaluation of Current Distribution in Electrode Systems by High-Speed Digital Computers, *Electrochim. Acta*, Vol. 9, pp. 297 - 311.

Koseki K., Hashimoto Y., Yoshida T., 1967b, Extended Equation for Current Distribution in Rectangular Cells (Part 2), *J. Electrochem. Soc. Japan*, Vol. 35, No. 2, pp. 88 - 96.

Koseki K., 1968, Extended Equation for Current Distribution in Rectangular Cells (Part 3), *J. Electrochem. Soc. Japan*, Vol. 36, No. 4, pp. 226 - 236.

Krohn A., 1974, Other Alloys, in *Modern Electroplating*, 3rd ed., Lowenheim F.A., Editor, Wiley-Interscience Publication, pp. 542 - 551.

Landau U., 1988, Plating - New Prospects for an Old Art, pp. 215 - 245.

Lanzi III, Landau U., J.D. Reid and R.T. Galasco, 1989, Effect of Local Kinetic Variations on Through-Hole Plating, *Journal of the Electrochemical Society*, Vol. 136, No. 2, pp. 368 - 374.

Lanzi O., Landau U., 1988, Analysis of Mass Transport and Ohmic Limitations in Through-Hole Plating, *Journal of the Electrochemical Society*, Vol. 135, No. 8, pp. 1922 - 1930.

Lanzi O., 1985, M.S. Thesis, Case Western Reserve University, Cleverland, OH.

Leisner P., Ulrich D., Moller P., 1992, Applying Taguchi Statistics to Optimize Current Efficiency in Hard Chromium Pulse Plating, *Plating and Surface Finishing*, Vol. 79, Iss. 7, p. 62 - 66.

Lin K.M., Kackar R.N., 1985, Wave Soldering Process Optimization by Orthogonal Arrary Design Method, *Electronic Packing and Production*, Feb., pp. 108 - 115.

Lyons E.H., 1974, Fundamental Principles, in *Modern Electroplating*, 3rd ed., Lowenheim F.A., Editor, Wiley-Interscience Publication, pp. 19.

Madore C., Matlosz M., Landolt D., 1996, Blocking Inhibitors in Cathodic Levelling, *Journal of the Electrochemical Society*, Vol. 143, No. 12, pp. 3927 - 3943.

Mallows C.L., 1973, Some Comments on C_p, *Technometrics*, Vol. 15, pp. 661 - 675.

Matlosz M., Creton C., Clerc C. and Landolt D., 1987, Secondary Current Distribution in a Hull Cell, *Journal of the Electrochemical Society*, Vol. 134, No. 12, pp. 3015 - 3021.

Mattson E., and Bockris J. O'M., 1959, Galvanostatic Studies of the Kinetics of Deposition and Dissolution in the Copper + Copper Sulphate System, *Trans. Faraday Soc.*, Vol. 55, pp. 1586 - 1601.

Mayer L., Barbieri S., 1981, Characteristics of Acid Copper Deposits for PCB Applications, *Plating and Surface Finishing*, Vol. 68, pp. 46 - 50.

Mehdizadeh S., Dukovic J., Andricacos P.C. and Romankiw L.T., 1993, The Influence of Lithographic Patterning on Current Distribution in Electrodeposition : Experimental Study and Mass-Transfer Effects, *Journal of the Electrochemical Society*, Vol. 140, No. 12, pp. 3497 - 3505.

Mehdizadeh S., Dukovic J.O., Andricacos P.C., Romankiw L.T. and Cheh H.Y., 1992, The Influence of Lithographic Patterning on Current Distribution : A Model for Microfabrication by Electrodeposition, *Journal of the Electrochemical Society*, Vol. 139, No. 1, pp. 78 - 91.

Mehdizadeh S., Dukovic J., Andricacos P.C., Romankiw L.T., 1990, Optimization of Electrodeposit Uniformity by the Use of Auxiliary Electrodes, *Journal of the Electrochemical Society*, Vol. 137, No. 1, pp. 110 - 117.

Mehdizadeh S., J.O. Dukovic, P.C. Andricacos, Romankiw L.T. and Cheh H.Y., 1988, *Current Distribution in Electrodeposition on Resist-Patterned Substrates*, Extended Abstract 42D, AIChE 1988 Annual Meeting, Washington DC.

Middleman S., 1986, Factors that Affect Uniformity of Plating of Through-holes in Printed Circuit Boards II. Periodic Flow Reversal through the Holes, *Journal of the Electrochemical Society*, Vol. 133, No. 3, pp. 492 - 496.

Miller A.J., 1990, *Subset Selection in Regression*, Chapman and Hall.

Mirkova L., Rashkov S., Nanev C, 1982, Levelling Mechanism During Bright Acid Copper Plating, *Surface Technology*, Vol. 15, pp. 181 - 190.

Montgomery D.C., 1997, *Design and Analysis of Experiments*, Wiley, pp. 1 - 19, 318 - 336, 575 - 641.

Moulton H.F, 1905, Current Flow in Rectangular Conductors, *Proceedings of the London Mathematical Society*, Series 2, No. 3, pp. 104 - 110.

Myers R.H., Montgomery D.G., 1995, *Response Surface Methodology : Process and Product Optimization Using Designed Experiments*, Wiley, pp. 640 - 655.

Nair V.N. (ed.), 1992, Taguchi's Parameter Design : A Panel Discussion, *Technometrics*, Vol. 34, No. 2, pp. 127 - 161.

Newman J.S., 1991a, *Electrochemical Systems*, 2nd ed., Prentice Hall, pp. 378 - 396.

Newman J.S., 1991b, *Electrochemical Systems*, 2nd ed., Prentice Hall, pp. 410 - 415.

Newman J.S., 1991c, *Electrochemical Systems*, 2nd ed., Prentice Hall, pp. 437 - 453.

Newman J., 1966, Resistance for Flow of Current to a Disk, *Journal of the Electrochemical Society*, Vol. 113, No. 5, pp. 501 - 502.

Norm 50957 DIN (Duetsches Institut für Normung), 1983, Mikroskopische Messung der Schichtdicke, TAB 175, Beuth Verlag GmbH, Berlin Köln.

Pao T.W., Phadke M.S., Sherred C.S., 1985, Computer Response Time Optimization Using Orthogonal Array Experiments, *IEEE International Communications Conference*, Chicago, IL Conference Record, Vol. 2, pp. 890 -895.

Patel R.D., McFeeley J.J., Jolls K.R., 1975, Wall Mass Transfer in Laminar Pulsatile Flow in a Tube, *AIChE Journal*, Vol. 21, No. 2, pp. 259 - 267.

Parrish W.R. and Newman J., 1969, Current Distributions on a Plane Electrodes below the Limiting Current, *Journal of the Electrochemical Society*, Vol. 116, No. 1, pp. 169 - 172.

Parrish W.R. and Newman J., 1970, Current Distributions on Plane, Parallel Electrodes in Channel Flow, *Journal of the Electrochemical Society*, Vol. 117, No. 1, pp. 43 - 48.

Parthasaradhy N.V., 1989, *Practical Electroplating Handbook*, Prentice-Hall, pp. 57 - 100, 178 - 182, 279 - 281, 352 - 357.

Pesco A.M., Cheh H.Y., 1989, The Current Distribution within Plated Through-Holes I. The Effect of Electrolyte Flow Restriction during DC Electrolysis, *Journal of the Electrochemical Society*, Vol. 136, No. 2, pp. 399 - 407.

Phadke M.S., Design Optimization Case Studies, *AT&T Technical Journal*, Vol. 65, No. 2, pp. 51 - 68.

Pinkerton H.L., 1984, Current and Metal Distribution, in *Electroplating Engineering Handbook*, revised by Durney L.J., Van Nostrand Reinhold, pp. 461 - 473.

Pletcher D., 1982, *Industrial Electrochemistry*, Chapman and Hall, New York.

Powers J.V. and Romankiw L.T. , 1972, U.S. Patent No. 3652442.

Prentice G., 1991, Numerical Techniques for Modeling Current Distribution at Plane and Flow-by Electrodes, in *Techniques for Characterization of Electrodes and Electrochemical Processes*, R. Varma and J.R. Selman, Editors, Wiley, pp. 650.

Romankiw L.T., 1979, Abstract 462, pp. 1165, *The Electrochemical Society Extended Abstract*, Vol. 79-2, Los Angeles, CA Meeting.

Romankiw L.T., Krongelb S., Castellani E.E., Pfeiffer A.T., Stoeber J. and Olsen J.D., 1974, Advantages and Special considerations in Fabricating Bubble Circuits by Electroplating and Sputter Etching, *IEEE Trans. Magnetics* MAG-10, No. 3, pp. 828 - 831.

Romankiw L.T., Krongelb S., Castellani E.E., Pfeiffer A.T., Stoeber J. and Olsen J.D., 1973, *Proceedings of the International Conference on Magnetics, ICM-73*, Vol. 6, pp. 104 -111.

Ryan T.P., 1988, Taguchi's Approach to Experimental Design : Some Concerns, *Quality Progress*, Vol. 21, No. 5, pp. 34 - 36.

Sanicky M.K., 1985, A Versatile Plater's Tool : All About the Hull Cell, *Plating and Surface Finishing*, Vol. 72, No. 10, pp. 20 -21

Sarma R.L., and Nageswar S., 1984, Electrodeposition of Copper in the Presence of 2-Mercaptoethanol, *J. Appl. Electrochem.*, Vol. 12, pp. 329.

Shih H. and Pickering H.W., 1987, Three-Dimensional Modelling of the Potential and Current Distributions in an Electrolytic Cell, *Journal of the Electrochemical Society*, Vol. 134, No. 3, pp. 551 - 558.

Shinoura O., 1996, High Density Magnetic Recording Heads Prepared by Electrochemical Deposition, *Electrochemical Technology : Innovation and New Developments*, Masuko N., Osaka T., Ito Y, Editors, Kodansha, Tokyo, pp. 219 - 238.

Smyrl W.H. and Newman J., 1989, Current Distribution at Electrode Edges at High Current Densities, *Journal of the Electrochemical Society*, Vol. 136, No. 1, pp. 132 - 139.

Skowronsk S, Reinoso E., 1927, The Specific Resistivity of Copper Refining Electrolytes and Method of Calculation, *Trans. Am. Electrochem. Soc.*, Vol. 52, pp. 205 - 223.

Steinberg D.M., Huntre W.G., 1984, Experimental Design : Review and Comment, *Technometrics*, Vol. 26, No. 2, pp. 71 - 97.

Taguchi G., 1987, *System of Experimental Design*, UNIPUB, White Plains, New York.

Taguchi G., 1986, *Introduction to Quality Engineering*, Asian Productivity Organization, UNIPUB, White Plains, New York.

Taguchi G., 1980, *Jikken Keikakuho*, 3rd ed., Maruzen, Tokyo, Vol. 1 and 2 (in Japanese).

Taguchi G., Wu Y., 1980, *Introduction to Off-Line Quality Control*, Central Japan Quality Control Association, Nagoya, Japan.

Taylor G.A.R., 1989, Fractional factorial experimental designs and orthogonal arrarys, *Quality Assurance*, Vol. 15, No. 3, pp. 117 - 122.

Tobias C.W., Wijsman R., 1953, , *Journal of the Electrochemical Society*, Vol. 100, No. 2, , pp. 459 - 4.

Turner D.R., Johnson G.H., 1962, The Effect of Some Addition Agents on the Kinetics of Copper Electrodeposition from a Sulfate Solution I : Cathode Potential-Current Density Relation, *Journal of the Electrochemical Society*, Vol. 109, No. 9, pp. 798 - 804.

Wagner C., 1951, Theoretical Analysis of the Current Density Distribution in Electrolytic Cells, *Journal of the Electrochemical Society*, Vol. 98, No. 1, pp. 116 - 128.

Wagner C., 1954, Contribution to the Theory of Electropolishing, *Journal of the Electrochemical Society*, Vol. 101, No. 1, pp. 225 - 228.

West A.C. and Newman J., 1991, Current Distributions on Recessed Electrodes, *Journal of the Electrochemical Society*, Vol. 138, No. 10, pp. 1620 - 1625.

West A.C. and Newman J., 1989, Current Distribution near an Electrode Edge as a Primary Distribution is Approached, *Journal of the Electrochemical Society*, Vol. 136, No. 10, pp. 2935 - 2939.

West A.C., Matlosz M., Landolt D., 1992, Primary current distribution in the Hull cell and related trapezoidal geometries, *Journal of Applied Electrochemistry*, Vol. 22, pp. 301 - 303.

Yoshida T., Koseki K., 1967a, Extended Equation for Current Distribution in Rectangular Cells (Part 1), *J. Electrochem. Soc. Japan*, Vol. 35, No. 1, pp. 24 - 35.

Yung E.K. and Romankiw L.T., 1989, Fundamental Study of Acid Copper Through-Hole Electroplating Process, *Journal of the Electrochemical Society*, Vol. 136, No. 3, pp. 756 - 767.

Yung E.K., Romankiw T.L.. and Alkire R.C., 1989, Plating of Copper into Through-Holes and Vias, *Journal of the Electrochemical Society*, Vol. 136, No. 1, pp. 206 - 215.

Appendix 3.1

List of Apparatus and Equipment

Fig. A3.1 : Photo-plotter : GSI Model 3244

Fig. A3.2 : Shearing machine : RS#609-398

Fig. A3.3 : Deburring machine : Hipass Moduline 600

Fig. A3.4 : Convection Oven : Binder EF240

Fig. A3.5 : Laminator : Circuitage

Fig. A3.6 : Exposure machine : Cologht DMVL 930 SA

Fig. A3.7 : Developing machine : Simona GmbH D-6570

Fig. A3.8 : Hull cell : Kocovr 7CA-267

Fig. A3.9 : Power supply : Kocour Rectifier 15A

Fig. A3.10 : Water purification system : B-pure D4511

Fig. A3.11 : Analytical balance : BOSCH S2000

Fig. A3.12 : A PCB being Plated in the Agitated 200 litre Plating Bath

Fig. A3.13 : The Electroless Copper Plating Process

(a) The Set of Six Electroless Copper Plating Solutions

(b) A PCB undergoing the Electroless Copper Process in an Agitated bath

Fig. A3.14 : CNC drilling machine : Excellon EX-110

Fig. A3.15 : Struer Dap-V polishing machine

Fig. A3.16 : Measurement of Deposit Thickness with X-ray Coating Thickness Gauge

(a) A PCB with Sectioned PTHs supported by Rounded Leaf Spring

(b) Measurement of a Through-hole as shown in the Screen of the X-ray Thickness Gauge

Fig. A3.17 : MEIJI Microscope

Fig. A3.18 : Cross-sectional Profile of the Plated Copper obtained by the Roughness Measurement Machine

Appendix 3.1 (Fig. A3.1, Fig. A3.2)

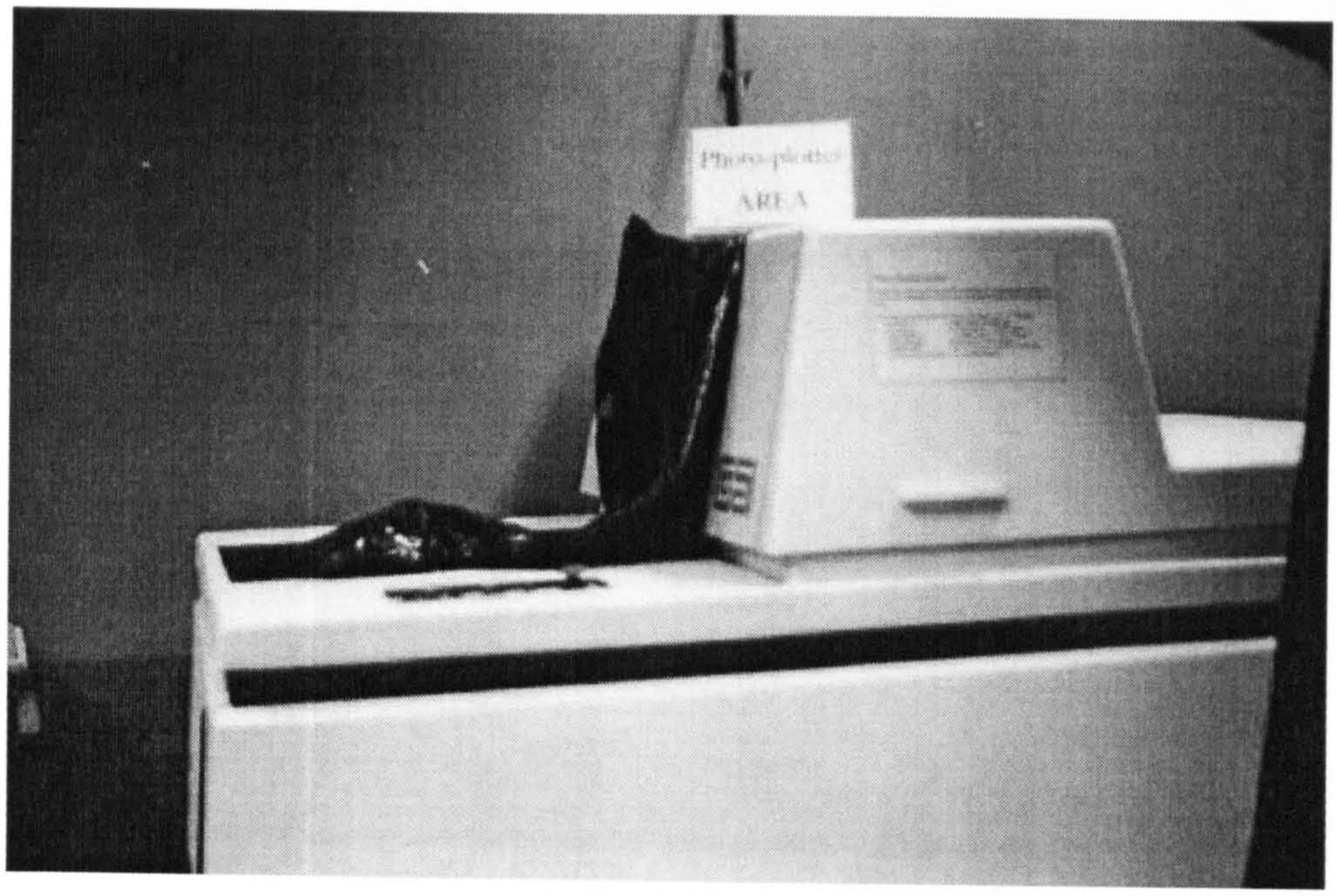

Fig. A3.1 : Photo-plotter : GSI Model 3244

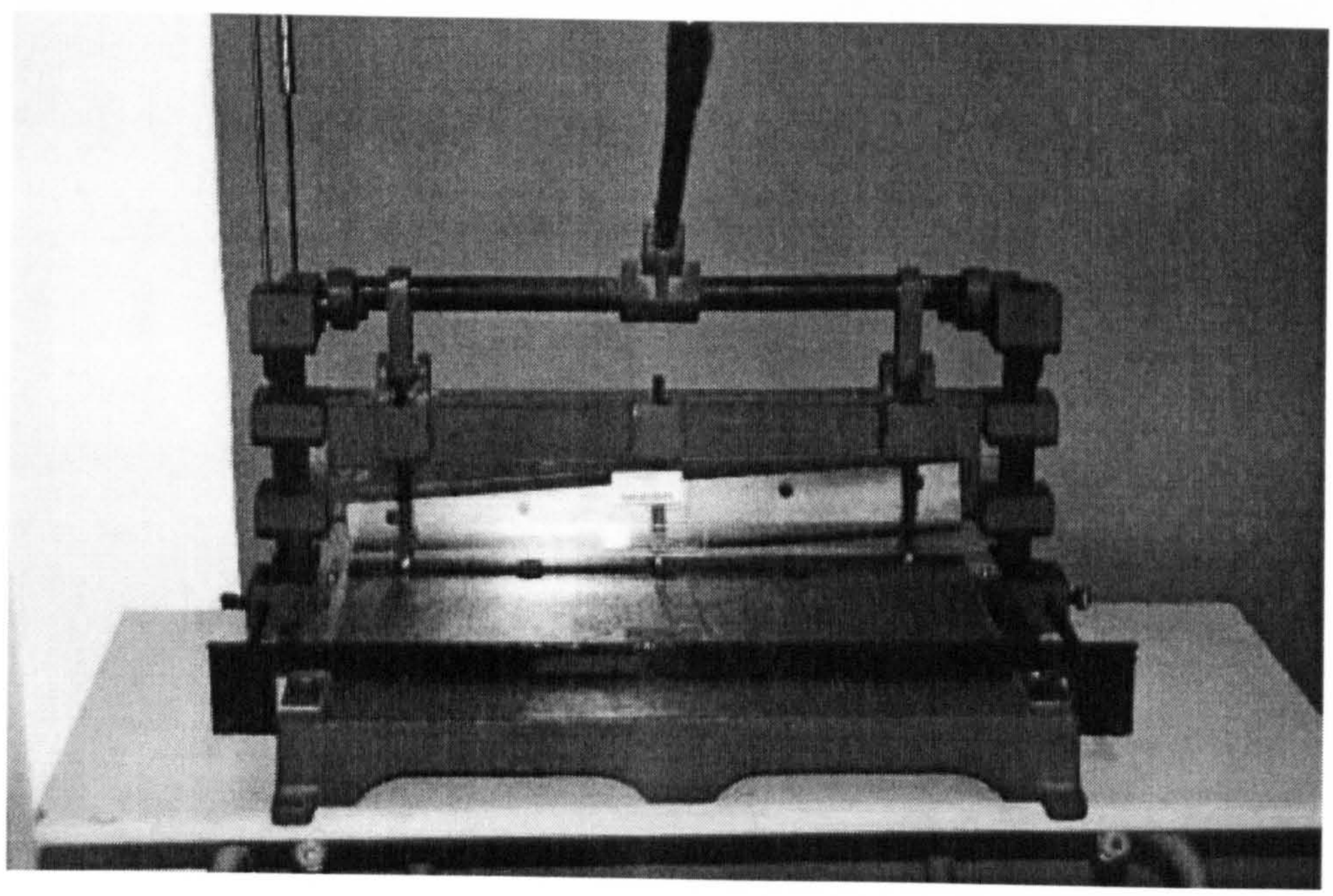

Fig. A3.2 : Shearing machine : RS#609-398

Appendix 3.1 (Fig. A3.3, Fig. A3.4)

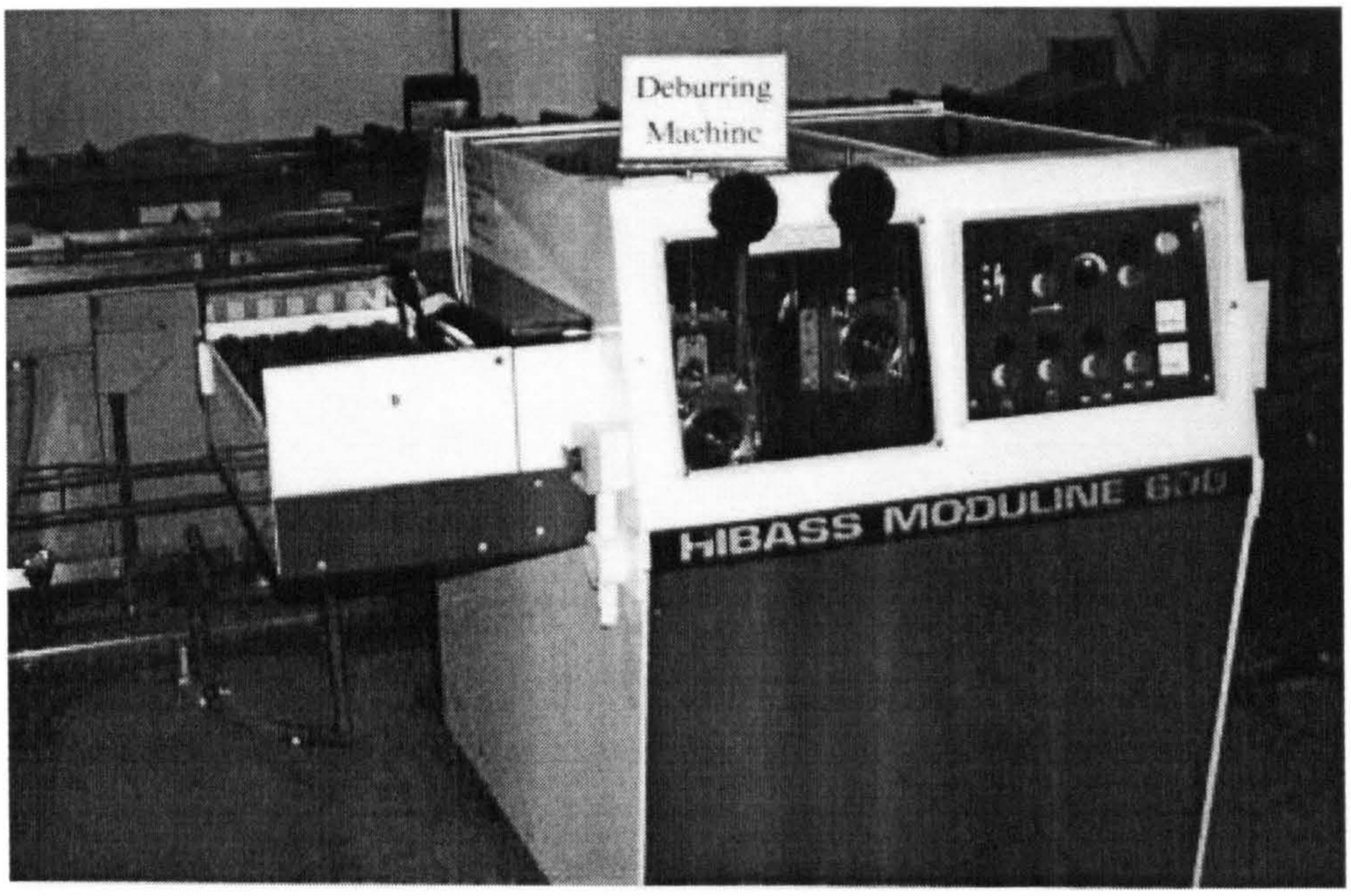

Fig. A3.3 : Deburring machine : Hipass Moduline 600

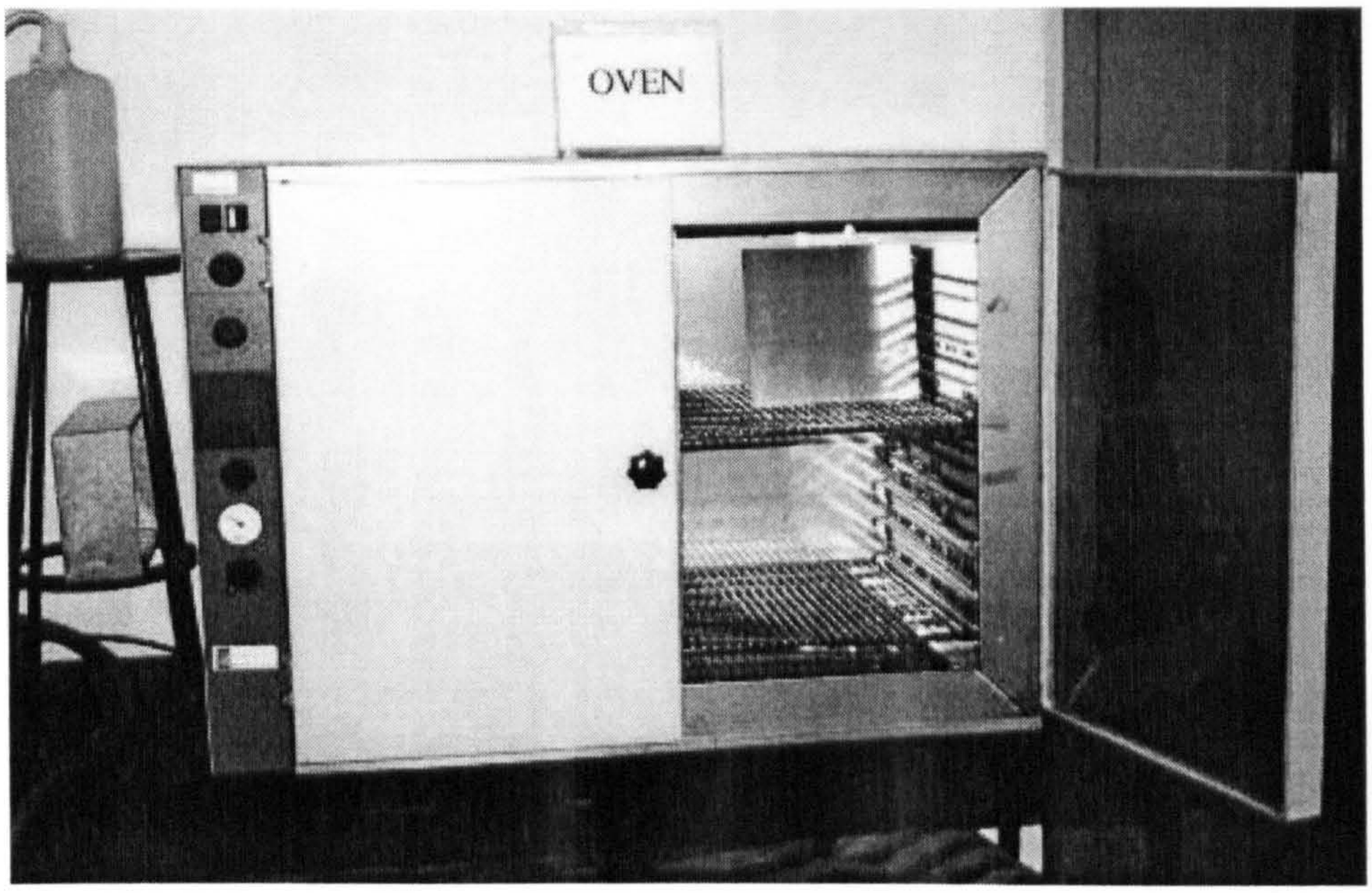

Fig. A3.4 : Convection Oven : Binder EF240

Appendix 3.1 (Fig. A3.5, Fig. A3.6)

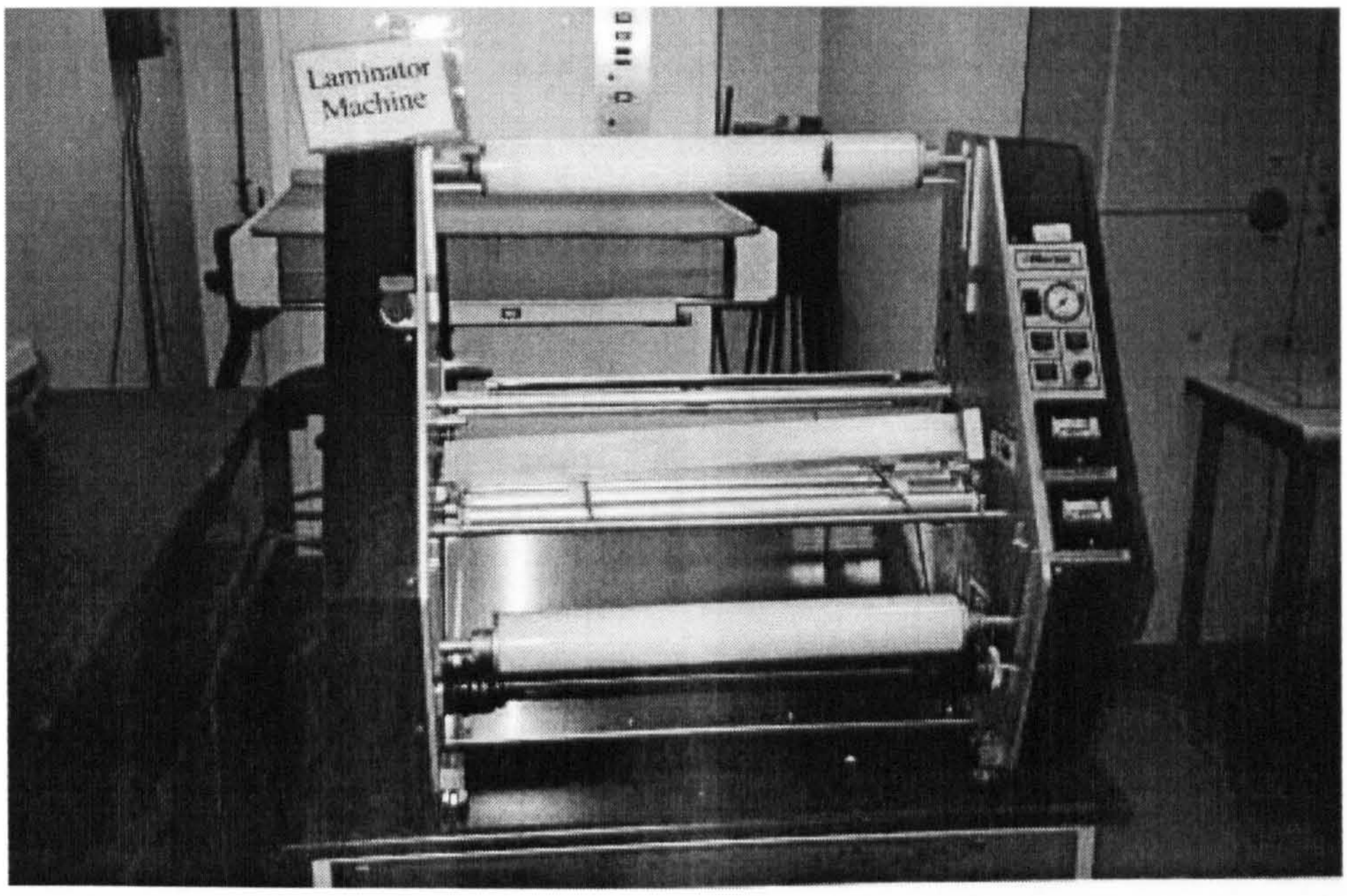

Fig. A3.5 : Laminator : Circuitage

Fig. A3.6 : Exposure machine : Cologht DMVL 930 SA

Appendix 3.1 (Fig. A3.7, Fig. A3.8)

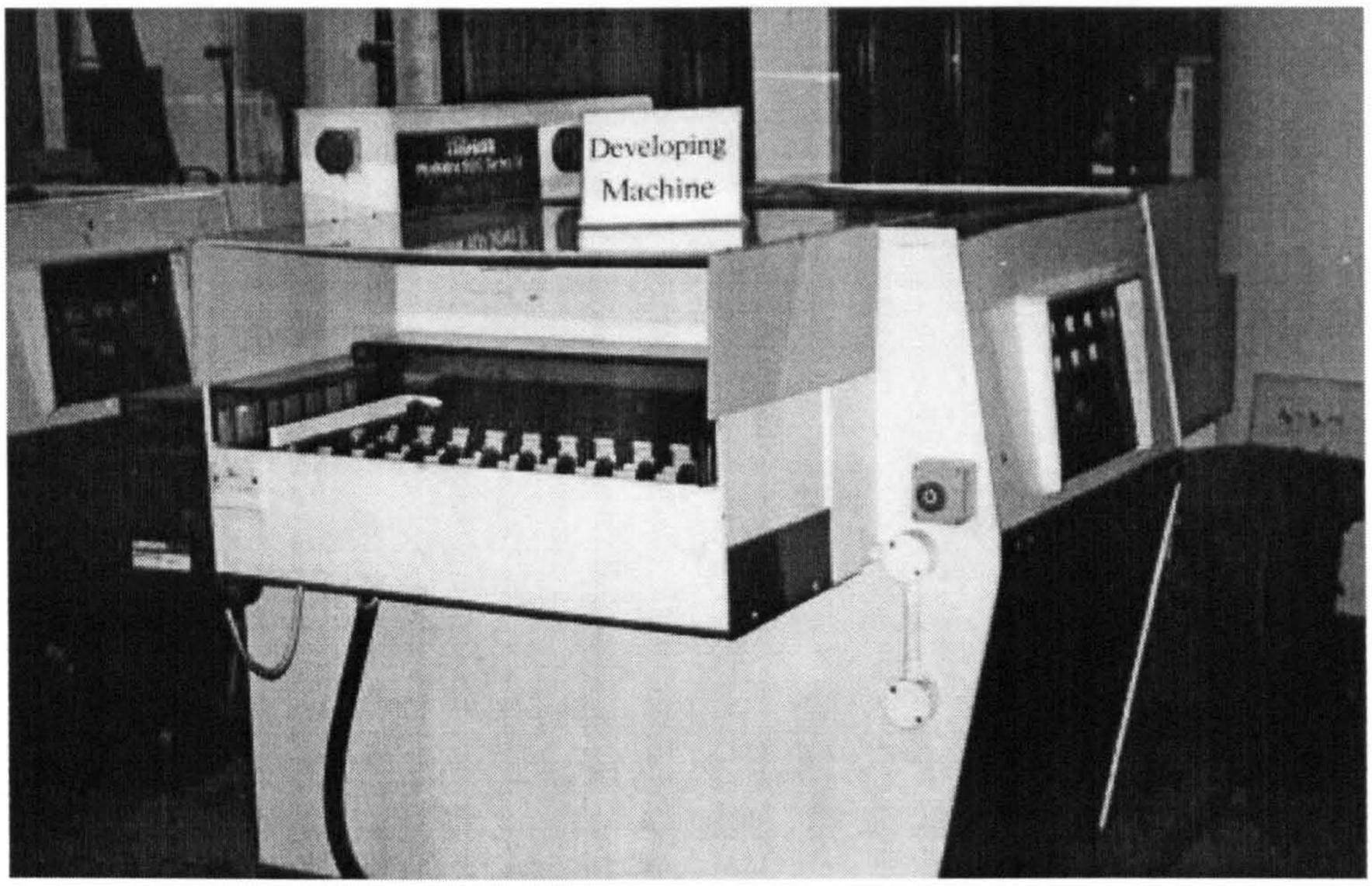

Fig. A3.7 : Developing machine : Simona Gmbh D-6570

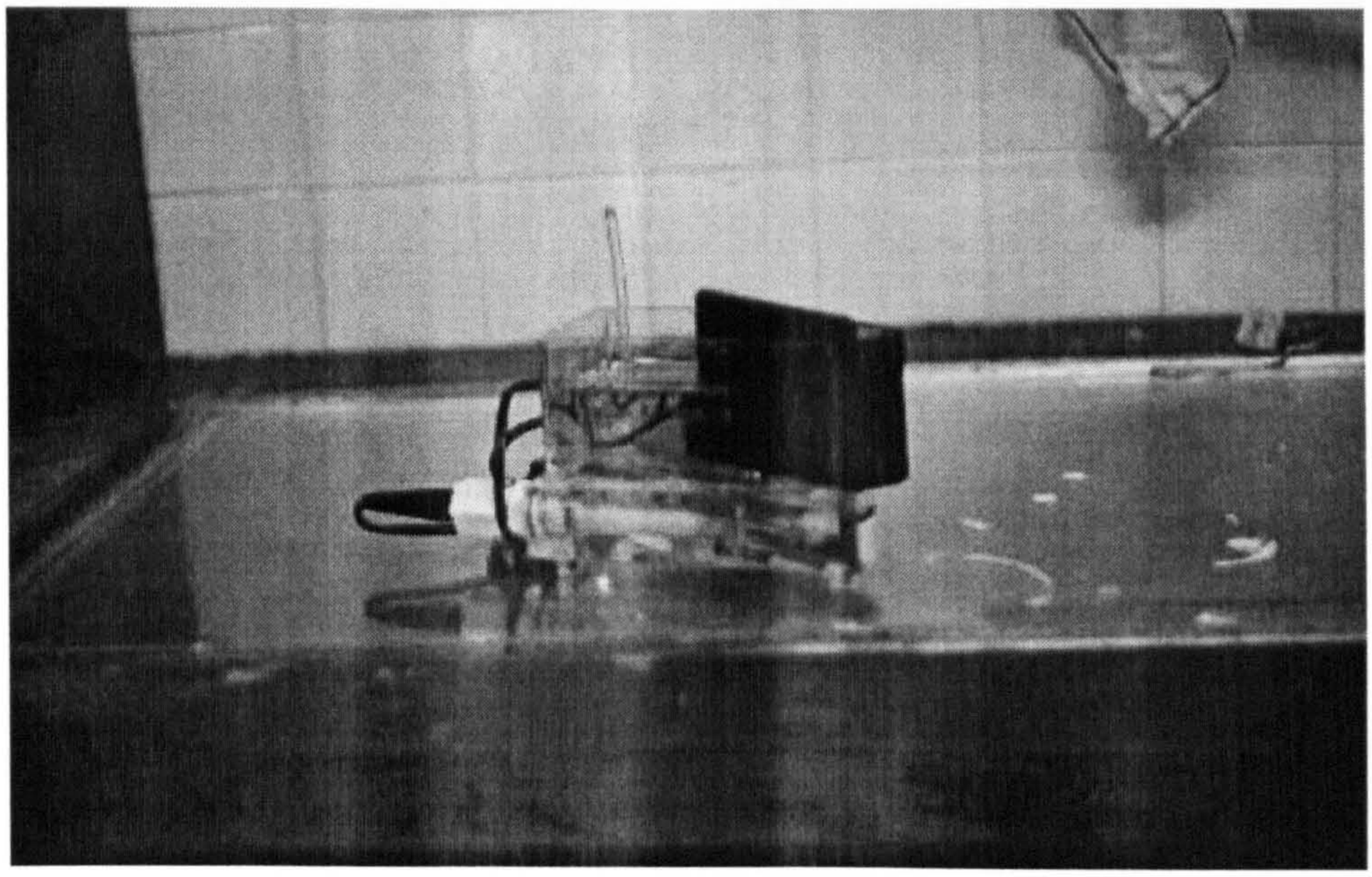

Fig. A3.8 : Hull cell : Kocovr 7CA-267

Appendix 3.1 (Fig. A3.9, Fig. 3.10)

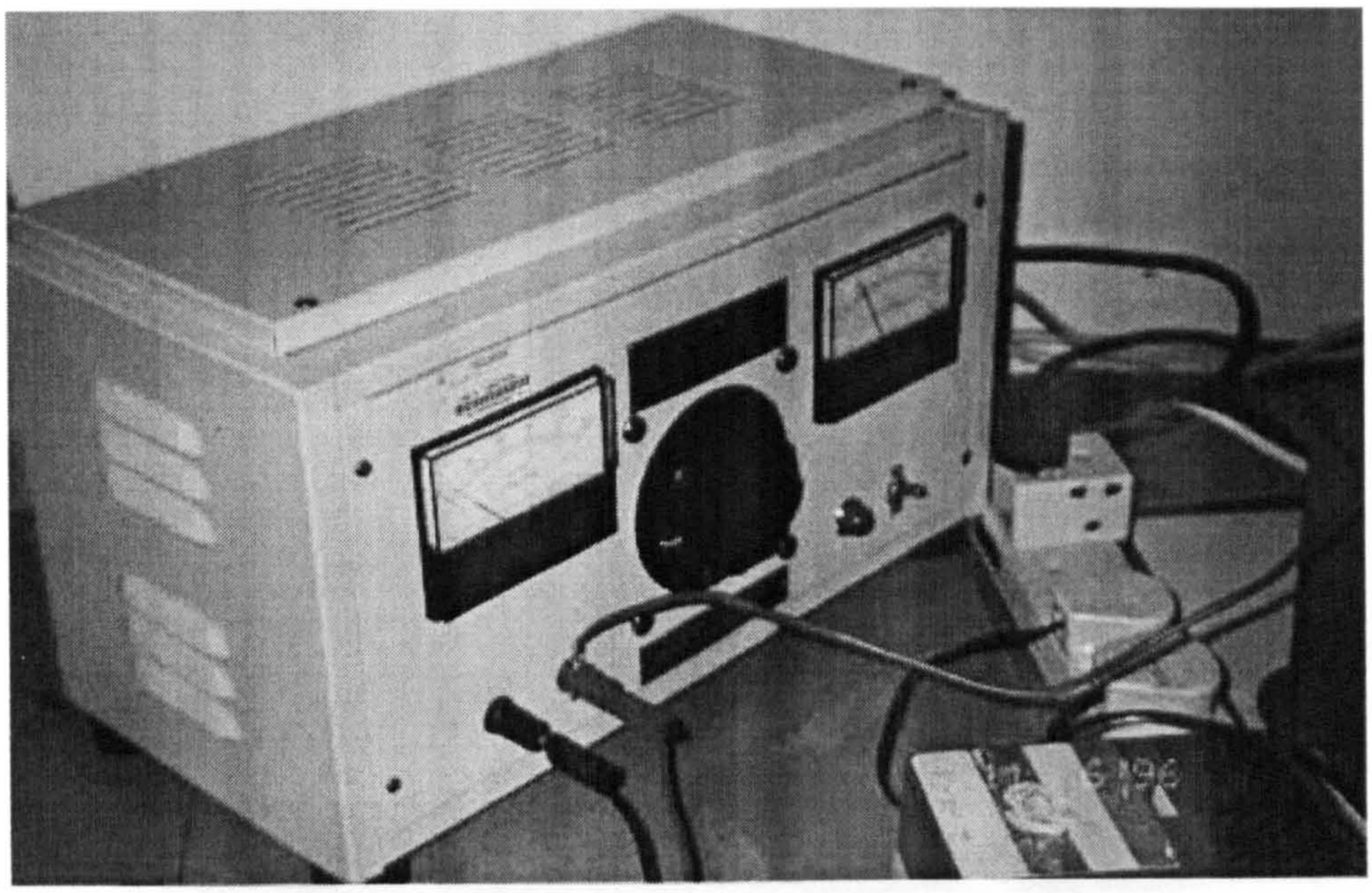

Fig. A3.9 : Power supply : Kocour Rectifier 15A

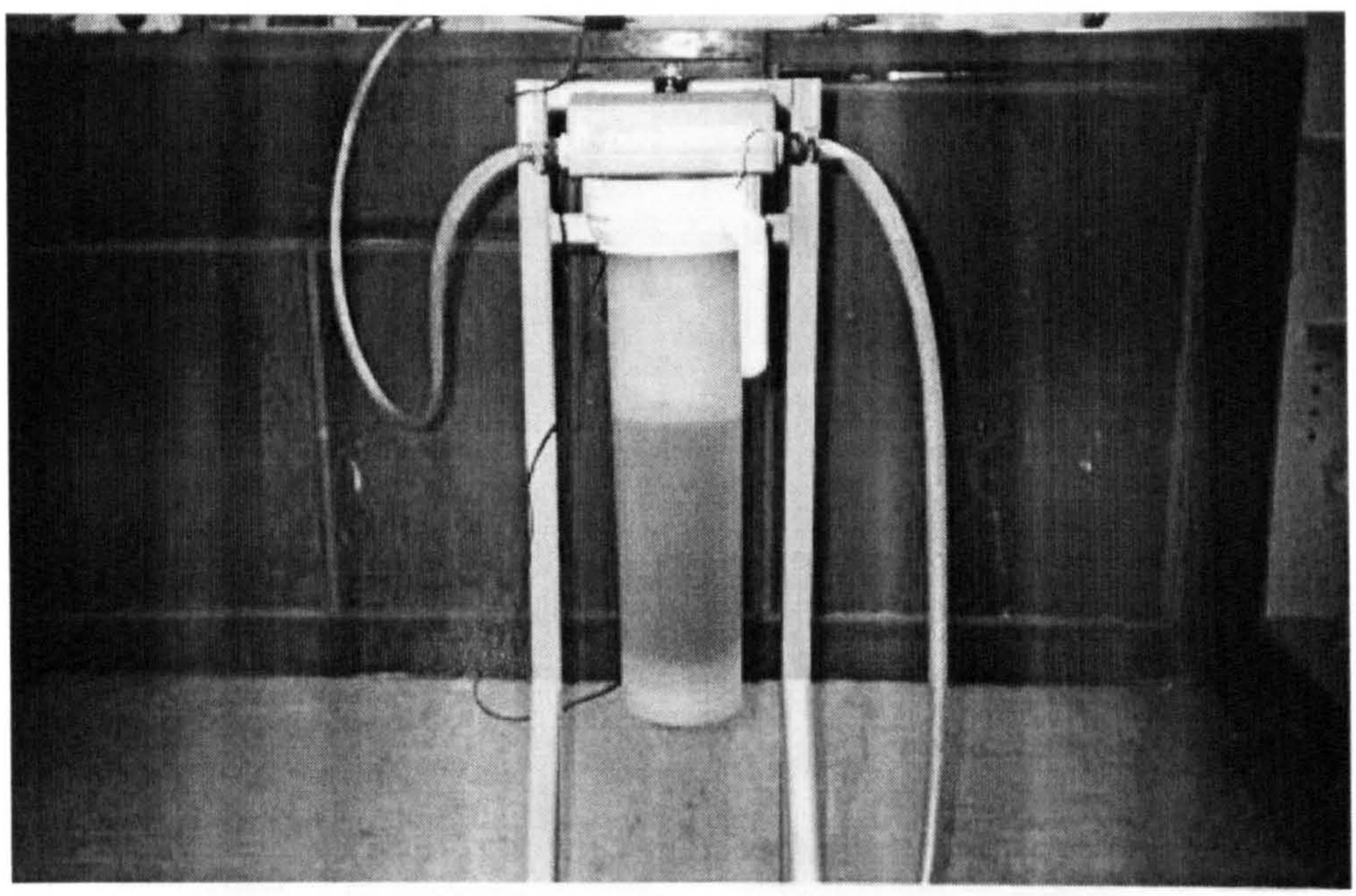

Fig. A3.10 : Water purification system : B-pure D4511

Appendix 3.1 (Fig. A3.11, Fig. A3.12)

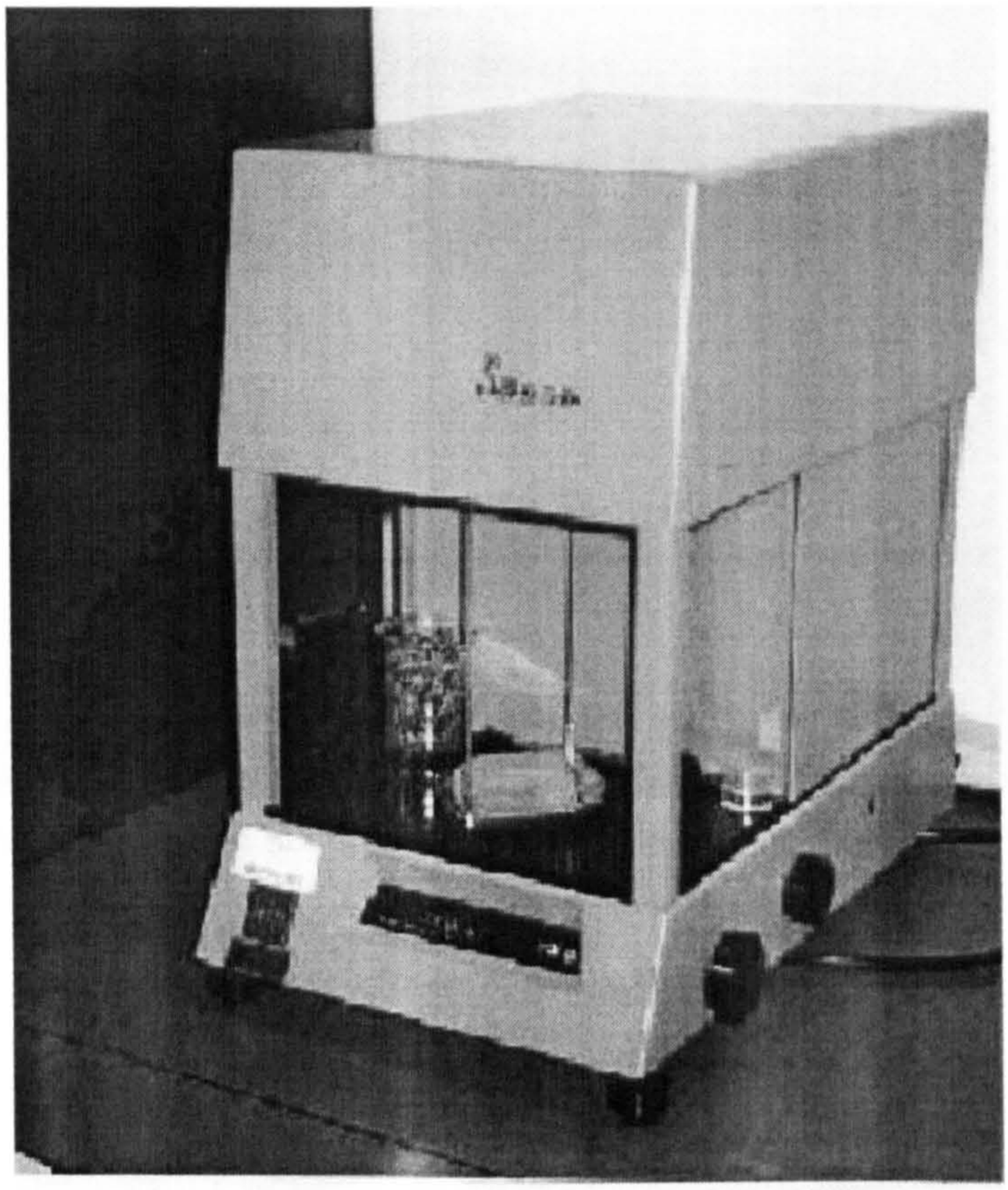

Fig. A3.11 : Analytical balance : BOSCH S2000

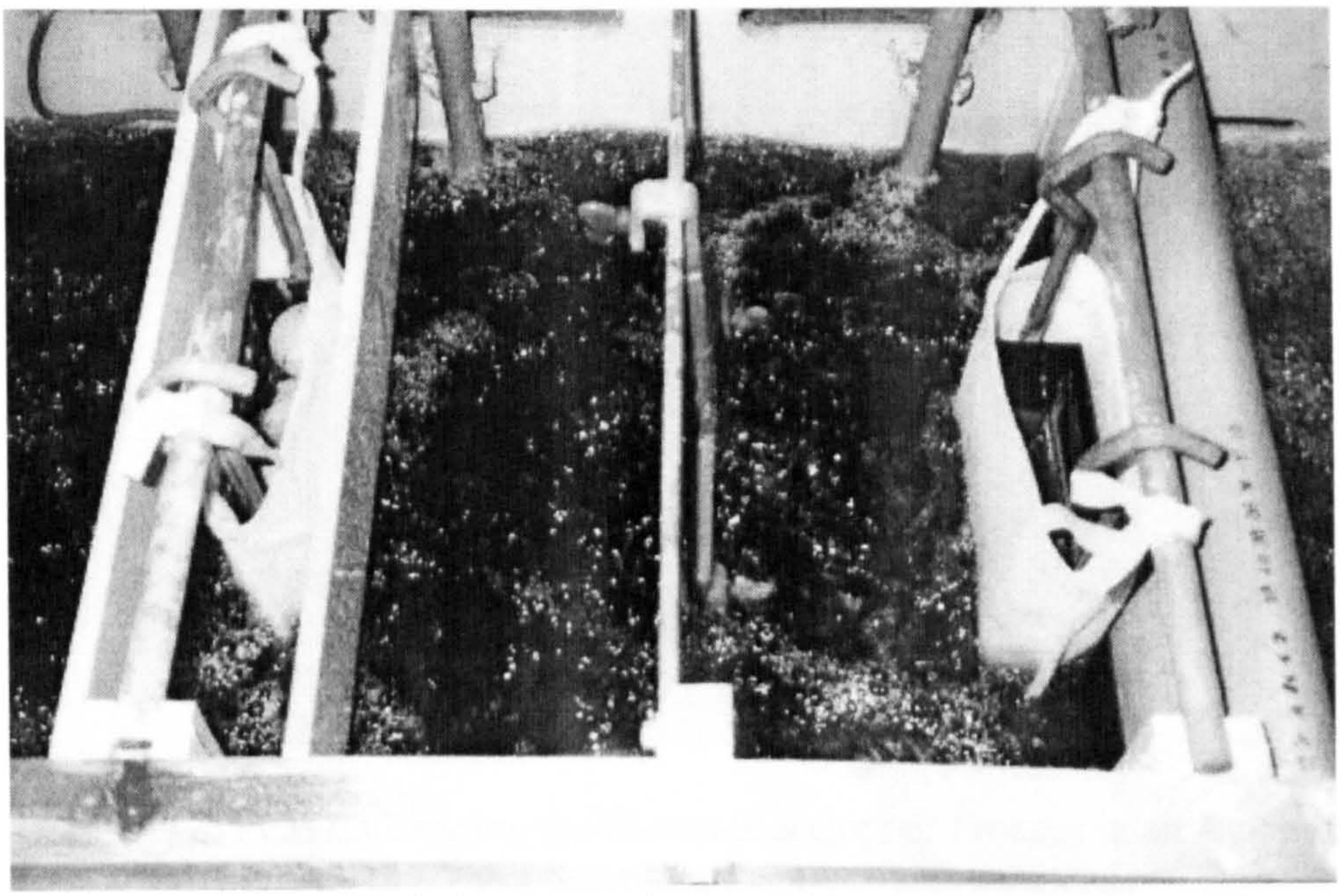

Fig. A3.12 : A PCB being Plated in the Agitated 200 litre Plating Bath

Appendix 3.1 (Fig. 3.13 (a), (b))

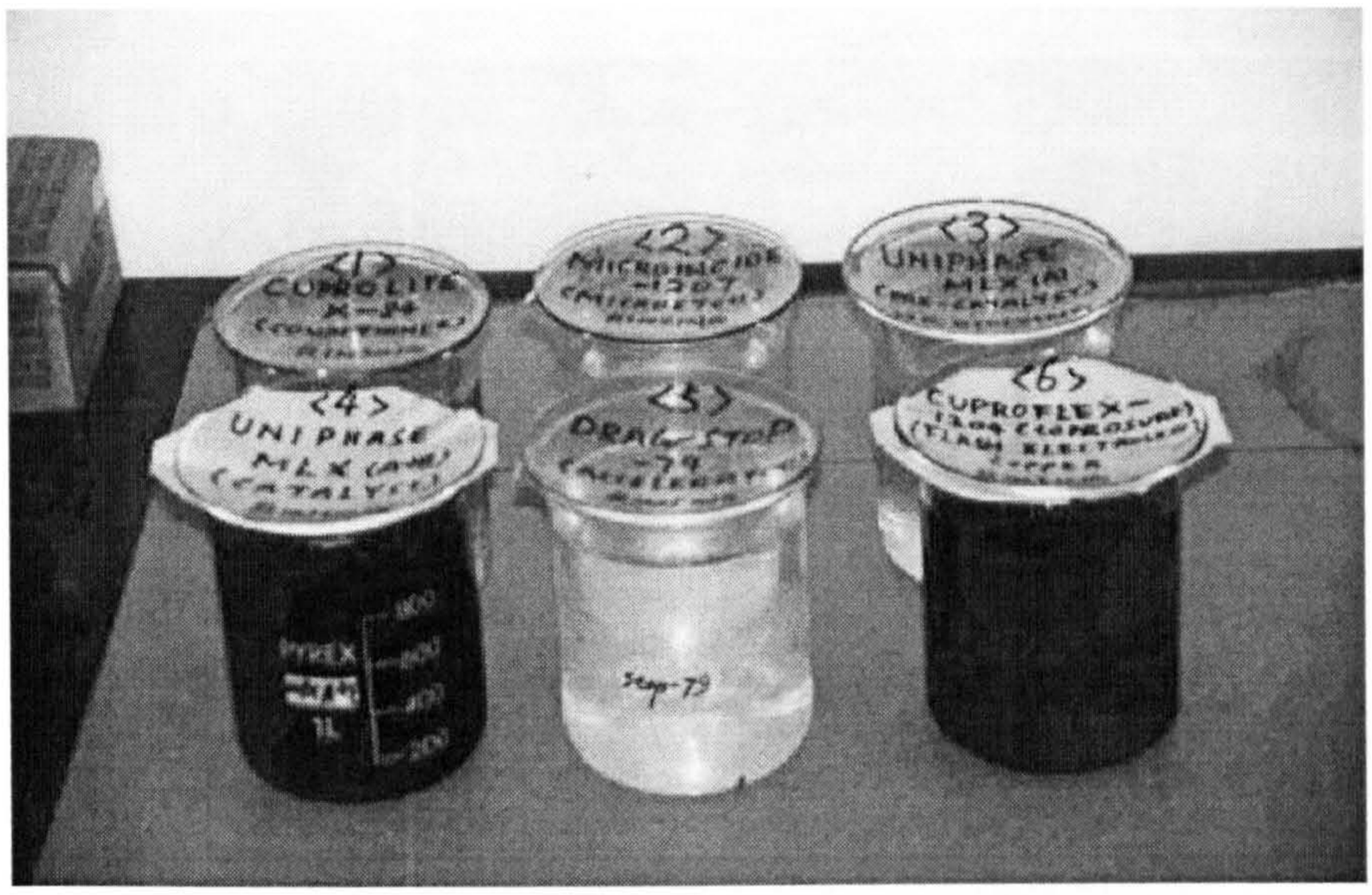

Fig. A3.13(a) : The Set of Six Electroless Copper Plating Solutions

Fig. A3.13(b) : A PCB undergoing the Electroless Copper Process in an Agitated bath
Fig. A3.13 : The Electroless Copper Plating Process

Appendix 3.1 (Fig. A3.14, Fig. A3.15)

Fig. A3.14 : CNC drilling machine : Excellon EX-110

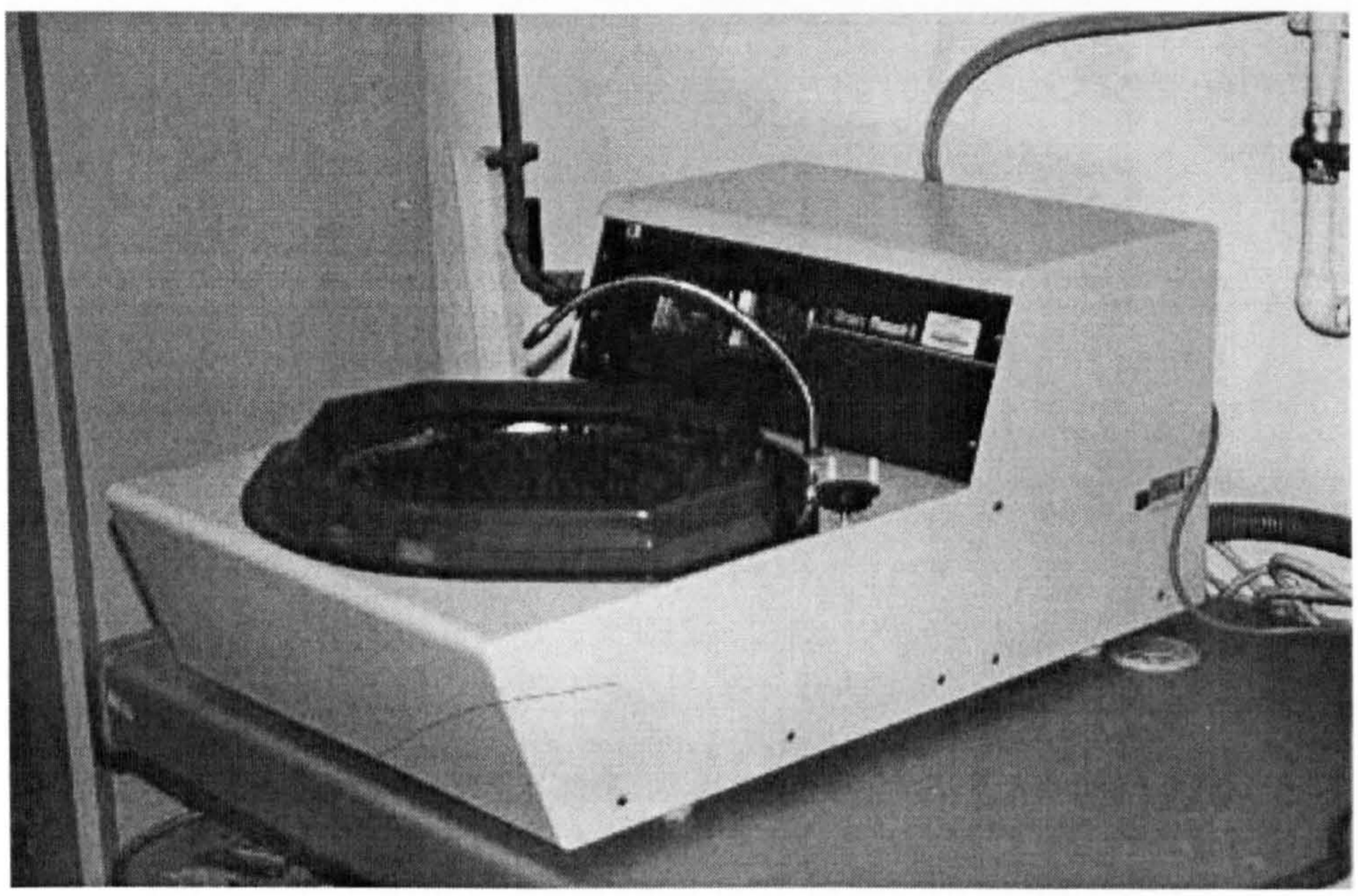

Fig. A3.15 : Struer Dap-V polishing machine

Appendix 3.1 (Fig. A3.16(a), (b))

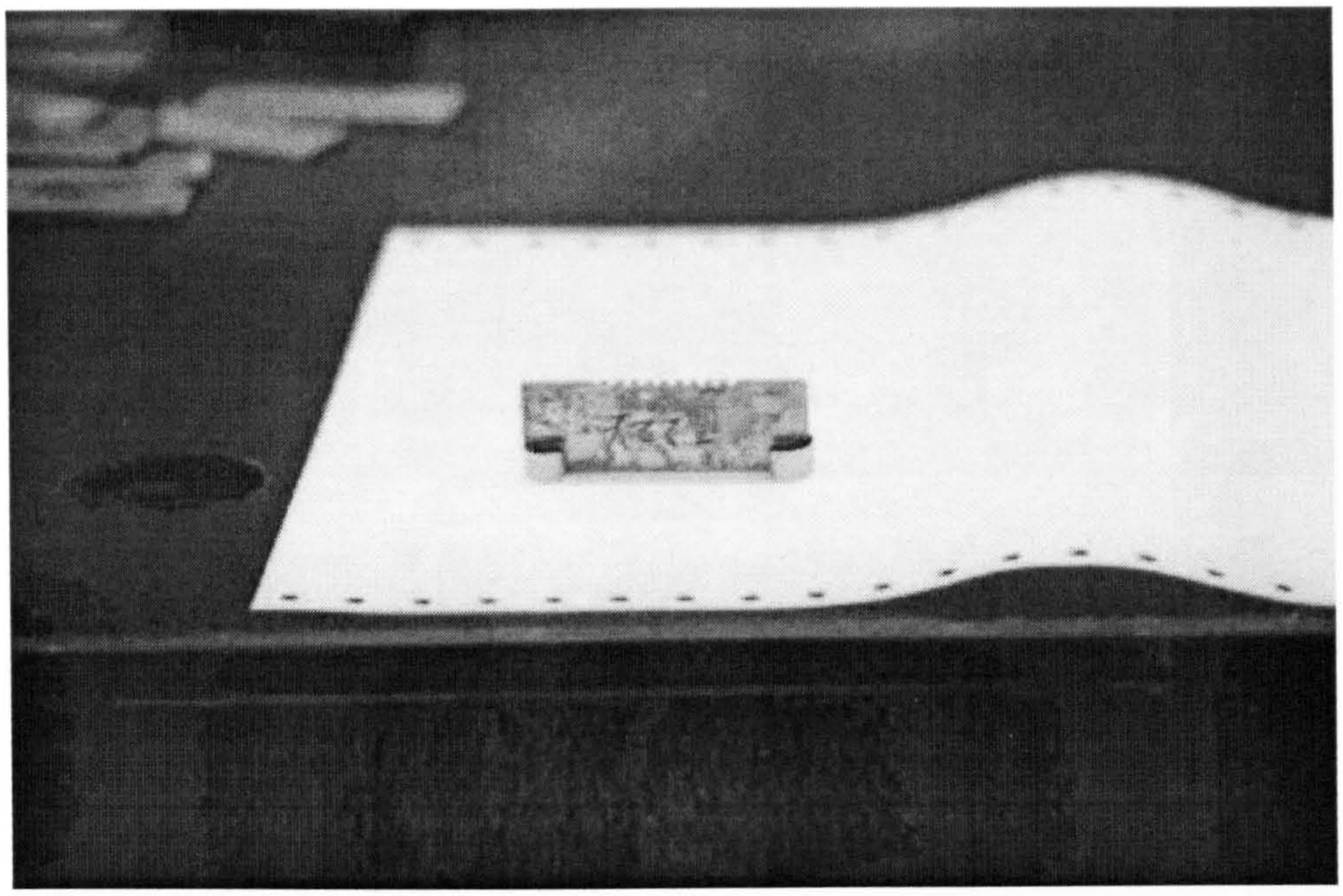

(a) A PCB with Sectioned PTHs supported by Rounded Leaf Springs

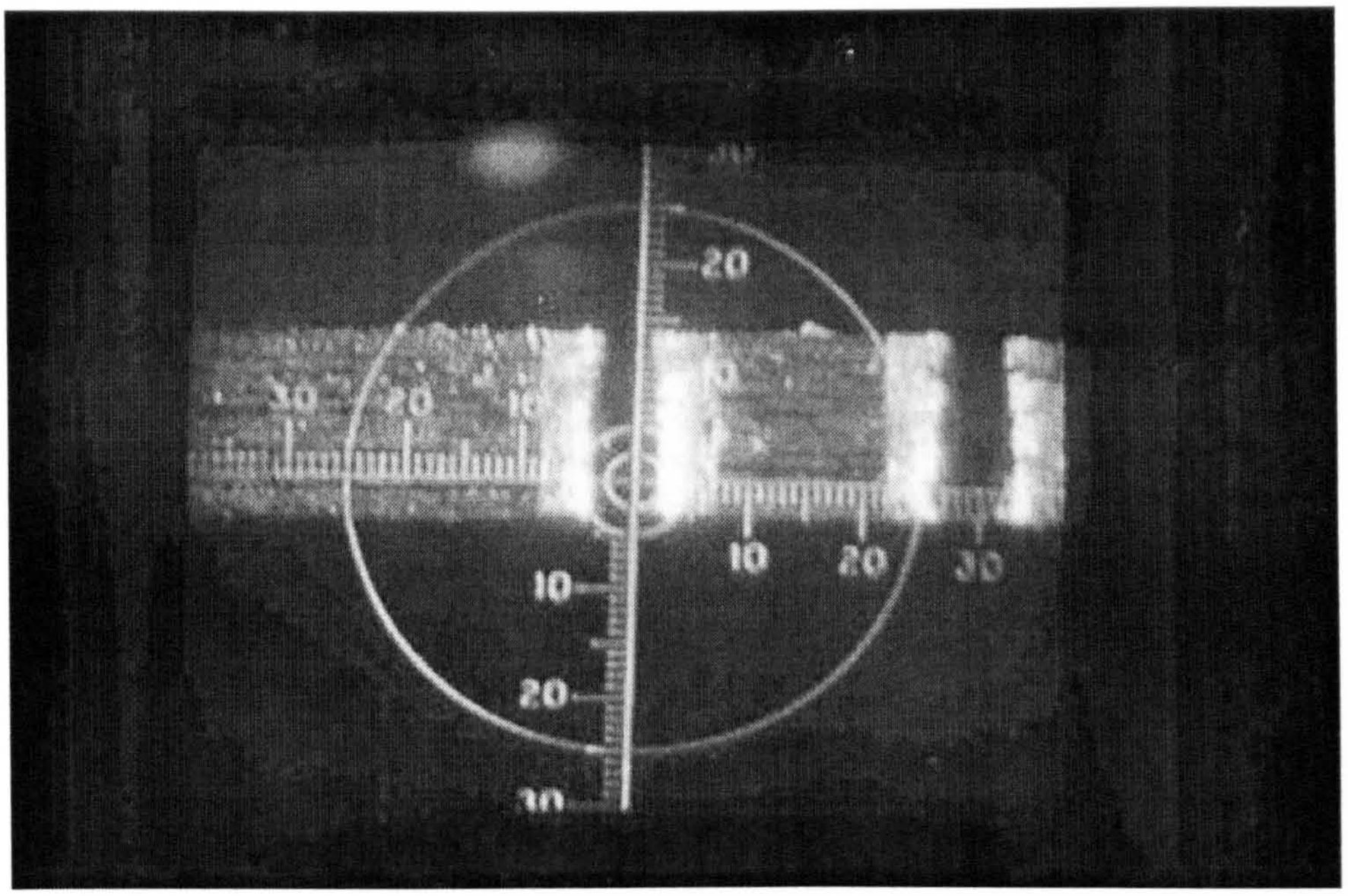

(b) Measurement of a Through-hole as shown in the Screen of the X-ray Thickness Gauge

Fig. A3.16 : Measurement of Deposit Thickness with X-ray Coating Thickness Gauge

Appendix 3.1 (Fig. A3.17, Fig. A3.18)

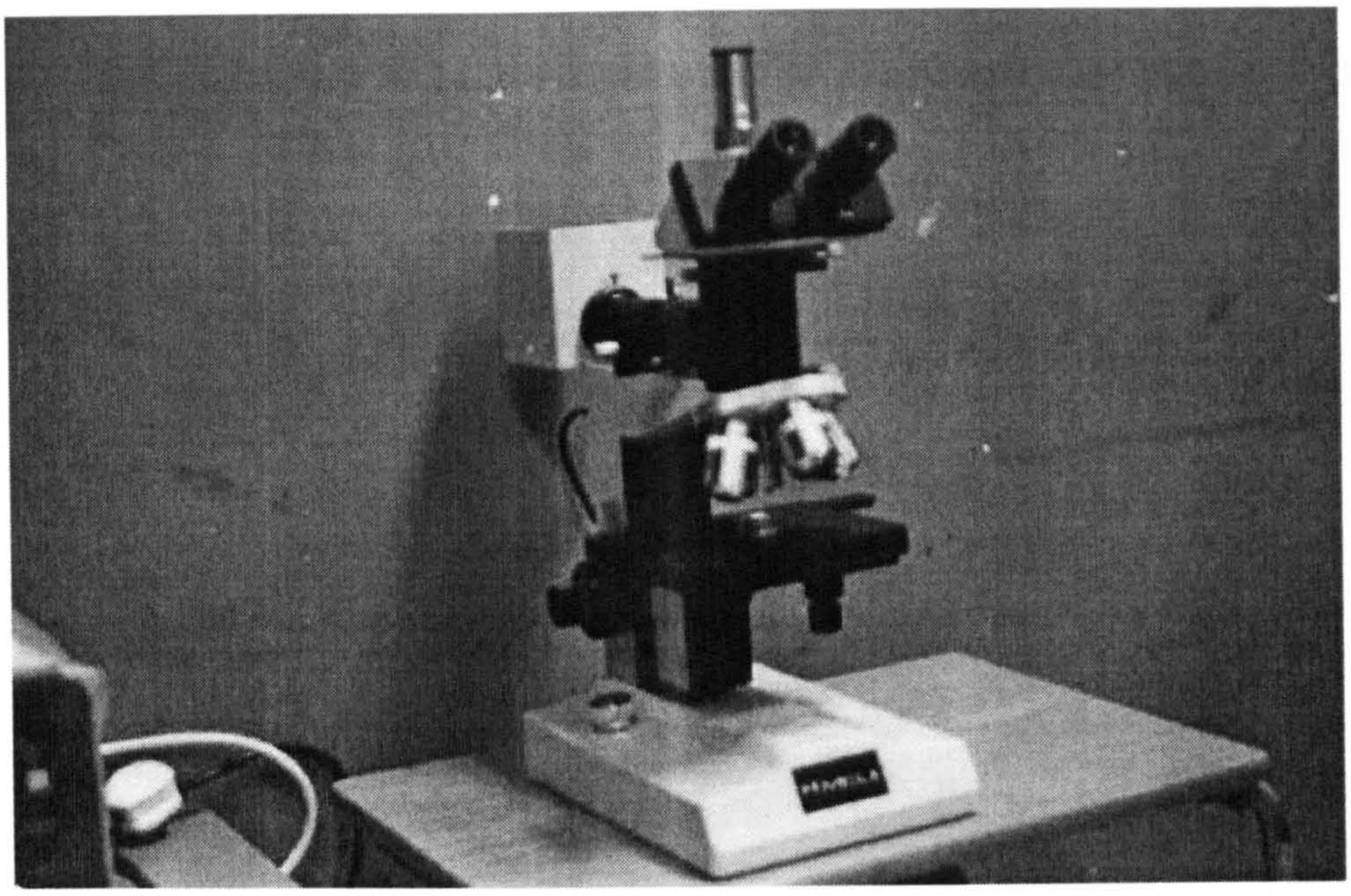

Fig. A3.17 : MEIJI Microscope

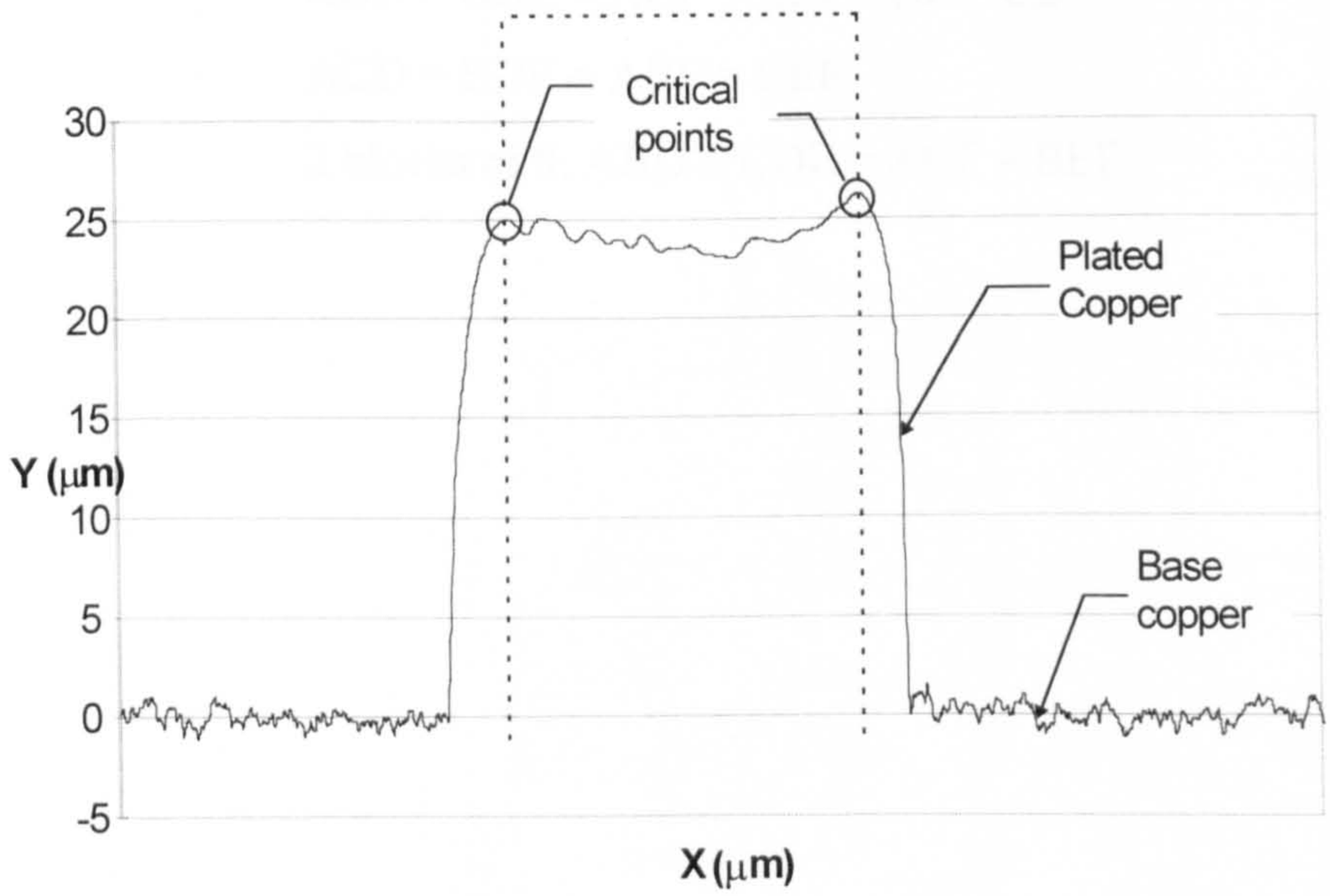

Fig. A3.18 : Cross-sectional Profile of the Plated Copper obtained by the Roughness Measurement Machine

Appendix 4.1

Alias Structure of the 2_{IV}^{6-2} Fractional Factorial Design used in the Screening Experiments of Uniform Pattern Plating

2_{IV}^{6-2} ¼ , ¼ fraction of 6 factors in 16 runs

Design Generators

E = ABC F = BCD

Defining relation: I = ABCE = BCDF = ADEF

Aliases

A = BCE = DEF	AB = CE
B = ACE = CDF	AC = BE
C = ABE = BDF	AD = EF
D = BCF = AEF	AE = BC = DF
E = ABC = ADF	AF = DE
F = BCD = ADE	BD = CF
ABD = CDE = ACF = BEF	BF = CD
ACD = BDE = ABF = CEF	

2 blocks of 8: ABD = CDE = ACF = BEF

Appendix 4.2

Raw Data of the Screening Runs of the Hull Cell Experiment
Uniform Pattern Plating Experiment

Run Order	Copper Plating Thickness (μm)								Mean Thickness (μm)	Standard Deviation (μm)
11	45	45	45	50	45	40	42	40	44	3.295018
10	30	40	40	40	40	45	40	45	40	4.6291
16	35	30	38	30	35	32	32	35	33.375	2.825269
1	32	32	32	38	40	40	40	40	36.75	3.991061
14	55	60	65	68	45	62	60	58	59.125	6.978283
9	40	50	50	52	55	50	50	52	49.875	4.35685
15	28	30	32	30	38	35	35	32	32.5	3.295018
2	25	30	35	30	32	35	40	38	33.125	4.853202
4	80	90	90	100	95	85	102	100	92.75	7.869471
8	90	100	90	100	105	105	110	110	101.25	7.905694
13	28	30	35	40	38	40	35	35	35.125	4.35685
7	25	30	30	30	35	38	35	30	31.625	4.10357
6	65	70	72	70	78	72	70	80	72.125	4.793969
3	50	68	70	75	60	75	55	52	63.125	10.17613
12	60	70	60	60	65	60	60	68	62.875	4.189698
5	50	55	62	70	68	70	60	58	61.625	7.327785

Appendix 4.3
Raw Data of the Screening Runs of the Plating Bath Experiment, Uniform Pattern Plating

Width	Duration	Average Current Density	Electrode Separation	Board No.	Measuring Points 1	2	3	4	5	6	7	8	9
-1	-1	-1	-1	1a	40.382	40.698	45.128	45.367	45.399	45.872	35.298	35.733	35.678
-1	-1	-1	-1	1b	48.015	41.856	25.693	45.437	35.198	45.491	41.897	39.324	26.724
1	-1	-1	-1	2a	51.303	39.876	44.111	48.339	32.804	32.219	39.706	44.754	34.672
1	-1	-1	-1	2b	32.833	44.779	46.389	46.118	41.497	49.365	32.409	40.232	39.727
-1	1	-1	-1	3a	50.841	49.136	59.691	45.388	46.472	48.706	47.822	60.925	53.014
-1	1	-1	-1	3b	48.166	57.629	60.177	48.118	46.437	61.825	62.696	60.382	50.803
1	1	-1	-1	4a	53.254	47.944	52.837	54.232	54.022	35.075	52.676	49.229	45.143
1	1	-1	-1	4b	41.985	53.63	48.321	42.461	51.614	49.336	47.249	54.126	45.944
-1	-1	1	-1	5a	54.417	54.798	58.024	47.444	50.309	42.511	52.163	61.927	66.003
-1	-1	1	-1	5b	45.398	45.999	58.623	52.558	45.521	61.998	49.138	49.883	58.563
1	-1	1	-1	6a	48.267	45.212	59.179	45.084	59.7	45.243	45.809	50.126	44.995
1	-1	1	-1	6b	39.282	36.91	45.687	56.233	42.182	47.002	41.326	52.733	63.073
-1	1	1	-1	7a	85.625	90.684	93.334	102.951	87.879	91.755	86.061	102.695	103.459
-1	1	1	-1	7b	87.668	94.203	100.953	96.756	86.122	102.361	96.424	85.739	86.649
1	1	1	-1	8a	95.165	83.206	101.269	87.14	86.076	96.912	104.15	87.979	84.382
1	1	1	-1	8b	81.765	85.545	83.787	91.606	83.648	93.217	83.31	94.984	96.662
-1	-1	-1	1	9a	37.508	39.736	30.109	27.076	28.688	37.952	35.099	37.353	32.94
-1	-1	-1	1	9b	27.954	31.306	34.633	41.473	42.019	41.876	29.818	44.184	30.816
1	-1	-1	1	10a	25.347	27.541	40.568	40.465	38.775	34.338	42.12	25.561	22.99
1	-1	-1	1	10b	31.21	40.764	38.283	44.06	35.616	29.865	35.033	36.642	33.417
-1	1	-1	1	11a	34.235	33.136	35.327	49.958	37.936	30.654	49.991	48.603	53.199
-1	1	-1	1	11b	38.543	45.745	44.684	45.276	41.257	50.519	39.289	41.084	37.476
1	1	-1	1	12a	25.734	31.604	30.716	46.077	36.527	42.165	48.038	42.342	52.112
1	1	-1	1	12b	37.81	36.131	39.704	41.646	43.21	33.479	43.129	36.774	30.373
-1	-1	1	1	13a	43.267	40.29	42.716	47.557	41.578	39.994	45.311	42.515	45.473
-1	-1	1	1	13b	39.322	43.782	47.374	38.433	42.057	45.319	40.388	51.4	44.574
1	-1	1	1	14a	38.237	41.619	37.637	39.712	36.745	38.951	35.433	30.048	37.282
1	-1	1	1	14b	43.903	42.299	36.986	38.675	44.654	41.367	47.589	43.359	44.981
-1	1	1	1	15a	53.6	62.329	49.885	54.994	54.765	53.076	48.3	46.553	50.899
-1	1	1	1	15b	54.385	59.444	57.518	55.592	55.378	60.296	53.565	59.065	45.685
1	1	1	1	16a	44.914	53.82	50.389	54.496	55.021	62.592	46.905	57.411	46.08
1	1	1	1	16b	55.225	63.846	55.401	56.432	59.437	64.077	56.577	58.679	51.792

All thickness and Standard Deviation Data in μm

Appendix 4.3
Raw Data of the Screening Runs of the Plating Bath Experiment, Uniform Pattern Plating

Measuring Points

10	11	12	13	14	15	16	17	18	19	20	21	22	23
38.921	35.311	35.085	48.122	48.679	42.192	48.083	42.925	45.367	45.217	48.358	48.219	42.351	40.087
45.267	49.397	46.528	47.736	32.726	58.372	40.261	34.107	33.172	40.271	46.399	31.634	40.419	34.037
37.846	35.072	41.014	35.921	52.461	41.556	41.507	34.489	49.32	52.121	35.002	54.518	52.903	47.318
41.392	43.389	43.556	32.411	32.572	32.663	31.614	45.754	41.714	46.583	31.49	39.905	38.897	40.683
44.908	53.857	48.102	57.228	50.54	52.751	58.934	52.925	62.107	66.14	62.513	56.399	63.803	51.268
52.524	50.113	46.156	49.064	51.038	57.059	61.062	62.043	61.668	64.075	62.488	58.431	60.726	56.553
41.553	49.42	51.883	63.239	46.818	50.32	57.713	45.669	56.118	64.24	54.816	52.52	55.454	58.43
56.681	51.548	46.379	51.81	47.364	57.382	60.126	57.459	50.972	58.121	50.315	62.463	60.322	59.539
63.198	42.178	57.8326	48.946	42.162	43.565	60.471	66.852	62.788	55.237	58.18	66.06	58.48	52.781
63.711	46.052	59.049	56.635	54.258	60.935	50.252	45.511	50.791	54.006	50.121	51.418	61.106	46.358
46.447	55.533	47.321	55.873	59.013	58.64	64.588	49.59	47.979	47.794	53.939	60.591	51.941	49.724
60.129	63.289	46.454	43.179	54.99	42.706	57.336	59.409	46.689	43.86	54.38	55.972	54.481	50.241
103.892	103.816	106.062	88.102	97.401	103.937	96.429	103.139	99.382	104.576	102.434	96.622	100.548	101.654
90.807	84.742	98.858	92.21	92.374	92.04	84.834	94.404	93.202	98.76	101.716	96.729	95.752	98.684
99.025	97.655	91.936	98.862	102.066	84.585	83.615	88.69	84.808	84.106	102.575	99.669	84.073	82.362
86.903	98.615	96.489	86.274	94.261	91.648	94.505	94.085	88.936	90.005	91.632	93.342	92.58	85.716
32.517	30.686	41.327	28.067	39.347	37.539	29.668	36.091	23.55	44.647	42.463	39.456	39.019	40.873
34.332	52.237	42.688	39.803	36.308	34.558	27.735	36.511	30.986	33.143	27.564	30.483	34.307	30.128
32.56	35.826	24.489	29.345	31.489	40.984	32.149	42.675	44.027	35.264	36.921	35.468	42.052	40.792
40.09	44.212	44.311	34.061	36.177	34.352	31.259	36.285	40.239	33.417	43.555	33.457	32.393	32.316
51.812	31.919	39.807	48.873	49.642	50.782	32.597	46.911	42.196	34.553	46.506	36.541	48.604	50.162
40.362	38.991	43.246	37.152	40.067	37.945	44.1	36.369	36.07	45.928	40.26	37.595	39.615	41.252
38.223	45.425	50.573	35.189	32.719	42.845	45.373	46.972	36.485	39.473	47.701	50.078	36.917	37.82
30.08	32.889	34.739	42.083	33.6	43.823	43.551	44.191	43.973	45.575	39.053	44.22	40.123	44.8
49.894	53.545	51.795	47.329	47.923	44.766	34.812	49.233	46.866	50.313	48.666	44.105	49.578	52.987
50.381	46.076	46.448	51.139	46.649	45.116	50.089	51.318	51.071	48.351	48.259	46.451	54.973	45.822
42.724	49.024	41.749	49.147	47.893	49.815	42.628	48.274	46.716	50.588	44.179	46.01	45.393	49.434
43.54	40.07	43.211	43.16	45.033	38.92	41.308	44.529	40.126	49.235	48.686	47.524	42.367	42.497
53.807	51.874	52.947	46.086	62.153	52.672	50.892	52.891	55.065	52.947	58.245	51.47	60.761	58.752
57.134	54.802	54.054	48.024	58.037	54.096	47.454	53.929	55.852	58.37	58.486	55.514	48.185	55.125
52.734	54.156	47.877	55.688	51.337	58.108	51.015	49.444	56.237	52.583	47.998	50.984	57.191	54.334
55.959	59.178	56.844	56.791	64.062	62.175	61.196	57.2	69.534	64.697	63.955	58.804	61.271	56.374

All thickness and Standard Deviation Data in μm

Appendix 4.3
Raw Data of the Screening Runs of the Plating Bath Experiment, Uniform Pattern Plating

24	Average Thickness	Overall me	cell mean	Standard Deviation	Mean SD	Cell Mean SD	Faraday	Bd no.
48.267	42.54226			4.788463				1a
43.491	40.43309	41.48767		7.73813	6.263297			1b
38.376	42.55791			7.133482				2a
35.864	39.82487	41.19139	41.33953	5.637477	6.38548	6.324388	23.80832	2b
63.033	54.06391			6.429545				3a
51.76	56.05361	55.05876		5.989996	6.20977			3b
60.39	51.85239			6.631702				4a
57.851	52.3977	52.12504	53.5919	5.824712	6.228207	6.218989	35.71249	4b
52.674	55.05768			7.744579				5a
51.109	52.95148	54.00458		5.904265	6.824422			5b
49.413	51.85165			5.951938				6a
50.449	50.32796	51.0898	52.54719	7.653724	6.802831	6.813626	33.33165	6b
100.559	97.93204			6.520278				7a
98.007	93.56465	95.74835		5.514474	6.017376			7b
84.694	91.75243			7.606268				8a
93.476	90.4137	91.08307	93.41571	4.828344	6.217306	6.117341	49.99748	8b
27.281	35.29178			5.71618				9a
31.132	35.42878	35.36028		6.256197	5.986188			9b
41.249	34.85852			6.527831				10a
27.989	36.56583	35.71217	35.53623	4.763196	5.645513	5.815851	23.80832	10b
33.048	42.78017			7.844838				11a
36.181	40.99239	41.88628		3.711849	5.778343			11b
39.895	40.91774			6.935034				12a
35.043	39.34591	40.13183	41.00905	4.896915	5.915974	5.847159	35.71249	12b
50.493	46.10926			4.567854				13a
46.216	46.73009	46.41967		4.088494	4.328174			13b
53.759	43.01035			5.864876				14a
37.971	43.21822	43.11428	44.76698	3.280369	4.572622	4.450398	33.33165	14b
58.045	53.69404			4.397746				15a
51.169	54.78217	54.23811		3.983785	4.190766			15b
51.214	52.66583			4.24544				16a
60.198	59.54374	56.10478	55.17145	4.05091	4.148175	4.16947	49.99748	16b

Board no.	Average Thickness	Standard Deviation
1a	42.54226	4.788463
2a	42.55791	7.133482
3a	54.06391	6.429545
4a	51.85239	6.631702
5a	55.05768	7.744579
6a	51.85165	5.951938
7a	97.93204	6.520278
8a	91.75243	7.606268
9a	35.29178	5.71618
10a	34.85852	6.527831
11a	42.78017	7.844838
12a	40.91774	6.935034
13a	46.10926	4.567854
14a	43.01035	5.864876
15a	53.69404	4.397746
16a	52.66583	4.24544
1b	40.43309	7.73813
2b	39.82487	5.637477
3b	56.05361	5.989996
4b	52.3977	5.824712
5b	52.95148	5.904265
6b	50.32796	7.653724
7b	93.56465	5.514474
8b	90.4137	4.828344
9b	35.42878	6.256197
10b	36.56583	4.763196
11b	40.99239	3.711849
12b	39.34591	4.896915
13b	46.73009	4.088494
14b	43.21822	3.280369
15b	54.78217	3.983785
16b	59.54374	4.05091

All thickness and Standard Deviation Data in μm

Appendix 4.4
Normal Probability Plot of the Residuals of the Plating Bath Experiment, Uniform Pattern Plating

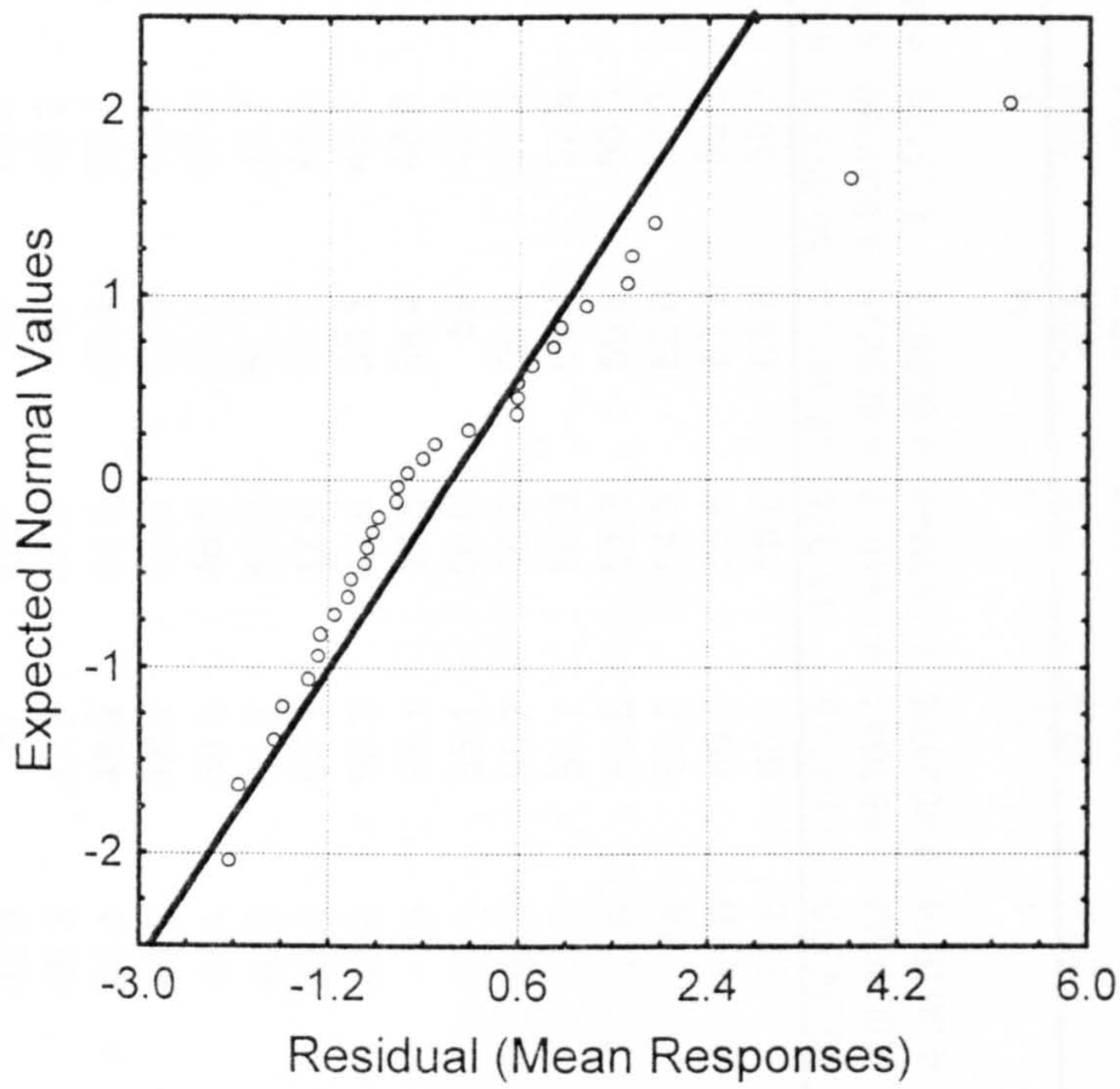

Normal Probability Plot of Residuals for Mean Responses

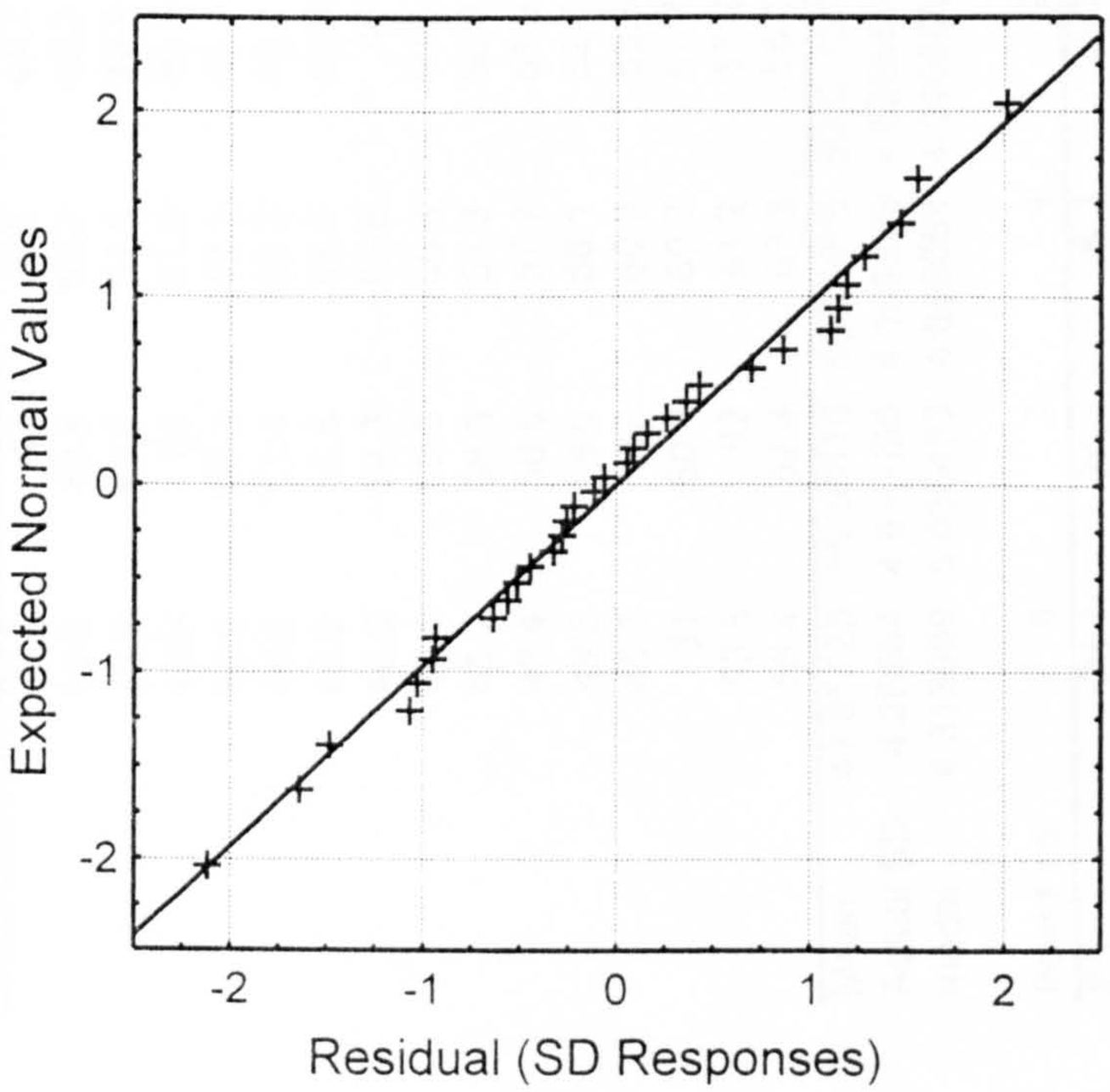

Normal Probability Plot of Residuals for SD Responses

Appendix 4.5

Raw Data of the Verification Run
Second Order Model, Uniform Pattern Plating Experiment

Board no.	1	2	3	4	5	6	7	8	9	10	11	12
	42.7	49	49.8	44.7	46.7	42.9	47	40.7	49	45.9	43.7	40.9
	43.2	49.8	50.7	43.3	47.6	45.3	47.3	42.9	49	46.2	43.8	41.3
	43.3	49.8	51.8	43.4	47.6	45.4	48.4	44.8	50.4	46.7	44.8	43.2
	43.9	50	51.9	46.3	48.1	46.3	48.4	46.4	52.8	46.9	45.5	43.3
	44.5	50.3	52.1	46.4	48.3	46.4	50.2	46.5	55.2	47.5	46.1	43.8
	44.6	51.4	52.3	48.3	48.7	46.9	51.5	47.3	57.3	47.7	46.6	45
	46.8	52.6	55.5	48.6	49.6	47.4	52.1	47.4	57.7	48.2	47	45.5
	46.9	54.3	55.6	49	50.5	48.6	52.2	47.4	58.1	48.7	47.3	46.2
	49.1	55.3	56.4	50.9	51.2	49	53.1	49.5	58.4	48.8	47.3	48.1
	49.2	58.3	57.3	50.6	51.5	49.1	55.1	50.9	59	49.3	48.5	48.2
	49.4	58.5	57.7	51.9	52.2	50.9	55.2	50.7	59.9	51.3	48.7	50
	49.5	58.6	58.1	52.5	54.7	50.9	57.7	50.9	60.4	52.9	50.8	50.3
	49.7	60	60.3	53.6	55.7	51.6	59.6	51.3	60.8	56.3	51.9	51.2
	51	60.4	60.7	57.7	57	54	60.2	54.3	62.6	57.3	53.1	53.6
	53.5	62	61.2	57.2	62.6	55.6	60.5	55.6	63.7	58.2	56.2	55.1
	58.4	62.4	63.3	56.1	63 5	57.6	60.6	58.6	63.8	59.2	56.6	55.4
Mean	47.85625	55.16875	55.91875	50.03125	52.21875	49.24375	53.69375	49.075	57.38125	50.69375	48.61875	47.56875
Actual SD	4.26864	4.830696	4.165288	4.628566	5.198489	4.004992	4.867644	4.648512	4.863225	4.600068	4.041818	4.688243
model	4.318999	5.036493	4.856064	4.340505	4.850353	4.361914	4.402175	4.783944	4.900978	4.25125	4.461166	4.725081

Board no.	8	7	4	2	12	1	10	3	14	6	16	5
ES	26.7	26.7	26.7	26.7	27.9	27.9	27.9	27.9	28.6	28.6	28.6	28.6
ACD	32.3	34.4	38.2	43.0	32.3	34.4	38.2	43.0	32.3	34.4	38.2	43.0
Actual SD	4.648512	4.867644	4.628566	4.830696	4.688243	4.26864	4.600068	4.165288	4.40651	4.004992	4.672967	5.198489
model	4.783944	4.402175	4.340505	5.036493	4.725081	4.318999	4.25125	4.856064	4.780153	4.361914	4.291126	4.850353
% error	-0.02913	0.095625	0.062236	-0.0426	-0.00786	-0.0118	0.075829	-0.16584	-0.08479	-0.08912	0.081713	0.066969

ES : Electrode Separation (cm) ACD : Average Current Density (mA/cm^2)
All thickness and standard deviation data in μm

Appendix 4.5

Raw Data of the Verification Run
Second Order Model, Uniform Pattern Plating Experiment

13	14	15	16
43	41.7	42.5	46.2
43.1	41.3	43	45.8
43.2	45	43.1	47
45.1	45.7	43.7	47
45.8	46.5	43.7	47.5
45.9	46.6	43.8	48.8
46.2	47.5	44.5	49.9
46.4	48.2	44.8	51.5
47	49.3	45.9	52.8
47.3	49.6	46.2	52.3
47.8	50.1	46.6	54.5
49.5	51.2	52.8	55.1
50.4	52.4	53.9	56.1
52.5	54.1	55.1	57.2
54.5	55.1	55.3	58.9
57.7	56.5	56.1	59.9
47.8375	48.8	47.5625	51.90625
4.173068	4.40651	5.099526	4.672967
4.387339	4.780153	4.891561	4.291126

15	11	13	9
29.2	29.2	29.2	29.2
32.3	34.4	38.2	43.0
5.099526	4.041818	4.173068	4.863225
4.891561	4.461166	4.387339	4.900978
0.040781	-0.10375	-0.05135	-0.00776

ES : Electrode Separation (cm) ACD : Average Current Density (mA/cm^2)
All thickness and standard deviation data in μm

Appendix 4.6

Measurement Scheme and Typical Thickness Profile of the Nonuniform Pattern Plating Experiment

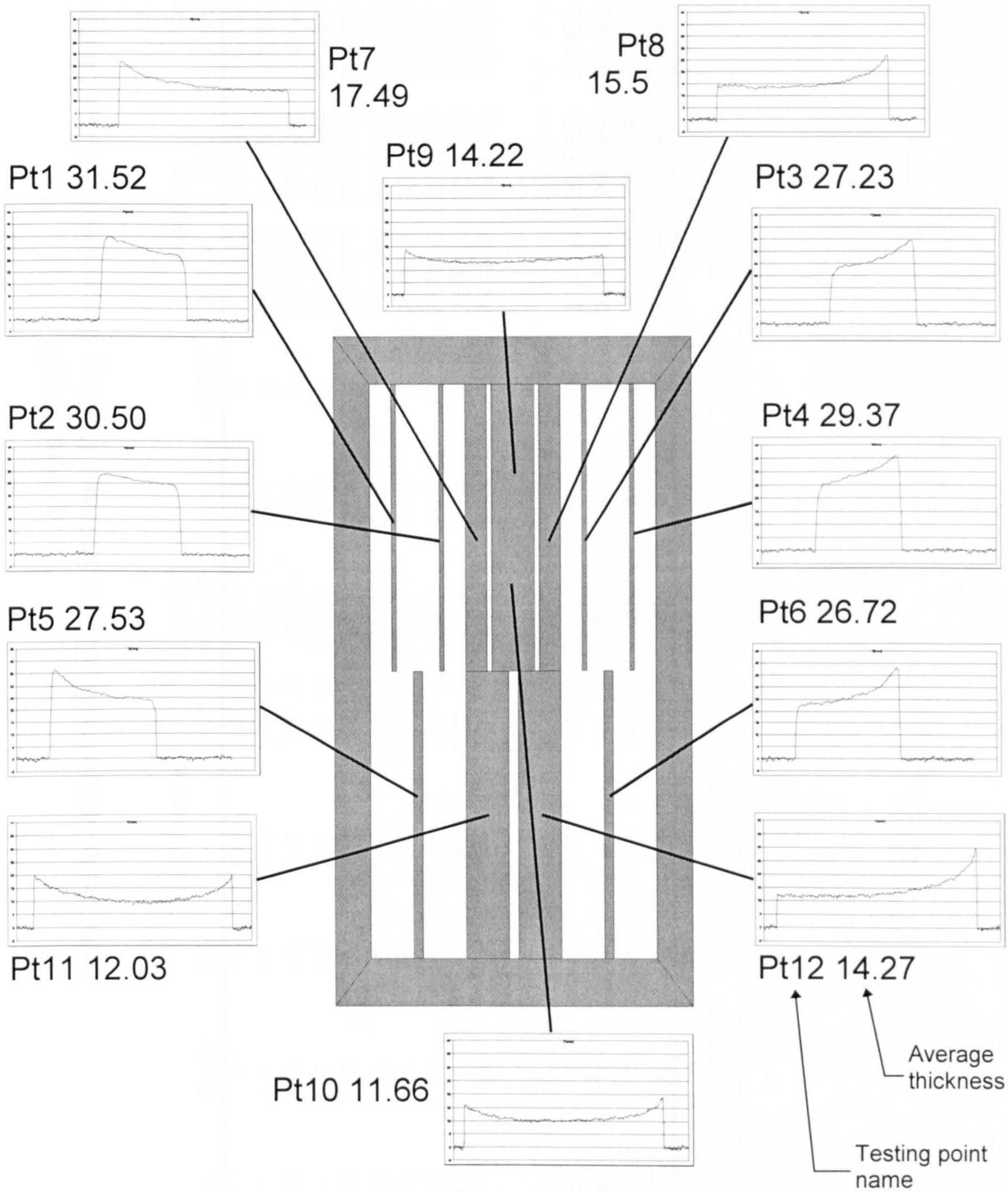

Appendix 4.7
Raw Data of the Nonuniform Pattern Plating Experiment, First-Order Model

		Coded Variable			CD (A/ft2)	ES		Weight (g)		Experimental results			
Board	Order	CD	L	AAD	mA/cm2	cm	AADR	Before	After	Difference	Ave. Thick		Efficiency
13	1	+1	+1	+1	40.9	25.4	9	29.1800	29.6599	0.4799	15.60	0.8616	86.16%
1	2	+1	+1	-1	40.9	25.4	2	29.0220	29.3675	0.3455	15.66	0.8649	86.49%
14	3	+1	-1	+1	40.9	15.2	9	29.1694	29.6670	0.4976	16.17	0.8934	89.34%
2	4	+1	-1	-1	40.9	15.2	2	29.2013	29.5470	0.3457	15.67	0.8654	86.54%
16	5	-1	+1	+1	30.1	25.4	9	28.8277	29.1756	0.3479	11.31	0.8477	84.77%
3	6	-1	+1	-1	30.1	25.4	2	29.0222	29.2725	0.2503	11.34	0.8504	85.04%
15	7	-1	-1	+1	30.1	15.2	9	28.9676	29.3190	0.3514	11.42	0.8562	85.62%
4	8	-1	-1	-1	30.1	15.2	2	28.7856	29.0317	0.2461	11.15	0.8361	83.61%
17	9	+1	+1	+1	40.9	25.4	9	29.3215	29.7986	0.4771	15.51	0.8566	85.66%
7	10	+1	+1	-1	40.9	25.4	2	29.1254	29.4800	0.3546	16.07	0.8877	88.77%
20	13	-1	+1	+1	28	10	9	29.4460	29.7892	0.3432	11.16	0.8362	83.62%
6	14	-1	+1	-1	28	10	2	29.1842	29.4384	0.2542	11.52	0.8636	86.36%
19	15	-1	-1	+1	28	6	9	28.8799	29.2309	0.3510	11.41	0.8552	85.52%
5	16	-1	-1	-1	28	6	2	29.1094	29.3547	0.2453	11.12	0.8334	83.34%
											Average	0.8639	

Appendix 4.7
Raw Data of the Nonuniform Pattern Plating Experiment, First-Order Model

	Board 13	Board 1	Board 14	Board 2	Board 16	Board 3	Board 15	Board 4	Board 17	Board 7	Board 18	Board 9	Board 20
pt1	38.230	25.846	36.411	26.869	22.128	18.718	28.136	19.601	32.288	27.635	31.525	28.900	22.793
pt2	37.722	31.827	35.653	27.173	21.381	19.778	25.099	16.247	30.454	26.246	30.501	31.977	21.638
pt3	20.280	21.724	24.963	23.400	19.557	18.069	21.190	19.048	38.910	35.137	27.234	25.114	18.998
pt4	14.503	22.663	32.980	25.699	20.906	17.339	24.296	19.759	39.977	31.081	29.372	26.243	20.263
pt5	12.747	14.455	14.725	17.236	14.526	12.434	9.549	10.723	15.214	15.556	27.527	26.148	15.428
pt6	14.835	12.803	20.317	16.025	18.289	13.930	17.125	15.285	15.545	15.926	26.717	25.395	16.443
pt7	27.573	23.341	18.633	21.624	12.449	16.014	11.453	12.961	15.482	20.606	17.493	24.946	13.055
pt8	29.695	21.419	11.698	15.805	11.218	12.400	11.460	13.406	19.787	17.807	15.503	22.334	10.865
pt9	18.243	19.914	13.511	18.605	10.080	14.077	8.254	11.033	14.476	24.962	14.223	21.946	10.169
pt10	16.607	15.572	14.507	15.304	8.822	15.713	8.925	14.289	11.930	23.677	11.662	18.709	9.435
pt11	11.489	11.700	7.603	12.766	7.201	12.960	6.372	13.171	6.783	11.452	12.048	16.671	7.571
pt12	8.528	10.889	11.156	12.628	9.856	12.529	10.447	11.352	6.030	10.577	14.267	20.691	8.771
Mean	20.871	19.346	20.180	19.428	14.701	15.330	15.192	14.740	20.573	21.722	21.506	24.090	14.619
SD	10.076	6.369	10.045	5.335	5.458	2.652	7.602	3.288	11.839	7.718	7.882	4.274	5.378
Avg Up	25.357	22.788	23.544	21.810	15.818	16.514	17.352	15.793	25.413	25.894	22.189	25.021	15.902
Avg Low	11.900	12.462	13.450	14.664	12.468	12.963	10.873	12.633	10.893	13.377	20.140	22.226	12.053
SD Up	9.359	4.701	10.351	4.791	5.670	2.460	8.129	3.373	11.330	5.537	8.232	4.165	5.570
SD Low	2.637	1.543	5.423	2.325	4.922	0.684	4.520	2.050	5.192	2.756	8.120	4.421	4.529
SD LC	11.296	6.952	10.538	5.491	5.348	2.798	7.753	2.829	9.252	6.344	8.079	4.890	5.570
SD CR	6.982	5.028	7.912	4.666	5.078	2.092	6.178	3.087	12.494	8.364	7.037	3.300	4.650

All thickness and Standard Deviation Data in μm
Avg Up : average thickness of the narrow region
Avg Low : average thickness of the thick region
SD Up : standard deviation of the upper region
SD Low : standard deviation of the lower region
SD LC : standard deviation of the left and center region
SD CR : standard deviation of the center and right region

Appendix 4.7
Raw Data of the Nonuniform Pattern Plating Experiment, First-Order Model

	Board 6	Board 19	Board 5
pt1	17.318	22.413	17.876
pt2	20.921	21.286	19.007
pt3	18.338	18.919	18.143
pt4	17.737	21.189	16.912
pt5	13.177	17.932	12.443
pt6	15.609	17.858	14.726
pt7	16.397	12.459	15.052
pt8	17.084	11.547	13.529
pt9	16.446	9.500	15.132
pt10	14.906	8.602	14.585
pt11	12.516	7.233	11.464
pt12	12.197	9.324	12.716
Mean	16.054	14.855	15.132
SD	2.556	5.614	2.419
Avg (narro	17.394	15.739	16.280
Avg (thick)	13.375	13.087	12.838
SD (narrov	1.758	5.773	1.968
SD (thick)	1.544	5.617	1.369
SD LC	2.789	5.713	2.495
SD CR	2.154	5.080	2.026

All thickness and Standard Deviation Data in μm
Avg Up : average thickness of the narrow region
Avg Low : average thickness of the thick region
SD Up : standard deviation of the upper region
SD Low : standard deviation of the lower region
SD LC : standard deviation of the left and center region
SD CR : standard deviation of the center and right region

Appendix 4.8
Raw Data of the Verification Experiment Using the 'Zebra Pattern' Nonuniform Pattern Plating

		Coded Variable			ACD	ES		Current	Weight (g)			
Board	Order	CD	L	AADR	mA/cm^2	cm	AADR	A	Before	After	Difference	Efficiency
4 I	1	-1	1	-0.42857	30.1	25.4	4	0.83	29.0561	29.3614	0.3053	0.932
8 I	2	-1	1	0.714286	30.1	25.4	8	1.00	28.5818	28.9462	0.3644	0.925
7 I	3	-1	1	0.428571	30.1	25.4	7	0.96	28.3883	28.7383	0.3500	0.928
5 I	4	-1	1	-0.14286	30.1	25.4	5	0.87	28.6805	28.9916	0.3111	0.904
6 I	5	-1	1	0.142857	30.1	25.4	6	0.91	28.3993	28.7346	0.3353	0.930
4 II	6	-1	1	-0.42857	30.1	25.4	4	0.83	28.8438	29.1437	0.2999	0.916
3 I	7	-1	1	-0.71429	30.1	25.4	3	0.79	28.8838	29.1650	0.2812	0.904
6 II	8	-1	1	0.142857	30.1	25.4	6	0.91	28.3627	28.6908	0.3281	0.910
7 II	9	-1	1	0.428571	30.1	25.4	7	0.96	28.4439	28.7888	0.3449	0.914
8 II	10	-1	1	0.714286	30.1	25.4	8	1.00	29.0037	29.3667	0.3630	0.922
3 II	11	-1	1	-0.71429	30.1	25.4	3	0.79	28.8346	29.1187	0.2841	0.914
5 II	12	-1	1	-0.14286	30.1	25.4	5	0.87	28.6486	28.9660	0.3174	0.922
											Average :	0.91842

AADR	3	4	5	6	7	8
Area (cm^2)	26.12898	27.52253	28.91607	30.30962	31.70316	33.09671

Appendix 4.8
Raw Data of the Verification Experiment Using the 'Zebra Pattern"
Nonuniform Pattern Plating

	From Table 4.12						Deposite Thickness (μm)					
	Board 3	Board 6	Board3i	Board3ii	Board4i	Board4ii	Board5i	Board5ii	Board6i	Board6ii	Board7i	Board7ii
AADR	2		3		4		5		6		7	
pt1	18.71765	17.31802	19.7014	20.9495	19.6289	20.4380	21.4119	20.0750	21.3125	21.0540	20.1554	21.5518
pt2	19.77798	20.92149	19.8827	20.5868	20.0245	20.2889	22.1936	19.1623	19.6292	19.3042	19.9958	20.4462
pt3	18.06908	18.33787	17.6659	18.8100	19.4704	19.6614	19.5712	17.4631	17.8921	17.9048	17.8572	20.4462
pt4	17.33908	17.73742	18.1689	19.2235	18.5413	19.2610	19.8001	18.8537	17.5748	17.6396	19.2607	19.6706
pt5	12.43427	13.17744	12.5294	12.2362	14.1211	13.5687	14.9520	12.4403	12.7554	12.9391	13.5408	13.5341
pt6	13.92975	15.60859	14.4756	13.9372	16.0196	15.2175	16.5666	15.0072	15.1747	15.1682	14.8556	14.9347
pt7	16.01414	16.39705	14.7507	13.6927	14.1803	13.9556	14.0524	13.2196	13.9633	14.2331	13.6684	13.4572
pt8	12.40039	17.08437	13.6660	12.4938	13.0986	12.7505	13.7285	11.7439	13.2087	13.1104	12.4439	12.1688
pt9	14.07676	16.44645	14.5830	14.0792	13.6765	14.1683	13.8597	13.0500	12.2815	13.6755	11.4704	11.1921
pt10	15.71299	14.90624	13.0019	12.5171	12.8432	12.9315	12.8743	11.5505	10.7378	12.7837	10.5092	9.8413
pt11	12.96042	12.51616	10.9315	10.7896	10.0015	9.9618	10.0955	9.4140	8.9435	8.9206	8.7138	8.3084
pt12	12.52923	12.19719	9.8640	10.7041	8.7332	8.7018	8.9072	8.3930	9.1790	9.0186	9.0219	9.5851
Std. Dev.	2.652148	2.555833	3.2802	3.8009	3.7652	3.9958	4.3002	3.8982	4.0141	3.7769	4.1578	4.7659
Ave SD	2.603991		3.540569		3.88052		4.099219		3.8955		4.461837	
Avg Up	16.5135	17.3936	16.4276	16.5441	16.4330	16.6819	17.1865	15.6398	15.8250	16.2131	15.6701	16.0968
Avg Low	12.96	13.37	11.95	11.92	12.22	11.86	12.63	11.31	11.5131	11.5116	11.53	11.59
SD Up	2.460026	1.758018	2.746337	3.681851	3.239503	3.503477	3.907591	3.589617	3.792215	3.153975	4.05664	4.868951
SD Low	0.68	1.54	2.01	1.52	3.42	3.04	3.70	3.00	3.000108	3.073384	3.13	3.15
Mean Th	15.33015	16.05402	14.93508	15.00166	15.02826	15.07541	15.66775	14.19771	14.38771	14.64597	14.29109	14.5947
Average	15.69208		14.96837		15.05183		14.93273		14.51684		14.4429	

All thickness and Standard Deviation Data in μm
Avg Up : average thickness of the narrow region
Avg Low : average thickness of the thick region
SD Up : standard deviation of the upper region
SD Low : standard deviation of the lower region

Appendix 4.8
Raw Data of the Verification Experiment Using the 'Zebra Pattern'
Nonuniform Pattern Plating

			From Table 4.12	
	Board8i	Board8ii	Board 16	Board 20
AADR	8		9	
pt1	21.8168	23.6885	22.12817	22.79299
pt2	20.8154	22.6723	21.38129	21.63797
pt3	19.4283	20.0306	19.55733	18.99778
pt4	20.4440	22.1781	20.90645	20.26327
pt5	13.9565	12.6379	14.52612	15.42792
pt6	16.5173	15.7339	18.28914	16.44344
pt7	13.5268	13.4603	12.44857	13.05464
pt8	13.0013	12.3358	11.21829	10.86488
pt9	10.0046	11.3036	10.07977	10.16918
pt10	9.4340	9.3081	8.822192	9.435455
pt11	8.6141	8.8118	7.200923	7.570747
pt12	9.3983	8.8853	9.855642	8.771477
Std. Dev.	4.9213	5.6281	5.457551	5.378209
Ave SD	5.274699		5.41788	
Avg Up	16.0589	16.8722	15.8178	15.9020
Avg Low	12.12	11.52	12.47	12.05
SD Up	5.108329	5.83923	5.669748	5.569726
SD Low	3.76	3.33	4.92	4.53
Mean Th	2875.91	3079.906	2921.121	2882.809
Average	14.91682		14.66015	

All thickness and Standard Deviation Data in μm
Avg Up : average thickness of the narrow region
Avg Low : average thickness of the thick region
SD Up : standard deviation of the upper region
SD Low : standard deviation of the lower region

Appendix 4.9 Response Graphs of the Upper, Lower, Left-centre, Centre-Right Regions of the Board

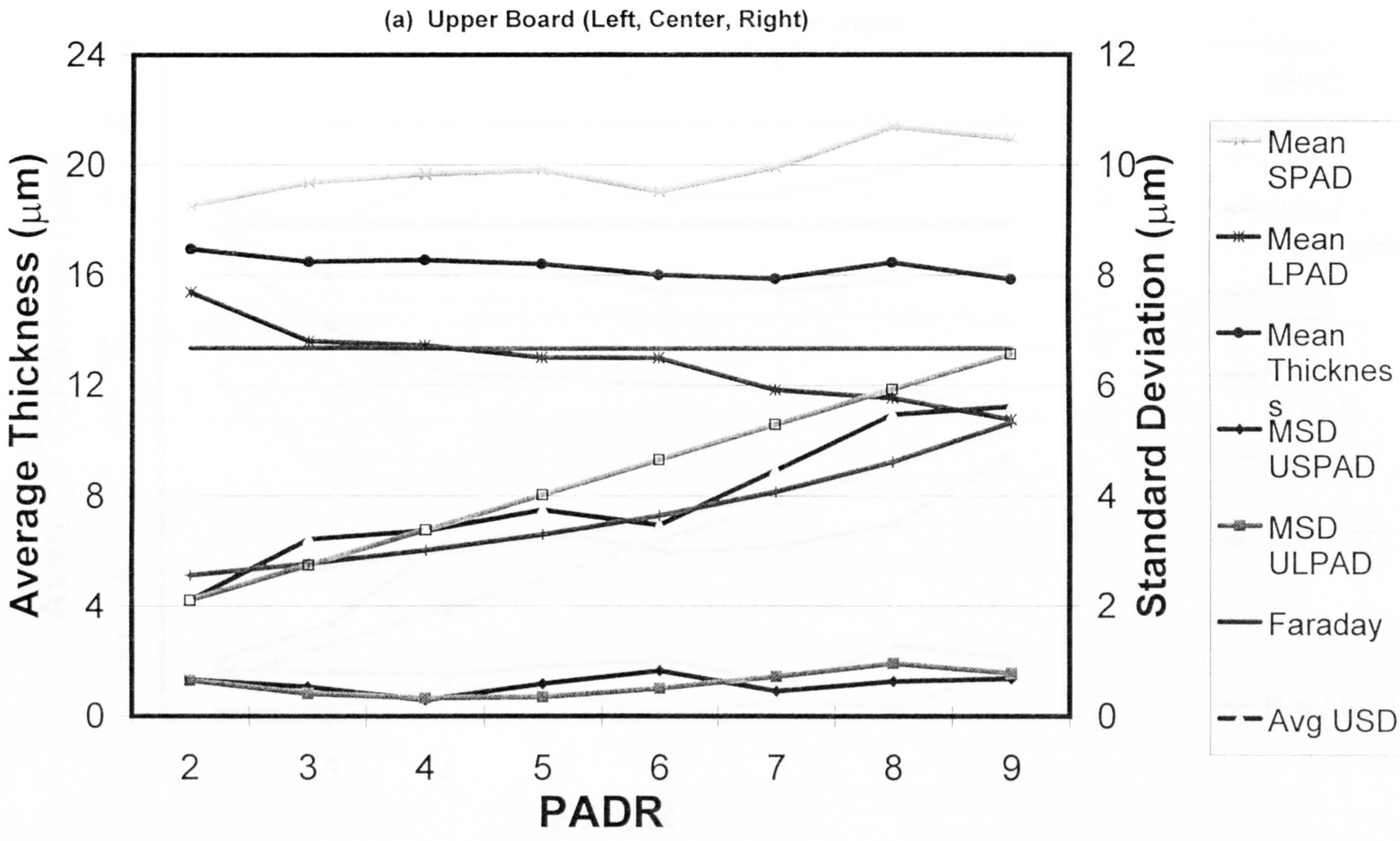

Appendix 4.9

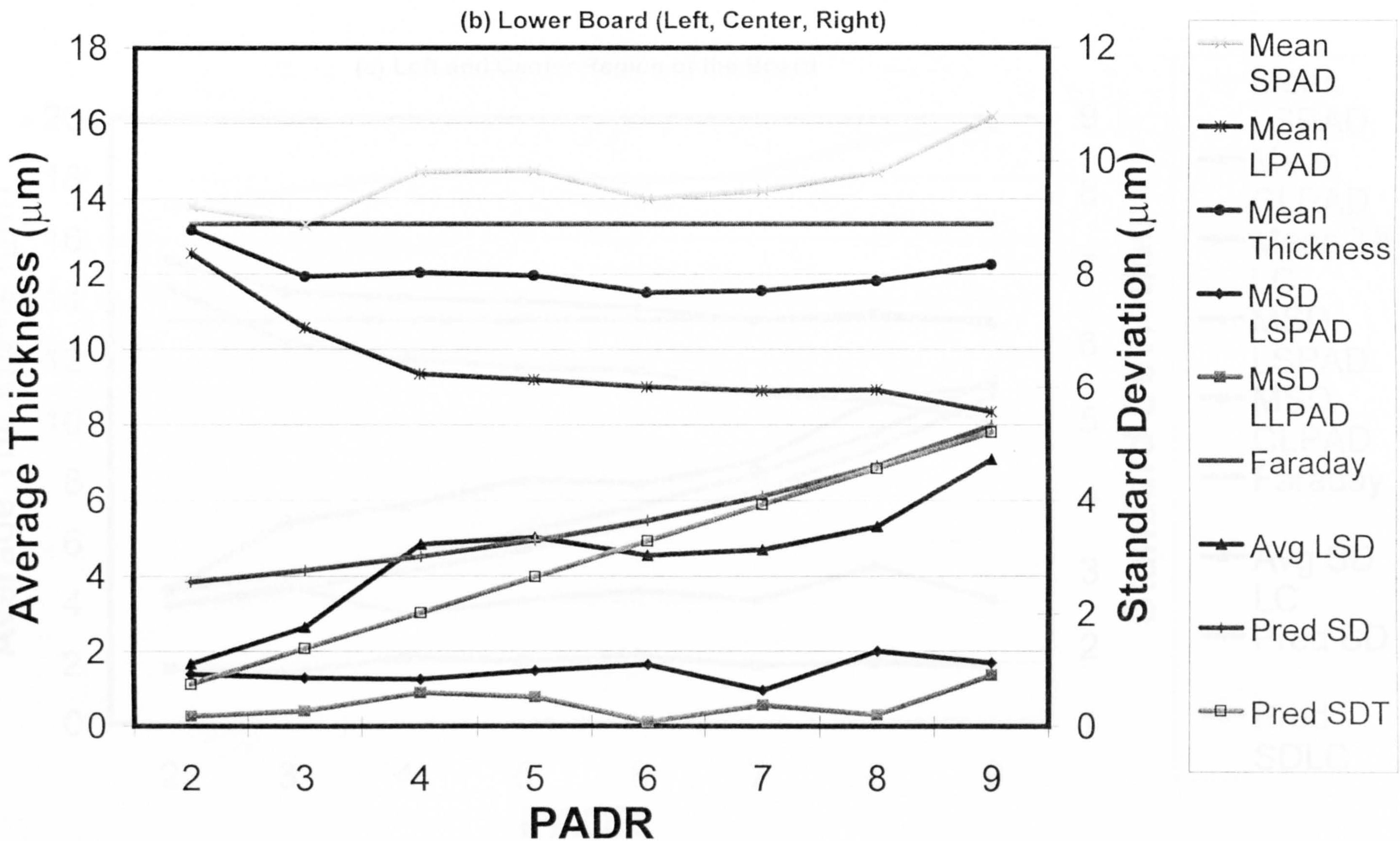
(b) Lower Board (Left, Center, Right)
Average Thickness (μm)
Standard Deviation (μm)
PADR
18
16
14
12
10
8
6
4
2
0
12
10
8
6
4
2
0
2
3
4
5
6
7
8
9
Mean SPAD
Mean LPAD
Mean Thickness
MSD LSPAD
MSD LLPAD
Faraday
Avg LSD
Pred SD
Pred SDT

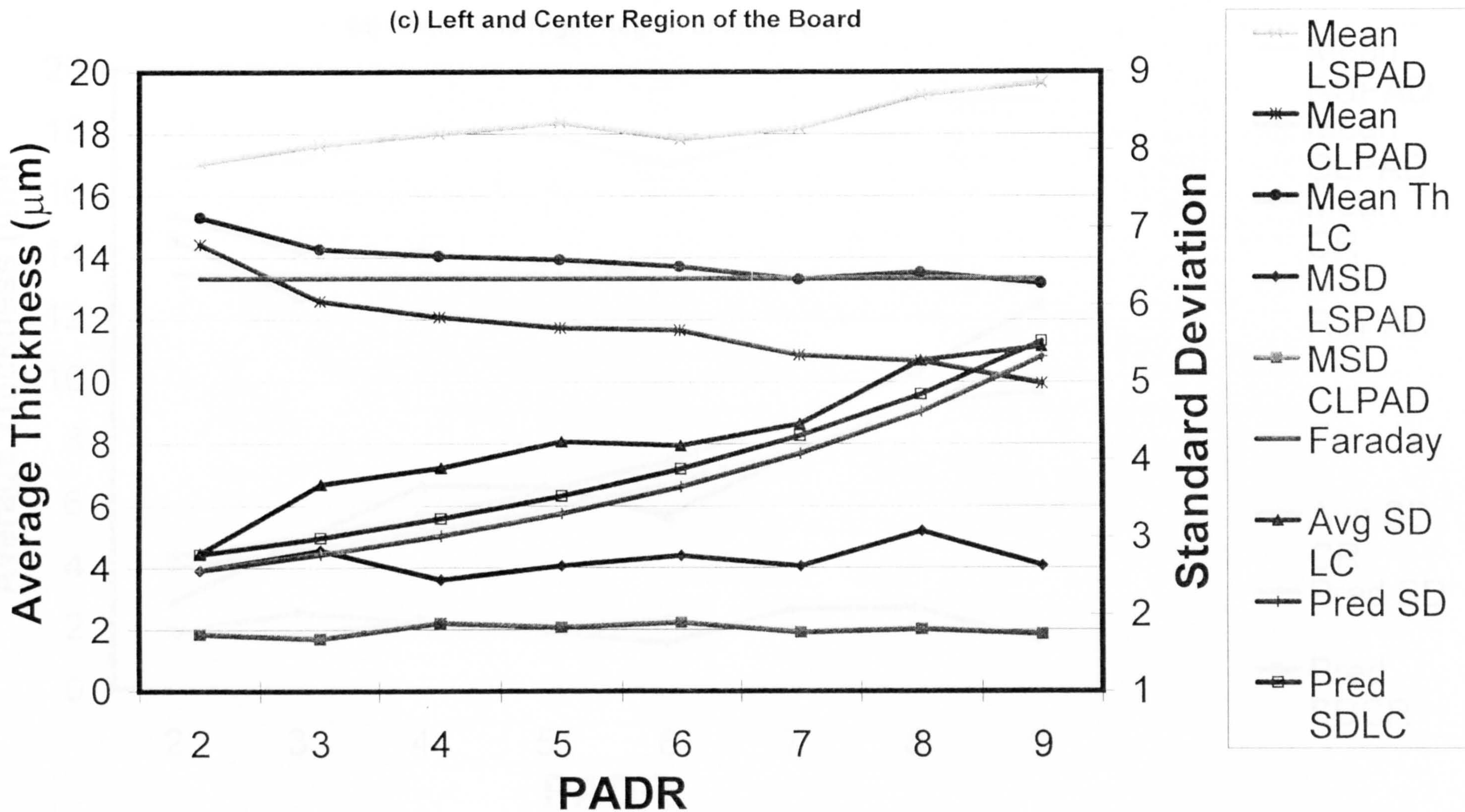
(c) Left and Center Region of the Board
Average Thickness (μm)
Standard Deviation
PADR
0
2
4
6
8
10
12
14
16
18
20
1
2
3
4
5
6
7
8
9
2
3
4
5
6
7
8
9
Mean LSPAD
Mean CLPAD
Mean Th LC
MSD LSPAD
MSD CLPAD
Faraday
Avg SD LC
Pred SD
Pred SDLC

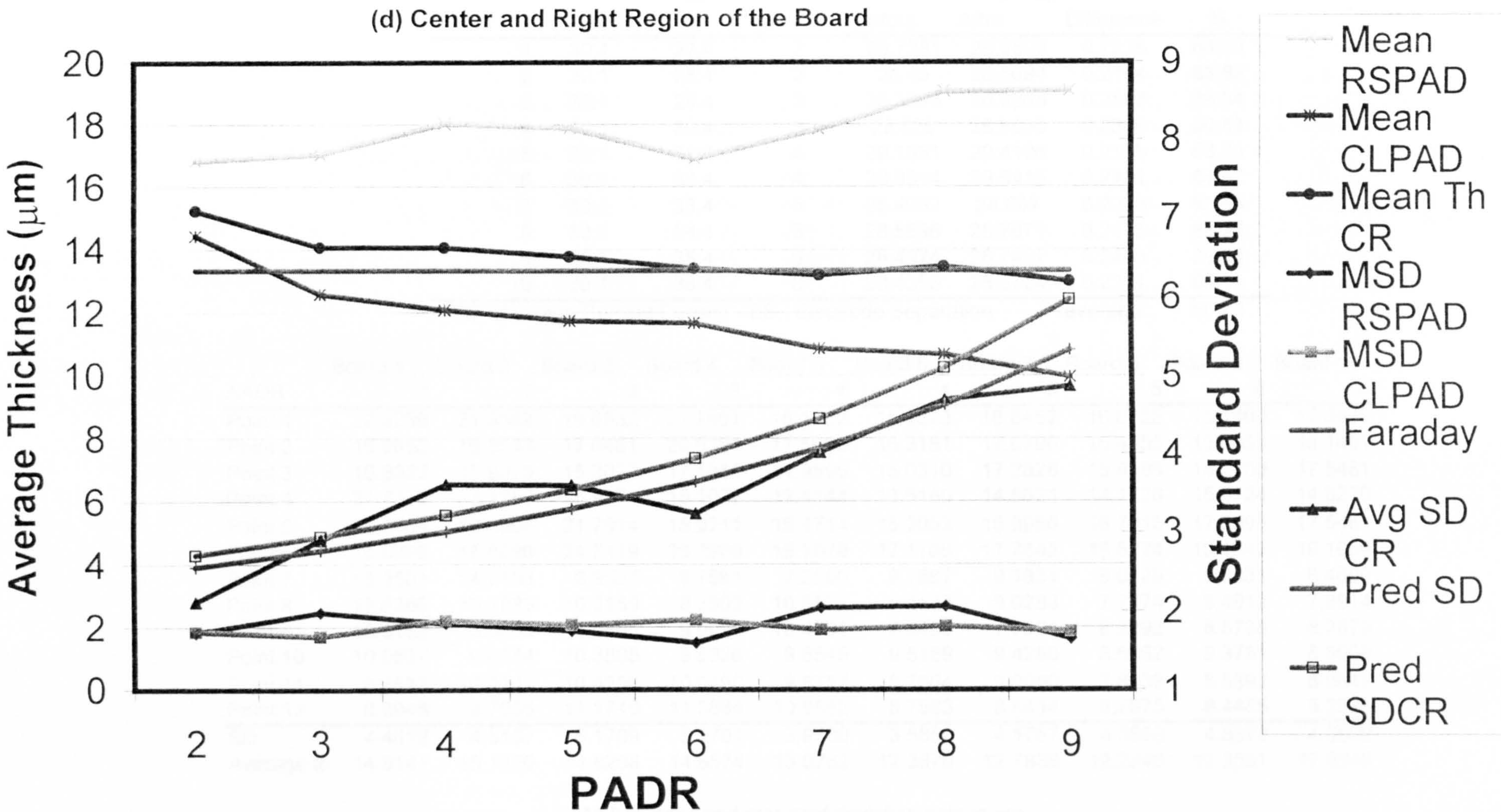
(d) Center and Right Region of the Board
Average Thickness (μm)
Standard Deviation
PADR
0
2
4
6
8
10
12
14
16
18
20
1
2
3
4
5
6
7
8
9
2
3
4
5
6
7
8
9
Mean RSPAD
Mean CLPAD
Mean Th CR
MSD RSPAD
MSD CLPAD
Faraday
Avg SD CR
Pred SD
Pred SDCR

Appendix 4.10
Raw Data of the Nonuniform Pattern Verification Experiment Using a Simple Circuit Pattern

Board	ACD mA/cm^2	ES cm	AADR	Weight (g) Before	After	Difference	Effeciency %
1	30.1	27.4	2	28.7381	28.9599	0.2218	84.79
2	30.1	28.4	2	28.45	28.6694	0.2194	83.88
3	30.1	29.4	3	28.3645	28.6208	0.2563	89.04
4	30.1	30.4	3	28.625	28.8856	0.2606	90.53
5	30.1	31.4	4	29.1951	29.4106	0.2155	86.74
6	30.1	32.4	4	29.3314	29.5415	0.2101	84.57
7	30.1	33.4	5	28.4632	28.687	0.2238	85.56
8	30.1	34.4	5	28.5696	28.7871	0.2175	83.15
9	30.1	35.4	6	28.4974	28.7437	0.2463	89.66
10	30.1	36.4	6	28.4353	28.6724	0.2371	86.31
ACD : Average Current Density			ES : Electrode Separation			average :	86.42

	Board 1	Board 2	Board 3	Board 4	Board 5	Board 6	Board 7	Board 8	Board 9	Board 10
AADR	2	2	3	3	4	4	5	5	6	6
Point 1	22.3256	21.9582	19.0532	21.7461	18.1382	15.9273	16.8452	16.0722	18.1809	17.0435
Point 2	16.8652	16.8533	17.6481	20.5391	17.5698	16.3181	17.6796	16.4255	19.0953	18.1491
Point 3	16.5322	15.9376	15.2022	17.1361	14.9595	16.0310	17.2828	15.8185	18.0700	17.5481
Point 4	21.7370	22.1383	16.9271	15.1027	12.4144	13.5180	14.5621	14.1728	15.4724	14.8220
Point 5	16.5904	19.1906	21.7914	18.9711	15.4714	15.2053	15.9956	16.7015	17.5999	17.5461
Point 6	15.0999	15.0690	24.7119	23.7269	19.7079	17.1760	17.7642	18.6274	19.1342	19.1659
Point 7	13.3501	14.7156	9.9567	8.7561	7.2560	9.1867	9.1831	8.0129	9.2831	8.4609
Point 8	12.8380	15.2083	10.3159	8.3909	10.5572	9.3533	9.0283	7.2774	8.4912	7.8914
Point 9	15.0183	13.3666	10.0665	9.9920	10.4791	8.6499	7.7901	8.3292	8.5738	8.2879
Point 10	10.0537	9.0284	10.3805	9.8926	9.6545	9.5189	9.4250	8.6862	9.3731	8.8009
Point 11	8.9637	10.0147	10.6206	10.0490	9.8757	8.7604	9.0080	7.8038	8.5391	8.0647
Point 12	8.3948	8.7035	11.1749	11.5864	10.8552	8.7583	8.8414	8.7675	8.4485	8.2335
SD	4.4612	4.5107	5.1709	5.5701	3.9700	3.5850	4.1787	4.3860	4.8673	4.8509
Average th	14.8141	15.1820	14.8208	14.6574	13.0782	12.3670	12.7838	12.2246	13.3551	12.8345

All thickness and standard deviation data in μm

Appendix 4.10
Raw Data of the Nonuniform Pattern Verification Experiment Using a Simple Circuit Pattern

Board	Coded Variable ACD	ES	AADR	Expected thickness	Actual thickness	Actual SD	Mean SD	Actual mean th.	uncoded OPAD	Coded OPAD	Predicted SD *
1	-1	1	-1.0000	13.3420	14.8141	4.4612			0.1499	-0.8583	2.8033
2	-1	1	-1.0000	13.3420	15.1820	4.5107	4.4860	14.9980	0.1499	-0.8583	2.8033
3	-1	1	-0.7143	13.3420	14.8208	5.1709			0.1999	-0.4297	3.4064
4	-1	1	-0.7143	13.3420	14.6574	5.5701	5.3705	14.7391	0.1999	-0.4297	3.4064
5	-1	1	-0.4286	13.3420	13.0782	3.9700			0.1249	-1.0727	2.5017
6	-1	1	-0.4286	13.3420	12.3670	3.5850	3.7775	12.7226	0.1249	-1.0727	2.5017
7	-1	1	-0.1429	13.3420	12.7838	4.1787			0.1498	-0.8585	2.8031
8	-1	1	-0.1429	13.3420	12.2246	4.3860	4.2823	12.5042	0.1498	-0.8585	2.8031
9	-1	1	0.1429	13.3420	13.3551	4.8673			0.1749	-0.6441	3.1047
10	-1	1	0.1429	13.3420	12.8345	4.8509	4.8591	13.0948	0.1749	-0.6441	3.1047

AADR	2	2	3	3	4	4	5	5	6	6
SAAD ASD	3.0498		3.3100		1.9283		1.3343		1.3966	
SAAD SD	3.0429	3.0568	3.4834	3.1365	2.6135	1.2432	1.2263	1.4424	1.3446	1.4487
LAAD ASD	2.6734	2.9332	0.4387	1.1288	1.3149	0.3630	0.5686	0.5659	0.4239	0.3172
LAAD ASD	2.8033		0.7838		0.8389		0.5672		0.3706	
Overall SD	4.4612	4.5107	5.1709	5.5701	3.9700	3.5850	4.1787	4.3860	4.8673	4.8509
Overall MSD	4.4860		5.3705		3.7775		4.2823		4.8591	
SAAD Avg	18.3581		19.3797		16.0364		16.4956		17.6523	
SAAD Mean Th	18.1917	18.5245	19.2223	19.5370	16.3769	15.6960	16.6883	16.3030	17.9255	17.3791
LAAD Mean Th	11.4365	11.8395	10.4192	9.7778	9.7796	9.0379	8.8793	8.1462	8.7848	8.2899
LAAD Avg	11.6380		10.0985		9.4088		8.5127		8.5373	
Overall Mean Th	14.8141	15.1820	14.8208	14.6574	13.0782	12.3670	12.7838	12.2246	13.3551	12.8345
Overall Mean Avg	14.9980		14.7391		12.7226		12.5042		13.0948	

SAAD ASD : average SD response of SAAD region
SAAD SD : SD response of SAAD region
LAAD ASD : SD response of LAAD region
LAAD ASD : average SD response of LAAD region
Overall SD : overall SD response of whole board
Overall MSD : average response of overall SD

SAAD Avg : average of mean response of SAAD region
SAAD Mean Th : mean deposite thickness of SAAD region
LAAD Mean Th : mean deposite thickness of LAAD region
LAAD Avg : average of mean response of LAAD region
Overall Mean Th : mean deposite thickness of whole board
Overall Mean Avg : average response of overall mean thickness

All thickness and standard deviation data in μm

Appendix 5.1

Alias Structure of the 2_{VI}^{6-1} Fractional Factorial Design used in the Screening Experiments of PTH Plating

2^{6-1}; ½ fraction of 6 factors in 32 runs

Design Generators

F = ABCDE

Defining relation: I = ABCDEF

Aliases

Each main effect is aliased with a single 5-factor interaction.

Each 2-factor interaction is aliased with a single 4-factor interaction.

ABC = DEF	ACE = BDF
ABD = CEF	ACF = BDE
ABE = CDF	ADE = BCF
ABF = CDE	ADF = BCE
ACD = BEF	AEF = BCD

2 blocks of 16: ABF = CDE

4 blocks of 8: BC

ABF = CDE

ACF = BDE

Appendix 5.2
Raw Data of the Screening Runs of the PTH Experiment

		Coded Variable								
		A	B	C	D	E	F			
Obs no.	RunOrd	Acid	Sulphate	ACD	ES	IHD	CAR	Mean	SD	Residual
1	7	-1	-1	-1	-1	-1	-1	12.1218	3.0123	0.6001
2	23	1	-1	-1	-1	-1	1	13.7170	3.2934	1.1429
3	28	-1	1	-1	-1	-1	1	13.2808	1.7032	-0.4471
4	8	1	1	-1	-1	-1	-1	9.4471	1.4222	-0.9899
5	10	-1	-1	1	-1	-1	1	13.0112	3.3774	0.2409
6	30	1	-1	1	-1	-1	-1	14.0936	2.5968	0.5066
7	13	-1	1	1	-1	-1	-1	14.7945	1.9410	-0.1494
8	24	1	1	1	-1	-1	1	14.2325	3.2320	0.0959
9	15	-1	-1	-1	1	-1	1	13.0545	2.5304	0.6321
10	2	1	-1	-1	1	-1	-1	12.5511	2.1296	-0.0298
11	27	-1	1	-1	1	-1	-1	14.2566	3.0531	0.8932
12	11	1	1	-1	1	-1	1	13.6548	2.2616	0.3641
13	17	-1	-1	1	1	-1	-1	14.0224	2.3827	-0.7853
14	1	1	-1	1	1	-1	1	16.2859	5.1943	0.9801
15	18	-1	1	1	1	-1	1	14.5384	4.1913	-0.0229
16	5	1	1	1	1	-1	-1	12.9081	2.6010	-0.5673
17	6	-1	-1	-1	-1	1	1	12.5063	1.9391	-0.2111
18	32	1	-1	-1	-1	1	-1	11.5025	3.4530	1.0411
19	20	-1	1	-1	-1	1	-1	11.4650	1.6555	-0.7569
20	29	1	1	-1	-1	1	1	10.5231	1.7706	-0.3791
21	3	-1	-1	1	-1	1	-1	12.7781	2.0854	-0.0054
22	9	1	-1	1	-1	1	1	15.1213	2.5210	-0.6151
23	22	-1	1	1	-1	1	1	15.7225	1.9742	-1.1621
24	31	1	1	1	-1	1	-1	10.5731	3.1788	1.0886
25	12	-1	-1	-1	1	1	-1	13.6763	1.8483	-0.3118
26	14	1	-1	-1	1	1	1	13.1113	1.1661	-0.7319
27	21	-1	1	-1	1	1	1	13.3319	1.5278	-0.3699
28	19	1	1	-1	1	1	-1	9.9700	1.7141	-0.4458
29	16	-1	-1	1	1	1	1	16.9606	3.8299	-0.3839
30	4	1	-1	1	1	1	-1	16.2756	3.1676	-0.0003
31	26	-1	1	1	1	1	-1	13.8700	3.0807	-0.0873
32	25	1	1	1	1	1	1	16.3088	5.0807	0.8671

Acid : Concentration of Sulphuric Acid
Sulphate : Concentration of Copper Sulphate
ACD : Average Current Density
ES : Electrode Separation
IHD : Inter-Hole Distance of the PTH / BV
CAR : Correct Aspect Ratio of the PTH / BV
Residual : based on the 6-term First-Order Model (Eq. 5.1)

Appendix 5.2

Observation number	1	2	3	4	5	6	7	8	9	10	11
	9.78	13.77	9.73	6.74	9.93	9.18	13.26	11.26	11.42	9.57	12.57
	10.01	13.66	11.54	6.09	10.15	10.87	14	11.97	13.14	9.55	12.55
	10.6	9.96	10.7	6.8	10.62	14.48	13.77	10.42	11.96	10.15	10.15
	9.45	9.24	9.99	9.21	9.66	14.23	13.73	11.15	13.25	11.35	11.35
	9.78	8.77	11.07	8.91	8.89	13.1	14.38	10.13	12.78	11.53	11.53
	8.33	8.99	10.78	6.16	8.14	12.99	14.39	10.25	10.15	10.64	9.64
	8.21	8.51	11.23	6.8	8.15	11.8	14.6	10.46	10.46	11.39	11.39
	8.45	8.59	11.83	8.43	9.03	13.78	14.14	11.71	9.42	9.02	12.06
	9.12	10.95	12.55	7.87	10.51	11.62	12.13	11.18	9.89	11.06	11.06
	10.1	9.74	11.98	9.01	9.98	10.56	13.48	12.22	9.61	9.4	12.4
	11.01	10.35	10.26	9.01	11.24	10.4	13.98	12.61	10.55	9.64	12.64
	8.6	13.04	11.68	9.35	12.04	11.23	13.04	12.1	10.59	11.89	11.89
	8.45	11.56	10.46	9.77	12.84	11.02	13.56	11.8	10.54	10.56	10.56
	9.12	10.99	12.81	9.7	9.6	11.65	12.81	11.5	9.17	10.9	10.9
Deposite	9.78	11.45	12.78	9.49	9.43	12.45	14.08	11.6	12.51	10.23	10.23
	8.5	12.81	13.08	10.26	9.65	12.1	11.58	11.09	11.31	11.4	11.4
thickness	9.12	11.64	13.11	9.42	11.91	10.68	14.46	11.15	11.67	11.56	11.56
	8.45	12.9	13.11	9.29	12.03	10.55	14.9	11.19	9.4	11.23	11.23
measured	8.12	11.3	13.06	10.21	8.24	10.47	13.31	10.84	12.91	10.99	9.99
	9.23	10.5	12.12	10.16	9.26	11.36	14.46	10.87	9.61	10.87	10.87
(μm)	9.45	9.46	12.14	9.44	9.79	11.46	12.25	10.89	10	11.23	11.23
	10	9.87	11.67	8.39	10.35	12.03	14.84	9.89	9.58	9.09	12.09
	16.19	9.2	15.22	7.71	10.39	11.88	13	17.16	11.08	15.34	18.34
	16.59	18.35	15.53	6.64	11.88	18.56	11.66	17.19	10.27	15.86	15.86
	15.46	16.95	15.46	7.92	11.9	17.63	11.12	15.37	16.46	14.9	17.9
	15.97	17.72	14.44	11.33	10.34	15.04	10.94	18	16.65	14.24	17.24
	14.09	18.53	15.38	11.21	17.46	14.54	13.84	15.11	13.81	14.28	17.28
	14.92	17.51	14.03	11.31	18.6	16.78	18.75	18.48	16.93	14.56	17.56
	14.19	15.88	15.4	10.04	19.52	16.58	17.97	15.97	13.26	13.55	16.55
	15.12	15.59	15.09	10.14	17.92	16.12	18.84	15.85	15.69	13.23	16.23
	16.14	18.6	15.71	10.15	17.88	16.35	18.31	19.63	14.49	15.56	17.56
	15.79	16.04	13.97	10.04	17	15.2	15.55	17.41	15.61	15.02	18.02
	14.22	15.59	13.71	11.09	16.88	15.14	15.93	16.32	15.53	14.44	17.44
	15.09	16.4	14.56	11.16	18.12	17.4	17.67	16.15	13.2	15	17
	14.3	15.35	14.56	11.99	18.53	17	16.56	16.89	15.71	15.3	17.3
	14.22	16.48	13.45	11.59	14.66	15.99	16.66	17.69	14.77	14.99	16.99
	13.89	16.12	13.75	11.01	14.66	15.2	16.96	19.41	16.56	13.3	16.3
	14.27	17.01	14.86	10.67	13.41	17.89	15.2	18.18	16.42	13.11	16.11
	14.69	16.22	14.45	10.3	14.42	17.1	15.75	17.85	14.24	14.46	17.46
	14.2	16.54	13.51	10.18	15.74	16.22	15.2	17.07	15.16	14.55	17.55
	15.74	16.88	13.99	10.23	13.35	15.99	14.63	16.54	15.18	14.23	17.23
	16.01	17	13.98	9.83	14.22	16.45	14.67	17.08	15.98	14.64	17.64
	14.33	18.03	15.63	9.97	16.03	16.32	16.01	19.29	14.91	13.94	16.94
	14.28	15.23	14.39	10.82	17.33	15.68	14.43	17.31	14.4	14.5	17.5
		15.46	14.71	9.8	15.74	16.02	14.87		14.99		
		16.25	15.36	9.12	14.04	16.22	15.44		16.49		
			14.13	9.19	17.28	17.09	15		15.85		
			14.53	9.04	15.03		16.98				
				9.53	13.78		16.24				
				9.61			17.09				
				9.67			18.1				
number of points measurec	44	46	48	51	49	47	51	44	47	44	44
Mean Thickness	12.12	13.72	13.28	9.447	13.01	14.09	14.79	14.23	13.05	12.55	14.26
standard deviation	3.012	3.293	1.703	1.422	3.377	2.597	1.941	3.232	2.53	2.13	3.053

Appendix 5.2

Observation number	12	13	14	15	16	17	18	19	20	21	22
	11.89	12.99	10.13	11.9	9.56	10.63	9.37	10.69	7.93	12.03	13.51
	11.64	10.45	12.73	9.19	7.96	10.53	9.96	11.34	8.27	11.44	14.4
	10.47	10.5	9.88	9.24	8.73	10.43	8.25	10.16	9.49	12.01	13.52
	10.32	10.15	12.56	11.37	10.25	9.7	6.84	9.66	9.58	11.17	12.22
	11.39	11.45	13.23	10.39	11.41	11.81	7.66	9.02	9.62	9.38	11.39
	11.81	11.5	9.09	10.6	9.92	11.22	7.44	9.28	8.99	10.4	12.45
	12.97	11.12	9.49	11.88	9.46	11.45	8.6	10.35	8.56	10.15	12.7
	12.87	11.5	12	10.57	8.08	10.99	8.19	10.24	9.02	11.04	13.61
	12.32	12.25	11.23	10.55	9.84	12.82	16.11	12.53	11.52	15.63	16.97
	10.11	12.45	11.56	11.26	12.42	13.25	13.34	12.07	11.58	14.99	17.47
	10.41	11.12	11.78	9.75	11.25	15.6	15.1	13.76	12.02	15.17	16.5
	12.78	11.56	11.4	10.69	9.86	14.56	15.97	12.87	13.24	14.86	16.03
	12.81	12.88	10.99	9.81	9.3	12.99	14.22	14.54	13.1	13.62	19.03
	12.83	12.54	10.89	9.36	10.29	13.56	14.16	13.08	12.29	12.84	19.45
Deposite	11.15	12.2	12.01	9.79	11.78	15.46	14.33	11.29	11.22	15.1	15.05
	11.14	12.6	11.56	9.12	11.3	15.1	14.5	12.56	11.94	14.62	17.64
thickness	12.78	11.45	10.77	11.77	11.26						
	10.44	12.08	10.5	11.2	12.12						
measured	10.68	11.97	11.64	10.05	10.62						
	12.46	12.21	11.75	9.33	10.23						
(μm)	11.45	12.3	11.46	11.66	11.99						
	12.74	12.76	11.47	11.2	12.01						
	12.68	12.71	21.71	18.74	11.66						
	12.69	15.23	23.5	18.44	14.43						
	11.9	15.56	19.25	20.76	15.58						
	11.41	15.45	22.12	20.33	14.88						
	15.16	16.87	19.24	17.97	15.61						
	16.47	16.5	23.76	18.89	16.31						
	15.3	16.45	20.15	18.01	16.1						
	15.53	16.78	20.79	18.47	15.97						
	16.61	17.88	20.4	17.44	14.01						
	16.45	16.99	20.3	17.55	15.6						
	15.52	16	21.55	18.56	15.45						
	14.84	15.55	21.07	18.07	15.55						
	16.87	16.45	22.13	19.18	13.82						
	16.84	15.45	22.56	18.7	14.99						
	16.47	15.7	21.87	19	15.18						
	14.37	16.65	22.06	18.47	14.44						
	16.9	17.52	19.89	18.44	14.31						
	14.09	16.63	20.43	19.03	15.3						
	14.99	17.89	20.17	18.1	16						
	16.19	15.06	20.5	19.2	15.43						
	14.55	15.08	23.01	17.88	15.2						
	16.6	16.19	22	17.78	14.66						
	15.8	16.39			14.55						
	16.29				15.81						
	16.89				16.2						
	16.56										

number of points measured	48	45	44	44	47	16	16	16	16	16	16
Mean Thickness	13.65	14.02	16.29	14.54	12.91	12.51	11.5	11.47	10.52	12.78	15.12
standard deviation	2.262	2.383	5.194	4.191	2.601	1.939	3.453	1.655	1.771	2.085	2.521

Appendix 5.2

Observation number	23	24	25	26	27	28	29	30	31	32
	14.07	7.67	13.72	11.75	11.22	8.5	14.74	14.45	10.51	12.74
	15.86	6.94	11.06	12.61	11.6	10.67	12.06	13.97	10.28	12.21
	12.35	7.05	11.54	12.83	12.02	9.76	12.48	12.36	10.67	10.85
	12.15	8.14	13.42	13.23	13.2	8.67	13.78	13.84	10.94	10.27
Deposite	13.99	8.45	11.29	11.24	12.88	7.96	13.2	13.7	11.01	10.56
	14.56	7.68	12.56	11.51	11.3	8.13	12.57	13.41	11.64	11.09
thickness	14.84	7.12	10.86	11.68	11.99	7.77	14.78	12.2	11.22	11.89
	15.01	7.44	12.27	12.09	12.1	7.55	13.21	14.09	11.1	12.54
measured	16.22	12.92	14.81	14.79	13.28	9.59	20.1	19.27	16.8	21.14
	16.21	14.89	15.26	14.17	13.98	11.4	19.74	17.8	16.39	22.01
(μm)	17.5	13.68	16	14.02	15.11	12.5	21.56	21.77	17.65	22.67
	17.24	14.19	16.41	13.47	15.3	12.5	21.47	17.86	17.37	22.89
	18.67	12.23	15.24	14.15	15.75	10.77	20.89	21.87	16.03	20.33
	18.1	13.44	14.9	14.39	13.94	10.63	20.01	18.53	16.49	21.22
	17.23	13.78	14.59	14.16	14.65	11.09	19.58	17.3	17.01	19.24
	17.56	13.55	14.89	13.69	14.99	12.03	21.2	17.99	16.81	19.29

number of points measured	16	16	16	16	16	16	16	16	16	16
Mean Thickness	15.72	10.57	13.68	13.11	13.33	9.97	16.96	16.28	13.87	16.31
standard deviation	1.974	3.179	1.848	1.166	1.528	1.714	3.83	3.168	3.081	5.081

Appendix 5.3
Normal Probability Plot of the Residuals of the PTH Plating Experiment, First-Order Model

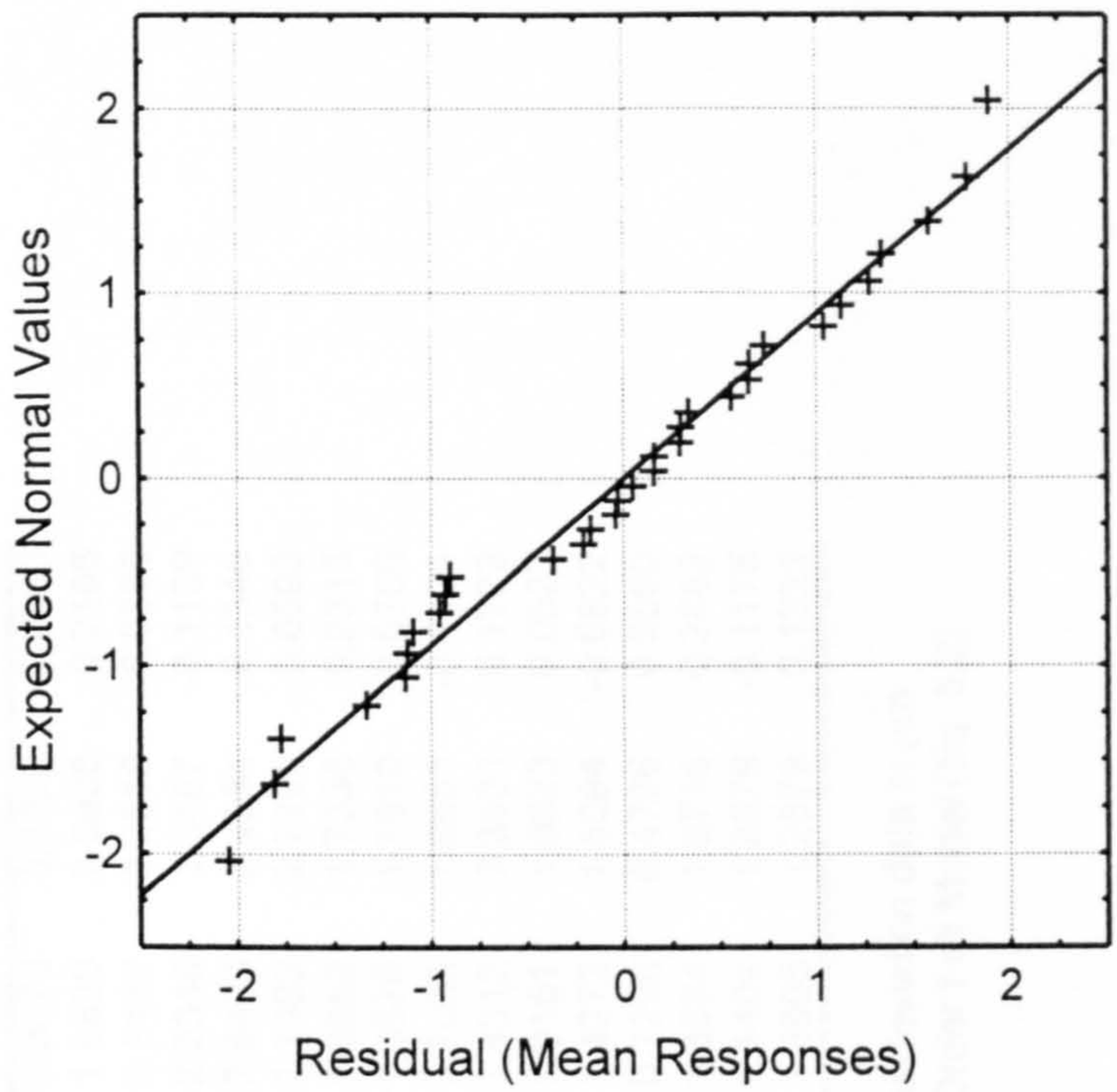

Normal Probability Plot of Residuals for the Mean Responses

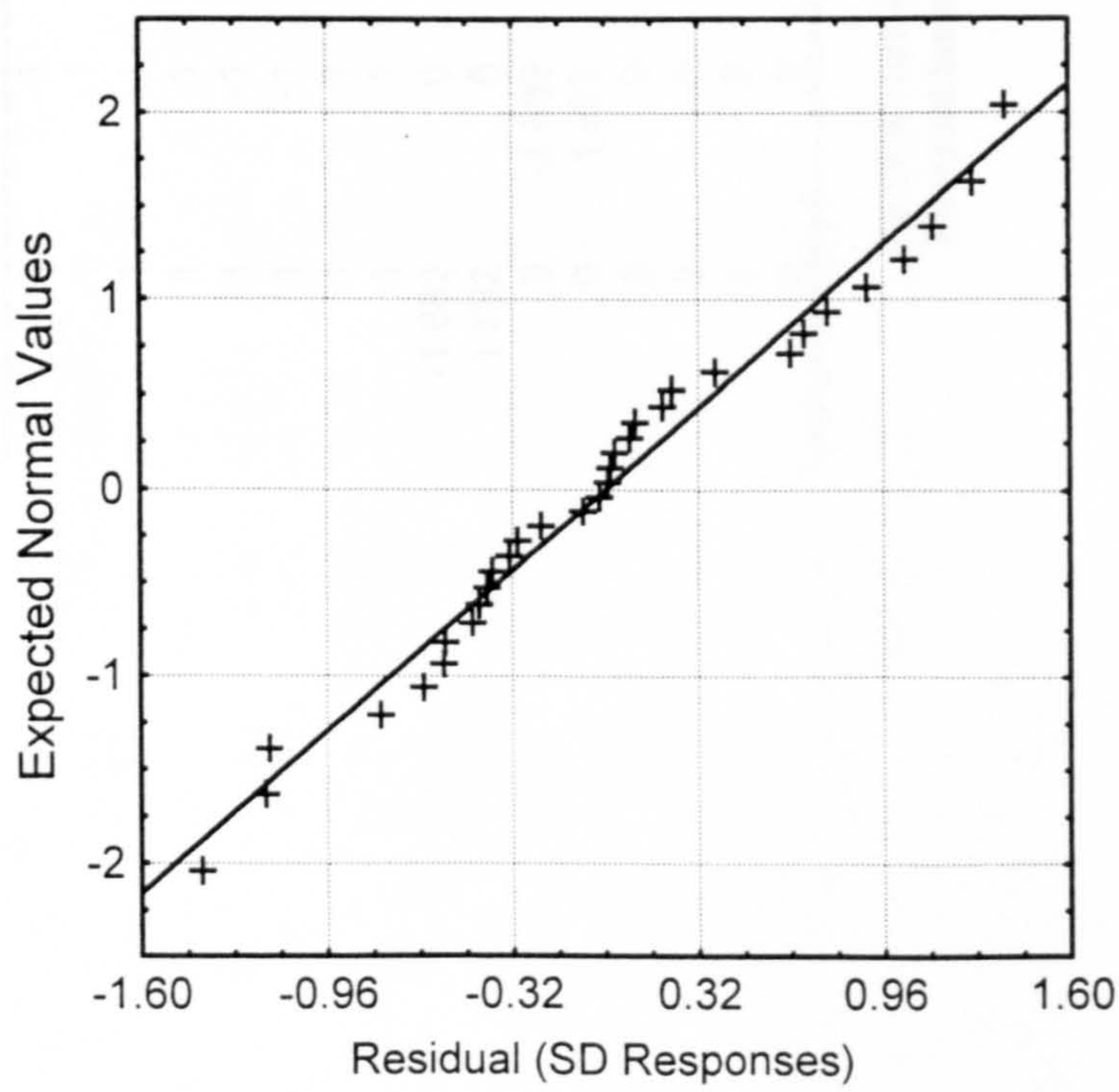

Normal Probability Plot of Residuals for the SD Reponses

Appendix 5.4
Raw Data of the PTH CCD Experiments for the Second-Order Model Building

i C ACD	D ES	F (mm) CAR	Actual SD	Predicted SD	Residual
-1	-1	-1	0.3673	0.4226	-0.0553
1	-1	-1	1.8830	2.0938	-0.2108
-1	1	-1	0.9132	0.9518	-0.0386
1	1	-1	2.2348	2.3487	-0.1139
-1	-1	1	2.5430	2.4084	0.1346
1	-1	1	2.7993	2.7399	0.0593
-1	1	1	1.9653	1.7338	0.2315
1	1	1	1.8670	1.7910	0.0760
-1.682	0	0	1.7033	1.8555	-0.1521
1.682	0	0	3.4312	3.3090	0.1222
0	-1.682	0	1.9151	1.8623	0.0527
0	1.682	0	1.4272	1.5094	-0.0822
0	0	-1.682	0.7296	0.4706	0.2590
0	0	1.682	1.3834	1.6716	-0.2882
0	0	0	1.1404	1.2579	-0.1175
0	0	0	1.3805	1.2579	0.1225

All thickness and standard deviation data in μm
Residual based on First-Order Full Model (Eq. 5.2)

Appendix 5.4
Raw Data of the PTH CCD Experiments for the Second-Order Model Building

observation number	1	2	3	4	5	6	7	8	9	10	11	12	13	14	15	16
	11.7	12.79	11.24	17.08	8.48	12.07	10.85	6.89	11.25	7.17	11.76	11.09	10.53	9.22	10.46	12.58
	11.26	13.5	10.96	15.53	7.04	12.62	10.2	7.92	10.89	6.27	12.01	10.81	10.22	9.17	10.69	12.62
	10.87	14.03	11.32	14.78	5.72	12.72	9.17	7.5	10.78	6.41	12.11	12.98	9.87	9.43	10.86	12.64
Deposite	11.04	13.73	10.72	14.93	7.1	12.74	10.6	8.14	11.03	6.78	13.16	12.64	10.67	9.55	11.46	12.28
	10.48	13.2	10.35	16.12	5.64	11.9	10.07	8.8	11.8	6.04	12	9.87	10.42	9.91	11.25	13.55
thickness	10.62	13.4	10.52	16.67	6.39	11.48	9.27	8.99	11.81	6.36	12.98	8.56	9.92	9.8	10.65	12.38
	11.2	13.03	11.24	18.26	6.71	11.26	9.47	8.03	11.92	7.48	13.29	10.2	10.05	10.21	10.78	12.16
measure	11.04	14.73	10.71	13.74	6.66	11.75	11.2	7.32	12.17	7.37	12.74	13.19	9.42	10.37	12.27	12.5
	10.95	11.75	9.76	13.81	12.18	7.23	6.65	9.69	7.38	13.43	9.36	9.99	8.97	7.95	8.98	9.09
(μm)	11.1	11.15	10.66	11.16	12.35	7.02	5.99	11.9	7.46	13.09	9.36	9.82	8.4	7.56	9.24	11.12
	10.77	8.84	9.89	12.63	12.06	6.83	7.61	11.85	7.72	13.35	9.07	10.7	8.68	7.47	9.35	10.32
	11.35	11.15	9.34	10.96	10.51	6.5	5.72	13.22	8.55	13.59	9.06	10.85	9.51	6.87	9.11	10.75
	11.2	10.18	8.59	10.09	10.48	6.4	5.78	11.48	8.73	13.49	8.83	10.35	8.8	6.39	8.85	9.36
	10.86	9.62	8.33	13.71	10.81	6.26	7.05	10.34	9.09	13.44	8.6	11.3	8.82	7.14	9	10.04
	9.89	10.2	9.3	12.78	10.39	6.59	5.79	11.32	9.9	12.75	8.33	10.81	8.59	7.47	9.1	10.04
	10.93	9.8	9.88	13.44	10.77	6.96	6.98	10.53	10.43	13	9.53	13.48	9.01	7.05	8.92	10.49
Mean Th	10.904	11.887	10.105	13.907	8.9873	9.2173	8.1033	9.802	9.9773	10.19	10.695	11.037	9.4233	8.4227	10.034	11.289
SD	0.3673	1.883	0.9132	2.2348	2.543	2.7993	1.9653	1.867	1.7033	3.4312	1.9151	1.4272	0.7296	1.3834	1.1404	1.3805

All thickness and standard deviation data in μm

Appendix 5.5
Normal Probability Plot of the Residuals of the PTH Plating Experiment, Second-Order Model

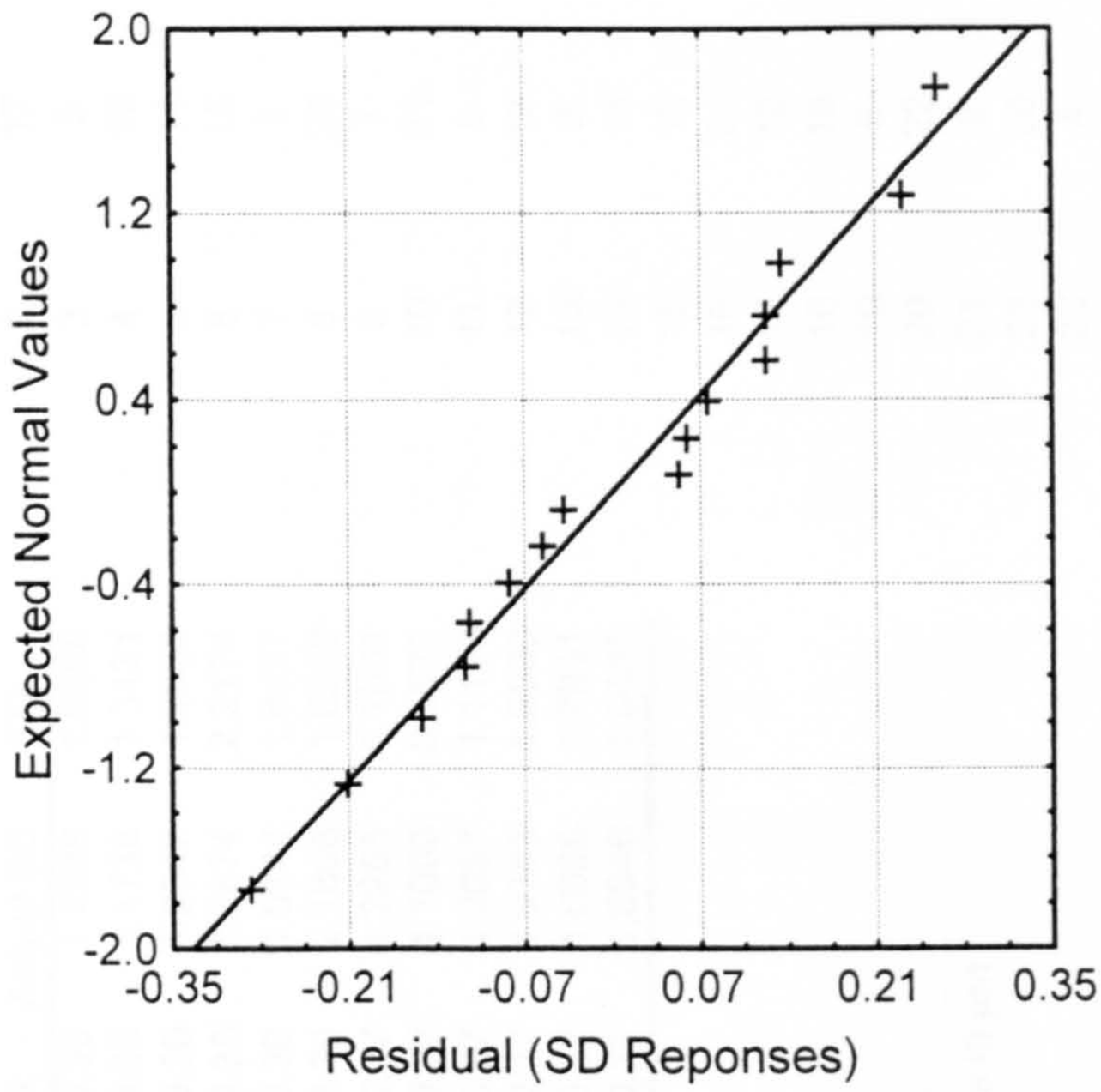

Normal Probability Plot of Residuals for the SD Responses

Appendix 5.6
Raw Data of the PTH Verification Experiments

ACD mA/cm²	ES cm	CAR mm	Coded Variable C ACD	D ES	F CAR	Mean Actual SD	Predicted SD
30.1	16.51	2.69	-0.8	-1	0.30	1.4288	1.6858
30.1	17.78	2.69	-0.8	0	0.30	1.1735	1.3121
30.1	19.05	2.69	-0.8	1	0.30	1.2347	1.2965
34.4	16.51	2.69	0.8	-1	0.30	2.2874	2.2174
34.4	17.78	2.69	0.8	0	0.30	1.5144	1.8437
34.4	19.05	2.69	0.8	1	0.30	2.1808	1.8282
30.1	16.51	2.44	-0.8	-1	-0.27	1.2265	1.1601
30.1	17.78	2.44	-0.8	0	-0.27	1.1000	0.9572
30.1	19.05	2.44	-0.8	1	-0.27	1.2057	1.1126
34.4	16.51	2.44	0.8	-1	-0.27	1.9763	1.9960
34.4	17.78	2.44	0.8	0	-0.27	1.6685	1.7931
34.4	19.05	2.44	0.8	1	-0.27	1.6946	1.9485

ACD : Average Current Density
ES : Electrode Separation

All thickness and standard deviation data in μm

Board No.	Order No.	Mean Thickness	SD	Average SD	Predicted SD
1	1	13.5235	1.4886	1.4288	1.6858
2	17	13.9745	1.3689		
3	5	13.7855	1.0663	1.1735	1.3121
4	19	13.9580	1.2806		
5	11	13.7240	1.2449	1.2347	1.2965
6	15	13.2805	1.2245		
7	3	19.3730	2.7733	2.2874	2.2174
8	23	19.3160	1.8014		
9	7	18.5855	1.4727	1.5144	1.8437
10	21	18.6020	1.5562		
11	9	18.2565	2.2427	2.1808	1.8282
12	13	17.8085	2.1188		
13	2	13.6415	1.2123	1.2265	1.1601
14	16	13.6035	1.2408		
15	10	14.1330	1.1906	1.1000	0.9572
16	24	14.0595	1.0094		
17	12	13.8155	1.2342	1.2057	1.1126
18	18	13.8905	1.1772		
19	6	19.5530	2.1881	1.9763	1.9960
20	22	19.2520	1.7645		
21	8	18.0815	1.4683	1.6685	1.7931
22	20	18.4415	1.8686		
23	4	15.1715	1.7201	1.6946	1.9485
24	14	15.2840	1.6691		

Appendix 5.6
Raw Data of the PTII Verification Experiments

Board no.	1	13	7	23	3	19	9	21	11	5	17	12	24	6
Order no.	1	2	3	4	5	6	7	8	9	11	12	13	14	15
	12.71	13.3	15.64	12.32	13.7	18.43	17.27	17.34	17.6	13	13.06	16.48	13.98	12.86
	12.69	12.98	15.95	14.31	13.85	17.75	17.68	17.84	16.89	12.76	12.75	16.29	14.64	12.83
	12.81	12.76	18.68	13.69	13.71	17.68	17.64	17.57	16.39	13.91	13.29	15.63	13.22	12.23
Upper	12.77	12.5	17.66	12.87	12.66	18.24	17.91	17.44	17.41	12.59	12.34	15.57	14.76	12.59
thickness	12.79	13.25	17.51	13.85	13.67	16.83	17.74	16.65	16.42	12.61	12.6	15.66	14.75	12.89
measured	12.48	12.62	17.9	13.66	12.83	17.58	17.51	16.75	15.85	12.82	12.73	15.87	13.63	12.65
	11.43	13.01	16.67	13.94	13.69	17.73	16.99	17.52	16.11	12.72	12.54	15.79	12.47	12.32
(μm)	11.55	13.23	16.05	13.92	13.79	17.88	17.55	17.31	16.25	12.48	13.67	15.91	13.73	12.43
	13.98	14.15	20.28	15.9	14.29	19.72	18.89	18.54	18.55	14.2	14.61	19.06	16.01	13.15
	10.19	10.77	14.59	13.27	9.97	15.6	16.5	14.92	14.86	11.31	11.38	13.81	12.58	10.3
	14.56	14.34	21.34	16.37	14.56	22.2	19.5	20.15	21.64	15.02	14.84	19.5	17.69	14.86
	14.79	14.57	22.59	17.19	14.63	22.43	18.89	20.04	20.33	14.2	14.1	19.63	16.45	14.66
	15.94	14.64	23.36	16.68	14.29	21.58	18.77	19.42	20.53	15.43	14.92	19.38	16.58	13.89
Lower	14.76	14.32	20.28	16.63	14.07	20.29	20.88	18.58	19.62	14.99	14.85	19.85	15.87	13.83
thickness	14.68	13.99	21.31	16.79	14.18	20.48	19.27	18.85	18.57	14.08	14.34	19.93	15.92	14.77
measured	15.3	14.15	21.48	16.45	14.1	20.5	19.36	17.84	18.55	14.82	14.38	19.37	15.75	14.23
	14.25	13.95	22.04	17.4	14.23	21.07	18.73	17.88	18.65	14.77	14.61	19.69	16.75	13.84
(μm)	14.43	13.87	21.34	16.34	14.88	21.14	19.91	18.92	19.39	14.34	14.79	19.44	17.72	13.99
	15.1	17.05	23.75	17.79	14.91	24.2	22.81	21.42	24.13	15.99	16.7	21.25	17.92	15.4
	13.26	13.38	19.04	14.06	13.7	19.73	17.91	16.65	17.39	12.44	13.81	18.06	14.76	11.89
Max.	15.94	17.05	23.75	17.79	14.91	24.2	22.81	21.42	24.13	15.99	16.7	21.25	17.92	15.4
Min.	10.19	10.77	14.59	13.27	9.97	15.6	16.5	14.92	14.86	11.31	11.38	13.81	12.58	10.3
Range	5.75	6.28	9.16	4.52	4.94	8.6	6.31	6.5	9.27	4.68	5.32	7.44	5.34	5.1
Mean	13.5235	13.6415	19.373	15.1715	13.7855	19.553	18.5855	18.0815	18.2565	13.724	13.8155	17.8085	15.259	13.2805
Std. dev.	1.488603	1.212311	2.773322	1.720105	1.066285	2.188071	1.472668	1.46828	2.242729	1.244907	1.234199	2.118821	1.669065	1.224532

All thickness and standard deviation data in μm

Appendix 5.6
Raw Data of the PTH Verification Experiments

Board no.	14	2	18	4	10	20	8	16
Order no.	16	17	18	19	21	22	23	24
	12.75	13.1	13.09	13.34	16.78	17.64	17.89	12.9
	12.63	13.84	12.92	13.41	17.54	17.93	17.77	12.85
	12.69	12.76	12.84	13.24	17.59	17.82	17.84	13.07
Upper	11.96	12.88	12.75	13.2	17.67	17.67	17.86	13.21
thickness	12.39	12.69	12.58	12.76	17.55	17.5	17.62	12.95
measured	12.48	12.81	12.63	12.9	17.43	17.38	17.59	13.83
	12.72	12.17	12.51	13.12	16.97	17.65	17.8	13.1
(μm)	12.61	13.02	13.8	13	16.84	17.9	18.03	13.26
	13.39	13.55	14.38	14.51	18.91	19.48	18.94	14.52
	11.25	11.81	12.05	10.65	15.94	16.81	16.18	12.84
	15.34	15.02	14.56	15.2	19.85	20.66	21.02	14.73
	14.78	14.88	14.99	15.31	20.15	21.22	20.91	14.8
	14.81	14.62	14.83	14.88	20.12	21.19	20.85	14.31
Lower	14.49	14.79	14.71	14.73	20.2	20.83	20.98	15.5
thickness	14.45	14.55	14.56	14.37	19.77	20.58	20.54	15.05
measured	14.61	14.85	14.65	14.52	19.54	20.33	20.47	14.73
	14.96	15.11	14.54	15.1	19.46	20.72	20.73	15.12
(μm)	14.84	15.92	14.77	15.02	19.23	21.05	21.15	15.27
	15.07	17.28	16.73	16.41	22.07	22.63	23.1	15.72
	13.85	13.84	13.92	13.49	18.43	18.05	19.05	13.43
Max.	16.07	17.28	16.73	16.41	22.07	22.63	23.1	15.72
Min.	10.25	11.81	12.05	10.65	15.94	16.81	16.18	11.84
Range	5.82	5.47	4.68	5.76	6.13	5.82	6.92	3.88
Mean	13.6035	13.9745	13.8905	13.958	18.602	19.252	19.316	14.0595
Std. dev.	1.240752	1.368931	1.177189	1.280623	1.556188	1.76447	1.801378	1.009447

All thickness and standard deviation data in μm

Appendix 5.7

Alias Structure of the 2_{IV}^{7-2} Fractional Factorial Design used in the Screening Experiments of BV Plating

2^{7-2}, ¼ fraction of 7 factors in 32 runs

Design Generators

F = ABCDE G = ABDE

Defining relation: I = ABCDF = ABDEG = CEFG

Aliases

A	AB = CDF = DEG	BC = ADF	CE = FG	ACE = AFG
B	AC = BDF	BD = ACF = AEG	CF = ABD = EG	ACG = AEF
C = EFG	AD = BCF = BEG	BE = ADG	CG = EF	BCE = BFG
D	AE = BDG	BF = ACD	DE = ABG	BCG = BEF
E = CFG	AF = BCD	BG = ADE	DF = ABC	CDE = DFG
F = CEG	AG = BDE	CD = ABF	DG = ABE	CDG = DEF
G = CEF				

2 blocks of 16: ACE = AFG 4 blocks of 8: ACE = AFG

BCE = BFG

AB = CDF=DEG

Appendix 5.8
Raw Data of the Screening Runs of the BV Experiments

Observa. No.	A Acid	B Sulphate	C ACD	D ES	E IHD	F CAR	G DR	MEAN	SD
1	-1	-1	-1	-1	-1	1	1	8.5832	1.1290
2	1	-1	-1	-1	-1	-1	-1	6.7996	0.9848
3	-1	1	-1	-1	-1	-1	-1	7.2780	1.3467
4	1	1	-1	-1	-1	1	1	8.7429	1.1506
5	-1	-1	1	-1	-1	-1	1	10.7509	2.1965
6	1	-1	1	-1	-1	1	-1	10.2334	1.8377
7	-1	1	1	-1	-1	1	-1	7.9116	1.7442
8	1	1	1	-1	-1	-1	1	10.6627	2.1009
9	-1	-1	-1	1	-1	-1	-1	9.2916	1.7604
10	1	-1	-1	1	-1	1	1	7.7839	1.6837
11	-1	1	-1	1	-1	1	1	8.5531	1.9568
12	1	1	-1	1	-1	-1	-1	9.0815	1.6556
13	-1	-1	1	1	-1	1	-1	11.1986	2.4720
14	1	-1	1	1	-1	-1	1	10.9224	2.1465
15	-1	1	1	1	-1	-1	1	11.9133	2.1424
16	1	1	1	1	-1	1	-1	11.2378	2.4233
17	-1	-1	-1	-1	1	1	-1	8.0669	1.2242
18	1	-1	-1	-1	1	-1	1	6.6988	1.0922
19	-1	1	-1	-1	1	-1	1	7.5694	1.2799
20	1	1	-1	-1	1	1	-1	7.8838	1.3811
21	-1	-1	1	-1	1	-1	-1	8.5950	1.8589
22	1	-1	1	-1	1	1	1	8.4719	1.8652
23	-1	1	1	-1	1	1	1	9.9138	1.8670
24	1	1	1	-1	1	-1	-1	8.7419	2.0046
25	-1	-1	-1	1	1	-1	1	8.4781	1.6742
26	1	-1	-1	1	1	1	-1	6.8431	1.2152
27	-1	1	-1	1	1	1	-1	7.4644	1.2753
28	1	1	-1	1	1	-1	1	8.2781	1.4461
29	-1	-1	1	1	1	1	1	12.0538	2.5851
30	1	-1	1	1	1	-1	-1	10.8956	2.5868
31	-1	1	1	1	1	-1	-1	11.4663	2.3390
32	1	1	1	1	1	1	1	13.0463	2.6290

Acid : Concentration of Sulphuric Acid
Sulphate : Concentration of Copper Sulphate
ACD : Average Current Density
ES : Electrode Separation
IHD : Inter-Hole Distance of the PTH / BV
CAR : Correct Aspect Ratio of the PTH / BV
DR : Depth Ratio of the BV

All thickness and standard deviation data in μm

Appendix 5.8
Raw Data of the Screening Runs of the BV Experiments

observation no.	1	2	3	4	5	6	7	8	9	10	11
	6.45	5.12	5.53	6.62	8.61	9.62	6.15	8.63	7.18	5.89	6.67
	6	6.45	5.25	7.12	10.67	9.17	5.45	8.36	7.81	7.12	6.37
	7.57	7.45	6.53	7.08	6.45	7.21	6.48	7.88	8.12	7.1	7.93
	8.88	6.87	5.68	6.39	6.79	7.29	5.42	7.2	8.97	6.13	7.79
	7.78	7.8	6.5	8.52	6.14	9.93	6.83	8.48	7.33	6.44	6.73
	7.31	7.91	6.87	8.56	6.45	8.84	6.86	9.33	7.56	7.22	6.06
	7.04	6.12	6.8	7.27	10.23	6.92	5.59	10.55	6.48	5.12	7.33
Deposite	7.12	6.25	6.56	7.67	6.38	10.01	5.31	9.85	6.49	5.13	6.66
	8.77	5.33	6.98	7.39	8.66	8.33	6.94	9.2	8.81	6.08	6.52
thickness	9.01	5.28	5.38	7.81	9.76	8.1	7.01	8.6	8.5	5.97	6.55
	8.4	5.81	6.74	6.8	10.42	9.12	6.38	9.41	8.33	6.23	5.85
measured	7.98	5.67	6.45	7.16	8.85	9.45	5.67	9.91	8.54	6.49	6.16
	7.32	5.69	6.7	6.94	9.09	8.87	6.43	7.58	7.88	6.58	6.72
(μm)	8.45	6.7	6.05	7.21	10.99	9.1	6.95	8.46	8.36	5.23	6.54
	7.97	7.02	6.46	8.96	8.78	8.44	6.84	7.89	6.2	7.06	7.01
	6.9	5.55	5.97	8.56	9.66	8.26	5.45	7.56	6.67	7.2	7.55
	6.99	5.39	5.52	8.13	9.78	9.3	7.57	9.59	7.06	6.88	5.83
	7.78	6.16	5	8.23	9.6	8.87	6.28	9.38	7.02	7.01	5.34
	8.9	6.74	5.46	8.33	10.45	8.32	7.99	9.21	8.3	6.5	7.62
	8.12	5.33	5.55	8.7	10.3	9.03	7.33	9.77	8.12	6.66	7.95
	7.89	5.66	5.7	7.51	10	7.33	7.89	8.51	8.56	5.99	7.4
	8.8	5.2	5.96	8.96	10.24	7.97	5.25	8.19	8.44	6.13	6.83
	9.63	8.97	9.45	8.73	13.52	12.48	5.67	13.35	11.45	6.33	8.51
	9.56	7.02	8.8	8.71	11.92	11.57	6.38	13.98	11.89	6.89	10.01
	8.1	8.23	9.45	7.48	15.16	12.43	7.75	12.92	9.45	8.54	8.78
	8.9	7.56	8.64	8.71	10.76	12.27	6.87	14.33	9.1	8.65	8.35
	8.45	6.89	7.87	9.81	12.39	11.11	6.1	11.9	11.99	10.2	9.59
	8.12	6.78	8.65	10.06	11.91	11.14	9.76	11.49	11.45	9.45	11.74
	9.06	8.05	8.45	9.76	12.09	12.33	9.27	13.35	11.3	9.05	10.84
	9.13	7.12	7.64	9.03	13.06	12.54	9.15	11.36	10.4	10.12	10.65
	10.49	7.46	8.01	9.24	10.4	12.99	9.14	13.05	10.45	8.64	10.38
	10.46	6.4	9.54	10.66	12.66	10.88	10.3	11.64	11.78	9.13	10.71
	8.24	6.99	8.09	9.51	12.54	10.64	10.26	13.02	11.56	9.79	10.25
	8.9	8.06	7.47	9.34	11.65	11.2	10.66	12.3	9.6	10.56	11.36
	9.12	7.45	8.45	9.11	11.87	11.64	9.84	13.51	9.5	10	9.26
	9.45	7.69	9.11	10.03	13.33	12.9	8.98	13.19	10.88	8.11	9.69
	9.6	7.88	8	10.28	13.54	12.41	9.55	12.59	10.88	8.45	9.64
	9.3	8.14	8.48	9.14	12.5	9.9	8.24	11.58	11.46	10.63	9.24
	8.99	6.11	8.13	9.58	12.7	12.2	8.29	11.81	11.7	9.54	9.25
	10.45	7.02	8.45	10.06	13.07	12.1	10.2	13.5	10.51	9.33	11.65
	10.6	6.45	8.05	9.11	12.07	11.45	9.88	12.78	10.01	9.2	11.29
	9.49	8.03	8.66	10.89	11.38	11.65	9.44	10.79	10.6	9.5	10.41
	10.1	8.2	8.54	10.56	12.56	12.66	9.9	12.11	10.92	10.03	10.71
	10.09	7	8.66	9.19	13.66	12.3	10.93	11.07	11.22	10.19	11.53
		7.44		9.06			8.55				11.64
		6.81		9.13			10.04				
		6.33		9.53			9.92				
				9.18			9.66				
				9.22			9.38				
				9.01			9.4				
				10.35							
				10.24							
No. of points measured	44	47	44	52	44	44	50	44	44	44	45
Mean Thickness	8.583	6.8	7.278	8.743	10.75	10.23	7.912	10.66	9.292	7.784	8.553
Standard Deviation	1.129	0.985	1.347	1.151	2.197	1.838	1.744	2.101	1.76	1.684	1.957

Appendix 5.8
Raw Data of the Screening Runs of the BV Experiments

observation no.	12	13	14	15	16	17	18	19	20	21	22	23
	6.65	7.87	8.77	9.56	10.12	7.32	5.38	7.16	7.07	6.25	5.99	7.44
	7.89	8.56	8.99	9.58	8.95	7.1	6.25	6.23	6.3	6.04	6.48	8.31
	6.53	9.4	8.51	8.14	9.93	6.36	5.9	7.15	6.8	8.63	7.46	7.78
	8.6	9.24	8.59	9.66	8.04	7.98	5.56	5.44	6.43	7.84	7.23	8
	8.21	8.21	9.74	11.09	9.04	6.15	5.3	5.98	6.08	6.75	7.14	8.04
	6.71	7.87	9.35	10.88	10.6	7.01	4.99	6.12	6.89	6.6	6.95	7.9
	6.89	8.98	8.88	10.12	9.41	6.68	6.19	7.02	6.34	6.99	6.77	9.06
Deposite	8.76	9.7	9.85	8.99	9.6	7.61	6.4	7.46	7.33	7.54	6.3	9.29
	7.05	9.5	9.24	9.46	9.66	9.35	7.22	8.9	9.94	8.59	9.77	10.25
thickness	6.53	8.46	9.46	10.55	9.48	8.99	8.46	9.76	8.2	9.37	9.12	11.79
	8.86	8.54	8.57	10.4	8.97	9.5	7.56	8.65	9.65	11.95	9.45	11.85
measured	8.64	8.3	8.07	10.6	8.97	9.57	7.49	8.98	9.11	10.65	9.6	11.83
	8.18	9.05	9.9	10.49	9.12	9.99	7.18	8.63	9.01	11.55	9.99	11.81
(μm)	7.56	9.45	9.8	9.64	8.6	8.67	8.02	8.95	8.6	10	11.6	10.65
	7.18	8.81	9.47	9.78	8.44	8.23	8.03	7.56	8.47	9.13	11.01	12.22
	8.81	7.3	9.65	8.16	8.56	8.56	7.25	7.12	9.92	9.64	10.69	12.4
	7.7	8.94	8.64	9.03	9							
	6.08	9.09	8.77	10.11	8.5							
	7.87	8.65	8.27	9.89	7.99							
	6.44	8.81	9.65	10.33	8.24							
	8.82	8.34	8.65	10.2	8.33							
	8.8	14.5	8.47	11	9.24							
	10.09	13.78	9.08	15.58	15.05							
	9.78	12.4	13.66	13.15	12.39							
	10.03	13.44	12.96	13.41	12.35							
	9.9	13.36	11.03	15.19	16.81							
	9.27	12.91	13.04	14.24	11.81							
	11.4	13.12	15.38	13.5	12.73							
	11.22	12.84	15.35	13.32	14.76							
	10.99	13.27	13.98	13.84	11.5							
	10.76	13.61	12.68	12.99	12.72							
	12.13	12.56	13.47	12.56	12.63							
	11.22	12.12	11.27	13.54	13.61							
	11.1	14.03	13.8	13.3	14.29							
	9.01	13.91	13.34	13.98	14.92							
	9.55	13.81	15.28	13.7	12.79							
	9.26	14	11.88	14.04	13.16							
	9.61	13.6	11.69	12.69	12.35							
	9.76	12.99	11.09	14.11	13.86							
	9.98	14.04	11	13.63	15							
	10.75	14.22	12.66	14.34	11.5							
	11.29	13.73	11.87	14.1	14.22							
	12.41	13.65	13.04	13.6	13.67							
	9.13	13.78	12.38	14.97	12.1							
	9.74		11.64	14.66	12.69							
	10.61		11.57									
No. of points me	46	44	46	45	45	16	16	16	16	16	16	16
Mean Thickness	9.082	11.2	10.92	11.91	11.24	8.067	6.699	7.569	7.884	8.595	8.472	9.914
Standard Deviat	1.656	2.472	2.147	2.142	2.423	1.224	1.092	1.28	1.381	1.859	1.865	1.867

Appendix 5.8
Raw Data of the Screening Runs of the BV Experiments

observation no.	24	25	26	27	28	29	30	31	32
	7.74	6.64	5.13	5.31	6.7	9.56	7.85	9.04	11.22
	6.36	6.77	5.78	6.71	8.15	9.12	8.49	9.73	11.21
	7.63	7.94	5.46	7.87	6.2	10.6	9.55	8.81	9.97
	6.35	6.37	5.7	5.68	7.82	10.3	9.6	9.63	10.02
	7.99	7.17	5.89	6.09	7.13	9.02	8.47	9.61	10.35
	6.12	7.44	5.43	7.11	7.75	9.78	7.69	9.86	10.6
	6.56	6.69	6.86	6.2	6.96	9.44	8.44	9.6	10.85
Deposite	6.6	6.87	6.39	6.56	6.23	9.55	7.99	8.33	10.31
	11.9	9.05	7.18	9.49	8.4	13.15	13.25	13.96	16.62
thickness	9.96	9.78	8.92	7.44	9.48	13.16	12.14	14.85	14.76
	10.4	10.64	7.17	9.03	8.97	14.45	14.66	13.11	16.22
measured	9.66	10.99	8.3	8.24	10.71	14.64	14.12	14.12	14.73
	10.55	10.3	8.16	8.51	10.64	15.77	14	12.04	15.33
(μm)	10.34	10.78	8.55	8.82	9.97	15.89	13.05	12.67	15.64
	11.01	9.21	7.46	7.81	8.35	14.1	12.56	14.7	16.01
	10.7	9.01	7.11	8.56	8.99	14.33	12.47	13.4	14.9

No. of points me	16	16	16	16	16	16	16	16	16
Mean Thickness	8.742	8.478	6.843	7.464	8.278	12.05	10.9	11.47	13.04625
Standard Deviat	2.005	1.674	1.215	1.275	1.446	2.585	2.587	2.339	2.628974

Appendix 5.9
Normal Probability Plot of the Residuals of the BV Plating Experiment, First-Order Model

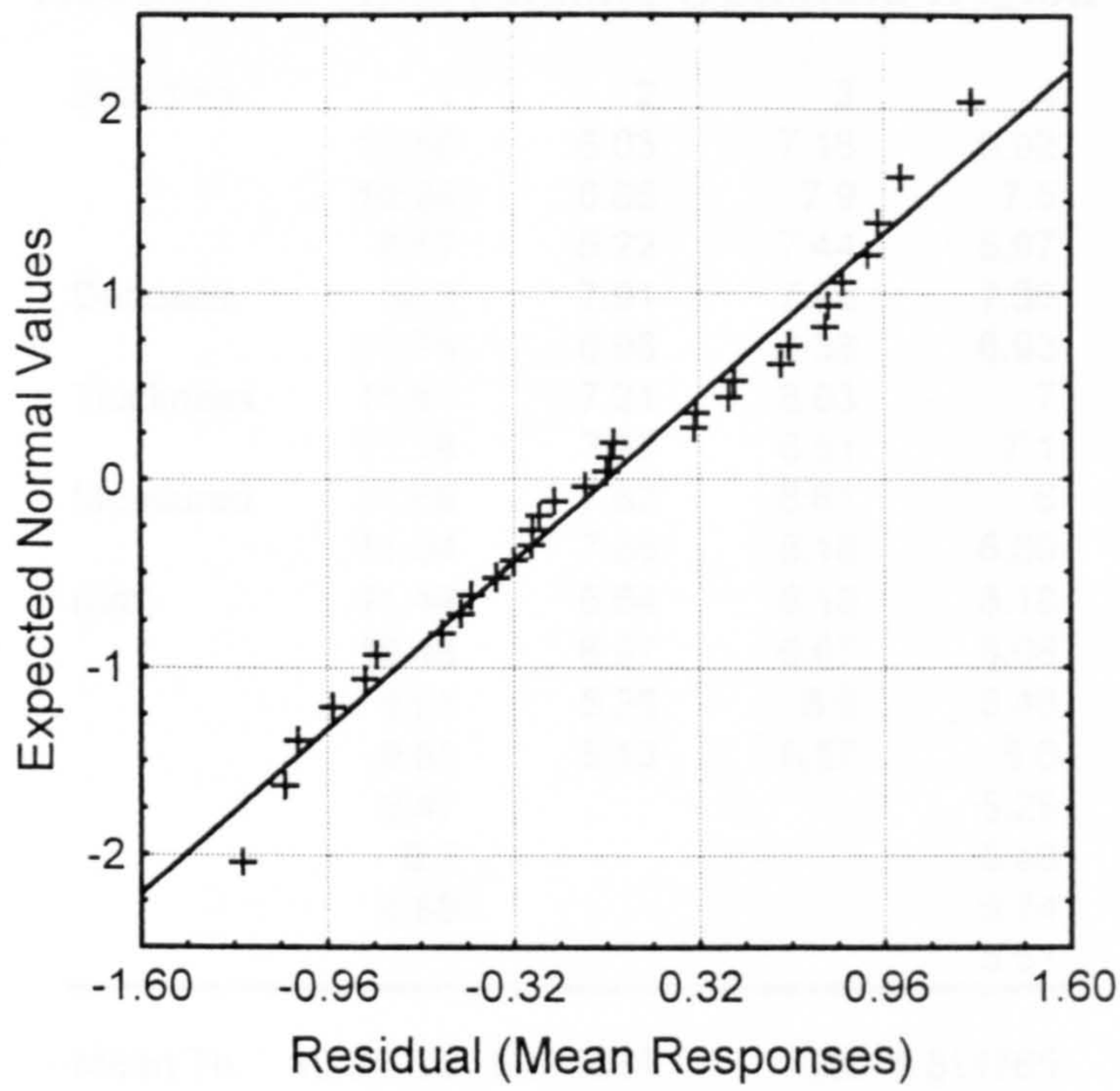

Normal Probability Plot of Residuals for the Mean Responses

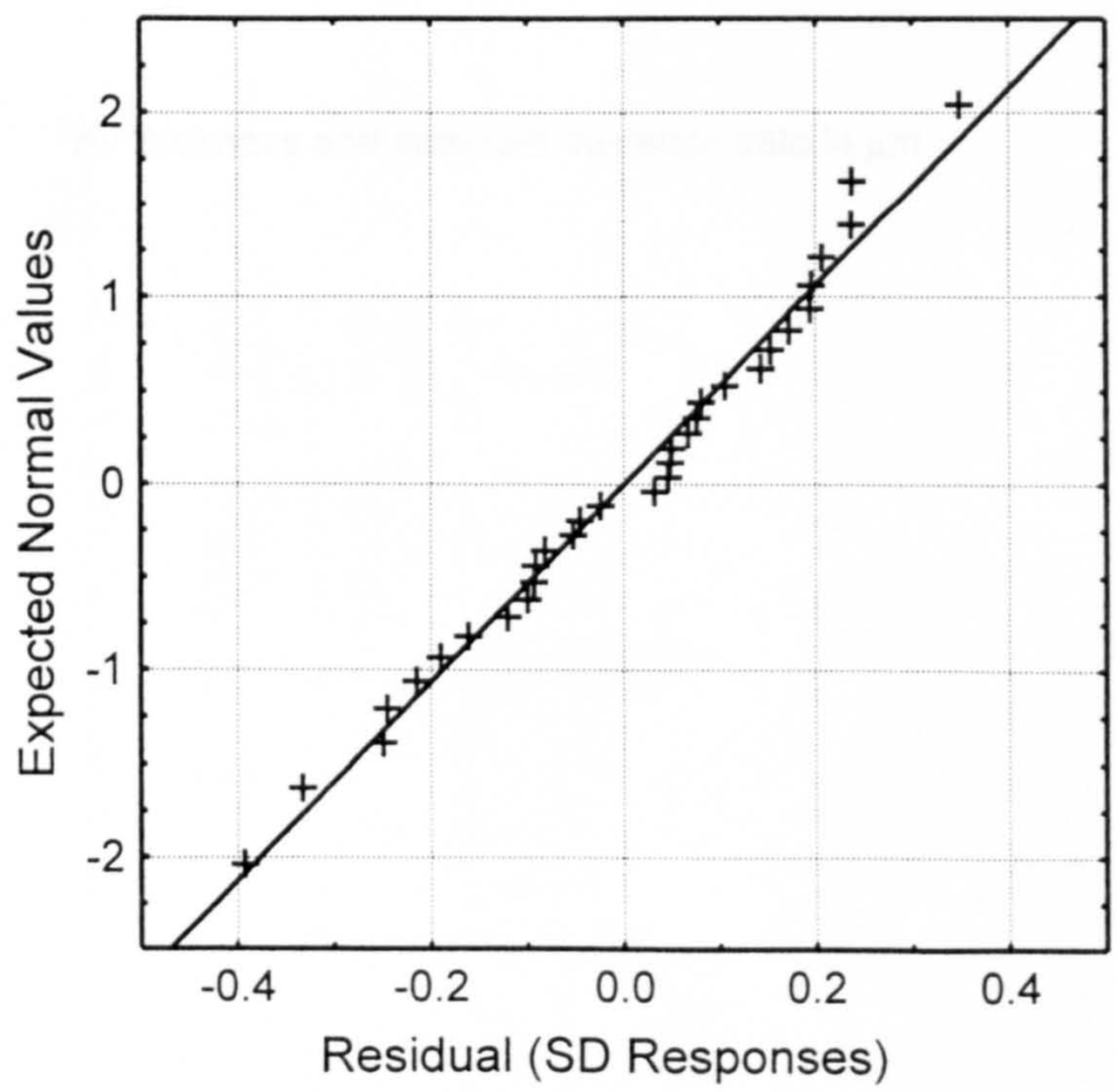

Normal Probability Plot of Residuals for the SD Responses

Appendix 5.10
Raw Data of the BV Experiments for locating the Approximate Optimum Region

Board no.	1	2	3	4
	10.86	6.03	7.16	6.92
	10.26	6.66	7.9	7.5
	9.57	6.22	7.44	5.97
Deposite	10.3	7.91	7.73	7.36
	10.79	6.98	8.33	6.93
Thickness	11.61	7.21	8.03	7
	11.19	7.97	8.51	7.1
Measured	11.68	7.62	6.61	6
	11.94	7.36	6.18	6.59
(μm)	11.44	6.64	6.13	8.18
	10.48	6.97	6.67	8.08
	9.91	5.38	6.6	5.46
	9.51	5.13	6.57	5.6
	8.47			5.28
	8.7			5.48
	8.88			5.74
				5.51
Mean Th.	10.34938	6.775385	7.22	6.511765
SD	1.101057	0.893883	0.820467	0.95343
Min.	11.94	7.97	8.51	8.18
Max.	8.47	5.13	6.13	5.28
Range	3.47	2.84	2.38	2.9

All thickness and standard deviation data in μm

Appendix 5.11
Raw Data of the BV CCD Experiments for the Second-Order Model Building

Obs. no.	ACD	ES	Actual SD	Predicted SD	Obs. no.	1	2	3	4	5	5	6	7	8	9
1	-1	-1	2.3858	2.492458		14.78	9.29	12.05	15.28	9.48	11.56	3	2	6.32	15.03
3	-1	1	2.314	2.11843		15.42	8.04	12.92	16.02	9.3	9.15	7.3	8.88	6.72	14.92
2	1	-1	1.0223	1.188511		13.92	7.78	13.05	16.37	9.7	10.76	7.05	8.72	7.16	14.22
4	1	1	3.1654	3.029383		13.19	8.6	12.45	14.09	7.95	12.88	6.78	8.51	8.69	14.34
6	-1.41421	0	1.361966	1.418756		14.23	8.71	11.51	14.52	11.2	10.84	6.86	8.34	7.04	12.27
7	1.414214	0	1.168298	1.140867		15	6.75	11.24	13.78	12.37	11.59	6.8	7.96	8.01	12.3
8	0	-1.41421	2.815	2.615972		16.14	7.11	11.62	11.14	11.34	12.47	6.74	7.83	6.8	13.73
9	0	1.414214	3.4248	3.653187		13.71	8.89	11.85	11.32	8.93	12.51	7.05	8.24	7.03	13.74
5	0	0	1.5544	1.6573		14.28	9.72	7.07	11.44	6.5	11.69	7.12	8.46	8.11	12.76
5	0	0	1.7602	1.6573		17.74	6.26	7.09	10.07	6.75	12.7	7.84	9.92	6.89	6.29
						16.17	7.92	7.84	9.45	7.33	15.66	6.17	7.45	12.15	6.4
						15.15	6.66	7.6	8.51	7.45	14.67	9.58	10.23	11.43	7.16
						14.36	7.03	7.93	9.19	8.14	11.35	9.27	10.02	12.37	7.76
						13.71	9.44	8.09	7.69	8.45	9.43	8.86	9.88	12.24	7.24
						16.79	7.84	8.57	10.73	9.7	12.22	9.11	9.61	12.39	8.2
						14.71	7	8.24	7.45	10.97	13.16	8.99	9.47	13.45	6.88
						16.3	7.44	7.27	7.17	9.8	10.75	8.78	9.33	12.85	7.43
						14.78	8.11	7.29	6.82	10.1	14.1	9.21	9.69	13.86	7.91
					Mean Th.	15.0211	7.9217	9.6489	11.1689	9.1922	12.0828	8.1285	9.2145	9.6394	10.4767
					SD	2.3858	1.0223	2.3140	3.1654	1.5544	1.7602	1.3620	1.1683	2.8150	3.4248
					Max	17.74	9.72	13.05	16.37	12.37	15.66	9.58	10.23	13.86	15.03
					Min	13.19	6.26	7.07	6.82	6.50	9.15	3.00	2.00	6.32	6.29
					Range	4.55	3.46	5.98	9.55	5.87	6.51	6.58	8.23	7.54	8.74

ACD : Average Current Density
ES : Electrode Separation

All thickness and standard deviation data in μm

Appendix 5.12
Normal Probability Plot of the Residuals of the BV Plating Experiment, Second-Order Model

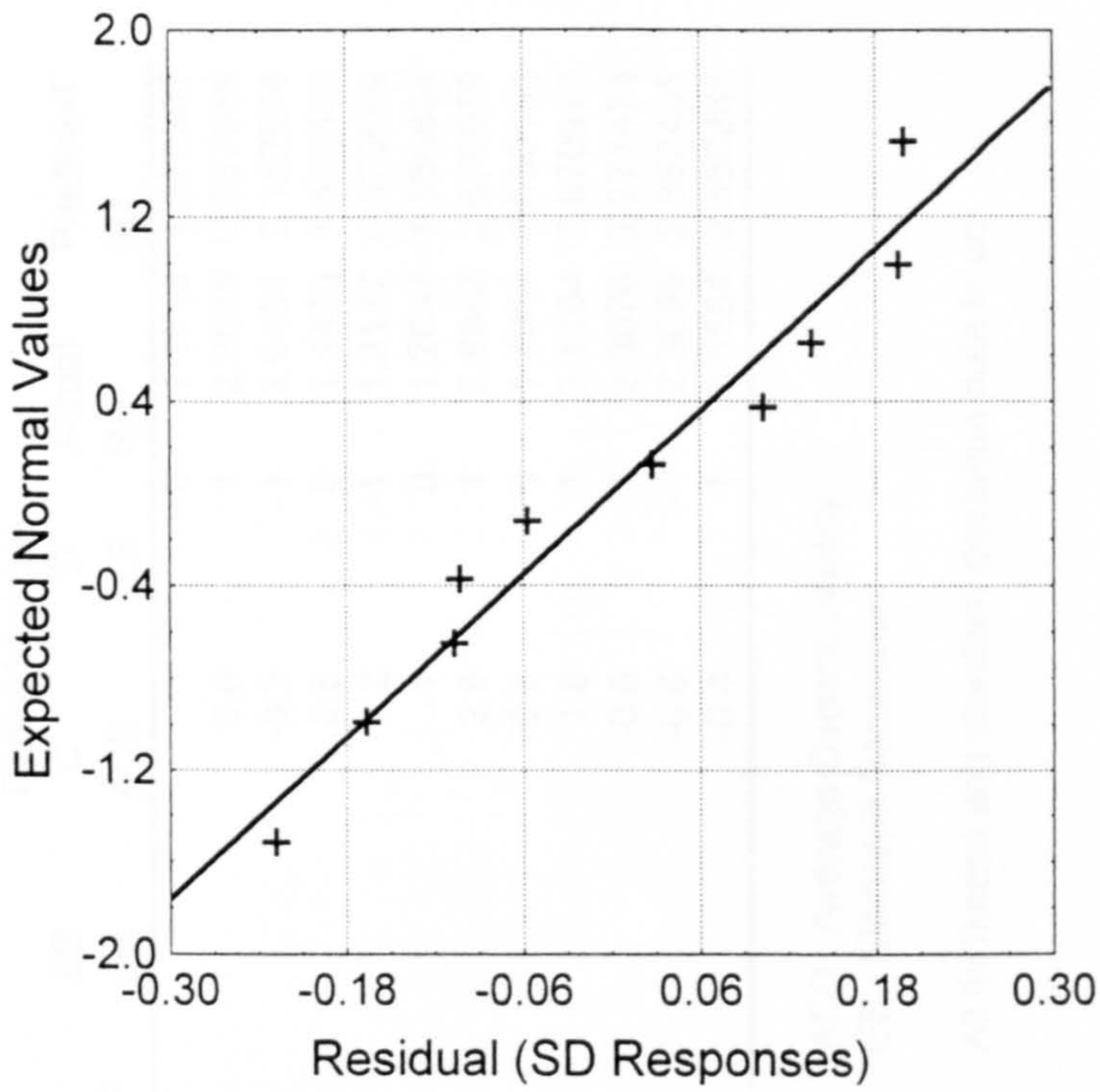

Normal Probability Plot of Residuals for the SD Responses

Appendix 5.13
Raw Data of the BV Verification Experiments

Obs. no.	ACD mA/cm^2	ES cm	Coded Variable C ACD	Coded Variable D ES	Actual SD	Predicted SD
1			1	0	1.1713	1.370307
2			0.6	1	2.8616	2.967989
3			-0.2	-1	2.0194	2.152074
4			0.6	0	1.4435	1.530403
5			1.2	-1	1.2117	0.975069
6			-1	0	1.2637	1.566804
7			2.6	1	2.8862	2.670979
8			0.2	0	1.7062	1.630101
9			1.8	1	3.1164	2.970977
10			-0.8	1	2.3076	2.277473
11			-0.6	-1	2.3699	2.352465
12			-0.4	1	2.5554	2.550261

ACD : Average Current Density
ES : Electrode Separation

All thickness and standard deviation data in μm

Appendix 5.13
Raw Data of the BV Verification Experiments

observatio BH number	1	2	3	4	5	6	7	17	18	19	20	21
	8.09	9.93	8.23	11.54	6.78	7.86	7.92	9.78	8.79	8.78	8.56	7.69
	8.67	9.81	8.15	11.02	6.89	8.11	7.43	9.68	8.11	8.59	8.78	8.16
	8.37	9.15	8.62	10.25	7.77	7.76	6.8	9.69	8.13	9.12	8.25	8.25
	8.19	8.18	8.28	10.24	7.21	8.46	6.89	10.78	7.56	9.29	8.69	7.96
	8.38	8.52	9.66	10.12	7.65	8.23	6.82	10.23	7.25	8.69	9.12	9.46
Deposite	7.79	6.35	9.29	10.19	8.23	8.22	7.14	10.28	6.86	9.28	9.13	9.26
	7.64	6.19	9.37	11.13	8.1	8.09	7.15	10.13	7.74	8.55	8.99	9.04
thickness	9.16	8.4	8.79	11.72	8.56	7.75	6.82	10.53	7.59	8.69	8.28	8.11
	7.15	8.04	8.99	11.88	7.82	7.78	13.67	9.38	7.25	8.33	8.19	8.63
measured	10.32	8.97	12.12	9.6	9.66	7.59	12.04	12.12	14.46	12.56	12.12	12.77
	9.93	12.63	12.25	11.31	9.45	10.4	12.63	12.37	13.89	12.47	12.56	12.12
(μm)	10.75	14.9	12.67	9.34	9.12	11.15	12.45	12.16	13.25	13.25	13.51	13.37
	10	14.32	13.46	9.24	10.33	11.26	12.75	13.29	14.68	13.46	13.46	13.2
	11.28	13.23	13.58	9.27	10.5	10.73	12.67	13.34	12.45	12.45	13.8	14.33
	10.14	11.69	12.43	9.51	10.45	8.46	12.09	13.56	12.69	13.76	12.77	14.01
	9.9	10.67	12.28	7.55	9.66	7.74	12.96	14.02	14.1	12.29	13.39	13.55
	9.67	12.95	12.05	7.28	9.45	7.82	12.86	13.05	14.23	14.06	13.46	13.53
	9.48	15.53	12.6	7.33	9.28	8.88	12.93	14.33	12.61	14.18	13.58	13.05
SD	1.171295	2.861573	2.019434	1.443499	1.211707	1.263677	2.886154	1.706156	3.116389	2.307578	2.369865	2.555364

All thickness and standard deviation data in μm

Appendix 5.14
Raw Data of the PTH Experiments conducted in the BV CCD

Obs. no.	Board no.	C ACD mA/cm²	D ES cm	F CAR mm	Coded Variable C ACD	D ES	F CAR	Actual SD	Plating area	Plating Current
1	6	32.3	12.7	2.226	-1	-1	-1	2.326645	0.0754	2.262
2	8	37.7	12.7	2.226	1	-1	-1	1.819012	0.0754	2.639
3	7	32.3	15.24	2.226	-1	1	-1	0.651703	0.0754	2.262
4	9	37.7	15.24	2.226	1	1	-1	1.852699	0.0754	2.639
5	2	32.3	12.7	3.012	-1	-1	1	1.889764	0.0758	2.274
6	4	37.7	12.7	3.012	1	-1	1	1.733635	0.0758	2.653
7	3	32.3	15.24	3.012	-1	1	1	1.702135	0.0758	2.274
8	5	37.7	15.24	3.012	1	1	1	0.484447	0.0758	2.653
9	10	30.3	13.97	2.560	-1.682	0	0	2.180023	0.0756	2.130408
10	11	39.6	13.97	2.560	1.682	0	0	1.890885	0.0756	2.784348
11	12	35.0	11.684	2.560	0	-1.682	0	1.433547	0.0756	2.457
12	13	35.0	16.256	2.560	0	1.682	0	2.188397	0.0756	2.457
13	18	35.0	13.97	2.048	0	0	-1.682	1.253303	0.0748	2.431
14	1	35.0	13.97	3.413	0	0	1.682	1.238938	0.0758	2.4635
15	14	35.0	13.97	2.560	0	0	0	1.540248	0.0756	2.457
16	15	35.0	13.97	2.560	0	0	0	1.521922	0.0756	2.457

Point	Raw Thickness Data (μm) Board 1	Board 2	Board 3
1	13.88	16.58	11.54
2	13.08	15.68	12.77
3	13.58	12.75	13.1
4	11.56	16.19	14.54
5	15.06	14.87	12.37
6	14.58	14.84	14.07
7	14.43	14.99	11.72
8	13.74	20.57	10.21
9	13.66	18.14	9.83
10	12.64	18.07	10.68
11	14.79	15.44	10.66
12	14.11	14.94	9.03
13	13.09	16.05	9
14	14.43	13.5	9.29
15	13.6	13.61	8.79
16	11.44	14.18	9.97
17	13.29	13.64	10.52
18	11.89	16.01	10.3
19	11.37	13.57	12.13
20	10.96	16.43	12.54
Mean Th.	13.259	15.5025	11.153
SD	1.238938	1.889764	1.702135

ACD : Average Current Density
ES : Electrode Separation
CAR : Correct Aspect Ratio of the PTH / BV

All thickness and standard deviation data in μm

Appendix 5.14
Raw Data of the PTH Experiments conducted in the BV CCD

Raw
Thickness Data (μm)

Point	Board 4	Board 5	Board 6	Board 7	Board 8	Board 9	Board 10	Board 11	Board 12	Board 13	Board 14	Board 15	Board 18
1	20.62	12.78	19.18	15.75	16.32	13.67	17.4	18.02	17.21	9.68	15.36	12.49	17.14
2	17.18	12.51	20.15	14.47	17.14	14.04	13.58	18.63	17.55	12.49	16.59	14.13	17.53
3	16.43	12.56	20.18	15.03	10.57	12.6	16.63	17.54	18.03	15.68	14.58	12.23	19.17
4	14.83	12.77	18.92	13.63	14.98	11.38	15.68	18.61	18.35	11.3	15.11	14.54	16.56
5	14.51	13.12	14.79	14.26	15.56	14.73	13.04	18.88	16.47	12.22	16.75	14.71	15.39
6	15.16	12.65	14.73	15.25	14.51	13.17	14.97	14.36	15.35	12.36	17.01	11.96	14.86
7	13.97	12.61	13.5	14.98	12.84	10.37	13.09	13.67	14.68	14.35	16.64	13.64	15.79
8	14.35	11.68	13.69	14.25	16.68	17.16	10.7	14.24	15.62	14.98	14.3	14.47	16.91
9	13.99	13.13	13.36	14.66	15.62	17.35	13.11	17.08	14.55	15.8	13.18	13.42	18.43
10	14.42	12.97	13.02	15.02	16.38	15.99	14.54	18.07	14.83	15.32	14.19	13.95	17.02
11	15.15	12.61	13.47	15.08	14.95	14.25	14.36	18.04	14.3	14.88	13.85	14.6	17.62
12	15.64	12.99	13.01	15.61	16.52	16.29	13.14	17.5	15.08	16.59	14.28	15.8	17.34
13	17.31	12.38	16.12	15.27	17.56	14.56	13.91	18.84	17.65	17.8	14.23	14.33	18.63
14	16.7	12.94	16.16	16.07	17.86	15.63	12.28	14.7	17.73	9.98	17.82	15.3	14.95
15	17.07	12.89	14.27	14.71	16.22	15.36	12.42	14.67	18.38	13.69	15.63	14.46	15.57
16	16.2	12.66	16.41	13.81	16.96	14.35	9.73	14.92	17.13	12.69	15.3	13.36	16.02
17	14.97	12.74	15.36	14.13	15.69	16.88	9.52	14.38	16.91	13.45	17.89	16.19	15.85
18	17.51	11.78	14.39	14.05	18.96	15.96	11.33	15.89	15.1	11.68	13.04	16.13	14.94
19	17.4	11.49	16.25	14.93	15.63	15.3	10.26	13.94	14.42	12.48	14.28	10.89	16.35
20	18.68	11.85	15.72	14.38	16.89	15.98	11.55	16.83	15.55	15.6	12.81	16.92	16.27
Mean Th.	16.1045	12.5555	15.634	14.767	15.892	14.751	13.062	16.4405	16.2445	13.651	15.142	14.176	16.617
SD	1.733635	0.484447	2.326645	0.651703	1.819012	1.852699	2.180023	1.890885	1.433547	2.188397	1.540248	1.521922	1.253303

Appendix 5.15
Raw Data of the BV Experiments conducted in the PTH CCD Space

		C	D	Coded Variable		
		ACD	ES	C	D	Actual
Obs. no.	Board no.	mA/cm^2	cm	ACD	ES	SD
1	1	29.6	16.51	-1	-1	1.263002
2	2	29.6	19.05	-1	1	1.979473
3	3	35.0	16.51	1	-1	2.851816
4	4	35.0	19.05	1	1	2.302962
5	5	28.5	17.78	-1.414	0	0.951371
6	6	36.1	17.78	1.414	0	2.198703
7	7	32.3	16.002	0	-1.414	2.080823
8	8	32.3	19.558	0	1.414	1.537737
9	9	32.3	17.78	0	0	2.009348
10	10	32.3	17.78	0	0	2.496408
11	11	32.3	17.78	0	0	1.865937

ACD : Average Current Density
ES : Electrode Separation
CAR : Correct Aspect Ratio of the PTH / BV

All thickness and standard deviation data in μm

Appendix 5.15
Raw Data of the BV Experiments conducted in the PTH CCD Space

	Raw Thickness (μm)										
Point	Board 1	Board 2	Board 3	Board 4	Board 5	Board 6	Board 7	Board 8	Board 9	Board 10	Board 11
1	7.85	10.28	6.13	13.44	7.09	12.23	12.53	11.26	11.04	11.88	12.1
2	6.12	11.23	7.93	12.96	7.35	11.56	11.12	10.68	11.12	10.41	7.24
3	6.96	5.66	6.87	10.07	7.56	11.44	6.62	6.56	10.71	5.31	5.85
4	7.8	6.55	6.15	11.14	8.79	6.63	6.27	6.72	10.63	5.91	8.94
5	6.19	6.22	6.94	12.37	6.09	8.88	5.9	6.12	6.97	5.14	6.08
6	7.79	5.32	6.72	7.29	7.78	8.52	6.67	6.28	6.39	6.8	7.44
7	7.49	6.89	6.02	7.99	6.72	7.55	6.78	7.05	5.93	7.67	7.02
8	7.65	6.65	8.97	8.34	7.32	12.65	11.73	6.43	6.7	11.22	7.64
9	6.96	8.23	6.53	7.25	7.57	11.82	6.08	6.69	7.18	12.06	8.49
10	7.61	7.94	5.88	7.19	7.97	10.96	7.69	7.79	11.12	11.56	12.01
11	10.06	10.78	13.82	6.83	5.84	8.94	6.68	6.86	6.7	6.71	6.28
12	9.95	5.31	12.28	6.99	7.62	7.71	7.02	6.92	6.8	7.95	7.88
13	9.69	6.6	12.47	7.14	5.03	8.96	7.31	9.02	6.08	6.08	6.62
14	8.73	5.41	12.54	7.65	6.66	6.58	6.93	7.05	7.29	8.95	6.27
15	6.51	5.87	5.77	7.49	6.26	6.83	7.38	8.42	7.52	6.72	7.81
16	6.73	5.77	6.42	8.62	6.12	6.71	8.47	8.12	7.9	5.95	7.21
Mean Th.	7.755625	7.169375	8.215	8.9225	6.985625	9.248125	7.82375	7.623125	8.13	8.145	7.805
SD	1.263002	1.979473	2.851816	2.302962	0.951371	2.198703	2.080823	1.537737	2.009348	2.496408	1.865937

Appendix 6.I

Approximation Solutions of Wa_T and Wa_L

Given that :

conc. $CuSO_4$	0.3	M
Conc. H_2SO_4	1.88	M
conductivity	0.580482	Ω^{-1} cm^{-1}
R	8.3134	J/K mol
T	298	K
Tafel slope $\left(\frac{RT}{a_c F}\right)$	0.07	V/decade, based on 0.3M CuSO4, 2.2M H2SO4, 0.3 g/l PEG, 0.625 mg/l MPSA solution in [Goodenough and Whitlaw, 89]
F	96487	c / g equiv
L	1.524	cm, based on the width of the 3 continuum over the board surface
$\alpha_c + \alpha_a$	2	based on formular of [Turner and Johnson, 62] for cupric ion
i_0	0.003584	A/cm2, based on the empirical formular of [Caban and Chapman, 77],

1. The conductivity of the electrolytic solution is determined by the empirical formular of [Caban and Chapman, 77],

$$\kappa = 0.011163 + 0.030798[CuSO_4] + 0.423553[H_2SO_4] - 0.045224[H_2SO_4]^2 - 0.13539[CuSO_4]\,[H_2SO_4]$$
$$= 0.58\ \Omega^{-1}cm^{-1}$$

2. The exchange current density is determined using the empirical formular of [Caban and Chapman, 77],

$$= 1.58 \times [Cu]^{0.67} e^{-0.36 \times [H_2SO_4]}$$
$$= 3.584 \text{ mA/cm}^2$$

3. The Wagner number at the Tafel and linear regime are calculated for the average current density and AADR values of the non-uniform pattern plating experiments using the formula in Sec. 2.4.3.